Distribution Agreement

In presenting this thesis or dissertation as a partial fulfillment of the requirements for an advanced degree from Emory University, I hereby grant to Emory University and its agents the non-exclusive license to archive, make accessible, and display my thesis or dissertation in whole or in part in all forms of media, now or hereafter known, including display on the world wide web. I understand that I may select some access restrictions as part of the online submission of this thesis or dissertation. I retain all ownership rights to the copyright of the thesis or dissertation. I also retain the right to use in future works (such as articles or books) all or part of this thesis or dissertation.

Signature:

_____ _____

Samantha Lynne Schwartz Date

Defining the RNA signatures detected by the innate immune sensor 2'-5'-oligoadenylate synthetase 1 (OAS1)

By

Samantha Lynne Schwartz
Doctor of Philosophy

Graduate Division of Biological and Biomedical Sciences
Biochemistry, Cell and Developmental Biology

_____

Graeme L. Conn, Ph.D.
Advisor

_____

Christine M. Dunham, Ph.D.
Committee Member

_____

Richard A. Kahn, Ph.D.
Committee Member

_____

Anice C. Lowen, Ph.D.
Committee Member

_____

Daniel Reines, Ph.D.
Committee Member

Accepted:

_____

Lisa A. Tedesco, Ph.D.
Dean of the James T. Laney School of Graduate Studies

_____

Date

Defining the RNA signatures detected by the innate immune sensor 2'-5'-oligoadenylate synthetase 1 (OAS1)

By

Samantha Lynne Schwartz
B.S., Armstrong Atlantic State University, 2012

Advisor: Graeme L. Conn, Ph.D.

An abstract of
A dissertation submitted to the Faculty of the
James T. Laney School of Graduate Studies of Emory University
in partial fulfillment of the requirements for the degree of
Doctor of Philosophy
in Biochemistry, Cell and Developmental Biology
2021

ABSTRACT

Defining the RNA signatures detected by the innate immune sensor
2'-5'-oligoadenylate synthetase 1 (OAS1)

By Samantha Lynne Schwartz

The innate immune system is a broad set of critical intracellular and extracellular processes that limit pathogen infectivity. To provide its essential first line of defenses, the innate immune system must identify and respond to foreign molecules. The 2'-5'-oligoadenylate synthetase (OAS) family of enzymes are important innate immune sensors of cytosolic double-stranded RNA (dsRNA), a potent signal and hallmark of viral infection. Defective or misregulated innate immune activity can cause increased persistence of and susceptibility to viral infection and human diseases, such as interferonopathies. My dissertation research investigates how specific molecular signatures within dsRNA molecules regulate OAS1 activity.

Structural studies previously revealed that dsRNA binding induces allosteric changes in OAS1 that reorganize its catalytic site and drive synthesis of 2'-5'-oligoadenylates from ATP. However, we still understand relatively little about how specific features of the dsRNA contribute to the level of OAS1 activation. I used a "simple" 18 bp dsRNA containing two copies of a previously identified OAS1 activation consensus sequence (WWN_9WG, where W is A or U, and N is any nucleotide) to identify and assess the contributions of specific dsRNA features required for potent OAS1 activation. Biochemical studies coupled with cell-based assays and computational modeling reveal that the 18 bp dsRNA contains two competing OAS1 binding sites with remarkably different capacities to activate the protein in a context-dependent manner. The dsRNA binding register was dictated by the position of the consensus sequence(s) and only when optimally positioned was potency of other RNA activating motifs observed. A new role was also identified for the non-conserved (N_9) nucleotides of the activation consensus in defining the dsRNA shape and flexibility important for OAS1 binding and recognition. The results indicate that OAS1 is unexpectedly sensitive to sequence, but also that the relative placement and organization of activating motifs is as critical as the sequences themselves. These studies define the molecular mechanism(s) that control OAS1 regulation by dsRNA and may reveal insight into viral evasion of the OAS1/RNase L pathway or avenues to new effective therapeutic strategies.

Defining the RNA signatures detected by the innate immune sensor 2'-5'-oligoadenylate synthetase 1 (OAS1)

By

Samantha Lynne Schwartz
B.S., Armstrong Atlantic State University, 2012

Advisor: Graeme L. Conn, Ph.D.

A dissertation submitted to the Faculty of the
James T. Laney School of Graduate Studies of Emory University
in partial fulfillment of the requirements for the degree of
Doctor of Philosophy
in Biochemistry, Cell and Developmental Biology
2021

ACKNOWLEDGMENTS

My success in graduate school and completion of this dissertation would not have been possible without the support of many people in my life. First and foremost, I would like to thank my research advisor and mentor, Dr. Graeme Conn. Thank you for taking a chance and hiring me to work as a Research Specialist in your lab (nearly ten years ago!) when graduate school and working towards a PhD was still *just* an idea I was entertaining. No words could accurately describe how grateful I am for your mentorship, patience, and for always pushing me to excel both at and away from the bench. Thank you for working tirelessly to read and provide feedback on everything I have ever written: pre-doctoral fellowship, manuscripts, job applications, and this thesis. Your care and attention to detail does not go unnoticed. Your passion for science is contagious and I hope one day I will be able to pay it forward and inspire others as you have, perhaps unknowingly, done for me. I cannot begin expressing my appreciation to my thesis committee members: Drs. Christine Dunham, Richard Kahn, Anice Lowen, and Daniel Reines, who always kept their doors open and came to every one of my meetings genuinely curious about my work. These years were not always easy, but your support was unwavering, you never gave up on me even in the darkest of moments when I may have considered throwing in the towel early. Thank you for pushing me beyond my comfort zone, asking the difficult questions, and never letting me sell myself short. I hope I made you all proud.

I am extremely grateful to all of my lab mates past (Jo, Pooja, Ginny, Sunita, Marta, Laís, Emily, Kellie, Brenda, Esther, Paige, and Meisam) and present (Natalia, Zane, Deb, Sarah, Logan, and Suparno). Thank you for taking the time out of your busy schedules to teach me the ropes and all things RNA biology; I will no doubt take these invaluable technical skills with me. More importantly, thank you for allowing me to interrupt your science to ask questions, encourage an impromptu lunch run to Indian buffet, or host a cake o'clock for no reason other than it was Tuesday. Research is rough sometimes with its many highs and lows, but I never squandered these moments – you all have a knack for making science (even more) *fun*!

Beyond the lab, I wish to thank my professors at both Emory University and Armstrong Atlantic State University (now Georgia Southern University, Armstrong campus). I appreciate the dedication you put into my training and for providing the tools necessary to build a solid foundation so I could become the budding scientist that I am today. Special thanks to Dr. Jennifer Brofft Bailey whose undergraduate course in applied microbiology opened my eyes to scientific careers that extended beyond the healthcare professions and teaching, and for taking me under your wing when I expressed interest in research. I would like to extend my deepest gratitude to everyone who ever read a version of my pre-doctoral fellowship, especially Dr. Anita Corbett, and to the National Institute of Allergy and Infectious Diseases (NIAID) for three years of funding to support my thesis project. Thank you to NIAID for also honoring me with the request to use my fellowship application as an example for future generations to reference. I wish to thank Mr. Skip and Leslie Petter and the Atlanta chapter of the Achievement Rewards for College Scientists (ARCS) Foundation for providing additional financial support and even more so for their all-around generosity.

I would not be here today without the love and support of my family and friends. The PhD really tests your limits both intellectually and emotionally, but without hesitation you were there to ensure we celebrated every accomplishment and dusted me off and picked me back up with every failure. I am especially grateful to my parents and my brother, Garrett, who have been my cheerleaders every step of the way. I must also thank Dr. Rachel Turn (Olbrych) for being my rock during the entire graduate school process. I am forever grateful for all of our late work nights, hiking adventures, and commiserating over failed experiments – you are more than my classmate, you are family. Last, but absolutely not least, I want to thank my partner-in-crime and in life, Darius Mahboubi. I cannot wait to see what the next chapter has in store for us.

TABLE OF CONTENTS

TABLE OF FIGURES

Chapter 1

Chapter 2

Chapter 3

Chapter 4

Chapter 5

LIST OF TABLES

CHAPTER ONE

Introduction

Innate immunity

Our cells must detect and respond to infection rapidly. Beyond initial physical barriers (such as the skin), the innate immune system serves as a first line of cellular and molecular defense with broad specificity. The innate immune system directly protects against pathogen replication, acts to warn neighboring cells, and primes the adaptive immune system to respond to infection. Innate immune system proteins take on a number of roles to prevent the spread of microbial invaders. One example is the ability to both accurately identify molecular features of foreign molecules, or pathogen-associated molecular patterns (PAMPs), in order to respond to infection while also avoiding inadvertent self-activation by endogenous molecules (1,2). The cellular proteins responsible for detecting these PAMPs are often referred to as pattern recognition receptors (PRRs). PRRs are found on the cell surface, membrane-bound in different cellular compartments, or free within the cytosol. A subset of PRRs are responsible for inducing the production of Type I Interferon (IFN), a family of cytokines responsible for triggering signaling cascades to limit both viral replication and prime neighboring cells to establish an antiviral state. Interferon also activates interferon-stimulated genes (ISGs) in a feedback loop that drives subsequent expression of genes with diverse antiviral functions (**Figure 1**). Tight regulation of these systems is required to achieve accurate detection of infecting pathogens while preventing spurious activation by cellular factors that would be detrimental to the cell.

Viral nucleic acid sensing

Nucleic acid sensing is one essential strategy used by the innate immune system to detect and clear viral infection. The sensitivity of these host antiviral sensors must be finely tuned in that they need to detect a broad range of viral nucleic acids while avoiding aberrant activation by host factors. Double-stranded RNA (dsRNA) is typically absent from uninfected cells and is therefore often a hallmark of viral infection, either present in viral genomes or produced as a consequence of viral gene expression or replication. Here, I will focus on a subset of nucleic

acid sensing PRRs responsible for detecting the presence of cytosolic dsRNA during viral infection (**Figure 1**).

Retinoic acid inducible gene I (RIG-I) and melanoma differentiation associated gene 5 (MDA5) are two members of the RIG-I-like receptor family of RNA helicases that share a similar domain architecture and signaling mechanism (3). RIG-I and MDA5 form filamentous oligomers (4,5) upon binding cytosolic dsRNA activating a signaling cascade that begins with the activation of the mitochondrial antiviral signaling protein (MAVS) via their caspase activation and recruitment domains (CARDs) (6). Activation of MAVS signals to transcription factors, IFN-regulatory factor 3 and 7 (IRF3/7), to induce the expression of Type I IFN (6,7). Type I IFN is secreted by the cell and binds to surface exposed IFN-alpha/beta receptor 1 and 2 (IFNAR1/2) on the same (autocrine signaling) and neighboring (paracrine signaling) cells to activate the expression of IFN-stimulated genes. Alternatively, MAVS can also trigger a pro-apoptotic cell fate directly via caspase 8 or indirectly via IRF3/7 to BCL-2-associated X protein (BAX) (8,9). RIG-I and MDA5 are expressed at low levels and latent in the uninfected cell, but activation of their respective pathways during a viral infection produces a positive feedback loop leading to increased protein expression (10,11). Despite their commonalities, RIG-I and MDA5 recognize distinct groups of viral RNAs. For example, one discriminating factor for the two enzymes is the size of dsRNA that each recognizes: RIG-I senses dsRNA <300 bp whereas MDA5 senses dsRNA >300 bp (12). Additionally, RIG-I is sensitive to dsRNA structure, particularly blunt ends with a 5'-triphosphate (13-16). Such a structure is indicative of RNAs produced outside of the nucleus as cellular RNAs are often masked by RNA binding proteins and/or post-transcriptional modifications (*e.g.* 7-methylguanosine cap, ribose 2'-O-methylation), thus protecting endogenous RNA from recognition by RIG-I (17-19). RIG-I and MDA5 can also function as effectors by displacing viral proteins bound to dsRNA that would otherwise be sequestered and undetected by the innate immune system (20).

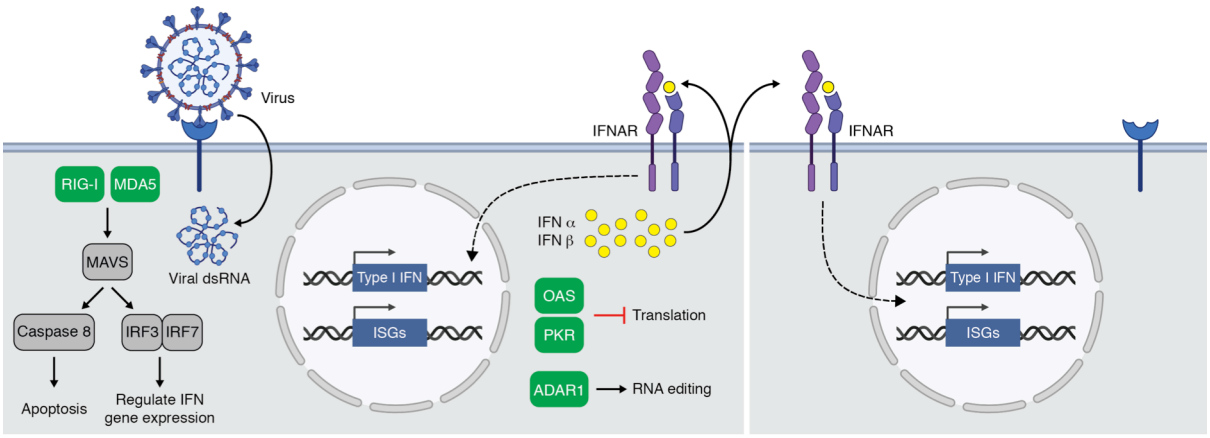

Figure 1. Overview of the innate immune system: cytosolic dsRNA receptors. Pathogen-derived nucleic acids are typically accompanied by defining features that can be recognized by cellular PRRs. PRRs must be able to detect molecules associated with infecting pathogens while readily distinguishing self from non-self. Because it is not normally present in the cytoplasm, dsRNA (*blue*) is an important signal of infection. The proteins responsible for detecting cytoplasmic dsRNA during viral infection are highlighted in *green*: RIG-I, MDA5, OAS, PKR, and ADAR1. The helicases RIG-I and MDA5 detect dsRNA in the cytoplasm and signal through mitochondrial antiviral signaling protein (MAVS, *grey*), which in turn can activate a pro-apoptotic pathway via caspase 8 (*grey*) or induce the production of Type I Interferon (IFN α/β, *yellow*) via the transcription factors IFN-regulatory factor 3 and 7 (IRF3/7, *grey*). IFN is secreted from the cell and binds to IFN-alpha/beta receptor 1 and 2 (IFNAR, *purple*) on the cell surface acting in an autocrine (same cell) or paracrine (neighboring cell) fashion. IFNAR activation signals for uninfected cells to also ramp up the expression of IFN-stimulated genes (ISGs) encoding for important antiviral restriction factors (RIG-I, MDA5, OAS, PKR, and ADAR1, *green*) in order to prime the cell in case of an impending infection. OAS, PKR, and ADAR1 restrict viral replication directly through distinct pathways that halt cellular translation (OAS, PKR) or interfere with RNA stability via A-to-I editing (ADAR1).

The 2'-5'-oligoadenylate synthetase (OAS) family of interferon-inducible nucleotidyl transferases are responsible for synthesizing 2'-5' phosphodiester-linked oligoadenylates (2-5A) upon binding to a dsRNA substrate (21-23). When comprised of three or more adenylates, these 2-5A activate their only known target, the latent cellular endoribonuclease L (RNase L) (24-26). RNase L establishes an antiviral state in several ways: direct cleavage of viral RNAs; degradation of cellular rRNA and tRNA halting general translation while still allowing for expression of innate immune system proteins (27-29); and tuning of the cellular transcriptome

through cleavage of specific mRNAs required for cell growth, proliferation, and differentiation (30-34). RNase L preferentially cleaves at single-stranded UA and UU sequences (35) generating RNA fragments with PAMPs that are able to enhance the immune response (36,37). **Chapter 2** provides a detailed overview of individual OAS family members and their specific RNA requirements for activation.

The dsRNA-activated protein kinase (PKR) is a member of the eIF2α kinase family responsible for initiating the shutdown of general translation, effectively blocking protein synthesis and inhibiting viral replication, cell cycle progression, and cell growth (38). PKR is activated upon binding a dsRNA molecule long enough (>30 bp) to recruit a second PKR monomer in close proximity to allow for dimerization and autophosphorylation of the kinase domains (39). Activated PKR in turn phosphorylates the alpha subunit of the eukaryotic initiation factor 2 (eIF2) (40,41), increasing affinity for its guanine nucleotide exchange factor (eIF2B) and thereby preventing eIF2B from releasing GDP efficiently to make way for GTP binding (42-44). eIF2 is responsible for delivering the initiator tRNA to the small ribosomal subunit and is essential for cap-dependent translation. PKR recognizes dsRNA in a sequence-independent manner by interacting directly with the phosphate and ribose backbones of two adjacent minor grooves (45,46) and is tolerant of structural elements like bulges and mismatches (47). Also, independent of RIG-I, PKR can be activated by single-stranded RNAs with limited secondary structure (*e.g.* short stem loops) if they contain a 5'-triphosphate (48). RIG-I and MDA5 are considered the major pathway for Type I IFN expression, but PKR has also been implicated in promoting Type I IFN production by stabilizing IFN-alpha/beta mRNA transcripts (49).

The adenosine deaminase acting on RNA (ADAR) class of enzymes are responsible for catalyzing the deamination reaction of adenosine (A) in dsRNAs resulting in A-to-I edits (50,51). These post-transcriptional modifications disrupt canonical Watson-Crick base pairing altering decoding during translation and overall stability of the dsRNA molecule. Consequently, inosine (I) modifications are typically read as guanosine (G) by reverse transcriptase and ribosomes,

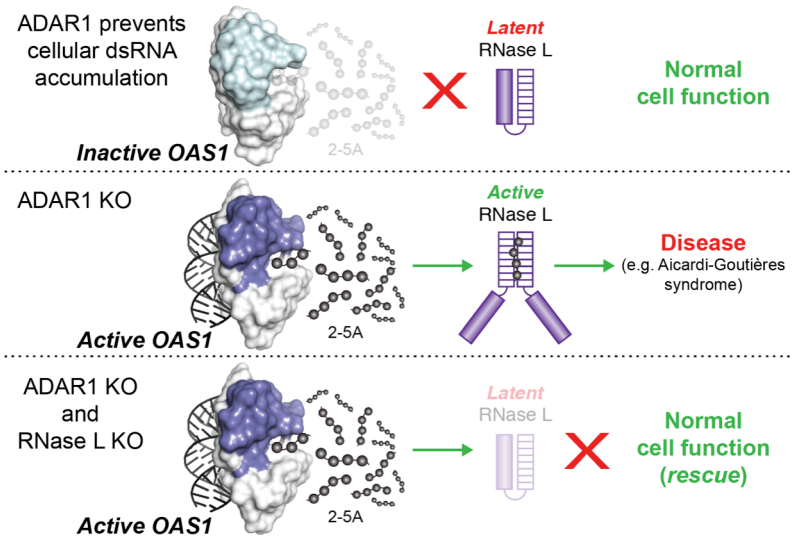

Figure 2. A-to-I editing by ADAR1 is proposed to reduce self-activation of innate immune response pathways. We still do not fully understand the molecular or cellular mechanisms that allow OAS1 to discriminate between viral and cellular RNAs. ***Top,*** However, A-to-I editing is proposed to be one way inadvertent activation by cellular RNAs is avoided: editing destabilizes dsRNA regions resulting in weaker or no OAS activation (54). ***Center,*** ADAR1 KO (deletion of *ADAR1*) eliminates this regulation resulting in activation of the OAS/RNase L pathway in the absence of infection causing diseases such as Aicardi-Goutières syndrome. ***Bottom,*** RNase L KO (deletion of *RNASEL*) rescues the ADAR1 KO phenotype by eliminating activation of RNase L restoring normal cell function.

potentially altering the copying of genetic information or leading to the translation of potentially non-functional protein products if edits occur in coding regions (52). RNA editing introduces mismatches and can disrupt secondary structure in dsRNA, which may no longer be sensed by other PRRs, thus impairing detection and providing a potential mode of viral escape (53). ADAR1 has also been implicated in preventing self-activation by endogenous dsRNAs in the absence of viral infection (**Figure 2**). Deletion of *ADAR1* in human lung carcinoma A549 cells produced a lethal phenotype that could be rescued by the subsequent deletion of *RNASEL* (54). These data suggest that loss of ADAR1 results in an accumulation of cellular dsRNAs that are capable of activating the OAS/RNase L pathway, thus indicating that ADAR1 is required to destabilize endogenous dsRNA to prevent aberrant activation of the innate immune system.

Viral evasion strategies for the OAS/RNase L pathway

Viruses depend on the host cell to complete their life cycle but at the same time must also avoid detection by innate antiviral factors that can potently restrict viral replication. These host-virus interactions are in a constant evolutionary arms race where the host must establish new ways to detect and limit viral infection while the virus must enter the cell and replicate all while navigating under the radar. A disparate pool of both DNA and RNA viruses have thus developed unique mechanisms to counter cellular antiviral defenses, including at each step in the OAS/RNase L pathway (**Figure 3**).

Inhibiting OAS activation is perhaps the most "direct" method for blocking the OAS/RNase L pathway. Hepatitis C virus encodes a non-structural protein, NS5A that binds directly to OAS to compete with dsRNA for binding (55). Many viruses also block dsRNA binding by encoding proteins utilized to protect viral RNA from detection and degradation by nucleic acid sensors. Some examples of this evasion strategy include Ebola virus VP35 (56,57), herpes simplex virus US11 (58), human immunodeficiency virus Tat (59), influenza A virus NS1 (60), reovirus outer capsid protein σ3 (61-63), and vaccinia virus E3L (64). Another related, but distinct, mechanism of evasion includes the targeted degradation of potential dsRNA activators. Herpes simplex virus encodes a virion-host shutoff (vhs) protein which functions as a viral RNase that preferentially degrades host and viral mRNAs (65), and vaccinia virus limits the formation of dsRNA via two virus-encoded decapping enzymes, D9 and D10, that are responsible for removing methylated mRNA cap structures leaving viral mRNAs susceptible to degradation by the cellular exonuclease Xrn1 (66,67). These viral countermeasures halt the OAS/RNase L pathway at its earliest stages by preventing the first key player, OAS, from ever becoming activated.

Next, to prevent dimerization and subsequent activation of RNase L, some viruses contain 2'-5'-phosphodiesterases (68) that are responsible for degrading 2-5A synthesized by OAS, namely coronavirus ns2 (69) and rotavirus VP3 (70,71). Additionally, herpes simplex virus

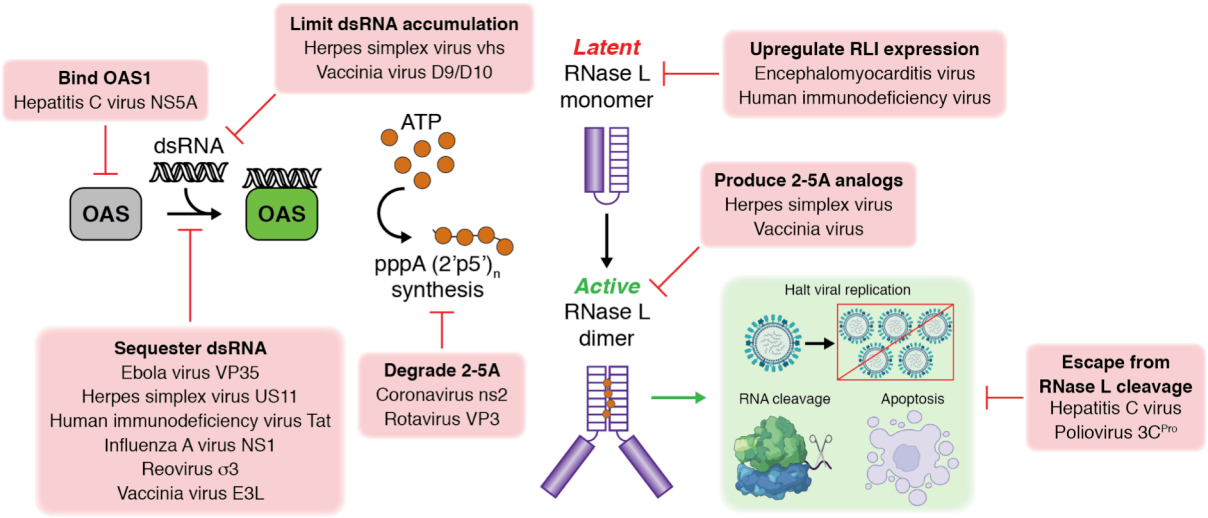

Figure 3. Viral evasion strategies to circumvent the OAS/RNase L pathway. 2'-5'-oligoadenylate synthetase (OAS, *grey*) expression is upregulated by Type I Interferon, a signaling molecule used to heighten the cell's antiviral defenses. OAS (*green*) is activated by double-stranded RNA (dsRNA) which allosterically induces structural rearrangements necessary to synthesize 2'-5'-linked oligoadenylates (2-5A, *orange*) from ATP. These 2-5A molecules are responsible for tethering inactive monomers of the latent cellular endoribonuclease L (RNase L, *purple*) to form a functionally active dimer. RNase L activation limits viral replication by degrading both viral and cellular RNA thus halting global translation, and depending on the severity of the infection, may result in apoptosis. Both DNA and RNA viruses have developed unique strategies to combat activation at each stage in the OAS/RNase L pathway highlighted in *red* and described in detail in the section "**Viral evasion strategies for the OAS/RNase L pathway**."

(72) and vaccinia virus (73,74) are proposed to hijack OAS in order to promote the synthesis of 2-5A analogs that are inactive or inhibitory against RNase L. These 2-5A analogs contain a complex mixture of phosphorylated and non-phosphorylated 2-5A species as well as additional derivative compounds (74), but their identity and mechanism of action still remain to be determined. The cellular RNase L inhibitor (RLI) is also responsible for inhibiting 2-5A binding to RNase L and may play a larger role in the absence of infection, as its expression is not regulated by interferon (75). However, observations of increased RLI expression and concomitant inhibition of RNase L have been noted during encephalomyocarditis virus (76) and human immunodeficiency virus (77) infection, although the latter is complicated by the role of

RLI in HIV capsid assembly. Some viruses can evade the OAS/RNase L pathway altogether by acquiring resistance to RNase L cleavage. For example, RNase L activity during hepatitis C virus infections results in the selection of viral strains with fewer RNase L target sequences, specifically UU and UA dinucleotides (78-80), and poliovirus contains a highly structured hairpin in the 3C protease ($3C^{Pro}$) open reading frame which acts as a cleavage-resistant substrate and thus a competitive inhibitor of RNase L (81).

In summary, numerous viral strategies for escape have been uncovered and these can occur at each stage of OAS/RNase L pathway activation, including inhibiting OAS, sequestering dsRNA, degrading 2-5A via viral-encoded phosphodiesterases, producing 2-5A analogs, inhibiting RNase L, or providing selective pressure to remove RNase L target sites within viral RNAs (summarized in **Figure 3**). The diverse strategies many different viruses have developed to evade detection clearly underscore the critical role the OAS/RNase L pathway plays in limiting viral infection.

Roles for the OAS/RNase L pathway in normal cell function

Another growing area of study is to understand the role of OAS and the OAS/RNase L pathway in normal cell function in the absence of viral infection. From an evolutionary perspective, OAS can be traced back to organisms lacking an interferon-regulated immune system (*e.g.* marine sponges), giving us some indication that the OAS family of proteins may have additional functions beyond those needed for antiviral defense. A recent study used whole-exome sequencing to identify three different human heterozygous missense mutations in OAS1 (A76V, C109Y, and L198V) implicated in infantile-onset pulmonary alveolar proteinosis, a disease characterized by dysfunction in lung surfactant homeostasis (82). A separate, but complementary, body of work in which our lab was involved, identified a fourth OAS1 mutation (V121G) and discovered that these four OAS1 mutations exhibit a gain-of-function phenotype contributing to dsRNA-independent OAS1 activation (Magg *et al.*, *submitted*). These studies led

to the identification of a novel interferonopathy, termed OAS1-associated polymorphic autoinflammatory immunodeficiency disorder (OPAID). In addition to increased susceptibility to viral infections (83,84), OAS1 single nucleotide polymorphisms (SNPs) have been linked to diabetes (85), multiple sclerosis (86,87), prostate cancer (88), and Sjögren's syndrome (89,90), as well as susceptibility to tuberculosis infection (91), suggesting that OAS1 has an important role in cellular processes that impact these human diseases.

The OAS/RNase L pathway is also gaining increasing appreciation for its anti-proliferative role. Specifically, RNase L has been implicated in tuning the human transcriptome by selectively destabilizing mRNAs responsible for suppressing cellular proliferation and adhesion (33,34). Controlled inhibition of cell growth and migration is important to limit the spread of infection, but is also required to monitor proper cell regulation to prevent cancer development and metastasis. OAS1 has also been shown to modify the DNA repair signal, poly(ADP-ribose) (PAR), by adding AMP residues in 2'-5'-linkages to attenuate PAR synthesis, thus improving cell viability following treatments with DNA damaging agents (92). The OAS/RNase L pathway has also been recently implicated in mediating the cytotoxicity of 5-azacytidine (AZA), a DNA methyltransferase inhibitor widely used in cancer treatment, further alluding to additional roles for the pathway, and OAS1 in particular, beyond innate immunity (93). Taken together, these observations suggest important roles for OAS1 in normal cellular processes that we have yet to fully elucidate. A critical element of determining such roles for OAS1 will be to fully define how OAS1 is regulated by dsRNA, including the contributions made by particular sequences and other molecular signatures that may be present in cellular or foreign dsRNAs.

OAS1 consensus sequences and activating motifs

OAS1 recognizes short dsRNAs (>18 bp) long enough to traverse its RNA-binding surface. Unlike other nucleic acid sensors, OAS1 does not possess a canonical RNA-binding motif or

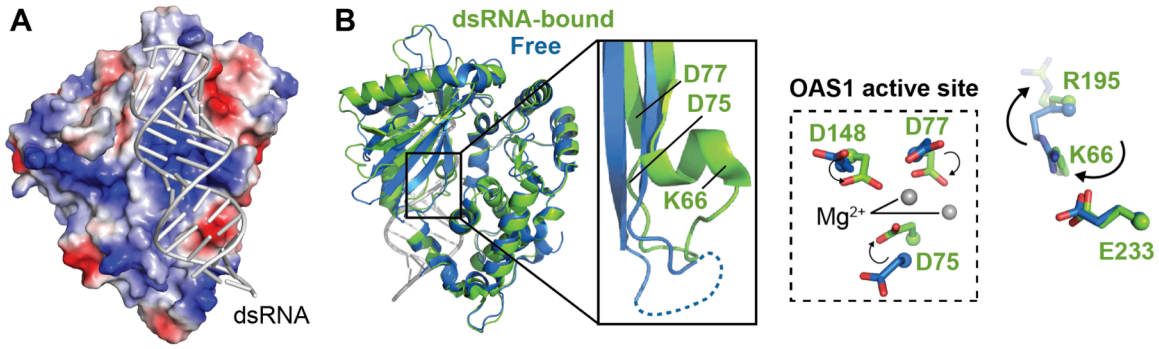

Figure 4. dsRNA binding induces conformational changes required for 2-5A synthesis by OAS1. ***A,*** OAS1 surface representation with electrostatic potential map showing the positive (*blue*) charge of the dsRNA binding surface. ***B,*** Overlay of free porcine OAS1 (PDB code 1PX5, *blue*) and dsRNA-bound human OAS1 (PDB code 4IG8, *green*). Binding dsRNA exchanges K66 and R195 (*right*) redirecting R195 from the protein core to the dsRNA binding surface which is coupled with the formation of a new alpha-helical structure (*solid box*). K66 replaces R195 in an electrostatic interaction with E233 (*right*) bringing residues D75, D77, and D148 into proximity promoting the formation of the catalytic triad and the coordination of two Mg^{2+} ions (*dashed box*).

domain (94); instead, OAS1 binds dsRNA via a relatively flat protein surface enriched with basic residues that contact the sugar-phosphate backbone at each end of the RNA helix (95) (**Figure 4A**). Upon dsRNA binding, OAS1 undergoes structural reorganization to narrow the ATP-binding cleft and reposition the catalytic residues to form the active site for 2-5A synthesis. Briefly, two basic residues (K66 and R195) swap positions to maintain an electrostatic interaction with E233, and these rearrangements direct R195 to the dsRNA binding surface driving formation of a new alpha helix thus organizing the OAS1 catalytic triad (D75, D77, and D148) and ATP donor/acceptor sites (**Figure 4B**). dsRNA binding is therefore required to allosterically induce the formation of the OAS1 active site containing the catalytic triad, two magnesium ions, and ATP (95,96) (*see* **Chapter 2** for more details). Because OAS1-dsRNA binding is predominantly driven by sequence-independent interactions (via phosphate and ribose groups), it was surprising when several studies identified consensus sequences and other activating motifs capable of potentiating OAS1 activation *in vitro* and in human cells, thus expanding OAS1 specificity beyond simple length requirements (97-100).

The first OAS1 activating consensus sequence was identified using systematic evolution of ligands by exponential enrichment (SELEX) to identify RNA aptamers able to bind OAS1 (97). Single-strand RNA aptamers, and in some cases corresponding dsRNAs, were tested for their ability to activate OAS1 *in vitro*. Sequence alignment was then used to reveal commonalities among the most potent activators. These OAS1 activators were found to have an overall high cytosine and low guanine content and contained the sequences APyAPy(N)nCC and UU(N)nACCC (where Py is C or U) within different regions of the RNA molecule (97). Although the resulting activating sequences are quite degenerate, these experiments were the first to lend insight into the possibility that OAS1 has some degree of sequence specificity. However, understanding the contribution of specific sequences was further complicated by the likelihood that single-stranded RNAs could form secondary structures or by the propensity of OAS1 to be activated by the flanking adapter sequences.

Another study tested a randomized panel of short (19 bp) dsRNAs with distinct sequences to probe for differences in their ability to activate OAS1 *in vitro* and in human A549 cells (98). Sequence alignment of the dsRNAs that most strongly promoted OAS1 activity identified a second, distinct activating consensus sequence, WWN_9WG (where W is A or U, and N is any nucleotide), which was then confirmed using a larger panel of dsRNA sequences. When mapped onto a dsRNA helix, the WW and WG consensus dinucleotide sequences were positioned in the two minor grooves spaced by the nine intervening base pairs and presented on the same face of the A-form helix for recognition by OAS1, as later confirmed in the OAS1-dsRNA crystal structure (95). Further, the G nucleotide of the WWN_9WG sequence makes one of the only base-specific interactions with OAS1, revealing part of the basis for the specificity of this novel activating consensus sequence.

Our lab's more recent findings using adenovirus VA RNA_I with altered 5'- and 3'-end sequences revealed that optimal OAS1 activation by this non-coding RNA required a 3'-end single-stranded pyrimidine-rich (C or U) sequence (99). In contrast, 3'-end single-stranded

purine-rich (G or A) sequences promoted a lower level of activation, while extension of the VA RNA_I terminal stem with an equivalent length of base paired nucleotides failed to enhance OAS1 activation. Deletion of the equivalent 3'-end sequences from two other RNA polymerase III non-coding transcripts, Epstein-Barr virus EBER-1 RNA and human cellular nc886 RNA, also exhibited reduced OAS1 activation. These observations thus led to the discovery of a novel RNA signature for OAS1 activation, the 3'-end single-stranded pyrimidine (3'-ssPy) motif (99). While the detailed mechanism of 3'-ssPy motif action remains to be determined, these studies identified one amino acid (Gly157) whose substitution with a bulkier residue did not impact overall OAS1 activity but fully eliminated sensitivity to the 3'-ssPy motif. Gly157 resides in a loop adjacent to the dsRNA binding surface suggesting that allosteric regulation of OAS1 by RNA may be more complex than previously determined.

Our group also discovered an activating structural element in the human cellular nc886 RNA with the ability to potentiate OAS1 activation. nc886 is a ubiquitously expressed cytosolic noncoding RNA that adopts two distinct structures which differ in their migration on native polyacrylamide gels: the slower migrating form ("Conformer 1") and the faster migrating form ("Conformer 2"). Studies of OAS1 activation by nc886 *in vitro* and in A549 cells revealed that most activity is conferred by a unique tertiary structural motif present only in the apical stem loop of nc886 Conformer 1 (100). Interestingly, this same Conformer 1 structural feature is critical for PKR inhibition by nc886 (101), suggesting the potential for cellular RNA-mediated communication between these two innate immune sensors. Analysis of nc886 with truncated terminal and central stem structures showed that the apical stem loop alone is not sufficient to activate OAS1. Rather, a predominantly base-paired region of the central stem, approximately 18 bp in length, is also required for OAS1 activation (100). These data suggest that the dsRNA region of the central stem is required for OAS1 binding and optimal positioning of the apical stem loop motif for OAS1 activation.

Structural studies have provided a clear rationale for the dsRNA length requirements needed for OAS1 (and other OAS family members) binding and catalysis. Despite these important advances, we still understand little about how other dsRNA features contribute to the extent of OAS1 activation. To date, four OAS1 activating motifs have been identified, but mechanistic insights on how these molecular signatures regulate OAS1 activity still remain unclear. However, one important consideration that has surfaced from this work is the idea that simply the presence or absence of a motif is not sufficient, but "accurate" placement within a dsRNA molecule can determine how much or how little a feature contributes to total activation. Thus, the context of these activating motifs is an additional variable to consider, which may become exceedingly more complicated in larger dsRNAs with the propensity to contain multiple and/or overlapping binding sites.

Research goals

The OAS/RNase L pathway is gaining new appreciation not just for its role in innate immunity but also for its growing prominence in regulating normal cell function. Although several crystal structures have been solved of OAS1 in complex with dsRNA, ATP analogs (dATP, ApCpp), or both (95,96), we still do not fully understand how dsRNA regulates the level of OAS activation or the mechanism(s) OAS1 employs to discriminate between viral and cellular RNA targets. Initially, the requirements for a good RNA activator were thought to include two main features: (i) a perfectly double-stranded RNA which also (ii) meets the specific length requirements (*e.g.* ranging from 18 bp for OAS1 to >50 bp for OAS3) to flank the dsRNA binding surface and activate the catalytic domain (95,102). However, recent work has revealed specific molecular signatures (*e.g.* nucleotide sequences and structural elements) able to enhance OAS1 activation *in vitro* and in human cells. These novel insights have allowed us to begin expanding our current understanding of dsRNA-mediated regulation of OAS1 to include additional considerations, such as the strong dependence on sequence for activation. Further research

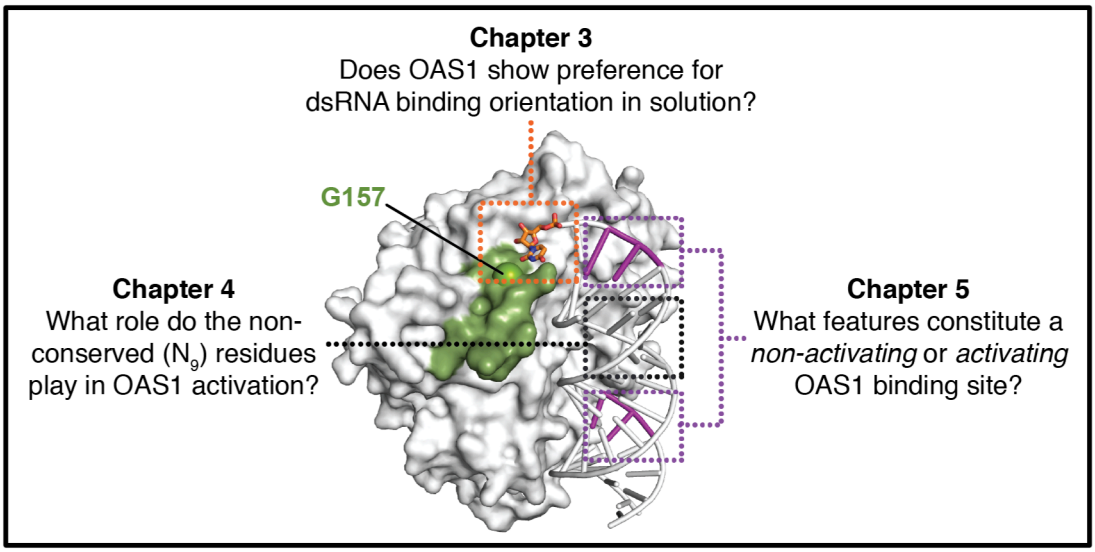

Figure 5. Overview of research objectives. OAS1 (*grey*) activation is regulated by dsRNA (*white*) and can be enhanced by the presence of unique molecular signatures, such as the 3'-ssPy motif (*orange box*) or WWN_9WG activation consensus sequence (*purple and black boxes*). These works are described in further detail in **Research goals** as well as their respective chapters.

needs to be done to identify and characterize additional sequence-specific determinants as well as identify the precise mechanism(s) that these dsRNA features exploit to enhance OAS1 activation.

Sequences have been identified that more strongly activate OAS1 (*e.g.* WWN_9WG consensus and 3'-ssPy motif), but none of these studies addressed the nature of these sequence preferences, the mechanisms that control OAS1 regulation by dsRNA containing these sequences, and how they affect the level of OAS1 activation *in vitro* or in human cells. We approached this work with the goal of elucidating the molecular signatures that define a sequence as activating or non-activating and the mechanism(s) OAS1 employs to discriminate between dsRNA molecules (or binding sites within a larger dsRNA) (**Figure 5**).

Chapter 3 describes a study that aimed to address whether OAS1 has a preference for binding directionality in solution as observed in a previously solved OAS1-dsRNA crystal structure (95) by using the 3'-ssPy motif as a tool for measuring dsRNA orientation. This study

not only demonstrated that OAS1 has preference for binding directionality within a simple 18 bp dsRNA in solution, but that features previously reported for an OAS1 consensus sequence needed to be followed up and possibly entirely redefined. Unexpectedly, the 3'-ssPy motif only potentiated activation of OAS1 when appended to the "top" strand of the 18 bp dsRNA. Additional mutations and modeling suggested that the 3'-ssPy cannot induce stronger OAS1 activation when appended on the "bottom" strand due to its inability to interact with the loop containing Gly157. This difference is the result of the additional nucleotide spacing in this orientation between the consensus guanine ($WWN_9W\underline{G}$) and the end of the dsRNA duplex where the 3'-ssPy is located. A series of "scramble" constructs were designed to test the influence of overall dsRNA sequence, which identified unexpected contributions originating from the non-conserved (N_9) residues of the OAS1 activation consensus sequence. These data suggest that sequence in this intervening region may play an important role in OAS1 activation by defining the dsRNA shape and flexibility upon protein binding and could potentially dictate how the conserved (WW/WG) nucleotides are sensed. These findings will allow us to begin redefining the criteria previously thought to be important for OAS1 regulation by dsRNA.

Chapter 4 further defines how the non-conserved (N_9) residues of the OAS1 activation consensus sequence dictate the extent of OAS1 activation. A-to-I editing is proposed to be one way the cell avoids inadvertent activation by cellular RNAs (54), so we hypothesized that inosine substitutions within the N_9 sequence of the 18 bp dsRNA would destabilize double-stranded regions resulting in weaker or no OAS1 activation. However, we find that inosine-containing dsRNAs in both a destabilized (I•U) and restored Watson-Crick (I-C) base pairings both resulted in enhanced OAS1 activation. Computational modeling using molecular dynamics (MD) simulations demonstrated that destabilization of the dsRNA with I•U and a second highly destabilizing mismatch base pair (A•C) increases global dynamics and helical bending. Surprisingly, restoration or increase in helical stability of the dsRNA with I-C and G-C base pairs also enhances OAS1 activation. Here, computational analyses suggest these changes promote

specific local helical features that may predispose these dsRNAs as better OAS1 activators. Together, these results led to the identification of a new role for the non-conserved (N_9) sequence defining dsRNA shape and flexibility important for OAS1 binding and recognition. More broadly, these findings show that OAS1 is able to tolerate mismatched base pairs, greatly expanding the number of potential OAS1 activating sequences in viral and cellular RNAs.

Chapter 5 sheds light on the role of the conserved (WW/WG) dinucleotides in the OAS1 activation consensus sequence. For this study, we used the same 18 bp model dsRNA containing two, antiparallel copies of the WWN_9WG consensus sequence. Mutating guanine (G) to adenine (A) in each of the two consensus sequences led to opposing activation profiles: one no longer activated OAS1 ("non-activating") while the other dramatically increased OAS1 activation ("hyper-activating"). Our model thus far is that, in the absence of mutations, OAS1 can sample both available binding sites for activation; however, mutation of the conserved guanine nucleotide(s) drives competition for binding between the productive and non-productive site. Here, we show another example of orientation-specific activation (*see* **Chapter 3**) in a dsRNA containing two "equivalent" consensus sequences.

Collectively, these studies shape our current understanding of how specific sequences in dsRNA, and their context, control regulation of OAS1. We have identified that the context in which the molecular signatures, WWN_9WG consensus and 3'-ssPy motif, are presented are just as important (if not more so) than the sequences themselves. Additionally, these data have allowed us to begin redefining the OAS1 activating consensus sequence as it appears more complicated than previously determined (*e.g.* WW/WG positioned into the two minor grooves of dsRNA). By determining the RNA features that create a preferred OAS1 binding site (activating or non-activating) and elucidating the mechanisms used to confer these activities greatly enhances our current understanding of host-pathogen interactions, such as how viruses could mask otherwise activating motifs to evade detection by the innate immune system.

References

1. Wu, J. and Chen, Z.J. (2014) Innate immune sensing and signaling of cytosolic nucleic acids. *Annu Rev Immunol*, **32**, 461-488.
2. Schlee, M. and Hartmann, G. (2016) Discriminating self from non-self in nucleic acid sensing. *Nat Rev Immunol*, **16**, 566-580.
3. Yoneyama, M., Kikuchi, M., Matsumoto, K., Imaizumi, T., Miyagishi, M., Taira, K., Foy, E., Loo, Y.M., Gale, M., Jr., Akira, S. *et al.* (2005) Shared and unique functions of the DExD/H-box helicases RIG-I, MDA5, and LGP2 in antiviral innate immunity. *J Immunol*, **175**, 2851-2858.
4. Peisley, A., Wu, B., Yao, H., Walz, T. and Hur, S. (2013) RIG-I forms signaling-competent filaments in an ATP-dependent, ubiquitin-independent manner. *Mol Cell*, **51**, 573-583.
5. Wu, B., Peisley, A., Richards, C., Yao, H., Zeng, X., Lin, C., Chu, F., Walz, T. and Hur, S. (2013) Structural basis for dsRNA recognition, filament formation, and antiviral signal activation by MDA5. *Cell*, **152**, 276-289.
6. Yoneyama, M., Kikuchi, M., Natsukawa, T., Shinobu, N., Imaizumi, T., Miyagishi, M., Taira, K., Akira, S. and Fujita, T. (2004) The RNA helicase RIG-I has an essential function in double-stranded RNA-induced innate antiviral responses. *Nat Immunol*, **5**, 730-737.
7. Seth, R.B., Sun, L., Ea, C.K. and Chen, Z.J. (2005) Identification and characterization of MAVS, a mitochondrial antiviral signaling protein that activates NF-kappaB and IRF 3. *Cell*, **122**, 669-682.
8. Besch, R., Poeck, H., Hohenauer, T., Senft, D., Hacker, G., Berking, C., Hornung, V., Endres, S., Ruzicka, T., Rothenfusser, S. *et al.* (2009) Proapoptotic signaling induced by RIG-I and MDA-5 results in type I interferon-independent apoptosis in human melanoma cells. *J Clin Invest*, **119**, 2399-2411.
9. El Maadidi, S., Faletti, L., Berg, B., Wenzl, C., Wieland, K., Chen, Z.J., Maurer, U. and Borner, C. (2014) A novel mitochondrial MAVS/Caspase-8 platform links RNA virus-induced innate antiviral signaling to Bax/Bak-independent apoptosis. *J Immunol*, **192**, 1171-1183.
10. Matsumiya, T. and Stafforini, D.M. (2010) Function and regulation of retinoic acid-inducible gene-I. *Crit Rev Immunol*, **30**, 489-513.
11. Loo, Y.M. and Gale, M., Jr. (2011) Immune signaling by RIG-I-like receptors. *Immunity*, **34**, 680-692.
12. Kato, H., Takeuchi, O., Mikamo-Satoh, E., Hirai, R., Kawai, T., Matsushita, K., Hiiragi, A., Dermody, T.S., Fujita, T. and Akira, S. (2008) Length-dependent recognition of double-stranded ribonucleic acids by retinoic acid-inducible gene-I and melanoma differentiation-associated gene 5. *J Exp Med*, **205**, 1601-1610.
13. Hornung, V., Ellegast, J., Kim, S., Brzozka, K., Jung, A., Kato, H., Poeck, H., Akira, S., Conzelmann, K.K., Schlee, M. *et al.* (2006) 5'-Triphosphate RNA is the ligand for RIG-I. *Science*, **314**, 994-997.
14. Pichlmair, A., Schulz, O., Tan, C.P., Naslund, T.I., Liljestrom, P., Weber, F. and Reis e Sousa, C. (2006) RIG-I-mediated antiviral responses to single-stranded RNA bearing 5'-phosphates. *Science*, **314**, 997-1001.

15. Schmidt, A., Schwerd, T., Hamm, W., Hellmuth, J.C., Cui, S., Wenzel, M., Hoffmann, F.S., Michallet, M.C., Besch, R., Hopfner, K.P. *et al.* (2009) 5'-triphosphate RNA requires base-paired structures to activate antiviral signaling via RIG-I. *Proc Natl Acad Sci U S A*, **106**, 12067-12072.

16. Kowalinski, E., Lunardi, T., McCarthy, A.A., Louber, J., Brunel, J., Grigorov, B., Gerlier, D. and Cusack, S. (2011) Structural basis for the activation of innate immune pattern-recognition receptor RIG-I by viral RNA. *Cell*, **147**, 423-435.

17. Zust, R., Cervantes-Barragan, L., Habjan, M., Maier, R., Neuman, B.W., Ziebuhr, J., Szretter, K.J., Baker, S.C., Barchet, W., Diamond, M.S. *et al.* (2011) Ribose 2'-O-methylation provides a molecular signature for the distinction of self and non-self mRNA dependent on the RNA sensor Mda5. *Nat Immunol*, **12**, 137-143.

18. Schuberth-Wagner, C., Ludwig, J., Bruder, A.K., Herzner, A.M., Zillinger, T., Goldeck, M., Schmidt, T., Schmid-Burgk, J.L., Kerber, R., Wolter, S. *et al.* (2015) A Conserved Histidine in the RNA Sensor RIG-I Controls Immune Tolerance to N1-2'O-Methylated Self RNA. *Immunity*, **43**, 41-51.

19. Devarkar, S.C., Wang, C., Miller, M.T., Ramanathan, A., Jiang, F., Khan, A.G., Patel, S.S. and Marcotrigiano, J. (2016) Structural basis for m7G recognition and 2'-O-methyl discrimination in capped RNAs by the innate immune receptor RIG-I. *Proc Natl Acad Sci U S A*, **113**, 596-601.

20. Yao, H., Dittmann, M., Peisley, A., Hoffmann, H.H., Gilmore, R.H., Schmidt, T., Schmidt-Burgk, J., Hornung, V., Rice, C.M. and Hur, S. (2015) ATP-dependent effector-like functions of RIG-I-like receptors. *Mol Cell*, **58**, 541-548.

21. Kerr, I.M., Brown, R.E. and Hovanessian, A.G. (1977) Nature of inhibitor of cell-free protein synthesis formed in response to interferon and double-stranded RNA. *Nature*, **268**, 540-542.

22. Justesen, J., Ferbus, D. and Thang, M.N. (1980) Elongation mechanism and substrate specificity of 2',5'-oligoadenylate synthetase. *Proc Natl Acad Sci U S A*, **77**, 4618-4622.

23. Hovanessian, A.G. and Justesen, J. (2007) The human 2'-5'-oligoadenylate synthetase family: Unique interferon-inducible enzymes catalyzing 2'-5' instead of 3'-5' phosphodiester bond formation. *Biochimie*, **89**, 779-788.

24. Dong, B., Xu, L., Zhou, A., Hassel, B.A., Lee, X., Torrence, P.F. and Silverman, R.H. (1994) Intrinsic molecular activities of the interferon-induced 2-5A-dependent RNase. *J Biol Chem*, **269**, 14153-14158.

25. Han, Y., Whitney, G., Donovan, J. and Korennykh, A. (2012) Innate immune messenger 2-5A tethers human RNase L into active high-order complexes. *Cell Rep*, **2**, 902-913.

26. Huang, H., Zeqiraj, E., Dong, B., Jha, B.K., Duffy, N.M., Orlicky, S., Thevakumaran, N., Talukdar, M., Pillon, M.C., Ceccarelli, D.F. *et al.* (2014) Dimeric structure of pseudokinase RNase L bound to 2-5A reveals a basis for interferon-induced antiviral activity. *Mol Cell*, **53**, 221-234.

27. Wreschner, D.H., James, T.C., Silverman, R.H. and Kerr, I.M. (1981) Ribosomal RNA cleavage, nuclease activation and 2-5A(ppp(A2'p)nA) in interferon-treated cells. *Nucleic Acids Res*, **9**, 1571-1581.

28. Donovan, J., Rath, S., Kolet-Mandrikov, D. and Korennykh, A. (2017) Rapid RNase L-driven arrest of protein synthesis in the dsRNA response without degradation of translation machinery. *RNA*, **23**, 1660-1671.

29. Chitrakar, A., Rath, S., Donovan, J., Demarest, K., Li, Y., Sridhar, R.R., Weiss, S.R., Kotenko, S.V., Wingreen, N.S. and Korennykh, A. (2019) Real-time 2-5A kinetics suggest that interferons beta and lambda evade global arrest of translation by RNase L. *Proc Natl Acad Sci U S A*, **116**, 2103-2111.

30. Al-Ahmadi, W., Al-Haj, L., Al-Mohanna, F.A., Silverman, R.H. and Khabar, K.S. (2009) RNase L downmodulation of the RNA-binding protein, HuR, and cellular growth. *Oncogene*, **28**, 1782-1791.

31. Fabre, O., Salehzada, T., Lambert, K., Boo Seok, Y., Zhou, A., Mercier, J. and Bisbal, C. (2012) RNase L controls terminal adipocyte differentiation, lipids storage and insulin sensitivity via CHOP10 mRNA regulation. *Cell Death Differ*, **19**, 1470-1481.

32. Brennan-Laun, S.E., Li, X.L., Ezelle, H.J., Venkataraman, T., Blackshear, P.J., Wilson, G.M. and Hassel, B.A. (2014) RNase L attenuates mitogen-stimulated gene expression via transcriptional and post-transcriptional mechanisms to limit the proliferative response. *J Biol Chem*, **289**, 33629-33643.

33. Banerjee, S., Li, G., Li, Y., Gaughan, C., Baskar, D., Parker, Y., Lindner, D.J., Weiss, S.R. and Silverman, R.H. (2015) RNase L is a negative regulator of cell migration. *Oncotarget*, **6**, 44360-44372.

34. Rath, S., Donovan, J., Whitney, G., Chitrakar, A., Wang, W. and Korennykh, A. (2015) Human RNase L tunes gene expression by selectively destabilizing the microRNA-regulated transcriptome. *Proc Natl Acad Sci U S A*, **112**, 15916-15921.

35. Wreschner, D.H., McCauley, J.W., Skehel, J.J. and Kerr, I.M. (1981) Interferon action--sequence specificity of the ppp(A2'p)nA-dependent ribonuclease. *Nature*, **289**, 414-417.

36. Malathi, K., Dong, B., Gale, M., Jr. and Silverman, R.H. (2007) Small self-RNA generated by RNase L amplifies antiviral innate immunity. *Nature*, **448**, 816-819.

37. Malathi, K., Saito, T., Crochet, N., Barton, D.J., Gale, M., Jr. and Silverman, R.H. (2010) RNase L releases a small RNA from HCV RNA that refolds into a potent PAMP. *RNA*, **16**, 2108-2119.

38. Garcia, M.A., Gil, J., Ventoso, I., Guerra, S., Domingo, E., Rivas, C. and Esteban, M. (2006) Impact of protein kinase PKR in cell biology: from antiviral to antiproliferative action. *Microbiol Mol Biol Rev*, **70**, 1032-1060.

39. Manche, L., Green, S.R., Schmedt, C. and Mathews, M.B. (1992) Interactions between double-stranded RNA regulators and the protein kinase DAI. *Mol Cell Biol*, **12**, 5238-5248.

40. Dar, A.C., Dever, T.E. and Sicheri, F. (2005) Higher-order substrate recognition of eIF2alpha by the RNA-dependent protein kinase PKR. *Cell*, **122**, 887-900.

41. Dey, M., Cao, C., Dar, A.C., Tamura, T., Ozato, K., Sicheri, F. and Dever, T.E. (2005) Mechanistic link between PKR dimerization, autophosphorylation, and eIF2alpha substrate recognition. *Cell*, **122**, 901-913.

42. Rowlands, A.G., Panniers, R. and Henshaw, E.C. (1988) The catalytic mechanism of guanine nucleotide exchange factor action and competitive inhibition by phosphorylated eukaryotic initiation factor 2. *J Biol Chem*, **263**, 5526-5533.

43. Sudhakar, A., Ramachandran, A., Ghosh, S., Hasnain, S.E., Kaufman, R.J. and Ramaiah, K.V. (2000) Phosphorylation of serine 51 in initiation factor 2 alpha (eIF2 alpha) promotes complex formation between eIF2 alpha(P) and eIF2B and causes

inhibition in the guanine nucleotide exchange activity of eIF2B. *Biochemistry*, **39**, 12929-12938.

44. Krishnamoorthy, T., Pavitt, G.D., Zhang, F., Dever, T.E. and Hinnebusch, A.G. (2001) Tight binding of the phosphorylated alpha subunit of initiation factor 2 (eIF2alpha) to the regulatory subunits of guanine nucleotide exchange factor eIF2B is required for inhibition of translation initiation. *Mol Cell Biol*, **21**, 5018-5030.

45. Bevilacqua, P.C. and Cech, T.R. (1996) Minor-groove recognition of double-stranded RNA by the double-stranded RNA-binding domain from the RNA-activated protein kinase PKR. *Biochemistry*, **35**, 9983-9994.

46. Nanduri, S., Carpick, B.W., Yang, Y., Williams, B.R. and Qin, J. (1998) Structure of the double-stranded RNA-binding domain of the protein kinase PKR reveals the molecular basis of its dsRNA-mediated activation. *EMBO J*, **17**, 5458-5465.

47. Bevilacqua, P.C., George, C.X., Samuel, C.E. and Cech, T.R. (1998) Binding of the protein kinase PKR to RNAs with secondary structure defects: role of the tandem A-G mismatch and noncontiguous helixes. *Biochemistry*, **37**, 6303-6316.

48. Nallagatla, S.R., Hwang, J., Toroney, R., Zheng, X., Cameron, C.E. and Bevilacqua, P.C. (2007) 5'-triphosphate-dependent activation of PKR by RNAs with short stem-loops. *Science*, **318**, 1455-1458.

49. Schulz, O., Pichlmair, A., Rehwinkel, J., Rogers, N.C., Scheuner, D., Kato, H., Takeuchi, O., Akira, S., Kaufman, R.J. and Reis e Sousa, C. (2010) Protein kinase R contributes to immunity against specific viruses by regulating interferon mRNA integrity. *Cell Host Microbe*, **7**, 354-361.

50. Bass, B.L. and Weintraub, H. (1988) An unwinding activity that covalently modifies its double-stranded RNA substrate. *Cell*, **55**, 1089-1098.

51. Wagner, R.W., Smith, J.E., Cooperman, B.S. and Nishikura, K. (1989) A double-stranded RNA unwinding activity introduces structural alterations by means of adenosine to inosine conversions in mammalian cells and Xenopus eggs. *Proc Natl Acad Sci U S A*, **86**, 2647-2651.

52. George, C.X., John, L. and Samuel, C.E. (2014) An RNA editor, adenosine deaminase acting on double-stranded RNA (ADAR1). *J Interferon Cytokine Res*, **34**, 437-446.

53. Samuel, C.E. (2011) Adenosine deaminases acting on RNA (ADARs) are both antiviral and proviral. *Virology*, **411**, 180-193.

54. Li, Y., Banerjee, S., Goldstein, S.A., Dong, B., Gaughan, C., Rath, S., Donovan, J., Korennykh, A., Silverman, R.H. and Weiss, S.R. (2017) Ribonuclease L mediates the cell-lethal phenotype of double-stranded RNA editing enzyme ADAR1 deficiency in a human cell line. *Elife*, **6**, e25687.

55. Taguchi, T., Nagano-Fujii, M., Akutsu, M., Kadoya, H., Ohgimoto, S., Ishido, S. and Hotta, H. (2004) Hepatitis C virus NS5A protein interacts with 2',5'-oligoadenylate synthetase and inhibits antiviral activity of IFN in an IFN sensitivity-determining region-independent manner. *J Gen Virol*, **85**, 959-969.

56. Cardenas, W.B., Loo, Y.M., Gale, M., Jr., Hartman, A.L., Kimberlin, C.R., Martinez-Sobrido, L., Saphire, E.O. and Basler, C.F. (2006) Ebola virus VP35 protein binds double-stranded RNA and inhibits alpha/beta interferon production induced by RIG-I signaling. *J Virol*, **80**, 5168-5178.

57. Hartman, A.L., Ling, L., Nichol, S.T. and Hibberd, M.L. (2008) Whole-genome expression profiling reveals that inhibition of host innate immune response pathways by Ebola virus can be reversed by a single amino acid change in the VP35 protein. *J Virol*, **82**, 5348-5358.

58. Sanchez, R. and Mohr, I. (2007) Inhibition of cellular 2'-5' oligoadenylate synthetase by the herpes simplex virus type 1 Us11 protein. *J Virol*, **81**, 3455-3464.

59. Schroder, H.C., Ugarkovic, D., Wenger, R., Reuter, P., Okamoto, T. and Muller, W.E. (1990) Binding of Tat protein to TAR region of human immunodeficiency virus type 1 blocks TAR-mediated activation of (2'-5')oligoadenylate synthetase. *AIDS Res Hum Retroviruses*, **6**, 659-672.

60. Min, J.Y. and Krug, R.M. (2006) The primary function of RNA binding by the influenza A virus NS1 protein in infected cells: Inhibiting the 2'-5' oligo (A) synthetase/RNase L pathway. *Proc Natl Acad Sci U S A*, **103**, 7100-7105.

61. Imani, F. and Jacobs, B.L. (1988) Inhibitory activity for the interferon-induced protein kinase is associated with the reovirus serotype 1 sigma 3 protein. *Proc Natl Acad Sci U S A*, **85**, 7887-7891.

62. Denzler, K.L. and Jacobs, B.L. (1994) Site-directed mutagenic analysis of reovirus sigma 3 protein binding to dsRNA. *Virology*, **204**, 190-199.

63. Beattie, E., Denzler, K.L., Tartaglia, J., Perkus, M.E., Paoletti, E. and Jacobs, B.L. (1995) Reversal of the interferon-sensitive phenotype of a vaccinia virus lacking E3L by expression of the reovirus S4 gene. *J Virol*, **69**, 499-505.

64. Xiang, Y., Condit, R.C., Vijaysri, S., Jacobs, B., Williams, B.R. and Silverman, R.H. (2002) Blockade of interferon induction and action by the E3L double-stranded RNA binding proteins of vaccinia virus. *J Virol*, **76**, 5251-5259.

65. Dauber, B., Saffran, H.A. and Smiley, J.R. (2019) The herpes simplex virus host shutoff (vhs) RNase limits accumulation of double stranded RNA in infected cells: Evidence for accelerated decay of duplex RNA. *PLoS Pathog*, **15**, e1008111.

66. Liu, S.W., Katsafanas, G.C., Liu, R., Wyatt, L.S. and Moss, B. (2015) Poxvirus decapping enzymes enhance virulence by preventing the accumulation of dsRNA and the induction of innate antiviral responses. *Cell Host Microbe*, **17**, 320-331.

67. Burgess, H.M. and Mohr, I. (2015) Cellular 5'-3' mRNA exonuclease Xrn1 controls double-stranded RNA accumulation and anti-viral responses. *Cell Host Microbe*, **17**, 332-344.

68. Silverman, R.H. and Weiss, S.R. (2014) Viral Phosphodiesterases That Antagonize Double-Stranded RNA Signaling to RNase L by Degrading 2-5A. *J Interferon Cytokine Res*, **34**, 455-463.

69. Zhao, L., Jha, B.K., Wu, A., Elliott, R., Ziebuhr, J., Gorbalenya, A.E., Silverman, R.H. and Weiss, S.R. (2012) Antagonism of the interferon-induced OAS-RNase L pathway by murine coronavirus ns2 protein is required for virus replication and liver pathology. *Cell Host Microbe*, **11**, 607-616.

70. Zhang, R., Jha, B.K., Ogden, K.M., Dong, B., Zhao, L., Elliott, R., Patton, J.T., Silverman, R.H. and Weiss, S.R. (2013) Homologous 2',5'-phosphodiesterases from disparate RNA viruses antagonize antiviral innate immunity. *Proc Natl Acad Sci U S A*, **110**, 13114-13119.

71. Ogden, K.M., Hu, L., Jha, B.K., Sankaran, B., Weiss, S.R., Silverman, R.H., Patton, J.T. and Prasad, B.V. (2015) Structural basis for 2'-5'-oligoadenylate binding and enzyme activity of a viral RNase L antagonist. *J Virol*, **89**, 6633-6645.

72. Cayley, P.J., Davies, J.A., McCullagh, K.G. and Kerr, I.M. (1984) Activation of the ppp(A2'p)nA system in interferon-treated, herpes simplex virus-infected cells and evidence for novel inhibitors of the ppp(A2'p)nA-dependent RNase. *Eur J Biochem*, **143**, 165-174.

73. Rice, A.P., Roberts, W.K. and Kerr, I.M. (1984) 2-5A accumulates to high levels in interferon-treated, vaccinia virus-infected cells in the absence of any inhibition of virus replication. *J Virol*, **50**, 220-228.

74. Rice, A.P., Kerr, S.M., Roberts, W.K., Brown, R.E. and Kerr, I.M. (1985) Novel 2',5'-oligoadenylates synthesized in interferon-treated, vaccinia virus-infected cells. *J Virol*, **56**, 1041-1044.

75. Bisbal, C., Martinand, C., Silhol, M., Lebleu, B. and Salehzada, T. (1995) Cloning and characterization of a RNAse L inhibitor. A new component of the interferon-regulated 2-5A pathway. *J Biol Chem*, **270**, 13308-13317.

76. Martinand, C., Salehzada, T., Silhol, M., Lebleu, B. and Bisbal, C. (1998) RNase L inhibitor (RLI) antisense constructions block partially the down regulation of the 2-5A/RNase L pathway in encephalomyocarditis-virus-(EMCV)-infected cells. *Eur J Biochem*, **254**, 248-255.

77. Martinand, C., Montavon, C., Salehzada, T., Silhol, M., Lebleu, B. and Bisbal, C. (1999) RNase L inhibitor is induced during human immunodeficiency virus type 1 infection and down regulates the 2-5A/RNase L pathway in human T cells. *J Virol*, **73**, 290-296.

78. Han, J.Q. and Barton, D.J. (2002) Activation and evasion of the antiviral 2'-5' oligoadenylate synthetase/ribonuclease L pathway by hepatitis C virus mRNA. *RNA*, **8**, 512-525.

79. Han, J.Q., Wroblewski, G., Xu, Z., Silverman, R.H. and Barton, D.J. (2004) Sensitivity of hepatitis C virus RNA to the antiviral enzyme ribonuclease L is determined by a subset of efficient cleavage sites. *J Interferon Cytokine Res*, **24**, 664-676.

80. Washenberger, C.L., Han, J.Q., Kechris, K.J., Jha, B.K., Silverman, R.H. and Barton, D.J. (2007) Hepatitis C virus RNA: dinucleotide frequencies and cleavage by RNase L. *Virus Res*, **130**, 85-95.

81. Han, J.Q., Townsend, H.L., Jha, B.K., Paranjape, J.M., Silverman, R.H. and Barton, D.J. (2007) A phylogenetically conserved RNA structure in the poliovirus open reading frame inhibits the antiviral endoribonuclease RNase L. *J Virol*, **81**, 5561-5572.

82. Cho, K., Yamada, M., Agematsu, K., Kanegane, H., Miyake, N., Ueki, M., Akimoto, T., Kobayashi, N., Ikemoto, S., Tanino, M. *et al.* (2018) Heterozygous Mutations in OAS1 Cause Infantile-Onset Pulmonary Alveolar Proteinosis with Hypogammaglobulinemia. *Am J Hum Genet*, **102**, 480-486.

83. Yakub, I., Lillibridge, K.M., Moran, A., Gonzalez, O.Y., Belmont, J., Gibbs, R.A. and Tweardy, D.J. (2005) Single nucleotide polymorphisms in genes for 2'-5'-oligoadenylate synthetase and RNase L inpatients hospitalized with West Nile virus infection. *J Infect Dis*, **192**, 1741-1748.

84. Lim, J.K., Lisco, A., McDermott, D.H., Huynh, L., Ward, J.M., Johnson, B., Johnson, H., Pape, J., Foster, G.A., Krysztof, D. *et al.* (2009) Genetic variation in OAS1 is a risk factor for initial infection with West Nile virus in man. *PLoS Pathog*, **5**, e1000321.

85. Field, L.L., Bonnevie-Nielsen, V., Pociot, F., Lu, S., Nielsen, T.B. and Beck-Nielsen, H. (2005) OAS1 splice site polymorphism controlling antiviral enzyme activity influences susceptibility to type 1 diabetes. *Diabetes*, **54**, 1588-1591.

86. Fedetz, M., Matesanz, F., Caro-Maldonado, A., Fernandez, O., Tamayo, J.A., Guerrero, M., Delgado, C., Lopez-Guerrero, J.A. and Alcina, A. (2006) OAS1 gene haplotype confers susceptibility to multiple sclerosis. *Tissue Antigens*, **68**, 446-449.

87. O'Brien, M., Lonergan, R., Costelloe, L., O'Rourke, K., Fletcher, J.M., Kinsella, K., Sweeney, C., Antonelli, G., Mills, K.H., O'Farrelly, C. *et al.* (2010) OAS1: a multiple sclerosis susceptibility gene that influences disease severity. *Neurology*, **75**, 411-418.

88. Mandal, S., Abebe, F. and Chaudhary, J. (2011) 2'-5' oligoadenylate synthetase 1 polymorphism is associated with prostate cancer. *Cancer*, **117**, 5509-5518.

89. Li, H., Reksten, T.R., Ice, J.A., Kelly, J.A., Adrianto, I., Rasmussen, A., Wang, S., He, B., Grundahl, K.M., Glenn, S.B. *et al.* (2017) Identification of a Sjogren's syndrome susceptibility locus at OAS1 that influences isoform switching, protein expression, and responsiveness to type I interferons. *PLoS Genet*, **13**, e1006820.

90. Liu, X., Xing, H., Gao, W., Yu, D., Zhao, Y., Shi, X., Zhang, K., Li, P., Yu, J., Xu, W. *et al.* (2017) A functional variant in the OAS1 gene is associated with Sjogren's syndrome complicated with HBV infection. *Sci Rep*, **7**, 17571.

91. Wu, S., Wang, Y., Chen, G., Zhang, M., Wang, M. and He, J.Q. (2018) 2'-5'-Oligoadenylate synthetase 1 polymorphisms are associated with tuberculosis: a case-control study. *BMC Pulm Med*, **18**, 180.

92. Kondratova, A.A., Cheon, H., Dong, B., Holvey-Bates, E.G., Hasipek, M., Taran, I., Gaughan, C., Jha, B.K., Silverman, R.H. and Stark, G.R. (2020) Suppressing PARylation by 2',5'-oligoadenylate synthetase 1 inhibits DNA damage-induced cell death. *EMBO J*, **39**, e101573.

93. Banerjee, S., Gusho, E., Gaughan, C., Dong, B., Gu, X., Holvey-Bates, E., Talukdar, M., Li, Y., Weiss, S.R., Sicheri, F. *et al.* (2019) OAS-RNase L innate immune pathway mediates the cytotoxicity of a DNA-demethylating drug. *Proc Natl Acad Sci U S A*, **116**, 5071-5076.

94. Hartmann, R., Justesen, J., Sarkar, S.N., Sen, G.C. and Yee, V.C. (2003) Crystal structure of the 2'-specific and double-stranded RNA-activated interferon-induced antiviral protein 2'-5'-oligoadenylate synthetase. *Mol Cell*, **12**, 1173-1185.

95. Donovan, J., Dufner, M. and Korennykh, A. (2013) Structural basis for cytosolic double-stranded RNA surveillance by human oligoadenylate synthetase 1. *Proc Natl Acad Sci U S A*, **110**, 1652-1657.

96. Lohofener, J., Steinke, N., Kay-Fedorov, P., Baruch, P., Nikulin, A., Tishchenko, S., Manstein, D.J. and Fedorov, R. (2015) The Activation Mechanism of 2'-5'-Oligoadenylate Synthetase Gives New Insights Into OAS/cGAS Triggers of Innate Immunity. *Structure*, **23**, 851-862.

97. Hartmann, R., Norby, P.L., Martensen, P.M., Jorgensen, P., James, M.C., Jacobsen, C., Moestrup, S.K., Clemens, M.J. and Justesen, J. (1998) Activation of 2'-5' oligoadenylate

synthetase by single-stranded and double-stranded RNA aptamers. *J Biol Chem*, **273**, 3236-3246.

98. Kodym, R., Kodym, E. and Story, M.D. (2009) 2'-5'-Oligoadenylate synthetase is activated by a specific RNA sequence motif. *Biochem Biophys Res Commun*, **388**, 317-322.

99. Vachon, V.K., Calderon, B.M. and Conn, G.L. (2015) A novel RNA molecular signature for activation of 2'-5' oligoadenylate synthetase-1. *Nucleic Acids Res*, **43**, 544-552.

100. Calderon, B.M. and Conn, G.L. (2018) A human cellular noncoding RNA activates the antiviral protein 2'-5'-oligoadenylate synthetase 1. *J Biol Chem*, **293**, 16115-16124.

101. Calderon, B.M. and Conn, G.L. (2017) Human noncoding RNA 886 (nc886) adopts two structurally distinct conformers that are functionally opposing regulators of PKR. *RNA*, **23**, 557-566.

102. Donovan, J., Whitney, G., Rath, S. and Korennykh, A. (2015) Structural mechanism of sensing long dsRNA via a noncatalytic domain in human oligoadenylate synthetase 3. *Proc Natl Acad Sci U S A*, **112**, 3949-3954.

CHAPTER TWO

RNA regulation of the antiviral protein 2'-5'-oligoadenylate synthetase

Samantha L. Schwartz and Graeme L. Conn

The following chapter has been published:

Schwartz, S.L. and Conn, G.L. (2019). RNA regulation of the antiviral protein 2'-5'-oligoadenylate synthetase. *Wiley Interdiscip Rev RNA*, e1534 (PMID: 30989826).

Author Contributions: S.L.S. wrote the original draft. S.L.S. and G.L.C. reviewed, edited, and approved the final version.

ABSTRACT

The innate immune system is a broad collection of critical intra- and extracellular processes that limit the infectivity of diverse pathogens. The 2'-5'-oligoadenylate synthetase (OAS) family of enzymes are important sensors of cytosolic double-stranded RNA (dsRNA) that play a critical role in limiting viral infection by activating the latent ribonuclease L (RNase L) to halt viral replication and establish an antiviral state. Attesting to the importance of the OAS/RNase L pathway, diverse viruses have developed numerous distinct strategies to evade the effects of OAS activation. How OAS proteins are regulated by viral or cellular RNAs is not fully understood but several recent studies have provided important new insights into the molecular mechanisms of OAS activation by dsRNA. Other studies have revealed unanticipated features of RNA sequence and structure that strongly enhance activation of at least one OAS family member. While these discoveries represent important advances, they also underscore the fact that much remains to be learned about RNA-mediated regulation of the OAS/RNase L pathway. In particular, defining the full complement of RNA molecular signatures that activate OAS is essential to our understanding of how these proteins maximize their protective role against pathogens while still accurately discriminating host molecules to avoid inadvertent activation by cellular RNAs. A more complete knowledge of OAS regulation may also serve as a foundation for the development of novel antiviral therapeutic strategies and lead the way to a deeper understanding of currently unappreciated cellular functions of the OAS/RNase L pathway in the absence of infection.

Graphical/Visual Abstract and Caption

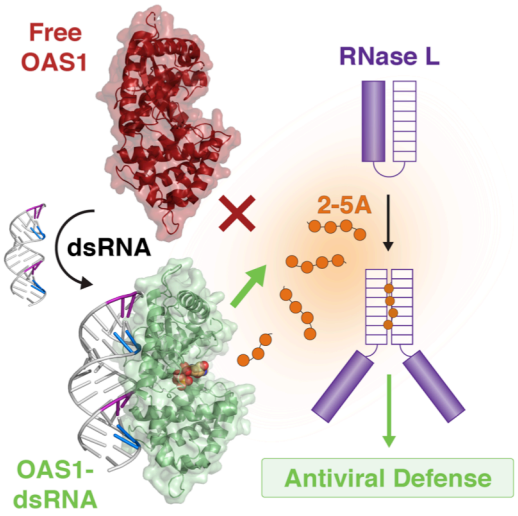

Caption: The 2'-5'-oligoadenylate synthetase/ ribonuclease L (OAS/RNase L) pathway is a critical component of human innate immunity: double-stranded RNA (dsRNA) binding to OAS drives activation of 2'-5'-oligoadenylate (2-5A) synthesis to trigger the antiviral properties of RNase L.

INTRODUCTION

The human innate immune system comprises a large collection of cellular and molecular defenses that provide a critical front line of protection against microbial infection (see Sidebar: *The innate immune system*). Molecular innate immune sensors, such as the 2'-5'-oligoadenylate synthetase (OAS) family of enzymes, may be present at basal levels in some cells and their expression is strongly upregulated by interferon. As such, they are referred to as interferon-stimulated genes (ISGs) (1). OAS enzymes are sensors of cytosolic double-stranded RNA (dsRNA), a potent indicator of viral infection (2,3). dsRNA binding to OAS promotes synthesis of unique 2'-5'-linked oligoadenylate (2-5A) molecules that act as a secondary messenger to activate their only known downstream target: the latent ribonuclease (RNase L) (4). RNase L is ubiquitously expressed and present in an inactive monomeric form in the cytoplasm; binding of 2-5A (≥3 nucleotides in length) drives RNase L dimerization and thus activation of its ribonuclease activity (**Figure 1A**) (5-7). RNA degradation by RNase L establishes an antiviral

state in several ways including direct cleavage of viral protein-encoding RNAs, degradation of cellular rRNA and tRNA which halts general translation while allowing expression of innate immune system proteins, and destabilization of the cellular transcriptome through cleavage of several specific mRNAs to suppress proliferation and adhesion (8-13). The OAS/RNase L pathway thus effectively halts viral replication and prevents viral spread to neighboring cells.

Sidebar: THE INNATE IMMUNE SYSTEM

The cells in our body must identify foreign (non-self) molecules to detect and respond to infection. Beyond initial physical barriers, a front line of cellular and molecular defenses with broad specificity is provided by the innate immune system. This system directly protects against microbial replication, acts to warn neighboring cells, and primes the other (adaptive) arm of the immune system to respond to infection. A critical feature of innate immune proteins is that they must accurately identify molecular features of foreign molecules – referred to as pathogen-associated molecular patterns (PAMPs) – in order to rapidly respond to the threat of infection while avoiding unwanted self-activation (14,15). The cellular proteins responsible for detecting PAMPs are known as pattern recognition receptors (PRRs). Double-stranded ribonucleic acid (dsRNA) is not normally present in uninfected cells but is present in some viral genomes or produced as a consequence of viral gene expression or replication. dsRNA is therefore an important and potent PAMP, detected by multiple cellular PRRs, and a strong signal for activation of the innate immune system (16). In addition to the OAS proteins, other RNA sensing PRRs limit infection by amplifying signaling cascades for interferon expression or by serving as direct effectors in their respective viral defense pathways (17-19). Additionally, cellular processes are in place to avoid aberrant activation of PRRs by host RNAs (e.g. via RNA modification or editing). A recent study, for example, provided evidence that activation of the OAS/RNase L pathway by host dsRNA is controlled by the action of double-stranded RNA-specific adenosine deaminase 1 (ADAR1) (20). As a result of these host defense systems, viruses have evolved diverse countermeasures to either mask their RNAs or to limit (or exploit) the effectiveness of specific PRRs and thus evade detection.

The OAS proteins are members of an ancient class of template-independent RNA polymerases that also includes 3'-end specific polyadenosine polymerase (PAP) and tRNA CCA adding enzyme (CCA). OASs are thought to have diverged from these other RNA polymerases early in metazoan evolution (21). All three RNA polymerases are also members of the wider nucleotidyl transferase superfamily which includes another innate immune sensor (of cytosolic

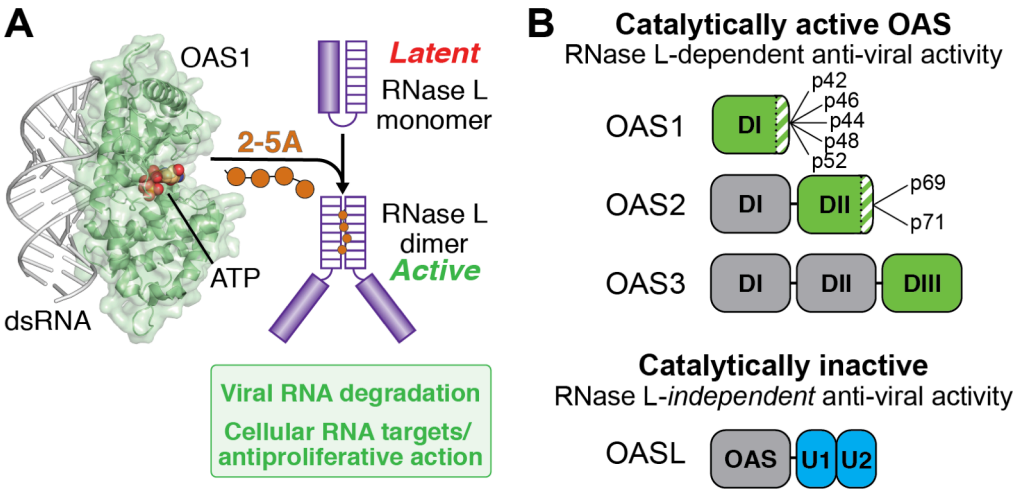

Figure 1. Overview of the OAS/RNase L pathway. ***A.*** dsRNA binding to OAS (here shown as OAS1) promotes synthesis of 2'-5'-linked oligoadenylates (2-5A) which in turn induce dimerization and activation of the latent ribonuclease (RNase L). RNase L degrades viral and cellular RNA targets to promote antiviral responses. ***B.*** Summary of domain organization and activities of the four human OAS proteins: OAS1, OAS2, OAS3, and OASL. For the active OAS proteins (OAS1, OAS2, and OAS3), the domain responsible for 2-5A catalysis is shown in green; other OAS domains (grey) contribute to dsRNA binding. Splicing isoforms are indicated for OAS1 and OAS2 (OAS3 is expressed as a single isoform); these proteins differ in their C-terminus (green/ white striped region). Human OASL contains a single non-catalytically active OAS domain appended with tandem ubiquitin-like domains (U1/U2; blue) and functions in antiviral innate immunity independent of RNase L.

DNA), cyclic GMP-AMP synthase (cGAS) (22,23). However, OAS is distinct from these structurally related proteins in several important ways. First, unlike PAP and CCA, OAS proteins do not require an RNA primer to initiate synthesis of polynucleotide chains from ATP. Second, OAS produces linear chains of unique 2'-5'-linked oligoadenylates, compared to the canonical 3'-5' linkages synthesized by PAP and CCA, and the combination of 2'-5' and 3'-5' linkages that form the cyclic dinucleotide product of cGAS. Third, the OAS proteins are distinct from PAP and CCA in their absolute requirement for dsRNA as an allosteric activator of their activity. As described further below, dsRNA binding to OAS results in unique structural rearrangements necessary to form the enzyme active site and promote synthesis of 2-5A (24). This requirement appears to be a relatively recent evolutionary adaptation driven specifically by OAS's role as an

innate immune sensor in higher organisms (25-27). In terms of its properties as an RNA-binding protein, OAS also appears quite distinct: it does not contain a canonical dsRNA-binding domain or other RNA recognition motif but instead recognizes dsRNA through a patch of positively charged amino acids located on the protein's surface. Notably, this dsRNA binding surface is absent in OAS proteins in lower organisms that lack interferon signaling (26,27). This mode of dsRNA recognition by OAS is also distinct from other well-studied innate immune sensors of dsRNA, like retinoic acid-inducible gene I (RIG-I) or dsRNA-activated protein kinase (PKR) (28-32), and suggests that OAS proteins might have only very weak discriminatory ability between different dsRNA sequences. This raises important questions about how OAS proteins specifically respond to viral RNAs and whether RNA sequence or structural motifs have any role to play in regulating OAS activity.

Recent evolutionary changes in OAS gene families add significant complexity in terms of the number of genes present, as well as their expression, cellular localization, and catalytic activity of their products, in a given organism. The human genome contains four distinct genes that encode a family of three catalytically active OAS enzymes (OAS1, OAS2, and OAS3) and one catalytically inactive member (OASL). All OAS proteins contain at least one copy of the globular OAS protein fold: OAS1, OAS2, and OAS3, contain one, two, and three OAS units, respectively, while OASL contains a single OAS unit embellished by two C-terminal copies of a ubiquitin-like domain (**Figure 1B**). Diversity of OAS expression is further increased by alternative splicing that result in at least ten different human protein isoforms (see Sidebar: *Alternative splicing expands human OAS protein diversity*). Comparisons between species adds yet further complexity. The murine genome, in particular, is notable for its extensive recent OAS gene duplication events (33). Further, while human OASL lacks enzymatic activity, mouse OASL2 and chicken OASL have retained their ability to produce 2-5A (34). Human OASL is nonetheless an important part of innate immunity and is thought to have evolved to exert its antiviral effect by binding RIG-I and enhancing its signaling (35,36). Loss-of-function mutations

in primate OAS1 have also been identified that substantially impair 2-5A synthesis or completely eliminate enzymatic activity altogether (37). Such species-specific differences in the OAS family presumably have their origins, at least in part, in the distinct viral challenges experienced by each species as well as the associated evolutionary "arms race" between host immune defense and viral countermeasure.

Sidebar: ALTERNATIVE SPLICING EXPANDS HUMAN OAS PROTEIN DIVERSITY

Alternative (or differential) splicing is a process that allows a single gene to code for multiple final protein products, greatly increasing the protein diversity encoded by the genome. During the process of mRNA transcription and maturation, specific exon(s) of a given gene can be included or excluded thereby increasing the pool of distinct mRNAs from a given gene to be directed for translation by the ribosome. All four human OAS genes are co-located in a single cluster on chromosome 12 and alternative splicing can generate a total of ten distinct mRNA products encoding OAS1 isoforms p42, p44, p46, p48 and p52, OAS2 isoforms p69 and p71, and OASL isoforms p39 and p59 (38). OAS3 is expressed as a single isoform (p100) (39). For both OAS1 and OAS2, alternative splicing involves the final gene exon and thus changes the sequence present at the C-terminus of each protein (**Figure 1B**) (40). While such changes in sequence have potential to alter protein function, a clear understanding of the impacts of alternative splicing of OAS genes are not currently available. OAS proteins are differentially induced by interferon and may localize to different subcellular fractions varying by cell type (41-43). Such observations suggest that regulation at the level of gene expression may have important consequences for OAS protein function both as a sensor of viral infection as well as in potential, currently unappreciated roles in the absence of infection.

Numerous studies of OAS proteins and the OAS/RNase L pathway over the last several decades have focused on their antiviral activity. Although the first X-ray crystal structure of an OAS protein was determined more than 15 years ago, relatively little was known regarding the molecular details of OAS regulation beyond the absolute requirement for a dsRNA activator and a rudimentary understanding of relative sensitivities of each OAS protein to dsRNA length, which increases from OAS1 (>17 bp) to OAS3 (>50 bp). However, as described in the sections that follow, recent structures of OAS1 and OAS3 domains bound to dsRNAs, combined with detailed biochemical analyses, have provided critical new molecular and functional insights into

the mechanism of OAS regulation by dsRNA. Further, evidence has also begun to emerge that specific RNA sequences and structural motifs, which may be present in cellular or viral RNAs, have the potential to profoundly impact the extent of OAS activation. Defining the rules governing RNA regulation of OAS proteins represents a critical but largely unexplored frontier in our understanding of this important protein family and the full complement of strategies used by viruses to evade detection by the innate immune system.

MOLECULAR BASIS OF OAS 1-3 REGULATION BY dsRNA

OAS1 regulation by short dsRNAs

The first high-resolution structure of an OAS family member, that of porcine OAS1, was determined in 2003 and revealed the overall architecture of the OAS protein domain (44). OAS1 adopts a bilobed structure with the N-terminal ("N-lobe") and C-terminal ("C-lobe") regions forming the two major domains of the protein; these lobes are connected by a central linker and their interaction is further stabilized by an N-terminal extension that wraps around the C-lobe (**Figure 2A**). Despite the absence of either dsRNA activator or ATP substrate, structural comparisons and mutagenesis studies confirmed the expected similarity of OAS to other members of the nucleotidyl transferase superfamily as well as potentially conserved features of the catalytic activities of these enzymes. Further, though OAS1 was found to lack a previously characterized RNA binding domain or motif, residues critical for dsRNA binding were identified across an extended, positively charged surface between the N- and C-lobes on the opposite side of the protein from the ATP-binding cleft and catalytic center (**Figure 2B**) (44). The authors further speculated that the role of dsRNA binding might be to widen the catalytic center to facilitate ATP substrate binding for 2-5A synthesis. However, the molecular mechanism underpinning the absolute requirement for dsRNA activation of 2-5A synthesis by OAS1 still remained unclear.

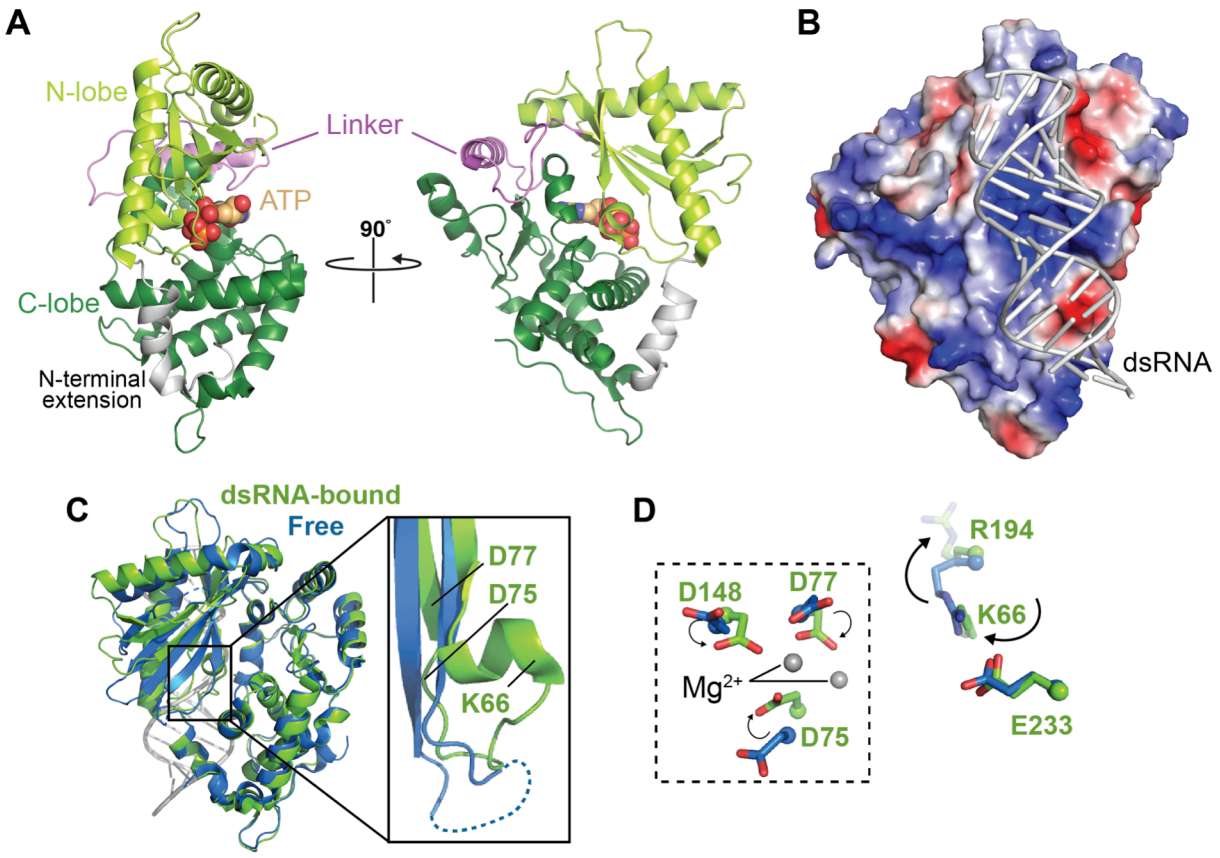

Figure 2. Conformational changes induced by dsRNA binding promote synthesis of 2-5A by OAS1. ***A.*** Cartoon of the OAS1 structure in its dsRNA-bound state (PDB code 4IG8). ATP binding sites and other structural features described in the main text are indicated. ***B.*** Electrostatic surface potential representation of OAS1 showing the positive (blue) charge of the dsRNA binding surface. ***C.*** Superposition of free porcine OAS1 (PDB code 1PX5; blue) and dsRNA-bound human OAS1 (green) with a zoomed view showing a secondary structure change induced by dsRNA binding. ***D.*** Reorganization of key residues upon dsRNA binding: a functionally critical positional switch in which K66 replaces R195 in an electrostatic interaction with E233 (*right*), helps promote reorganization of the OAS1 catalytic triad (D75, D77, and D148; *dashed box, left*).

An initial answer to this question came a decade later with the crystal structure of human OAS1 bound to a short (18 bp) dsRNA duplex in the presence of the substrate analog, dATP (24). This first structure of an OAS1-dsRNA complex beautifully revealed the molecular basis for dsRNA recognition and the fundamental mechanism of OAS1 activation by dsRNA: dsRNA binding drives an essential structural reorganization within OAS1 that narrows, rather than

widens, the ATP-binding cleft and repositions the catalytic residues to complete its active site. Subsequent structures of porcine OAS1-dsRNA complexes in the absence and presence of one or two molecules of AMPCPP (an ATP analog with a carbon atom linking the α and β phosphate groups) later revealed further important insights into the key drivers of dsRNA-induced conformational changes, the role of Mg^{2+} ions bound in the catalytic center, and the molecular basis for the specificity of 2'-5'-linkage formation by OAS1 (45).

As noted above, OAS1 lacks a canonical RNA-binding motif or domain and instead dsRNA interacts with a relatively flat surface of the protein on the opposite face from its catalytic site as previously predicted (**Figure 2B**). The OAS1-dsRNA complex structure revealed that this surface of OAS1 is distinct from that used by the structurally related but constitutively active CCA adding enzyme for tRNA binding (46,47). The 18 bp dsRNA used in the co-crystal structure spans the full length of its OAS1 binding surface and is recognized in two consecutive minor grooves, separated by approximately 30 Å, by two clusters of predominantly positively charged residues (one in each of the two OAS1 lobes). This mode of recognition defines the minimum length of dsRNA needed to bind and activate OAS1 at ~17 bp. The majority of interactions are made to phosphate groups and to the ribose 2'-OH in the minor groove, in common with many other dsRNA binding proteins (48,49). The importance of these interactions is supported by prior mutagenesis studies showing loss of activity upon substitution of these OAS1 residues (21,44,50), and the more general observations that dsRNA 2'-O-methylation significantly reduces OAS/RNase L pathway and recombinant OAS1 activation by dsRNA in cells and *in vitro*, respectively (51,52). Further, the finding that dsRNA binding is predominantly driven by non-sequence specific interactions to phosphate and ribose groups is also consistent with the ability of OAS1 to bind and become activated by a diverse range of RNA sequences. However, the OAS1-dsRNA complex structure also provides some mechanistic explanation for the emerging idea that some specific RNA sequences are capable of more potently activating OAS1 (discussed further below). In contrast, the largely sequence non-specific nature of OAS1-

dsRNA interaction less readily explains the finding that RNA modification via replacement of uridine with pseudouridine significantly reduces OAS1 activation by a given dsRNA (53). Rather, the origin for this phenomenon might reside in the rigidifying effect of this base modification on the dsRNA helical structure: in the co-crystal structure, the dsRNA is significantly distorted from ideal A-form helical geometry which would be less readily accomplished with a pseudouridine-containing dsRNA.

Crystal structures of OAS1-dsRNA complexes also revealed how binding of dsRNA drives functionally critical conformational changes in OAS1 necessary for activation of 2-5A synthesis. When bound by dsRNA, large conformational changes occur in the N-lobe, including large movements (>10 Å) of some secondary structure elements, while maintaining the two OAS1 lobes in their same relative positions as in the free protein. Overall, these changes in the N-lobe narrow the ATP binding cleft on the opposite side of the protein with rearrangements in OAS1 propagating from the dsRNA binding surface through the protein core to its catalytic center. Most critically, two basic residues (K66 and R195) exchange their positions to maintain an electrostatic interaction with the functionally critical E233; this switch directs R195 to the dsRNA binding surface, drives formation of a new α-helical structure and organizes the OAS1 catalytic triad (D75, D77, and D148) and ATP donor and acceptor sites (**Figure 2C,D**). Thus, dsRNA binding allosterically induces the formation of the catalytically competent OAS1 active site with correctly positioned catalytic triad, bound Mg^{2+} ions, and ATP substrates (24,45). It is noteworthy that the other structurally related nucleotidyl transferase enzymes PAP and CCA lack the potential for this charge switch and structural reorganization, and are locked in an “on” state, consistent with their constitutive (but primer-dependent) activity. Thus, dsRNA activation of OAS1’s polymerase activity is a unique adaptation necessitated by its role as a cytosolic dsRNA sensor within the innate immune system.

Basis of long dsRNA sensing by OAS3

OAS3 is the largest OAS variant and is composed of three OAS domains (DI, DII, and DIII; **Figure 1B**). Initial sequence-based analyses suggested DIII is the sole catalytically active domain while DI and DII are both "pseudoenzymes" that have lost the ability to synthesize 2-5A due to mutations of their catalytic aspartic acid residues (39). The first functional studies on OAS3 suggested that it preferentially synthesizes 2-5A dimers, a species that would be unable to activate RNase L, leading to speculation that OAS3 could have roles independent of RNase L activation (54). However, more recent analyses have shown that OAS3 is activated at a lower concentration of dsRNA, compared to OAS1, and is in fact capable of synthesizing 2-5A long enough to activate RNase L (55). The same study used mutational analysis to confirm the exclusive role of the OAS3 DIII domain in catalysis, as predicted given the lack of a complete catalytic center in the two other domains (DI and DII). However, the functionally critical changes in DI and DII apparently extend beyond the catalytic center as restoration of altered catalytic residues by mutagenesis failed to restore enzymatic activity (56).

These findings raise an important question: in the absence of catalytic activity, what functional role, if any, do DI and DII play? To address this question, Donovan *et al.* (2015) purified each OAS3 domain separately and tested their individual abilities to interact with dsRNA and produce 2-5A as compared to OAS1. While all three isolated domains retained their ability to bind dsRNA, none could synthesize 2-5A under previously determined conditions for OAS activity. Interestingly, however, isolated DIII was found to have some activity in the presence of Mn^{2+} as the divalent cation but the basis and potential relevance of this phenomenon is unclear. OAS3 DI was found to bind dsRNA ~14-fold more tightly than OAS1 which, together with the crystal structure determined of this domain bound to a 19 bp dsRNA, suggests that DI plays an essential role in RNA recognition (56). The higher dsRNA affinity of OAS3 DI can likely be explained by the fact that while OAS1 possesses the enzyme's catalytic activity and must therefore retain the ability to bind and release dsRNA for multiple rounds of catalysis, OAS3 DI

is a pseudoenzyme that serves exclusively as a dsRNA binding platform for presentation of the activator to the catalytic DIII domain. A second study used small angle X-ray scattering (SAXS) to show that the individual domains of OAS3 form a linear arrangement which would allow them to work in concert to specifically sense long RNAs (55). Consistent with this idea, OAS3 DI and DIII appear to be most critical for RNA binding and catalysis, while DII binds dsRNA more weakly and may act as a spacer allowing OAS3 to expand the RNA length requirement beyond that of OAS1 and OAS2 (56). This domain organization allows OAS3 to bind the largest dsRNA molecules (minimum RNA length requirement of ~50 bp), while short dsRNAs cannot simultaneously bind to each of the domains and thus induce the conformational changes in the catalytic DIII required for 2-5A production.

OAS2 is activated by dsRNA of intermediate length

Studies of OAS2 activity and structure have significantly lagged behind those of OAS1 and OAS3. *In vitro* studies in particular have been hindered by the need to express OAS2 using insect (52) or mammalian (57,58) expression systems in order to obtain catalytically active recombinant protein. The lack of activity in bacterially expressed OAS2 has been attributed to a requirement for post-translational modifications that are apparently unique to OAS2 among the active OAS proteins. OAS2 has four potential sites of glycosylation and a role for one or more of these was strongly suggested by the finding that inhibiting glycosylation in insect cells also leads to the production of inactive protein (52).

OAS2 functions as a homodimer and each protomer is comprised of two OAS domains: a catalytically inactive N-terminal domain (DI) and a catalytically active C-terminal domain (DII) (**Figure 1B**). Like OAS3, the individually expressed and purified OAS2 domains cannot produce 2-5A in isolation or when reconstituted (57,58). Isolated OAS2 DI has reduced affinity for dsRNA while DII can bind dsRNA with similar affinity to the full-length protein (57). These findings reveal that both OAS domains are required for OAS2 activity and suggest that the domains

must work cooperatively, possibly to form OAS2 dimers or to induce the structural rearrangements necessary in DII for catalysis. Therefore, OAS2 gains a level of specificity as it can only be activated by RNAs long enough to bind and span both domains, in a similar structural arrangement as observed for OAS3.

Early studies suggested that OAS2 is activated by dsRNAs of an intermediate size between those of OAS1 and OAS3, with a minimum length requirement of 25 bp (52). More recently, OAS2 activation was assessed *in vitro* using a series of dsRNAs ranging from 19 to 123 bp in length and found to increase consistently with increasing dsRNA length above a slightly longer minimum of 35-40 bp (58). Consistent with these analyses, the authors also found that a range of structured viral RNAs lacking helical regions >35 bp all failed to activate OAS2. If OAS2 requires a minor groove interaction site for each lobe (like the interactions made by OAS1 and DI of OAS3) within each of its two OAS domains, then OAS2 would require four consecutive minor grooves for interaction, consistent with the experimentally determined 35-40 bp minimum dsRNA length requirement. Several fundamental questions still remain regarding OAS2 regulation by dsRNA. For example, since OAS2 appears to be a homodimer, is dimerization necessary and, if so, must dsRNA bind to both OAS2 proteins within the dimer for activation or do the two active domains function independently of each other? Defining the OAS2 dimer and domain organization is also a critical next step that will address whether each OAS2 protomer can bind a separate dsRNA molecule or if a single dsRNA binds simultaneously to both. With tools in place to produce active OAS2 in sufficient quantities (58) for detailed biochemical and biophysical studies, we can anticipate answers to such questions arriving in the near future.

ROLE OF RNA SEQUENCE AND STRUCTURE IN OAS ACTIVATION

The recent structural and functional studies discussed so far have provided a new rational basis for the observed sensitivities of each OAS protein to dsRNA of different lengths and their

minimum requirements for activation. Despite these important advances, the new structures offer only limited clues on the role of RNA sequence specificity or how OAS proteins are potentially influenced by structured motifs within larger RNAs containing double-stranded regions, as might be found in viral or cellular RNAs. The following sections describe other recent advances centered on RNA sequence and structure determinants of OAS activation. Identifying and defining RNA molecular signatures for OAS activation (or inhibition) will be an essential step towards a complete understanding of OAS/RNase L pathway regulation by the host cell and in antiviral activity.

RNA sequence specificity in OAS activation

OAS1 "consensus" sequences

One emerging area has been to explore dsRNA features other than length, such as specific sequence, that potentially dictate the extent of OAS activation. One study tested a panel of short (19 bp) dsRNAs with distinct sequences to probe for differences in their ability to activate OAS1 *in vitro* and the OAS/RNase L pathway in human A549 cells (59). Sequence alignment of the dsRNAs that most strongly promoted OAS1 activity thus identified a consensus activation sequence WWN_9WG (where W is A or U, and N is any nucleotide). Analysis of a larger panel of over 100 dsRNA sequences was then used to confirm that this consensus sequence strongly correlated with the ability of a given short dsRNA to activate OAS1. When mapped onto a dsRNA helix, the minor grooves of the WW and WG consensus dinucleotide sequences are spaced by the nine intervening base pairs and presented on the same face of the A-form helix for recognition by OAS1, as observed in the OAS1-dsRNA crystal structure (24), which used an RNA duplex containing two copies of this sequence (**Figure 3A**). Further, the G nucleotide of the WWN_9WG sequence presented to OAS1 is the only base specifically recognized via a hydrogen bond from OAS1 residue Ser56, revealing at least part of the basis for the specificity of this consensus sequence. To date, the effect of this consensus sequence has only been

tested for OAS1; whether this or other specific sequence(s) can similarly enhance OAS2 or OAS3 activity remains to be determined.

A second, bipartite OAS1 activating sequence was identified in a separate study that used systematic evolution of ligands by exponential enrichment (SELEX) to identify RNA aptamers able to bind OAS1 (60). The RNA aptamers were 103 nucleotides in length and contained 34 random internal nucleotides for the SELEX process. Single-strand RNA aptamers and, in some cases corresponding dsRNA created by annealing of a complementary RNA strand, were tested for their ability to activate OAS1 *in vitro*. Sequence alignment was then used to reveal commonalities among the most potent activators. Good OAS1 activators were found to have an overall high cytosine and low guanine content and contained the sequences APyAPy(N)nCC and UU(N)nACCC (where Py is C or U) in different parts of the RNA molecule (60). These findings further support the idea that nucleotide content (especially cytosine) and specific RNA sequences can play an important role in defining the extent of OAS1 activation. Most studies on the innate immune response use the synthetic compound poly(I:C) as a positive control for PRR activation, but how poly(I:C) activates OAS1 is poorly understood (51). The relative importance of cytosine in dsRNA identified in this study could be one explanation of why poly(I:C) is such a potent activator of OAS1.

Sequence and structural motifs: 3'-ssPy motif and nc886 RNA

The non-coding adenoviral "virus-associated" RNA I (VA RNA_I; **Figure 3B**) possesses several pro-viral activities but is most widely recognized for its ability to inhibit PKR, relieving a cellular blockade on initiation of protein synthesis by this kinase (61). Curiously, however, despite these multiple inhibitory actions against host antiviral and other cellular processes, VA RNA_I was also reported to promote 2-5A synthesis by OAS1 (62). With our lab's long-standing interests in VA RNA_I structure and activity, we set out to further understand the molecular basis for this apparently paradoxical activity; remarkably, however, our *in vitro* transcribed VA RNA_I failed to

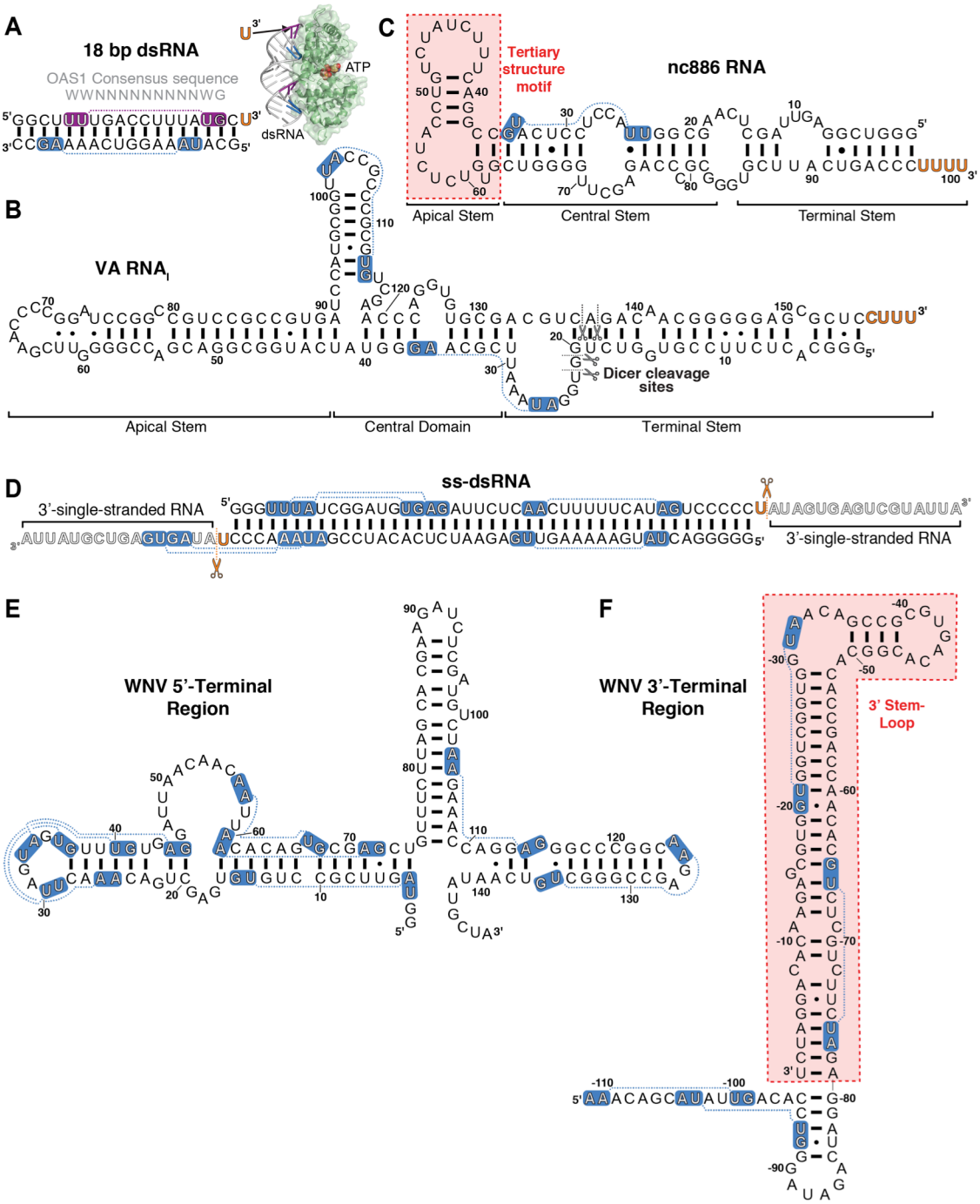

Figure 3. Double-stranded and structured RNA activators of OAS. Select RNAs discussed in the main text: ***A.*** 18 bp dsRNA used in the OAS1-dsRNA crystal structure and identification of the 3'-ssPy motif, ***B.*** Adenovirus (Ad2) VA RNA$_I$ with sites of Dicer cleavage indicated (black scissors), ***C.*** cellular nc886 RNA with location of OAS1 activating structural motif indicated (red shading), ***D.*** Example ss-dsRNA (43 bp) with sites of RNase cleavage to generate a minimal 3'-ssPy motif indicated (orange scissors), ***E.*** WNV 5'-terminal region, and ***F.*** WNV 3'-terminal region with OAS1 activating stem-loop highlighted (red shading). For all RNAs 3'-ssPy motifs are indicated by the orange text and the OAS1 consensus activation sequence WWN$_9$WG (shown above the 18 bp dsRNA in *Panel A*) by white text on blue background. The purple background for the 18 bp dsRNA top strand denotes the consensus sequence directly contacted by OAS1 in the OAS1-dsRNA crystal structure (*inset* in *Panel A*).

activate OAS1 to the extent previously reported (63). The basis of this difference was ultimately traced to the absence of a 3'-end CUUU sequence in our *in vitro* construct, which would normally be present in VA RNA_I as a result of RNA polymerase III termination (64). This observation thus led to the serendipitous discovery of a novel motif for OAS1 activation, the 3'-end single-stranded pyrimidine (3'-ssPy) motif.

Studies using VA RNA_I variants with altered 5'- and 3'-end sequences revealed that optimal OAS1 activation required a 3'-end pyrimidine-rich (C or U) single-stranded sequence (63). While 3'-end single-stranded purine-rich (G or A) sequences promoted an intermediate level of activation, extension of the VA RNA_I terminal stem with an equivalent length of base pairs failed to enhance OAS1 activation. Deletion of the equivalent 3'-end sequences from two other RNA polymerase III non-coding transcripts, Epstein-Barr virus EBER-1 RNA and human cellular nc886 RNA (**Figure 3C**), also reduced OAS1 activation by these RNAs, albeit to a significantly lesser extent in the latter case. To facilitate modeling of the effect of the 3'-ssPy motif, the 18 bp dsRNA duplex used in the OAS1-dsRNA crystal structure (**Figure 3A**) was also examined: addition of one 3'-end single-stranded U residue was sufficient to significantly enhance OAS1 activation by this model dsRNA. While the mechanism of 3'-ssPy motif action remains to be determined in detail, modeling using the OAS1-dsRNA structure was used to direct mutagenesis of surrounding conserved OAS1 residues. These studies identified one amino acid, G157, whose substitution with a bulkier residue did not impact overall OAS1 activity but fully eliminated sensitivity to the 3'-ssPy motif. G157 resides in a loop adjacent to the dsRNA binding surface suggesting that allosteric regulation of OAS1 by RNA may be more complex than currently appreciated (**Figure 4**). The implications for OAS1 antiviral activity, and in other potential roles in the uninfected cell, warrant further investigation. For example, given RNase L's preferential cleavage at single-stranded UA or UU sequences, production of dsRNAs appended with these sequences from larger structured RNAs with single-stranded regions could produce additional OAS1-activating dsRNAs with 3'-ssPy motifs, thus potentiating signaling via the

OAS/RNase L pathway (63,65,66). Additionally, OAS1 could play a role in sensing of aberrant 3'-end processing of cellular RNAs.

A more recent study by McKenna and colleagues examined the impact of single-stranded 3'-end sequences on OAS2 activation (58). A series of RNA *in vitro* transcription constructs was created to produce dsRNAs of various lengths (19-123 bp), with both 3'-ends in each dsRNA appended with a 17 nucleotide single-stranded sequence (ss-dsRNA; **Figure 3D**). This 3'-end sequence was also truncated to a single U residue by RNase treatment to generate a minimal 3'-ssPy motif. While the 3'-ssPy motif had no effect on OAS2 activation, dsRNAs with 17 nucleotide 3'-overhangs ("ss-dsRNAs") were consistently found to more strongly activate OAS2 once the helical region was >35 bp in length. This finding suggests OAS2 may have some selectivity for dsRNAs appended with longer single-stranded sequences. However, an additional element of complexity was revealed by parallel studies of OAS1 with the same dsRNA constructs: here, OAS1 was found to be insensitive to both the longer single-stranded sequence and the single 3'-end U residue (i.e. 3'-ssPy motif). This observation suggests that the context in which the 3'-ssPy is presented to OAS1 may be critical for the ability of this RNA signature to enhance 2-5A synthesis. Specifically, while our earlier studies used an 18 bp dsRNA containing an OAS1 activation consensus sequence (with the 3'-ssPy motif appended to the strand immediately following the G residue of the WWN_9WG consensus), the dsRNAs used by Koul *et al.* lacked this sequence in a corresponding position (**Figure 3D**). These findings suggest that RNA signatures like the 3'-ssPy motif do not directly influence OAS1 (or possibly, OAS2) binding to dsRNAs but, when positioned optimally by other features of the adjacent dsRNA binding site, can serve to strongly enhance 2-5A synthesis.

Further support for this idea also comes from recent studies of the human cellular nc886 RNA. nc886 is a ubiquitously expressed cytosolic non-coding RNA that was first identified during studies of PKR's proliferative role in some cancers (67,68) and has since been shown to directly bind and inhibit the kinase (69,70). nc886 adopts two distinct structures which differ in

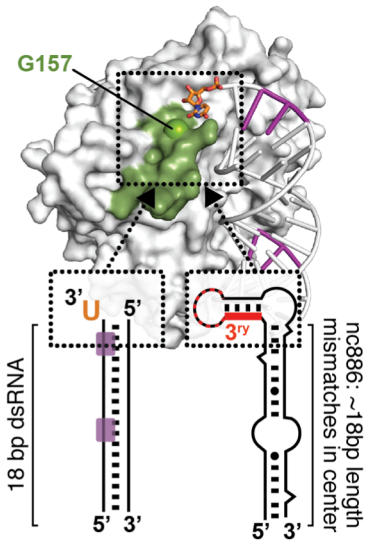

Figure 4. Model for enhancement of OAS1 activation by RNA sequence and structural motifs. OAS1 requires at least ~17 bp dsRNA for binding, shown here on the *left* for the model 18 bp dsRNA duplex with OAS1 consensus activation sequence (purple) and *right* the nc886 central stem sequence. Once positioned by the OAS1 binding site, RNA signatures such as the 3'-ssPy motif (orange) or the tertiary structure of nc886 (red) can dramatically increase OAS1 activation. The mechanism of activation by these RNA features is currently unknown but modeling and mutagenesis analyses suggest the OAS1 loop containing G157 may be important (see main text for details).

their migration on native polyacrylamide gels and their ability to inhibit PKR: the slower migrating form ("Conformer 1") is a potent PKR inhibitor while the faster migrating form ("Conformer 2") is a weak PKR activator that acts as a pseudoinhibitor at higher concentrations in the presence of another PKR-activator such as poly(I:C) RNA. As noted earlier, we also showed that nc886 can activate OAS1 *in vitro* as a mixture of conformers (63). A more recent detailed study of OAS1 activation by nc886 *in vitro* and in A549 cells revealed that most activity is conferred by a unique tertiary structure motif present only in the apical stem-loop of nc886 Conformer 1 (71). Interestingly, this same Conformer 1 structural feature is critical for PKR inhibition by nc886, suggesting the potential for cellular RNA-mediated communication between these two dsRNA-sensing elements of the innate immune system. Analysis of nc886 with truncated terminal and central stem structures showed that, although formation of the OAS1-

activating structure requires only the apical stem-loop RNA sequence, this domain is not alone sufficient to activate OAS1. Rather, a predominantly base-paired region of the central stem, approximately 18 bp in length, is also required for OAS1 activation (71). Our interpretation of these observations is that OAS1 binding to nc886 is dictated by the dsRNA region of the central stem, which optimally positions the apical stem-loop motif to potentiate OAS1 activation.

Collectively, these studies suggest a potential common theme for OAS1 activation by sequence and structural motifs appended to preferred OAS1 binding sites (**Figure 4**). The range of dsRNA sequences that preferentially bind OAS1, motifs that promote OAS1 activation once positioned optimally, and whether OAS2 or OAS3 are subject to similar regulation require further investigation.

Coding and non-coding viral RNAs containing dsRNA regions

Viruses may present dsRNA in the host cell through their genomes, during viral gene expression or replication, or through the expression of abundant non-coding RNA species like adenovirus VA RNA_I. However, many important details about how the sequences and/or structures of these viral RNAs contribute to OAS regulation and host-virus interaction have remained elusive. One early analysis of OAS/RNase L pathway activation by a viral RNA was performed with hepatitis C virus (HCV) genomic RNA (72). Specifically, the HCV RNA genome was found to activate OAS, leading to its cleavage by RNase L and thus limiting viral infection. In addition to this direct action of the OAS/RNase L pathway, a product of HCV RNA cleavage by RNase L can also act as a PAMP that activates the RIG-I pathway, propagating immune signaling and upregulation of interferon-stimulated genes to prevent HCV replication (66). Further supporting this idea, some HCV genotypes are deficient in the single-stranded UA- and UU-containing sequences preferred by RNase L (72) suggesting that HCV has developed a novel viral OAS/RNase L pathway evasion strategy wherein sequences preferentially cleaved by RNase L are selected against. While OAS can still bind HCV RNA and produce 2-5A, the

viral genome suffers minimal damage due to downstream RNase L activity thus allowing viral replication to persist. Differences observed in efficacy of interferon therapy for HCV infection may also be directly related to the sensitivity of the viral RNA to RNase L cleavage (72).

The 5'- and 3'-end regions of the West Nile virus (WNV) RNA genome (**Figure 3E,F**) have also been identified as potential activators of OAS1 (73,74). The isolated 5'-terminal region and mixture of the two terminal region RNAs activated OAS1 most robustly *in vitro* while the isolated 3'-terminal region and a single stem-loop structure from this region activated OAS1 to a lesser extent. These findings reveal both the potential for activation of the OAS/RNase L pathway by multiple regions of the WNV genome and that genome cyclization via interaction of the 5'- and 3'-terminal regions, a required step for viral replication, may not be sufficient for the virus to evade this detection (74). However, the full impact of OAS activation by WNV genomic RNA, its relevance to detection of infection, and potential for viral evasion all require further study. Both WNV RNA regions contain multiple WWN_9WG consensus activation sequences though their specific contributions to OAS1 activation were not directly tested and most do not fall in dsRNA regions. However, strong OAS1 activation by the isolated WNV RNA regions clearly shows that bulges, non-canonical base pairs, and mismatches within the ~18 bp regions are readily tolerated and that OAS1 can be activated by a diverse group of structured RNAs.

As noted earlier, a number of abundantly expressed non-coding RNAs can activate OAS1 but not OAS2 (or presumably OAS3 given its even greater dsRNA length requirement). These RNAs include adenovirus VA RNA_I, Epstein-Barr virus EBER-1 RNA, and human immunodeficiency virus TAR RNA (58,62,75,76). Our analysis revealed that the 3'-end sequence (3'-ssPy motif) is critical in the context of the wild-type full-length VA RNA_I (63), but this cannot be the complete picture of OAS1 regulation by this RNA transcript. First, in the original study that identified OAS1 activation by VA RNA_I, increasing the Watson-Crick base pairing in both the terminal and apical stem was found to increase OAS1 activation, with the greatest effect observed for the latter region, which is most distant from the 3'-ssPy motif (62).

Second, a shorter VA RNA_I fragment, roughly corresponding to the product of VA RNA_I cleavage by Dicer (**Figure 3B**) (77,78), binds OAS1 with higher affinity, but is a very poor activator (pseudoinhibitor) of OAS1 (79). OAS1 activation by EBER-1 and TAR RNAs have not been studied in detail but it is likely that the activity of these structured non-coding RNAs is similarly complex. All three non-coding RNAs contain more than one copy of the WWN_9WG consensus activation sequence but, as for the WNV terminal region RNAs, their contribution to OAS1 activation has not been determined. Regardless of these uncertainties in detail, it is intriguing and worthy of further investigation that three viral non-coding RNAs, which possess other well-established antiviral activities, are capable of activating a second parallel host antiviral pathway. This could be a tolerated consequence or an activity that is exploited for pro-viral purposes at late stages of infection when these non-coding RNAs are highly abundant.

CONCLUSIONS

Viruses depend on the host cell translational machinery for protein synthesis and thus their replication. To accomplish this, viruses must expose their proteins and nucleic acids to the cellular milieu but avoid detection by innate immune antiviral factors capable of restricting viral replication. The OAS family of enzymes comprise a group of cytosolic dsRNA innate immune sensors whose importance in this process is underscored by the numerous ways diverse viruses have developed to evade detection. These include directly inhibiting OAS, sequestering dsRNA produced as a result of viral infection, producing 2-5A analogs, degrading 2-5A via viral-encoded phosphodiesterases, expression of protein or RNA inhibitors of 2-5A interaction with RNase L or its ribonuclease activity, or through selective pressure to remove RNase L target sites within viral RNAs (16,72,80-90). While there is strong evidence for critical roles for each OAS family member in at least some context, defining the protective effects of each family member is an active area of investigation. For example, a recent study indicated OAS3 may be the main effector of the OAS/RNase L pathway in response to a range of viruses including WNV

and influenza A virus (IAV) (91). In this study, knockout of OAS3, but not OAS1 or OAS2, prevented 2-5A synthesis and rRNA degradation resulting in significantly higher viral titers. However, deletion of OAS1 or OAS2 had no detectable effects on 2-5A or rRNA and exhibited only minor effects on viral titers suggesting OAS1 and OAS2 may exert their antiviral functions through alternative pathways. Further, another study in which each of the ten human OAS proteins was expressed in A549 cells revealed that only OAS1 (p42 and p46 isoforms) and OAS3 exhibited measurable antiviral effects against Dengue virus, leading to the conclusion that OAS gene family members contribute differently to antagonize this virus (92). Yet, other evidence from analysis of OAS single nucleotide polymorphisms (SNPs) also appears to complicate these conclusions: SNPs in both *OAS1* and *OAS3* are known to increase susceptibility to WNV infection (93-95), while two SNPs in *OAS2* have been suggested to increase the susceptibility to Dengue virus (96,97). Delineating the specific, potentially overlapping, roles of each OAS protein family member is likely to continue to be an active area of investigation along with studies to define the nature of the viral RNAs detected by these proteins.

As discussed in this review, recent structural studies have revealed the molecular details of OAS allosteric regulation by dsRNA. Together with complementary biochemical and biophysical studies, this work has also provided a clear rationale for the observed dsRNA length requirements and the contribution of each OAS domain in dsRNA binding or catalysis (summarized in **Figure 5**). The OAS protein family's ability to discriminate dsRNAs based on length is likely an essential adaptation that allows detection and response to a wider range of virus-derived dsRNA during infection. However, despite these important advances, we still understand relatively little about how distinct features of the dsRNA contribute to the extent of OAS activation. Studies identifying specific sequences and single-stranded or structured motifs that enhance OAS1 activation (**Figure 5**), as well as identification of viral and cellular non-coding or coding RNA regions that strongly activate OAS1, suggest that much remains to be

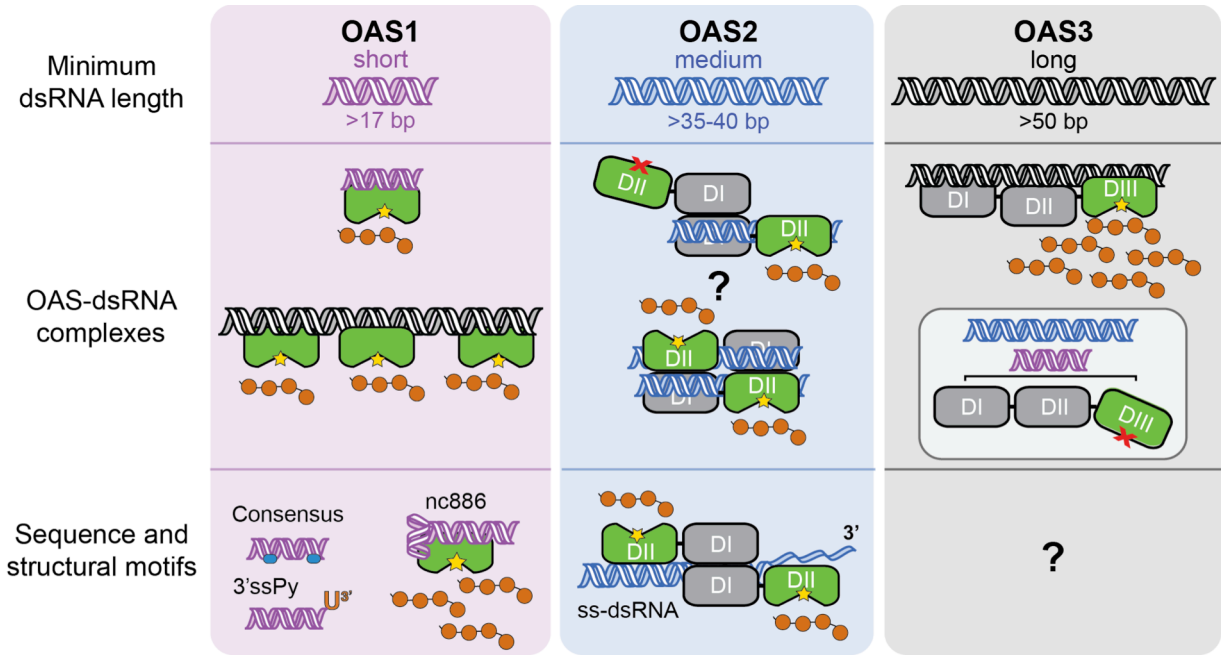

Figure 5. Summary of OAS protein activation by RNA. Current understanding of OAS protein regulation by dsRNA, as discussed in the main text, is summarized in the three vertical panels for OAS1 (purple), OAS2 (blue), and OAS3 (grey). *Top*, minimum dsRNA lengths required to activate each OAS protein. *Center*, OAS activation by dsRNA with dsRNA induced organization of the catalytic center (green domain) denoted by the yellow star. **OAS1** binds short dsRNAs and can also be strongly activated by longer dsRNAs with multiple binding sites. **OAS2** functions as a dimer of currently unknown organization (two potential dimer interactions are shown; also possible are via DII-DII only and DI/DI-DII/DII head-head). Also unknown is whether both OAS2 proteins must bind to dsRNA and whether they function independently or cooperatively. **OAS3** is activated only by longer dsRNAs due to the requirement to span three OAS domains; shorter RNAs are unable to induce the conformational change in DIII (*inset*). *Bottom*, other RNA sequences and motifs identified to enhance 2-5A synthesis.

learned. The case for larger RNAs with complex structures is likely further complicated by the potential for multiple OAS interaction sites (especially for the single domain OAS1). Even the "simple" 18 bp dsRNA used for structural studies (24) contained two overlapping antiparallel copies of the WWN_9WG consensus sequences, and yet the dsRNA bound in a single orientation and only one consensus was apparently sensed by OAS1. This issue is further complicated by studies of OAS1 activation by the same consensus sequence and 3'-ssPy motif which suggest that the context in which these features are presented is also a critical determinant of their

ability to promote OAS activation. Thus, it may not be simply the presence or absence of an RNA feature, but also their placement within the RNA that determines how much or little each contributes to OAS activation. A final consideration is whether such molecular signatures act in concert or competition to affect the level of OAS1 activity. Our current studies suggest that there are preferred OAS binding sites with weak ability to activate OAS1 and that these can diminish activation by other sites within the same dsRNA. Collectively, these considerations likely have important implications for how OAS proteins are able to selectively sense viral RNAs and it will be important to tease apart the details of how individual and combinations of RNA features control OAS activation. Equally, selection within viral RNAs for OAS binding sites that mask or compete with activating features could potentially be a mechanism to allow viral replication to persist by acting as a "sponge" for OAS activity.

While OAS's major function in the antiviral OAS/RNase L pathway is well-established, differential OAS expression and induction by interferon in different cell types (4), as well as OAS conservation in organisms without interferon, collectively imply these proteins play important cellular roles outside of innate immunity. Additionally, SNPs associated with the human *OAS1* gene have also been connected to diabetes (98), multiple sclerosis (99,100), and prostate cancer (101) suggesting some role in processes that impact these human diseases. A complete understanding of how RNA controls OAS activity is critical to gain a deeper understanding of multiple facets of innate immunity, host-virus interactions, and fundamental mechanisms of cellular translational control.

ACKNOWLEDGMENTS

We thank Drs. Christine M. Dunham, Daniel Reines, and Anice C. Lowen for discussions and comments on the manuscript. We are also grateful to Dr. Sean McKenna for sharing details of his group's recent work on OAS2 ahead of publication to allow its inclusion in this review.

FUNDING INFORMATION

This work was supported by T32-GM008367 and F31-AI133950 from the National Institutes of Health (to SLS), the Emory University Research Council (to GLC), and Emory University School of Medicine Bridge Funding Program (to GLC). SLS is also grateful for support from the Achievement Rewards for College Scientists (ARCS) Foundation, Atlanta Chapter.

REFERENCES

1. Schneider, W.M., Chevillotte, M.D. and Rice, C.M. (2014) Interferon-stimulated genes: a complex web of host defenses. *Annu Rev Immunol*, **32**, 513-545.
2. Takeuchi, O. and Akira, S. (2010) Pattern recognition receptors and inflammation. *Cell*, **140**, 805-820.
3. Sparrer, K.M. and Gack, M.U. (2015) Intracellular detection of viral nucleic acids. *Curr Opin Microbiol*, **26**, 1-9.
4. Hovanessian, A.G. and Justesen, J. (2007) The human 2'-5'-oligoadenylate synthetase family: Unique interferon-inducible enzymes catalyzing 2'-5' instead of 3'-5' phosphodiester bond formation. *Biochimie*, **89**, 779-788.
5. Dong, B., Xu, L., Zhou, A., Hassel, B.A., Lee, X., Torrence, P.F. and Silverman, R.H. (1994) Intrinsic molecular activities of the interferon-induced 2-5A-dependent RNase. *J Biol Chem*, **269**, 14153-14158.
6. Han, Y., Whitney, G., Donovan, J. and Korennykh, A. (2012) Innate immune messenger 2-5A tethers human RNase L into active high-order complexes. *Cell Rep*, **2**, 902-913.
7. Huang, H., Zeqiraj, E., Dong, B., Jha, B.K., Duffy, N.M., Orlicky, S., Thevakumaran, N., Talukdar, M., Pillon, M.C., Ceccarelli, D.F. *et al.* (2014) Dimeric structure of pseudokinase RNase L bound to 2-5A reveals a basis for interferon-induced antiviral activity. *Mol Cell*, **53**, 221-234.
8. Malathi, K., Dong, B., Gale, M., Jr. and Silverman, R.H. (2007) Small self-RNA generated by RNase L amplifies antiviral innate immunity. *Nature*, **448**, 816-819.
9. Banerjee, S., Li, G., Li, Y., Gaughan, C., Baskar, D., Parker, Y., Lindner, D.J., Weiss, S.R. and Silverman, R.H. (2015) RNase L is a negative regulator of cell migration. *Oncotarget*, **6**, 44360-44372.
10. Rath, S., Donovan, J., Whitney, G., Chitrakar, A., Wang, W. and Korennykh, A. (2015) Human RNase L tunes gene expression by selectively destabilizing the microRNA-regulated transcriptome. *Proc Natl Acad Sci U S A*, **112**, 15916-15921.
11. Siddiqui, M.A., Mukherjee, S., Manivannan, P. and Malathi, K. (2015) RNase L Cleavage Products Promote Switch from Autophagy to Apoptosis by Caspase-Mediated Cleavage of Beclin-1. *Int J Mol Sci*, **16**, 17611-17636.
12. Donovan, J., Rath, S., Kolet-Mandrikov, D. and Korennykh, A. (2017) Rapid RNase L-driven arrest of protein synthesis in the dsRNA response without degradation of translation machinery. *RNA*, **23**, 1660-1671.

13. Chitrakar, A., Rath, S., Donovan, J., Demarest, K., Li, Y., Sridhar, R.R., Weiss, S.R., Kotenko, S.V., Wingreen, N.S. and Korennykh, A. (2019) Real-time 2-5A kinetics suggest that interferons beta and lambda evade global arrest of translation by RNase L. *Proc Natl Acad Sci U S A*, **116**, 2103-2111.

14. Wu, J. and Chen, Z.J. (2014) Innate immune sensing and signaling of cytosolic nucleic acids. *Annu Rev Immunol*, **32**, 461-488.

15. Schlee, M. and Hartmann, G. (2016) Discriminating self from non-self in nucleic acid sensing. *Nat Rev Immunol*, **16**, 566-580.

16. Hur, S. (2019) Double-Stranded RNA Sensors and Modulators in Innate Immunity. *Annu Rev Immunol*, **37**, 349-375.

17. Loo, Y.M. and Gale, M., Jr. (2011) Immune signaling by RIG-I-like receptors. *Immunity*, **34**, 680-692.

18. Hull, C.M. and Bevilacqua, P.C. (2016) Discriminating Self and Non-Self by RNA: Roles for RNA Structure, Misfolding, and Modification in Regulating the Innate Immune Sensor PKR. *Acc Chem Res*, **49**, 1242-1249.

19. Samuel, C.E. (2011) Adenosine deaminases acting on RNA (ADARs) are both antiviral and proviral. *Virology*, **411**, 180-193.

20. Li, Y., Banerjee, S., Goldstein, S.A., Dong, B., Gaughan, C., Rath, S., Donovan, J., Korennykh, A., Silverman, R.H. and Weiss, S.R. (2017) Ribonuclease L mediates the cell-lethal phenotype of double-stranded RNA editing enzyme ADAR1 deficiency in a human cell line. *Elife*, **6**, e25687.

21. Torralba, S., Sojat, J. and Hartmann, R. (2008) 2'-5' oligoadenylate synthetase shares active site architecture with the archaeal CCA-adding enzyme. *Cell Mol Life Sci*, **65**, 2613-2620.

22. Sun, L., Wu, J., Du, F., Chen, X. and Chen, Z.J. (2013) Cyclic GMP-AMP synthase is a cytosolic DNA sensor that activates the type I interferon pathway. *Science*, **339**, 786-791.

23. Hornung, V., Hartmann, R., Ablasser, A. and Hopfner, K.P. (2014) OAS proteins and cGAS: unifying concepts in sensing and responding to cytosolic nucleic acids. *Nat Rev Immunol*, **14**, 521-528.

24. Donovan, J., Dufner, M. and Korennykh, A. (2013) Structural basis for cytosolic double-stranded RNA surveillance by human oligoadenylate synthetase 1. *Proc Natl Acad Sci U S A*, **110**, 1652-1657.

25. Kjaer, K.H., Poulsen, J.B., Reintamm, T., Saby, E., Martensen, P.M., Kelve, M. and Justesen, J. (2009) Evolution of the 2'-5'-oligoadenylate synthetase family in eukaryotes and bacteria. *J Mol Evol*, **69**, 612-624.

26. Fish, I. and Boissinot, S. (2016) Functional evolution of the OAS1 viral sensor: Insights from old world primates. *Infect Genet Evol*, **44**, 341-350.

27. Hu, J., Wang, X., Xing, Y., Rong, E., Ning, M., Smith, J. and Huang, Y. (2018) Origin and development of oligoadenylate synthetase immune system. *BMC Evol Biol*, **18**, 201.

28. Hornung, V., Ellegast, J., Kim, S., Brzozka, K., Jung, A., Kato, H., Poeck, H., Akira, S., Conzelmann, K.K., Schlee, M. *et al.* (2006) 5'-Triphosphate RNA is the ligand for RIG-I. *Science*, **314**, 994-997.

29. Devarkar, S.C., Wang, C., Miller, M.T., Ramanathan, A., Jiang, F., Khan, A.G., Patel, S.S. and Marcotrigiano, J. (2016) Structural basis for m7G recognition and 2'-O-methyl discrimination in capped RNAs by the innate immune receptor RIG-I. *Proc Natl Acad Sci U S A*, **113**, 596-601.

30. Manche, L., Green, S.R., Schmedt, C. and Mathews, M.B. (1992) Interactions between double-stranded RNA regulators and the protein kinase DAI. *Mol Cell Biol*, **12**, 5238-5248.

31. Nallagatla, S.R., Toroney, R. and Bevilacqua, P.C. (2011) Regulation of innate immunity through RNA structure and the protein kinase PKR. *Curr Opin Struct Biol*, **21**, 119-127.

32. Nallagatla, S.R., Toroney, R. and Bevilacqua, P.C. (2008) A brilliant disguise for self RNA: 5'-end and internal modifications of primary transcripts suppress elements of innate immunity. *RNA Biol*, **5**, 140-144.

33. Kakuta, S., Shibata, S. and Iwakura, Y. (2002) Genomic structure of the mouse 2',5'-oligoadenylate synthetase gene family. *J Interferon Cytokine Res*, **22**, 981-993.

34. Eskildsen, S., Justesen, J., Schierup, M.H. and Hartmann, R. (2003) Characterization of the 2'-5'-oligoadenylate synthetase ubiquitin-like family. *Nucleic Acids Res*, **31**, 3166-3173.

35. Zhu, J., Zhang, Y., Ghosh, A., Cuevas, R.A., Forero, A., Dhar, J., Ibsen, M.S., Schmid-Burgk, J.L., Schmidt, T., Ganapathiraju, M.K. *et al.* (2014) Antiviral activity of human OASL protein is mediated by enhancing signaling of the RIG-I RNA sensor. *Immunity*, **40**, 936-948.

36. Ibsen, M.S., Gad, H.H., Andersen, L.L., Hornung, V., Julkunen, I., Sarkar, S.N. and Hartmann, R. (2015) Structural and functional analysis reveals that human OASL binds dsRNA to enhance RIG-I signaling. *Nucleic Acids Res*, **43**, 5236-5248.

37. Carey, C.M., Govande, A.A., Cooper, J.M., Hartley, M.K., Kranzusch, P.J. and Elde, N.C. (2019) Recurrent Loss-of-Function Mutations Reveal Costs to OAS1 Antiviral Activity in Primates. *Cell Host Microbe*, **25**, 336-343.e334.

38. Hovnanian, A., Rebouillat, D., Mattei, M.G., Levy, E.R., Marie, I., Monaco, A.P. and Hovanessian, A.G. (1998) The human 2',5'-oligoadenylate synthetase locus is composed of three distinct genes clustered on chromosome 12q24.2 encoding the 100-, 69-, and 40-kDa forms. *Genomics*, **52**, 267-277.

39. Rebouillat, D., Hovnanian, A., David, G., Hovanessian, A.G. and Williams, B.R. (2000) Characterization of the gene encoding the 100-kDa form of human 2',5' oligoadenylate synthetase. *Genomics*, **70**, 232-240.

40. Bonnevie-Nielsen, V., Field, L.L., Lu, S., Zheng, D.J., Li, M., Martensen, P.M., Nielsen, T.B., Beck-Nielsen, H., Lau, Y.L. and Pociot, F. (2005) Variation in antiviral 2',5'-oligoadenylate synthetase (2'5'AS) enzyme activity is controlled by a single-nucleotide polymorphism at a splice-acceptor site in the OAS1 gene. *Am J Hum Genet*, **76**, 623-633.

41. Chebath, J., Benech, P., Hovanessian, A., Galabru, J. and Revel, M. (1987) Four different forms of interferon-induced 2',5'-oligo(A) synthetase identified by immunoblotting in human cells. *J Biol Chem*, **262**, 3852-3857.

42. Hovanessian, A.G., Laurent, A.G., Chebath, J., Galabru, J., Robert, N. and Svab, J. (1987) Identification of 69-kd and 100-kd forms of 2-5A synthetase in interferon-treated human cells by specific monoclonal antibodies. *EMBO J*, **6**, 1273-1280.

43. Besse, S., Rebouillat, D., Marie, I., Puvion-Dutilleul, F. and Hovanessian, A.G. (1998) Ultrastructural localization of interferon-inducible double-stranded RNA-activated enzymes in human cells. *Exp Cell Res*, **239**, 379-392.

44. Hartmann, R., Justesen, J., Sarkar, S.N., Sen, G.C. and Yee, V.C. (2003) Crystal structure of the 2'-specific and double-stranded RNA-activated interferon-induced antiviral protein 2'-5'-oligoadenylate synthetase. *Mol Cell*, **12**, 1173-1185.

45. Lohofener, J., Steinke, N., Kay-Fedorov, P., Baruch, P., Nikulin, A., Tishchenko, S., Manstein, D.J. and Fedorov, R. (2015) The Activation Mechanism of 2'-5'-Oligoadenylate Synthetase Gives New Insights Into OAS/cGAS Triggers of Innate Immunity. *Structure*, **23**, 851-862.

46. Tomita, K., Fukai, S., Ishitani, R., Ueda, T., Takeuchi, N., Vassylyev, D.G. and Nureki, O. (2004) Structural basis for template-independent RNA polymerization. *Nature*, **430**, 700-704.

47. Xiong, Y. and Steitz, T.A. (2004) Mechanism of transfer RNA maturation by CCA-adding enzyme without using an oligonucleotide template. *Nature*, **430**, 640-645.

48. Chang, K.Y. and Ramos, A. (2005) The double-stranded RNA-binding motif, a versatile macromolecular docking platform. *FEBS J*, **272**, 2109-2117.

49. Masliah, G., Barraud, P. and Allain, F.H. (2013) RNA recognition by double-stranded RNA binding domains: a matter of shape and sequence. *Cell Mol Life Sci*, **70**, 1875-1895.

50. Sarkar, S.N., Kessler, S.P., Rowe, T.M., Pandey, M., Ghosh, A., Elco, C.P., Hartmann, R., Pal, S. and Sen, G.C. (2005) Natural mutations in a 2'-5' oligoadenylate synthetase transgene revealed residues essential for enzyme activity. *Biochemistry*, **44**, 6837-6843.

51. Minks, M.A., West, D.K., Benvin, S., Greene, J.J., Ts'o, P.O. and Baglioni, C. (1980) Activation of 2',5'-oligo(A) polymerase and protein kinase of interferon-treated HeLa cells by 2'-O-methylated poly(inosinic acid).poly(cytidylic acid), Correlations with interferon-inducing activity. *J Biol Chem*, **255**, 6403-6407.

52. Sarkar, S.N., Bandyopadhyay, S., Ghosh, A. and Sen, G.C. (1999) Enzymatic characteristics of recombinant medium isozyme of 2'-5' oligoadenylate synthetase. *J Biol Chem*, **274**, 1848-1855.

53. Anderson, B.R., Muramatsu, H., Jha, B.K., Silverman, R.H., Weissman, D. and Kariko, K. (2011) Nucleoside modifications in RNA limit activation of 2'-5'-oligoadenylate synthetase and increase resistance to cleavage by RNase L. *Nucleic Acids Res*, **39**, 9329-9338.

54. Marie, I., Blanco, J., Rebouillat, D. and Hovanessian, A.G. (1997) 69-kDa and 100-kDa isoforms of interferon-induced (2'-5')oligoadenylate synthetase exhibit differential catalytic parameters. *Eur J Biochem*, **248**, 558-566.

55. Ibsen, M.S., Gad, H.H., Thavachelvam, K., Boesen, T., Despres, P. and Hartmann, R. (2014) The 2'-5'-oligoadenylate synthetase 3 enzyme potently synthesizes the 2'-5'-oligoadenylates required for RNase L activation. *J Virol*, **88**, 14222-14231.

56. Donovan, J., Whitney, G., Rath, S. and Korennykh, A. (2015) Structural mechanism of sensing long dsRNA via a noncatalytic domain in human oligoadenylate synthetase 3. *Proc Natl Acad Sci U S A*, **112**, 3949-3954.

57. Marie, I., Rebouillat, D. and Hovanessian, A.G. (1999) The expression of both domains of the 69/71 kDa 2',5' oligoadenylate synthetase generates a catalytically active enzyme and mediates an anti-viral response. *Eur J Biochem*, **262**, 155-165.

58. Koul, A., Deo, S., Booy, E.P., Orriss, G.L., Genung, M. and McKenna, S.A. (2020) Impact of double-stranded RNA characteristics on the activation of human 2'-5'-oligoadenylate synthetase 2 (OAS2). *Biochem Cell Biol*, **98**, 70-82.

59. Kodym, R., Kodym, E. and Story, M.D. (2009) 2'-5'-Oligoadenylate synthetase is activated by a specific RNA sequence motif. *Biochem Biophys Res Commun*, **388**, 317-322.

60. Hartmann, R., Norby, P.L., Martensen, P.M., Jorgensen, P., James, M.C., Jacobsen, C., Moestrup, S.K., Clemens, M.J. and Justesen, J. (1998) Activation of 2'-5' oligoadenylate synthetase by single-stranded and double-stranded RNA aptamers. *J Biol Chem*, **273**, 3236-3246.

61. Vachon, V.K. and Conn, G.L. (2016) Adenovirus VA RNA: An essential pro-viral non-coding RNA. *Virus Res*, **212**, 39-52.

62. Desai, S.Y., Patel, R.C., Sen, G.C., Malhotra, P., Ghadge, G.D. and Thimmapaya, B. (1995) Activation of interferon-inducible 2'-5' oligoadenylate synthetase by adenoviral VAI RNA. *J Biol Chem*, **270**, 3454-3461.

63. Vachon, V.K., Calderon, B.M. and Conn, G.L. (2015) A novel RNA molecular signature for activation of 2'-5' oligoadenylate synthetase-1. *Nucleic Acids Res*, **43**, 544-552.

64. Nielsen, S., Yuzenkova, Y. and Zenkin, N. (2013) Mechanism of eukaryotic RNA polymerase III transcription termination. *Science*, **340**, 1577-1580.

65. Wreschner, D.H., McCauley, J.W., Skehel, J.J. and Kerr, I.M. (1981) Interferon action--sequence specificity of the ppp(A2'p)nA-dependent ribonuclease. *Nature*, **289**, 414-417.

66. Malathi, K., Saito, T., Crochet, N., Barton, D.J., Gale, M., Jr. and Silverman, R.H. (2010) RNase L releases a small RNA from HCV RNA that refolds into a potent PAMP. *RNA*, **16**, 2108-2119.

67. Lee, K., Kunkeaw, N., Jeon, S.H., Lee, I., Johnson, B.H., Kang, G.Y., Bang, J.Y., Park, H.S., Leelayuwat, C. and Lee, Y.S. (2011) Precursor miR-886, a novel noncoding RNA repressed in cancer, associates with PKR and modulates its activity. *RNA*, **17**, 1076-1089.

68. Kunkeaw, N., Jeon, S.H., Lee, K., Johnson, B.H., Tanasanvimon, S., Javle, M., Pairojkul, C., Chamgramol, Y., Wongfieng, W., Gong, B. *et al.* (2013) Cell death/proliferation roles for nc886, a non-coding RNA, in the protein kinase R pathway in cholangiocarcinoma. *Oncogene*, **32**, 3722-3731.

69. Jeon, S.H., Lee, K., Lee, K.S., Kunkeaw, N., Johnson, B.H., Holthauzen, L.M., Gong, B., Leelayuwat, C. and Lee, Y.S. (2012) Characterization of the direct physical interaction of nc886, a cellular non-coding RNA, and PKR. *FEBS Lett*, **586**, 3477-3484.

70. Calderon, B.M. and Conn, G.L. (2017) Human noncoding RNA 886 (nc886) adopts two structurally distinct conformers that are functionally opposing regulators of PKR. *RNA*, **23**, 557-566.

71. Calderon, B.M. and Conn, G.L. (2018) A human cellular noncoding RNA activates the antiviral protein 2'-5'-oligoadenylate synthetase 1. *J Biol Chem*, **293**, 16115-16124.

72. Han, J.Q. and Barton, D.J. (2002) Activation and evasion of the antiviral 2'-5' oligoadenylate synthetase/ribonuclease L pathway by hepatitis C virus mRNA. *RNA*, **8**, 512-525.

73. Deo, S., Patel, T.R., Dzananovic, E., Booy, E.P., Zeid, K., McEleney, K., Harding, S.E. and McKenna, S.A. (2014) Activation of 2' 5'-oligoadenylate synthetase by stem loops at the 5'-end of the West Nile virus genome. *PLoS One*, **9**, e92545.

74. Deo, S., Patel, T.R., Chojnowski, G., Koul, A., Dzananovic, E., McEleney, K., Bujnicki, J.M. and McKenna, S.A. (2015) Characterization of the termini of the West Nile virus genome and their interactions with the small isoform of the 2'-5'-oligoadenylate synthetase family. *J Struct Biol*, **190**, 236-249.

75. Sharp, T.V., Raine, D.A., Gewert, D.R., Joshi, B., Jagus, R. and Clemens, M.J. (1999) Activation of the interferon-inducible (2'-5') oligoadenylate synthetase by the Epstein-Barr virus RNA, EBER-1. *Virology*, **257**, 303-313.

76. Maitra, R.K., McMillan, N.A., Desai, S., McSwiggen, J., Hovanessian, A.G., Sen, G., Williams, B.R. and Silverman, R.H. (1994) HIV-1 TAR RNA has an intrinsic ability to activate interferon-inducible enzymes. *Virology*, **204**, 823-827.

77. Andersson, M.G., Haasnoot, P.C., Xu, N., Berenjian, S., Berkhout, B. and Akusjarvi, G. (2005) Suppression of RNA interference by adenovirus virus-associated RNA. *J Virol*, **79**, 9556-9565.

78. Wahid, A.M., Coventry, V.K. and Conn, G.L. (2008) Systematic deletion of the adenovirus-associated RNAI terminal stem reveals a surprisingly active RNA inhibitor of double-stranded RNA-activated protein kinase. *J Biol Chem*, **283**, 17485-17493.

79. Meng, H., Deo, S., Xiong, S., Dzananovic, E., Donald, L.J., van Dijk, C.W. and McKenna, S.A. (2012) Regulation of the interferon-inducible 2'-5'-oligoadenylate synthetases by adenovirus VA(I) RNA. *J Mol Biol*, **422**, 635-649.

80. Cayley, P.J., Davies, J.A., McCullagh, K.G. and Kerr, I.M. (1984) Activation of the ppp(A2'p)nA system in interferon-treated, herpes simplex virus-infected cells and evidence for novel inhibitors of the ppp(A2'p)nA-dependent RNase. *Eur J Biochem*, **143**, 165-174.

81. Taguchi, T., Nagano-Fujii, M., Akutsu, M., Kadoya, H., Ohgimoto, S., Ishido, S. and Hotta, H. (2004) Hepatitis C virus NS5A protein interacts with 2',5'-oligoadenylate synthetase and inhibits antiviral activity of IFN in an IFN sensitivity-determining region-independent manner. *J Gen Virol*, **85**, 959-969.

82. Silverman, R.H. (2007) Viral encounters with 2',5'-oligoadenylate synthetase and RNase L during the interferon antiviral response. *J Virol*, **81**, 12720-12729.

83. Keel, A.Y., Jha, B.K. and Kieft, J.S. (2012) Structural architecture of an RNA that competitively inhibits RNase L. *RNA*, **18**, 88-99.

84. Zhang, R., Jha, B.K., Ogden, K.M., Dong, B., Zhao, L., Elliott, R., Patton, J.T., Silverman, R.H. and Weiss, S.R. (2013) Homologous 2',5'-phosphodiesterases from disparate RNA viruses antagonize antiviral innate immunity. *Proc Natl Acad Sci U S A*, **110**, 13114-13119.

85. Silverman, R.H. and Weiss, S.R. (2014) Viral Phosphodiesterases That Antagonize Double-Stranded RNA Signaling to RNase L by Degrading 2-5A. *J Interferon Cytokine Res*, **34**, 455-463.

86. Thornbrough, J.M., Jha, B.K., Yount, B., Goldstein, S.A., Li, Y., Elliott, R., Sims, A.C., Baric, R.S., Silverman, R.H. and Weiss, S.R. (2016) Middle East Respiratory Syndrome Coronavirus NS4b Protein Inhibits Host RNase L Activation. *MBio*, **7**, e00258.

87. Zhao, L., Jha, B.K., Wu, A., Elliott, R., Ziebuhr, J., Gorbalenya, A.E., Silverman, R.H. and Weiss, S.R. (2012) Antagonism of the interferon-induced OAS-RNase L pathway by murine coronavirus ns2 protein is required for virus replication and liver pathology. *Cell Host Microbe*, **11**, 607-616.

88. Drappier, M., Jha, B.K., Stone, S., Elliott, R., Zhang, R., Vertommen, D., Weiss, S.R., Silverman, R.H. and Michiels, T. (2018) A novel mechanism of RNase L inhibition: Theiler's virus L* protein prevents 2-5A from binding to RNase L. *PLoS Pathog*, **14**, e1006989.

89. Townsend, H.L., Jha, B.K., Han, J.Q., Maluf, N.K., Silverman, R.H. and Barton, D.J. (2008) A viral RNA competitively inhibits the antiviral endoribonuclease domain of RNase L. *RNA*, **14**, 1026-1036.

90. Townsend, H.L., Jha, B.K., Silverman, R.H. and Barton, D.J. (2008) A putative loop E motif and an H-H kissing loop interaction are conserved and functional features in a group C enterovirus RNA that inhibits ribonuclease L. *RNA Biol*, **5**, 263-272.

91. Li, Y., Banerjee, S., Wang, Y., Goldstein, S.A., Dong, B., Gaughan, C., Silverman, R.H. and Weiss, S.R. (2016) Activation of RNase L is dependent on OAS3 expression during infection with diverse human viruses. *Proc Natl Acad Sci U S A*, **113**, 2241-2246.

92. Lin, R.J., Yu, H.P., Chang, B.L., Tang, W.C., Liao, C.L. and Lin, Y.L. (2009) Distinct antiviral roles for human 2',5'-oligoadenylate synthetase family members against dengue virus infection. *J Immunol*, **183**, 8035-8043.

93. Yakub, I., Lillibridge, K.M., Moran, A., Gonzalez, O.Y., Belmont, J., Gibbs, R.A. and Tweardy, D.J. (2005) Single nucleotide polymorphisms in genes for 2'-5'-oligoadenylate synthetase and RNase L inpatients hospitalized with West Nile virus infection. *J Infect Dis*, **192**, 1741-1748.

94. Lim, J.K., Lisco, A., McDermott, D.H., Huynh, L., Ward, J.M., Johnson, B., Johnson, H., Pape, J., Foster, G.A., Krysztof, D. *et al.* (2009) Genetic variation in OAS1 is a risk factor for initial infection with West Nile virus in man. *PLoS Pathog*, **5**, e1000321.

95. Bigham, A.W., Buckingham, K.J., Husain, S., Emond, M.J., Bofferding, K.M., Gildersleeve, H., Rutherford, A., Astakhova, N.M., Perelygin, A.A., Busch, M.P. *et al.* (2011) Host genetic risk factors for West Nile virus infection and disease progression. *PLoS One*, **6**, e24745.

96. Alagarasu, K., Honap, T., Damle, I.M., Mulay, A.P., Shah, P.S. and Cecilia, D. (2013) Polymorphisms in the oligoadenylate synthetase gene cluster and its association with clinical outcomes of dengue virus infection. *Infect Genet Evol*, **14**, 390-395.

97. Thamizhmani, R. and Vijayachari, P. (2014) Association of dengue virus infection susceptibility with polymorphisms of 2'-5'-oligoadenylate synthetase genes: a case-control study. *Braz J Infect Dis*, **18**, 548-550.

98. Field, L.L., Bonnevie-Nielsen, V., Pociot, F., Lu, S., Nielsen, T.B. and Beck-Nielsen, H. (2005) OAS1 splice site polymorphism controlling antiviral enzyme activity influences susceptibility to type 1 diabetes. *Diabetes*, **54**, 1588-1591.

99. Fedetz, M., Matesanz, F., Caro-Maldonado, A., Fernandez, O., Tamayo, J.A., Guerrero, M., Delgado, C., Lopez-Guerrero, J.A. and Alcina, A. (2006) OAS1 gene haplotype confers susceptibility to multiple sclerosis. *Tissue Antigens*, **68**, 446-449.

100. O'Brien, M., Lonergan, R., Costelloe, L., O'Rourke, K., Fletcher, J.M., Kinsella, K., Sweeney, C., Antonelli, G., Mills, K.H., O'Farrelly, C. *et al.* (2010) OAS1: a multiple sclerosis susceptibility gene that influences disease severity. *Neurology*, **75**, 411-418.

101. Mandal, S., Abebe, F. and Chaudhary, J. (2011) 2'-5' oligoadenylate synthetase 1 polymorphism is associated with prostate cancer. *Cancer*, **117**, 5509-5518.

CHAPTER THREE

Human OAS1 activation is highly dependent on both RNA sequence and context of activating RNA motifs

Samantha L. Schwartz, Esther N. Park, Virginia K. Vachon, Shamika Danzy,
Anice C. Lowen and Graeme L. Conn

The following chapter has been published:

Schwartz, S.L., Park, E.N., Vachon, V.K., Danzy, S., Lowen, A.C. and Conn, G.L. (2020). Human OAS1 activation is highly dependent on both RNA sequence and context of activating RNA motifs. *Nucleic Acids Res.* **48**(13), 7520-7531 (PMID: 32678884).

Author Contributions: S.L.S., V.K.V., A.C.L., and G.L.C. participated in research design. S.L.S.*, E.N.P., and S.D. performed experiments. S.L.S., A.C.L., and G.L.C. analyzed data. S.L.S. and G.L.C. wrote the manuscript.

[*S.L.S. performed the majority of experiments shown in Figures 2 and 4-6.]

ABSTRACT

2’-5’-oligoadenylate synthetases (OAS) are innate immune sensors of cytosolic double-stranded RNA (dsRNA) and play a critical role in limiting viral infection. dsRNA binding induces allosteric structural changes in OAS1 that reorganize its catalytic center to promote synthesis of 2’-5’-oligoadenylate and thus activation of endoribonuclease L. Specific RNA sequences and structural motifs can also enhance activation of OAS1 through currently undefined mechanisms. To better understand these drivers of OAS activation, we tested the impact of defined sequence changes within a short dsRNA that strongly activates OAS1. Both *in vitro* and in human A549 cells, appending a 3’-end single-stranded pyrimidine (3’-ssPy) can strongly enhance OAS1 activation or have no effect depending on its location, suggesting that other dsRNA features are necessary for correct presentation of the motif to OAS1. Consistent with this idea, we also find that the dsRNA binding position is dictated by an established consensus sequence (WWN_9WG). Unexpectedly, however, not all sequences fitting this consensus activate OAS1 equivalently, with strong dependence on the identity of both partially conserved (W) and non-conserved (N_9) residues. A picture thus emerges in which both specific RNA features and the context in which they are presented dictate the ability of short dsRNAs to activate OAS1.

INTRODUCTION

The innate immune system detects diverse foreign molecules, or pathogen-associated molecular patterns (PAMPs), to provide a critical line of defense against infection (1,2). Double-stranded RNA (dsRNA) is often a hallmark of viral infection, present in viral genomes or produced as a consequence of viral gene expression or replication (3-5). dsRNA is thus a potent PAMP detected by several distinct human cellular pattern recognition receptors, including the 2'-5'-oligoadenylate synthetase (OAS) family of cytosolic dsRNA sensors which restrict replication of multiple viruses (6,7).

In humans, the *OAS* family contains four genes that encode three catalytically active enzymes (OAS1, OAS2, and OAS3) and one catalytically inactive protein (OASL) (8). Activation of each catalytically active OAS enzyme by dsRNA leads to the non-processive synthesis of 2'-5'-linked oligoadenylate (2-5A) molecules which promote dimerization and activation of latent endoribonuclease L (RNase L) (9-12). Activated RNase L degrades single-stranded viral and cellular RNA, including specific mRNAs, tRNA, and rRNA (13-18), thereby halting viral replication and limiting the spread of infection (19,20). The central importance of the OAS/RNase L pathway in control of infection is also reflected by the diverse array of viral mechanisms that inhibit this pathway or subvert the consequences of OAS activation (21-33).

OAS1 is capable of sensing short dsRNAs (>18 bp) and its antiviral role is supported by the identification of OAS1 single nucleotide polymorphisms (SNPs) important for determining susceptibility to West Nile virus infections (34-36). There is also accumulating evidence for essential roles played by OAS1 in normal cell function. For example, OAS1 SNPs have also been implicated in altered cellular function leading to diseases including diabetes (37), multiple sclerosis (38,39), prostate cancers (40), and Sjögren's syndrome (41,42), as well as susceptibility to tuberculosis infection (43). OAS1 has also been recently implicated in cancer cell survival after treatment with DNA damaging agents (44) and in mediating the cytotoxicity of 5-azacytidine (AZA), a DNA methyltransferase inhibitor widely used in cancer treatment (45).

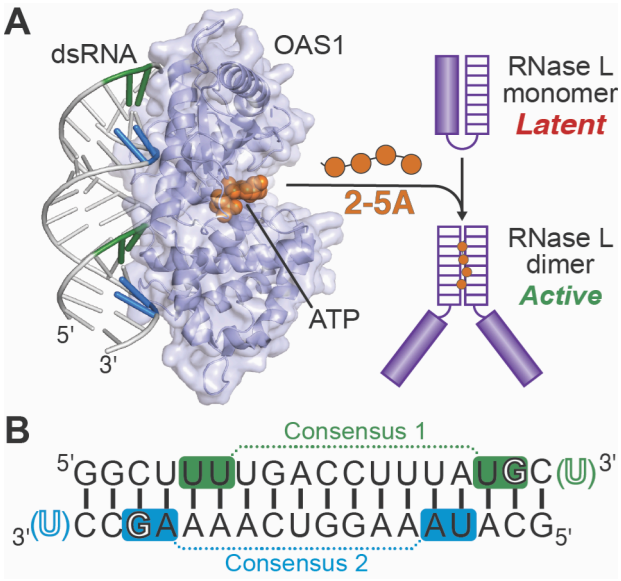

Figure 1. The OAS1/RNase L pathway and 18 bp dsRNA design. ***A,*** Upon binding dsRNA (*left*), OAS1 (shown as a cartoon with semi-transparent surface; PDB ID 4IG8) produces 2'-5'-oligoadenylate molecules (2-5A; *orange*) which promote dimerization and activation of RNase L (*right*). ***B,*** Sequence of the 18 bp dsRNA used in structural studies of the human OAS1-dsRNA complex (47) and as a starting point for the studies described here. This dsRNA contains two copies of a known OAS1 activation consensus sequence (WWN_9WG) highlighted in both panels for Consensus 1 (*green*) and Consensus 2 (*blue*) on the top and bottom strands, respectively. The conserved consensus G nucleotide, which makes a base-specific contact with OAS1, and placements of the 3'-ssPy motif (*green* or *blue* U) used here in specific dsRNA constructs are also indicated with outline font.

Taken together, these studies suggest important roles for OAS1 in both innate immunity and other cellular processes that we have yet to fully elucidate.

OAS1 lacks a canonical RNA-binding motif and instead interacts with dsRNA through a relatively flat surface of positive residues on the opposite side of the protein from its ATP binding sites and catalytic center (46-48). dsRNA binding allosterically induces conformational changes in the OAS1 active site, driving polymerization of ATP into 2-5A (**Figure 1A**). Despite available OAS1 structural data, there is still relatively little known about how specific features of dsRNA contribute to the potency of OAS1 activation. Defining the contributions made by specific sequences and other RNA molecular signatures will be essential to fully elucidate how OAS1 is regulated by viral or cellular dsRNA.

OAS1 activation is strongly enhanced by at least two distinct activating consensus sequences (49,50): APyAPy(N)nCC, UU(N)nACCC (where Py is C or U, and N is any nucleotide) and WWN_9WG (where W is A or U). Our subsequent discovery of the 3'-end single-stranded pyrimidine (3'-ssPy) motif revealed that OAS1 activation can be further enhanced by single-stranded pyrimidine-rich (C or U) sequences appended to the 3'-end of a short (18 bp) activating dsRNA, as well as other more complex viral and cellular non-coding RNAs (51,52). The 3'-ssPy motif is naturally found on non-coding RNAs as a consequence of RNA polymerase III transcription termination (53), and we have previously speculated that such 3'-ends might also occur as a result of RNase L cleavage at preferred single-stranded UA or UU sequences within larger RNA molecules, further potentiating signaling via the OAS/RNase L pathway (51). In contrast, another recent study found that the 3'-ssPy motif had no effect on OAS1 activation (54). These conflicting observations suggest that the dsRNA context in which the 3'-ssPy motif is presented to OAS1 can affect its ability to enhance 2-5A synthesis and that, more generally, our understanding of how different activating motifs can combine for optimal OAS1 activation is incomplete.

The 18 bp dsRNA used in the human OAS1-dsRNA co-crystal structure (47) contains two overlapping, antiparallel copies of the WWN_9WG consensus sequence (**Figure 1B**). The complexities of elucidating the contributions of activating motifs even within short dsRNAs are highlighted by the fact OAS1 bound this dsRNA in a single orientation despite the presence of two potential binding sites containing a preferred activation sequence. Here, the requirements for OAS1 activation by short dsRNAs are explored further using variations on this model 18 bp dsRNA. These studies reveal that binding orientation-specific activation also exists in solution and that OAS1 activation by short dsRNAs is unexpectedly sensitive to both RNA sequence and the relative organization of activating motifs.

MATERIALS AND METHODS

OAS1 protein expression and purification

Human OAS1 was expressed in *Escherichia coli* BL21(DE3) as an N-terminal 6xHis-SUMO fusion of amino acids 1-346 (corresponding to the common, core residues of all OAS1 splicing isoforms) from vector pE-SUMO (LifeSensors). Cells were grown in lysogeny broth (LB) at 37°C to mid-log phase (optical density at 600 nm of ~0.5), and protein expression was induced with 0.5 mM isopropyl β-D-1-thiogalactopyranoside (IPTG) with continued growth overnight at 20°C. Cells were lysed by sonication in 50 mM Tris-HCl buffer (pH 8.0) containing 300 mM NaCl, 20 mM imidazole, 10% (v/v) glycerol, and 10 mM β-mercaptoethanol. SUMO-OAS^{1-346} fusion protein was purified from cleared lysate by Ni^{2+}-affinity chromatography on an ÄKTApurifier 10 FPLC system (GE Healthcare) and dialyzed overnight against SUMO cleavage buffer, containing 50 mM Tris-HCl (pH 8.0), 150 mM NaCl, 10% (v/v) glycerol, and 2 mM DTT. The partially purified fusion protein was then stored at -80°C. Prior to each experiment, the N-terminal 6xHis-SUMO tag was cleaved by incubating SUMO-OAS^{1-346} fusion protein with SUMO protease (Ulp1) for 90 minutes at 30°C and an additional hour at 4°C, followed by dialysis against the appropriate assay buffer. This process produces OAS^{1-346} with a native N-terminus after SUMO tag removal.

Generating 18 bp dsRNA duplexes

Each RNA strand was chemically synthesized (Integrated DNA Technologies) and used without further purification. Each 18 bp dsRNA duplex was generated by mixing individual strands at equimolar concentrations and annealing by heating to 65°C for 10 minutes followed by slow cooling to room temperature. Native PAGE (20% acrylamide in 0.5x Tris-Borate-EDTA) was used to verify the homogeneity of both single-strand RNAs and dsRNA duplexes prior to use. Each lane contained RNA (100 ng total) resolved on gels run at 120V for 3 hours at 4°C,

visualized by staining with SYBR Gold (1:10,000, Invitrogen), and imaged on a Typhoon Trio Imager (GE Healthcare).

Chromogenic assay of OAS1 activity

OAS^{1-346} was dialyzed overnight against OAS1 activity assay buffer: 50 mM Tris-HCl (pH 7.4) containing 100 mM NaCl, 1 mM EDTA, and 1 mM DTT. Pyrophosphate (PP_i), the reaction by-product of 2-5A synthesis by OAS1, was monitored using a chromogenic assay adapted from previously established methods for measurement of OAS1 activity (51,52,55). OAS^{1-346} (100 nM) was incubated with 10 µg/ml poly(rI:rC) or 300 nM dsRNA in reactions containing final solution conditions of 25 mM Tris-HCl (pH 7.4), 10 mM NaCl, 7 mM $MgCl_2$, 1 mM DTT, and 2 mM ATP at 37°C in a 150 µl total reaction volume. Aliquots (10 µl) were removed over a 0-120 minute time course and the reaction immediately quenched by adding directly to the wells of a 96-well plate pre-dispensed with 250 mM EDTA (pH 8.0, 2.5 µl). At completion of the time course, 2.5% (w/v) ammonium molybdate in 2.5 M H_2SO_4 (10 µl) and 0.5 M β-mercaptoethanol (10 µl) were added to each well and the final volume brought to 100 µl with water. Absorbance at 580 nm was measured using a Synergy Neo2 plate reader (BioTek). Readings were subtracted from background using an ATP-only control reaction (lacking both OAS^{1-346} and dsRNA) and then converted to pyrophosphate produced (nmols) using a pyrophosphate standard curve. Experiments were performed as four independent assays using two different preparations of OAS^{1-346}, each comprising three technical replicates which were averaged prior to data analysis. Final values were plotted with their associated standard error of the mean (SEM) in GraphPad Prism 8.

Kinetic analyses were performed similarly but using a range of dsRNA concentrations (0.1-5 µM) and measuring PP_i production only for the initial 12 minutes of the reaction with two technical replicates for each experiment. Linear regression analysis was used to obtain initial rates of reaction (nmol PP_i produced/minute) for each dsRNA concentration. These values were

plotted and a non-linear regression analysis performed to obtain V_{max} and K_{app} values using the Michaelis-Menten model equation $Y=(V_{max}X)/(K_{app}+X)$ in GraphPad Prism 8.

OAS1/RNase L activation in A549 cells

Human wild-type and RNase L knock-out A549 cells, constructed using CRISPR-Cas9 gene editing technology as reported previously (6), were cultured in RPMI1640 cell culture medium supplemented with 10% fetal bovine serum and 100 µg/ml Normocin™. Both cell lines were monitored regularly and tested negative for mycoplasma. Cells were seeded into 12-well plates at $3x10^5$ cells/well and were treated with 5000 U/ml Interferon-α (Sigma) prior to dsRNA transfection. Following overnight interferon treatment (16 hours), cells were transfected with dsRNAs (50 nM) or poly(rI:rC) (0.1 µg/ml) using siLentFect Lipid Reagent (BioRad) and incubated at 37°C for 6 hours. Cells were lysed and total RNA was isolated using a RNeasy Plus Mini Kit (Qiagen) following manufacturer instructions. Total RNA was resolved using an Agilent 2100 Bioanalyzer system. At least two independent sets of experiments were performed with essentially identical results for both the wild-type (n=3) and RNase L knock-out (n=2) cells, respectively. Bands resulting from 28S rRNA cleavage in wild-type A549 cells were quantified using ImageJ and relative cleavage was calculated for each set of averaged technical replicates by normalizing to activity induced by the 18 bp dsRNA with no 3'-ssPy.

OAS1-dsRNA 4-thiouridine (4-thioU) crosslinking

RNA strands containing a 3'-ssPy motif modified with a 4-thiouridine were chemically synthesized (Dharmacon), purified by high performance liquid chromatography (HPLC), and 2'-deprotected before use. RNA strands containing the 4-thiouridine modification (3'-end) were 5'-end labeled using [γ-^{32}P]-ATP and T4 polynucleotide kinase (PNK), excess [γ-^{32}P]-ATP was removed using an Illustra MicroSpin G-25 column (GE Healthcare), and radiolabel incorporation was quantified by scintillation counting. The radiolabeled 18 bp dsRNA duplexes were generated by mixing the radiolabeled strand (containing 4-thiouridine) with the same unlabeled

strand and a slight total excess of unlabeled complement. The mixed strands were annealed by heating to 65°C for 10 minutes followed by slow cooling to room temperature. OAS^{1-346} was dialyzed overnight against OAS1 activity assay buffer but lacking DTT, *i.e.* 50 mM Tris-HCl (pH 7.4) containing 100 mM NaCl and 1 mM EDTA.

OAS^{1-346} (5 μM) was incubated with radiolabeled, 4-thiouridine containing 18 bp dsRNA duplex (500 nM) for 30 minutes on ice with UV exposure at 365 nm and using a 96-well plate format at a distance of 3 cm. Reactions were stopped by addition of SDS loading buffer and heating to 95°C for 5 minutes. Reaction products were resolved on a 10% SDS-PAGE run at 200V for 45 minutes to allow for sufficient separation of OAS1-dsRNA complex and free RNA. Gels were soaked in destain solution (50:40:10% ethanol:water:acetic acid; 15 minutes), fixed (20% ethanol, 2% glycerol; 15 minutes), dried, and imaged using a Typhoon FLA 7000 PhosphorImager and ImageQuant software (GE Healthcare).

RESULTS

The 3'-ssPy motif enhances OAS1 activation only when appended to the *top* strand of the 18 bp dsRNA

Our previous analysis of OAS1 activation by the model 18 bp dsRNA revealed that a single 3'-end unpaired U nucleotide (3'-ssPy motif) appended to one strand of the dsRNA was sufficient to potentiate OAS1 activation *in vitro* (51). In this original study, the 3'-ssPy motif was placed on the "top" RNA strand (as depicted in **Figure 1B**), corresponding to the dsRNA end closest to the base-specific interaction made by OAS1 (via the Ser56 backbone carbonyl group) to the activation consensus guanosine nucleotide ($WWN_9W\underline{G}$) in the OAS1-dsRNA complex crystal structure. However, the question remained as to whether addition of a 3'-ssPy motif to the complementary ("bottom") strand of this dsRNA could similarly enhance OAS1 activity. Enhanced activation by a 3'-ssPy on the bottom strand would indicate a lack of dsRNA binding preference or absence of orientation-specific activation in solution. In contrast, a different impact

of a 3'-ssPy on the bottom strand would reveal a binding preference in solution similar to that observed in the human OAS1-dsRNA crystal structure. Thus, addition of a 3'-ssPy to either strand of this model dsRNA can serve as a tool to assess OAS1 sensitivity to dsRNA binding orientation and OAS1 activation in solution.

To address this open question, we generated and compared four 18 bp dsRNAs derived from the model dsRNA duplex used in the OAS1-dsRNA complex crystal structure (**Figure 1**): no 3'-ssPy motif, top strand only, bottom strand only, and on both strands. For these analyses, one 3'-end single-stranded U nucleotide was used to represent the 3'-ssPy motif as our previous study showed a single additional pyrimidine was sufficient and addition of U or C-rich sequences were functionally equivalent in their ability to enhance OAS1 activation (51). Each dsRNA was generated by annealing the corresponding single-strand RNAs and stable duplex formation confirmed by native polyacrylamide gel electrophoresis (PAGE; **Figure 2A**). Each dsRNA was then tested in an established *in vitro* OAS1 activation assay, which measures the amount of inorganic pyrophosphate (PP_i) produced as a consequence of dsRNA-induced 2-5A synthesis. As previously observed (51), the level of OAS1 activity is significantly enhanced by addition of a top strand 3'-ssPy motif compared to the unaltered dsRNA (**Table 1** and **Figure 2B**, compare green and black curves, respectively). In contrast, addition of a 3'-ssPy to the bottom strand had no effect on OAS1 activation (**Table 1** and **Figure 2B**, compare blue and black curves), while its addition in the context of a top strand 3'-ssPy motif only modestly further increased activation (**Table 1** and **Figure 2B**, compare orange and green curves). Thus, the 3'-ssPy motif only significantly impacts OAS1 activation by this short dsRNA when appended to the top strand.

To assess whether the 3'-ssPy location can affect dsRNA-OAS1 interaction, we used OAS1-dsRNA crosslinking by exploiting the presence of the 3'-ssPy motif to site-specifically incorporate the photoreactive crosslinker 4-thiouridine (4-thioU). The modified single uridine (3'-ssPy motif) was added individually to each end of the dsRNA to generate top or bottom strand

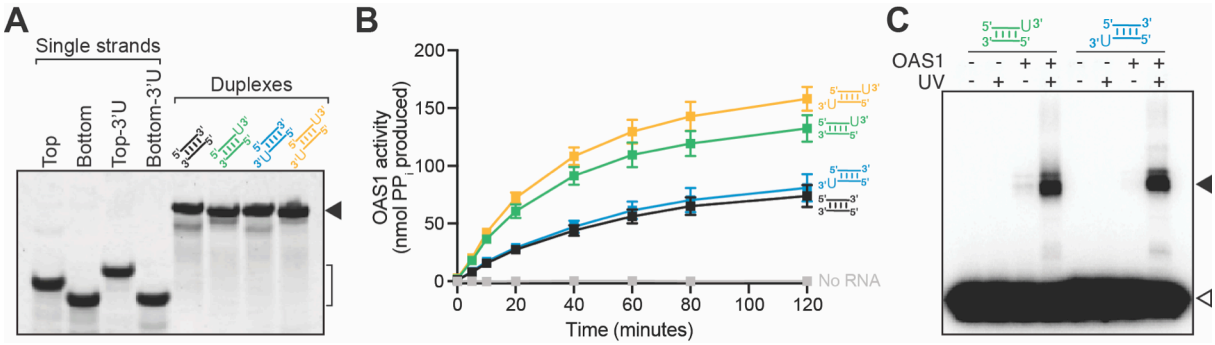

Figure 2. The 3'-ssPy motif impacts OAS1 activity *only* when appended to the top strand. ***A,*** Native PAGE analysis showing purity of the individual chemically synthesized ssRNAs and stable formation of each dsRNA, indicated by the bracket and solid arrowhead on the right of the image, respectively. ***B,*** Reaction progress curves from an *in vitro* chromogenic assay of OAS1 activity using a single dsRNA concentration (300 nM) for no 3'-ssPy (*black*), or with the motif appended to the top (*green*), bottom (*blue*), or both strands (*orange*). OAS1 activation is substantially enhanced only when the 3'-ssPy motif is placed on the top strand. ***C,*** OAS1-dsRNA crosslinking induced by irradiation with UV light (365 nm) resolved by SDS-PAGE to separate crosslinked complex (*solid arrow*) from free RNA (*open arrow*). ssRNAs containing 4-thioU modifications were 5'-end labeled with ^{32}P for visualization prior to annealing. Both dsRNAs crosslink to OAS1 via the 4-thioU regardless of 3'-ssPy motif location.

4-thioU 18 bp dsRNAs which were crosslinked to OAS1 (present in 10× excess) by exposure to 365 nm UV light. In each dsRNA, the RNA strand containing the 4-thioU modification was also 5'-end ^{32}P-labeled for visualization by autoradiography. Crosslinking and control reactions were resolved by SDS-PAGE to separate crosslinked OAS1-dsRNA complexes from free dsRNA (**Figure 2C**), revealing both 3'-ssPy-containing dsRNAs to be specifically, and to similar extents, crosslinked to OAS1 upon UV light treatment (**Figure 2C**, lanes 4 and 8). Therefore, the observed differences in OAS1 *in vitro* activity for these two dsRNAs (**Table 1** and **Figure 2B**; green and blue) do not appear to be due to significant differences in the nature or extent of OAS1-dsRNA complex formation (**Figure 2C**).

Short dsRNAs activate the OAS1/RNase L pathway in human A549 cells mirroring their capacity to activate OAS1 *in vitro*

We next tested the ability of the same four 18 bp dsRNAs to activate the OAS1/RNase L pathway in human lung carcinoma A549 cells as assessed by RNase L-mediated rRNA cleavage. A549 cells were selected for these experiments because they express OAS1 well, are amenable to transfection with small RNAs, and are the same background used to generate an RNase L CRISPR-Cas9 knock-out cell line (6). Because the model dsRNAs are only 18 bp in length, they are too short to activate either OAS2 or OAS3 (54,56,57) and must therefore act exclusively via OAS1 to promote RNase L activation. For these experiments, A549 cells were transfected with one of the four dsRNAs, containing (or lacking) 3'-ssPy motif(s), in parallel with poly(rI:rC) dsRNA transfection and mock transfected cells, as positive and negative controls, respectively.

Transfection with each dsRNA duplex or poly(rI:rC) dsRNA resulted in rRNA degradation (**Figure 3A** and **Table 1**) compared to the mock-transfected control and consistent with activation of the OAS1/RNase L pathway. Further, dsRNAs containing the 3'-ssPy on the top strand or on both strands (**Figure 3A**, green and orange, respectively) resulted in more cleavage overall compared to the dsRNAs containing 3'-ssPy on the bottom strand or lacking a 3'-ssPy (**Figure 3A**, blue and black, respectively). Thus, these cell-based assays of OAS1 activation correlate well with the respective capacity of each dsRNA to activate OAS1 in the *in vitro* activity assay. Additionally, a dsRNA with identical nucleotide content to the 18 bp dsRNA but with different sequence ("Scramble" dsRNA) completely failed to activate RNase L, also consistent with its *in vitro* activity (see below). The higher overall rRNA cleavage observed for poly(rI:rC) dsRNA is likely due to its higher potency and additional capacity to activate OAS2 and OAS3 (58). Furthermore, dsRNA-mediated rRNA cleavage activity is completely absent in A549 cells lacking RNase L (RNase L KO A549; **Figure 3B**) confirming that the observed rRNA

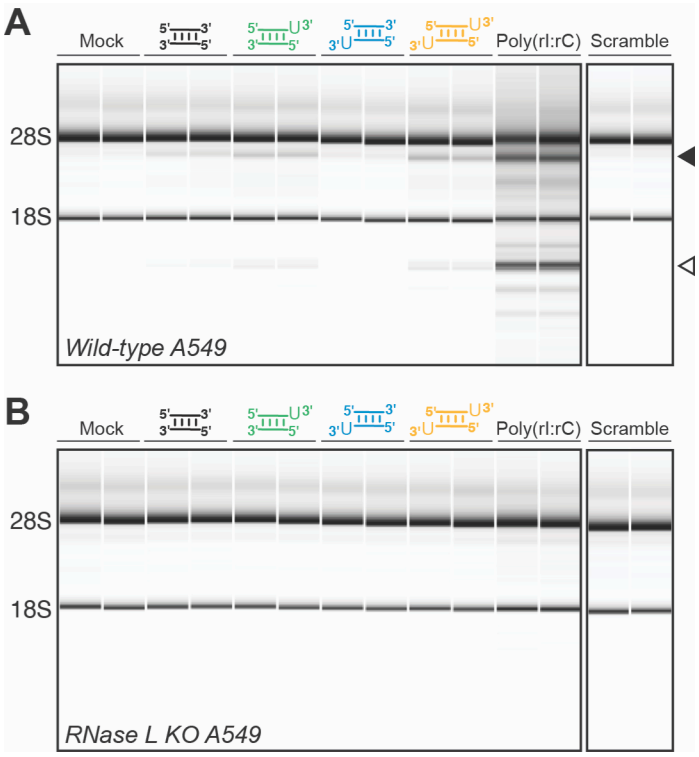

Figure 3. OAS/RNase L pathway activation in A549 cells by the short dsRNAs correlates with their ability to activate OAS1 *in vitro*. *A,* Bioanalyzer analysis of rRNA integrity in A549 cells following transfection with the indicated dsRNAs (18 bp dsRNAs with 3'-ssPy motifs appended as indicated and an 18 bp Scramble dsRNA). Mock transfection and transfection with poly(rI:rC) dsRNA serve as negative and positive controls, respectively. OAS1/RNase L pathway activation is indicated by 28S and 18S rRNA degradation (*arrows*). Quantification of the 28S rRNA cleavage product (*solid arrow)* is given in **Table 1**. ***B,*** As for *panel A* but using A549 RNase L KO cells (6). In both panels, a representative analysis with technical duplicates for each RNA is shown for one of at least two independent experiments which showed essentially identical results.

cleavage by the dsRNAs results exclusively from activation of the OAS/RNase L pathway via OAS1.

The results of both the *in vitro* and cell-based assays are consistent with either an OAS1 binding orientation preference for the 18 bp dsRNA (like that observed in the crystal structure), or a difference in ability of the dsRNA to activate OAS1 when bound in each of its two possible orientations. Either scenario is surprising, given that each strand of the dsRNA contains a sequence that conforms to the WWN_9WG activation consensus sequence. However, the two

potential binding orientations and the consensus sequence they each present to OAS1 are apparently non-equivalent in either their ability to bind OAS1, activate OAS1, or both.

The 3'-ssPy placement can alter apparent dsRNA affinity and maximal OAS1 activation

To define the basis of the differing capacity of the 18 bp dsRNAs to activate OAS1, we used the *in vitro* OAS1 activity assay to assess enzyme activation over a wide range of dsRNA concentrations. Initial rates of reaction at each dsRNA concentration were determined and used to derive the maximum reaction velocity (V_{max}) and apparent RNA dissociation constant (K_{app}), as a measure of OAS1 catalytic activity and proxy for dsRNA binding affinity, respectively (**Figure 4A**,**B** and **Table 1**). Both dsRNAs containing the motif exhibited a decreased K_{app}, corresponding to higher apparent dsRNA affinities, of 2.5-fold (top strand 3'-ssPy; **Figure 4B**, green) and 1.5-fold (bottom strand 3'-ssPy; **Figure 4B**, blue) compared to the dsRNA completely lacking a 3'-ssPy (**Figure 4B**, black). In contrast, while there was no measurable change in V_{max} with a top strand 3'-ssPy, we observed a modest decrease (1.5-fold) for a bottom strand placement of the motif. Therefore, the differences in OAS1 activity for these dsRNA duplexes appear to be due, at least in part, to changes in both apparent RNA affinity and maximum rate of 2-5A produced by OAS1 in the presence of each dsRNA. Specifically, a top strand 3'-ssPy reduces the dsRNA concentration required to reach maximal OAS1 activation but does not influence OAS1 V_{max}. In contrast, a bottom strand 3'-ssPy increases apparent dsRNA affinity (albeit to a lesser extent) and reduces the maximal activation of the enzyme. Thus, the 3'-ssPy appears to have context-dependent impacts on the kinetics of OAS1 activation.

Altering the distance between the 3'-ssPy motif and the consensus sequence impacts its ability to enhance OAS1 activation

We next asked whether the proximity of each consensus sequence to its corresponding 3'-end is the critical factor in determining the ability of a 3'-ssPy at each location on the 18 bp model

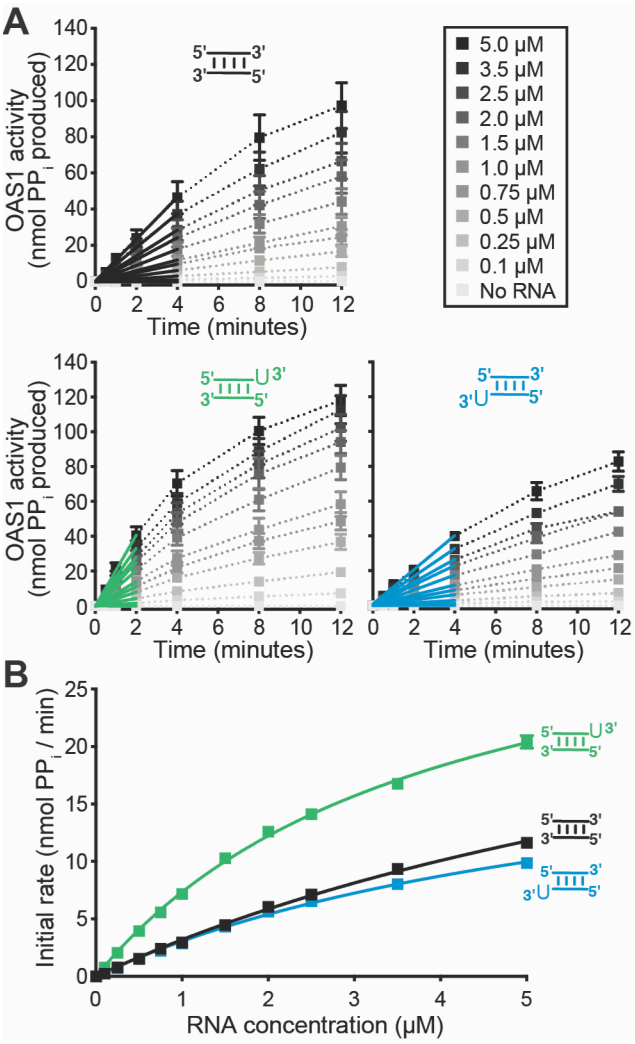

Figure 4. The 3'-ssPy motif differentially alters the kinetics of OAS1 activation when appended to the top or bottom strand. ***A,*** Progress curves for dsRNA containing no (*black*), top (*green*), or bottom (*blue*) 3'-ssPy motifs over a range of dsRNA concentrations (0-5 μM) to determine initial rates of pyrophosphate (PP_i) production. Data were fit using linear regression analysis for the first 2-4 minutes of the reaction (*color-coded solid lines*) in order to obtain the initial rate. ***B,*** Kinetic analyses using calculated initial rates from *panel A* for OAS1 activation by each dsRNA variant. Data were fit using non-linear regression analysis to obtain the V_{max} and K_{app} values shown in **Table 1**. All error bars indicate standard error of the mean (SEM) and may not be visible if their width is smaller than the data point used.

dsRNA to enhance OAS1 activation. Specifically, the top strand WWN_9WG consensus and adjacent 3'-ssPy are separated by one base pair, while the equivalent sequences on the bottom strand are separated by two base pairs. We therefore generated a new 18 bp dsRNA in which

the additional G-C base pair separating the terminal G of the consensus sequence on the lower strand from the 3'-end of the RNA was "moved" to the opposite end of the dsRNA (**Figure 5A**). Thus, this new dsRNA context ("Base Pair Move") has an increased distance between the top strand consensus sequence and its corresponding 3'-ssPy motif (by +1 bp) and an equivalent decrease in this distance for the bottom strand (by -1 bp), while maintaining the length of the dsRNA as 18 bp. We predicted that if the relative spacing of the consensus sequence and 3-ssPy is critical that we should observe an increase in activation resulting from a 3'-ssPy placed on the bottom strand, and a concomitant decrease in the effect conferred by the motif when appended on the top strand.

A set of four equivalent dsRNAs with the G-C base pair moved was generated (*i.e.* with no 3'-ssPy, top strand only, bottom strand only, and both strands) and each dsRNA was evaluated by native PAGE, as before (**Figure 5B**). The movement of this single base pair had two unanticipated effects on the extent of OAS1 activation, both modestly increasing activation in the absence of any appended 3'-ssPy while also decreasing activation by the most potent dsRNA, *i.e.* with the motif on both strands (**Table 1** and **Figure 5C**, black and orange curves, respectively). Pairwise comparisons of each 3'-ssPy addition in the context of both the 18 bp dsRNA and Base Pair Move dsRNA were conducted to determine whether the resulting activation level of OAS1 was altered in a manner corresponding with the spacing between each consensus and its associated 3'-end. As anticipated, addition of a 3'-ssPy to the bottom strand of the Base Pair Move dsRNA resulted in increased OAS1 activation (**Figure 5D**, *center*). In contrast, addition of the motif to the top strand of the Base Pair Move dsRNA (now with increased spacing between the consensus and 3'-ssPy) no longer increased OAS1 activation (**Figure 5D**, *left*). Addition of a 3'-ssPy motif to both strands of the Base Pair Move dsRNA resulted in no further activation of OAS1 compared to addition to the bottom strand only, (**Figure 5C** and **5D**, *right*), confirming the switch in 3'-ssPy sensitivity to the bottom strand in this altered dsRNA context.

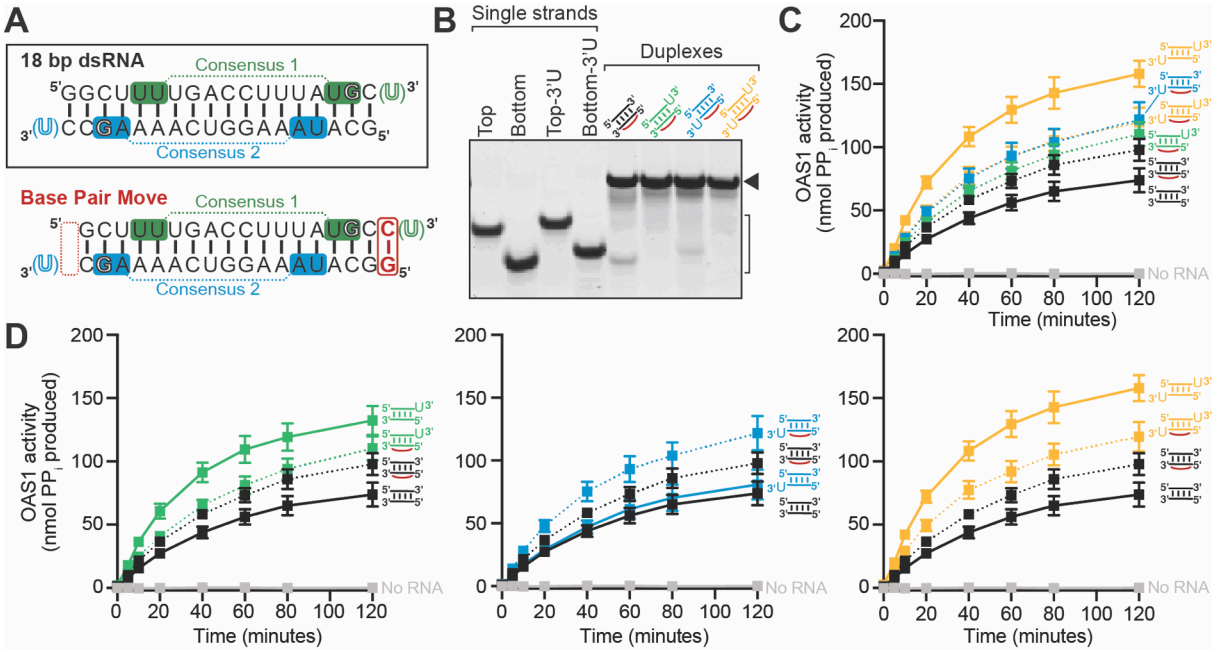

Figure 5. The relative context of the 3'-ssPy motif and consensus sequence is important for OAS1 activation. ***A,*** Schematic of the Base Pair Move dsRNA which is altered compared to the original 18 bp dsRNA by movement of a single G-C base pair from one end (*left, dotted red line*) to the other (*right, solid red line*). The original 18 bp dsRNA is shown (*black box*) for comparison. ***B,*** Native gel analysis showing purity of ssRNAs (*bracket*) and stable formation of each dsRNA (*solid arrow*). ***C,*** OAS1 enzyme progress curves comparing all Base Pair Move dsRNAs (*dotted lines*); curves for the original 18 bp dsRNA with no 3'-ssPy (*solid black line*) and 3'-ssPy appended on both strands (*solid orange line*) are the same as in **Figure 2B** and are shown for comparison to indicate the reduced overall range of activation by the Base Pair Move dsRNAs. ***D,*** OAS1 enzyme progress curves are shown as pair-wise comparisons for each 3'-ssPy variant in both the 18 bp dsRNA (*solid lines*) and Base Pair Move (*dotted lines*) contexts: no 3'-ssPy (*black*), top stand only (*green*), bottom strand only (*blue*), and on both strands (*orange*). The No RNA control (*grey*) is also shown in each panel.

These data thus support the idea that the nucleotide spacing between the consensus sequence and a 3'-ssPy appended to the end of the same strand is important for the latter motif's optimal placement and thus ability to potentiate OAS1 activation. These observations also suggest that OAS1 binds the 18 bp dsRNA in both orientations but that these binding modes do not result in equivalent OAS1 activation. Furthermore, the unexpected changes in activation with the single G-C base pair movement, which resulted in a narrower range of OAS1

activation, also suggest there are other elements of RNA sequence, in addition to the relative placement of the consensus sequence and 3'-ssPy, that contribute to the ability of a given dsRNA to activate OAS1.

OAS1 activation consensus sequence nucleotide identities (WW/WG) and their placement within a dsRNA are important for OAS1 activation

Given the unexpected sensitivity of the 18 bp dsRNA to the movement of a single base pair, we next asked whether the specific nucleotides within the consensus sequence (*i.e.* WW/WG and the intervening N_9 spacer) also influence the extent of OAS1 activation. Three new dsRNA constructs were designed (**Figure 6A**): (i) a "Scramble" dsRNA in which the order of most (15 of 18) nucleotides is altered while maintaining the nucleotide content of each strand; (ii) a "Scramble (Consensus)" dsRNA in which the top and bottom strand WW/WG consensus nucleotides of the original 18 bp dsRNA are maintained within this new scrambled background; and (iii) a "Consensus Strand Swap" variant in which only the top and bottom strand WW/WG consensus nucleotides of the original 18 bp dsRNA are exchanged. Collectively, these new dsRNAs were designed to test the influence of overall dsRNA sequence, the nucleotides flanking the consensus sequences, and the specific nucleotide identities of the two different consensus sequences. In all three new dsRNA constructs, additional changes were made as required to maintain perfect Watson-Crick dsRNA base pairing (**Figure 6A**,**B**).

Remarkably, the Scramble dsRNA was completely unable to activate OAS1 *in vitro* (**Figure 6C**; mauve and grey curves, respectively) or in A549 cells (**Figure 3**), underscoring the unexpectedly strong sensitivity of OAS1 to specific dsRNA sequence. Returning the nucleotides (WW/WG) of the two OAS1 consensus sequences to their original locations within this new dsRNA background restored OAS1 activation, but not to the same extent as for the original dsRNA sequence (**Figure 6C**; compare purple and black curves, respectively). In this partially restored dsRNA context, we also tested the impact of addition of the 3'-ssPy motif on OAS1

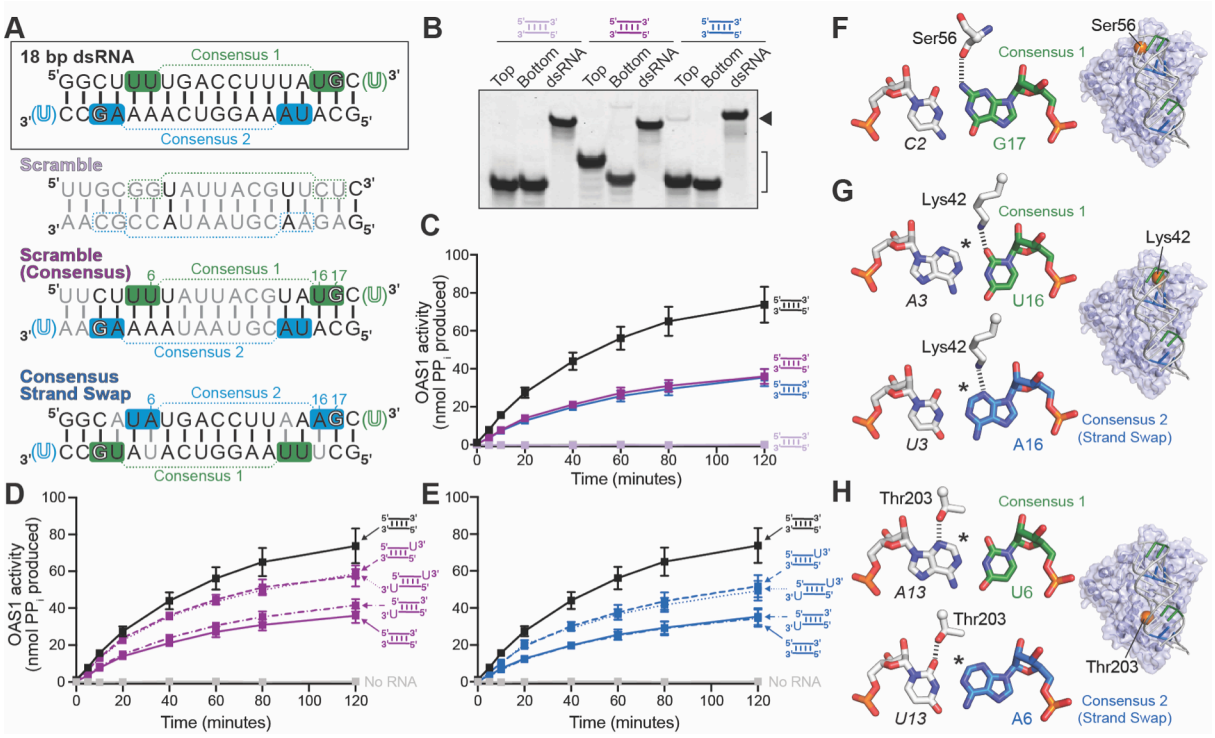

Figure 6. The OAS1 activation consensus sequence (WWN$_9$WG) and its placement within dsRNA are also important for OAS1 activation. ***A,*** Schematics of the additional 18 bp dsRNAs indicating the sequence changes to create the Scramble (nucleotides with altered identity are in *grey*), Scramble (Consensus), and Consensus Strand Swap. The original 18 bp dsRNA is shown (*black box*) for comparison. ***B,*** Native gel analysis showing purity of ssRNAs (*bracket*) and stable formation of each dsRNA (*solid arrow*). ***C,*** Progress curves for OAS1 activation by the Scramble (*mauve*), Scramble (Consensus) (*purple*), and Consensus Strand Swap (*blue*) dsRNAs compared to the original 18 bp dsRNA (*black*). ***D,*** Progress curves for OAS1 activation for the Scramble (Consensus) with each possible 3'-ssPy variation (*i.e.* none, top, bottom, or both strands). ***E,*** same as in *panel D*, except for the Consensus Strand Swap dsRNA. ***F-H,*** Views of the base pair interactions of consensus sequence nucleotides (WW^{6}/^{16}WG^{17}) directly contacted by OAS1 residues in the human OAS1-dsRNA structure (PDB 4IG8). The location of each OAS1 residue on the dsRNA binding surface is shown on a cartoon with semi-transparent surface rendering of the OAS1-dsRNA complex structure (indicated with an enlarged orange sphere at the residue's C_α atom). The view shown for each residue is related to that of **Figure 1A** by a 90° rotation around the y-axis. The asterisk in *panels G* and *H* denotes the approximate position of additional atoms of the exocyclic amino group that would be present if the A-U base pairing shown was replaced by G-C. Predicted interactions with Consensus 2 nucleotides in *panels G* and *H* were generated by mutation of the RNA sequence in PyMOL.

activation (*i.e.* appended to top or bottom strand only, or to both strands; **Figure 6D** and **Table**

1). Consistent, with the earlier experiments in the original dsRNA construct, OAS1 activation is enhanced by the 3'-ssPy only when appended on the top strand. These experiments reveal that while the presence of the WW/WG dinucleotide pairs and their specific location are important for OAS1 activity, additional features also contribute to optimal OAS1 activation. Specifically, given the identical placement of the top strand consensus in each dsRNA, these results point to an unexpected influence of the "N_9" sequence identity for OAS1 activation, raising the question of how these nucleotides may exert an effect on OAS1 activity.

Finally, we similarly assessed the activity of the Consensus Strand Swap construct, which possesses the original N_9 internal sequence but with the two consensus sequence WW/WG nucleotides on each strand switched (**Figure 6A**). This dsRNA also did not possess the same capacity to activate OAS1 as the original dsRNA (**Figure 6C**; compare blue and black curves, respectively), but resulted in an intermediate activation level, similar to that observed for the Scramble (Consensus) dsRNA. As before, addition of each potential combination of 3'-ssPy motifs on this dsRNA only showed enhanced OAS1 activation when the 3'-ssPy was appended on the top strand (**Figure 6E** and **Table 1**). These data indicate that the features which drive OAS1-dsRNA interaction and binding orientation-dependent OAS1 activation are conserved among these distinct dsRNA contexts. In particular, these results suggest that recognition of the conserved guanosine nucleotide (WW/W<u>G</u>), as previously observed in the OAS1-dsRNA complex structure, is a critical determinant of binding register (*i.e.* OAS1 location on the dsRNA helix) and thus optimal interaction and OAS1 activation. Additionally, examination of the three direct base interactions made by OAS1 to these base pairs in the human OAS1-dsRNA complex crystal structure (**Figure 6F**-**H**) allows rationalization of the differing abilities of UU/UG (Consensus 1) and UA/AG (Consensus 2) sequences to activate OAS1 (see Discussion).

DISCUSSION

Nucleic acid sensing is an essential innate immune strategy for pathogen detection and initiation

of downstream antiviral responses. Recent work has extended ideas of simple dsRNA length limitations for OAS protein activation (57), identifying sequence-specific motifs and activation sequences that can strongly enhance activation of the cytosolic dsRNA sensor OAS1 (49-52). However, the basis of their activity and whether they can act in concert (or competition) to control OAS1 activation is unknown. Fully defining these dsRNA features and their optimal contexts for OAS1 activation by viral or cellular RNAs is important because differing levels of pathway activation likely underpin regulation of distinct cellular processes or cell fates (e.g. apoptosis in response to viral infection).

Here, we used a model 18 bp dsRNA (47) to begin defining how specific RNA features affect OAS1 activation in a short dsRNA with more than one potential binding site. These studies revealed three key findings: (i) OAS1 is unexpectedly sensitive to RNA sequence as two dsRNAs of identical length and nucleotide content, but different sequence, could produce strong activation or no activation at all (18 bp dsRNA and Scramble dsRNA, respectively); (ii) interactions with the conserved nucleotides of the known activation consensus sequence (WWN_9WG) (50) can dictate the specific register of binding on the dsRNA helix; and (iii) only when appropriately positioned by these interactions can other activating motifs, such as 3'-ssPy, exert their effect on OAS1 activation. Additionally, we found that while the short dsRNA likely binds in both orientations in solution, unlike in the crystal structure (47), these two modes of OAS1 interaction are non-equivalent in their ability to promote 2-5A synthesis.

OAS1 binds dsRNA via a relatively flat protein surface that spans approximately the length of an 18 bp dsRNA helix. This surface is enriched with basic residues that contact the sugar-phosphate backbone at each end of the dsRNA but make relatively few contacts to the center of the RNA helix (47). A number of base-specific interactions are also observed in the structure, including those made by Lys42, Ser56, and Thr203 with three conserved nucleotides of the activating WWN_9WG consensus sequence (**Figure 6F**-**H**). These interactions appear to define the optimal register of binding on the dsRNA helix. Thus, when bound in the opposite

orientation from that observed in the crystal structure, *i.e.* to engage the bottom strand consensus, the shift in register by one base pair needed to maintain interactions with the consensus sequence would likely weaken contacts with the lower half of the dsRNA helix (**Figure 7**), resulting in inefficient allosteric promotion of 2-5A synthesis.

Our previous modeling and mutagenesis studies suggested that the top strand 3'-ssPy motif interacts with an OAS1 loop containing residue Gly157 on the protein surface adjacent to the bound dsRNA (**Figure 7A**). Substitution of this residue resulted in loss of sensitivity to the 3'-ssPy but with otherwise the same activity as the wild-type enzyme in response to dsRNA binding (51). Following the finding here that 3'-ssPy motifs on each end of the dsRNA are sensed differently by OAS1, we modeled the interaction of the 18 bp dsRNA in its opposite orientation while maintaining the three direct OAS1-dsRNA base contacts to the bottom strand consensus sequence noted above (**Figure 6F**-**H** and **7B**, *left*). In this orientation, the additional base pair between the bottom strand consensus sequence guanosine and its 3'-end shifts the modeled position of the 3'-ssPy such that it can no longer interact with the OAS1 Gly157 loop (**Figure 7A**,**B**) (51). However, when one base pair is removed, reducing the distance between the bottom strand consensus guanosine and the 3'-ssPy, the ability of the bottom 3'-ssPy motif to interact with the Gly157 would be restored (**Figure 7B**, *right*), consistent with the observed enhancement of OAS1 activation by the bottom strand 3'-ssPy in the context of the Base Pair Move dsRNA.

The 3'-ssPy thus appears to have context-dependent impacts on OAS1 activation: only when appropriately positioned by other dsRNA signatures, in this case by the precise binding register conferred by the activation consensus sequence, can the motif exert its effect on activation. This finding can readily explain the observation in another study using dsRNAs of various lengths (19-123 bp) that the 3'-ssPy motif had no effect on OAS1 activity (54): the dsRNAs used contained multiple WWN_9WG consensus sequences, however, none were located equivalently to the top strand of the 18 bp dsRNA to optimally position the motif to

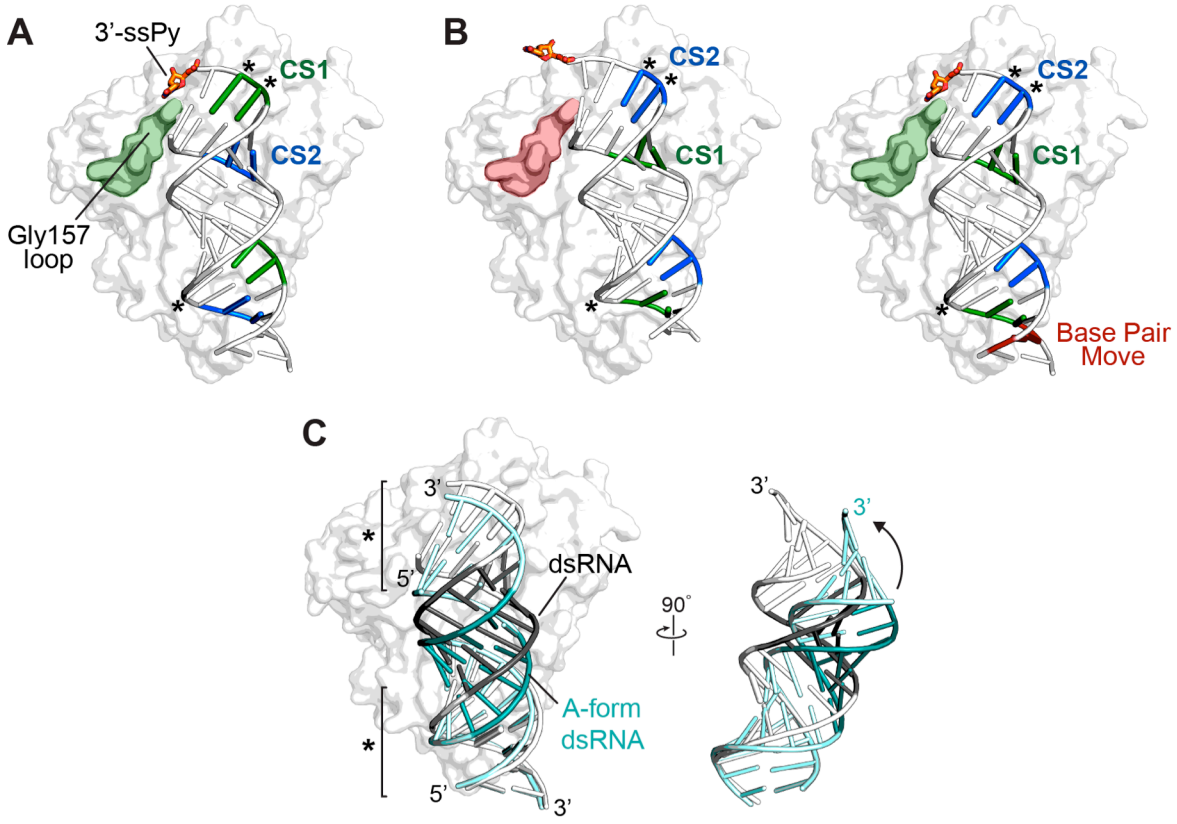

Figure 7. Models of OAS1 interactions with 18 bp dsRNA variants and the 3'-ssPy motif. *A*, Structure of the OAS1-dsRNA complex (PDB 4IG8) with a top strand 3'-ssPy motif (*orange sticks*) modeled as previously reported (51). The consensus sequences on the top (CS1; *green*) and bottom (CS2; *blue*) strands of the dsRNA, and the OAS1 loop containing Gly157 (*green*) are shown on the dsRNA cartoon and OAS1 surface, respectively. ***B*,** As in *panel A* but for the opposite dsRNA binding orientation, maintaining identical direct interactions between OAS1 and the dsRNA consensus nucleotides (marked *). The models shown are for the unaltered dsRNA in which the 3'-ssPy is no longer positioned to interact with the Gly157 loop (*left, red*) and the Base Pair Move dsRNA (*right*). ***C*,** Comparison of the dsRNA in the OAS1 complex structure with a regular A-form dsRNA helix generated using the 3DNA webserver (60). The regions marked * are the main protein-RNA interaction surfaces.

interact with the Gly157 loop. The same study also found no effect of the 3'-ssPy motif on OAS2 activity, but whether similar constraints influence optimal positioning of the dsRNA in this protein (or OAS3), or OAS2 is simply insensitive to the motif will require further investigation. Conversely, there are examples of larger viral and cellular non-coding RNAs whose ability to

activate OAS1 is enhanced by the 3'-ssPy motif in the absence of a "correctly" positioned consensus sequence (51), suggesting that there are other unrelated sequences that also allow for optimal positioning of OAS1.

Our OAS1 kinetics analyses showed that placement of the 3'-ssPy on the bottom strand of the 18 bp dsRNA both increases apparent dsRNA affinity but also, unexpectedly, reduces the maximal activation of the enzyme compared to either no 3'-ssPy or top strand 3'-ssPy. We note that this effect is consistent with the bottom strand 3'-ssPy promoting increased interaction with an OAS1 binding site that results in weaker OAS1 activation. The two-fold difference in V_{max} observed for the 18 bp dsRNA with 3'-ssPy on the bottom strand could thus be explained by an ability to bind the dsRNA approximately half of the time in the "incorrect" (or less productive) orientation. Further careful experiments will be required to fully test this concept of competing weaker or non-activating sites and the molecular basis of their action on OAS1. In the context of viral infection, for example, such insights would be important as a preferred OAS1 binding site in viral dsRNA with an intrinsically low ability to activate OAS1 could act as a "sponge" to diminish activation by other sites within the same dsRNA (59).

Finally, the intermediate activation induced by both the Scramble (Consensus) and Consensus Strand Swap dsRNAs indicates that both the specific identity of the partially conserved (W = A/U) consensus nucleotides as well as the intervening (N_9) sequence can strongly influence OAS1 activation. The role of the conserved WW/WG nucleotides can be partly rationalized based on interactions observed in the OAS1-dsRNA crystal structure. While the interaction with the consensus G nucleotide is conserved, different interactions are made at the other two positions directly contacted by OAS1 where the A-U base pair is reversed in both cases (**Figure 6F-H**). While Lys42 may be sufficiently flexible to make optimal interactions with A or U in the consensus sequence (though not a G-C pair with the additional amino group this would place in the dsRNA minor groove), we speculate that the closer placement of the U13 carbonyl group to Thr203 may be less readily accommodated, reducing OAS1 activation. The

role of the intervening sequence is less easily rationalized but the dsRNA in the co-crystal structure is distorted from a perfect A-form helix, adopting a bent conformation to allow both ends of the dsRNA are able to contact OAS1 (**Figure 7C**). Consistent with the limited RNA-protein interactions in the center of the dsRNA helix, OAS1 is highly tolerant of GU-wobble pairs in the intervening region (N_9) (47). We speculate that, rather than the nine non-conserved nucleotides being present simply to provide adequate spacing to place the WW and WG consensus nucleotides on the same face of the A-form helix (50), the specific sequence in this region also plays an indirect but important role in OAS1 activation by defining the dsRNA shape and flexibility upon protein binding.

The current work emphasizes the unexpectedly important role of RNA sequence and the context of activating motifs in OAS1 activation. While these facets of dsRNA-mediated OAS1 activation have been underappreciated to date, our findings are perhaps unsurprising given that OAS1-dsRNA interaction must be controlled to avoid aberrant activation by numerous cellular RNAs with sufficiently long dsRNA regions (47). These findings require us to begin redefining what constitutes a preferred sequence for promoting potent OAS1 activation and suggest there may be a continuum of activity with diverse sequences that fit a more general consensus. Further, the complexities revealed here in the context of a “simple” model dsRNA are likely to become substantially more complicated in larger dsRNA molecules with multiple potential overlapping OAS1 binding sites. More precisely defining preferred OAS1 activation sequences would facilitate accurate location of these features in specific viral or cellular RNAs to provide deeper insights into both OAS1 regulation and its roles in the uninfected cell. Further work is thus needed to identify and characterize additional sequence-specific determinants, how these RNA features work in concert or in competition, as well as the underlying molecular mechanism(s) by which they regulate OAS1 activation.

ACKNOWLEDGEMENTS

We thank Dr. Susan Weiss (University of Pennsylvania School of Medicine) for generously providing RNase L KO and associated parental A549 cells. We also thank Drs. Christine M. Dunham and Daniel Reines for discussions and comments on the manuscript.

FUNDING INFORMATION

This work was supported by National Institutes of Health awards R01-AI144067 (to GLC), T32-GM008367 (to SLS), and F31-AI133950 (to SLS); the Emory University Research Council (to GLC); and the Emory University School of Medicine Bridge Funding Program (to GLC). SLS also gratefully acknowledges support from the Atlanta Chapter of The ARCS Foundation. This study was supported in part by the Emory Integrated Genomics Core (EIGC), which is subsidized by the Emory University School of Medicine and is one of the Emory Integrated Core Facilities.

REFERENCES

1. Schneider, W.M., Chevillotte, M.D. and Rice, C.M. (2014) Interferon-stimulated genes: a complex web of host defenses. *Annu Rev Immunol*, **32**, 513-545.
2. Chow, J., Franz, K.M. and Kagan, J.C. (2015) PRRs are watching you: Localization of innate sensing and signaling regulators. *Virology*, **479-480**, 104-109.
3. Wu, J. and Chen, Z.J. (2014) Innate immune sensing and signaling of cytosolic nucleic acids. *Annu Rev Immunol*, **32**, 461-488.
4. Schlee, M. and Hartmann, G. (2016) Discriminating self from non-self in nucleic acid sensing. *Nat Rev Immunol*, **16**, 566-580.
5. Hur, S. (2019) Double-Stranded RNA Sensors and Modulators in Innate Immunity. *Annu Rev Immunol*, **37**, 349-375.
6. Li, Y., Banerjee, S., Wang, Y., Goldstein, S.A., Dong, B., Gaughan, C., Silverman, R.H. and Weiss, S.R. (2016) Activation of RNase L is dependent on OAS3 expression during infection with diverse human viruses. *Proc Natl Acad Sci U S A*, **113**, 2241-2246.
7. Schwartz, S.L. and Conn, G.L. (2019) RNA regulation of the antiviral protein 2'-5'-oligoadenylate synthetase. *WIREs RNA*, **10**, e1534.
8. Kristiansen, H., Gad, H.H., Eskildsen-Larsen, S., Despres, P. and Hartmann, R. (2011) The oligoadenylate synthetase family: an ancient protein family with multiple antiviral activities. *J Interferon Cytokine Res*, **31**, 41-47.

9. Dong, B., Xu, L., Zhou, A., Hassel, B.A., Lee, X., Torrence, P.F. and Silverman, R.H. (1994) Intrinsic molecular activities of the interferon-induced 2-5A-dependent RNase. *J Biol Chem*, **269**, 14153-14158.

10. Hovanessian, A.G. and Justesen, J. (2007) The human 2'-5'-oligoadenylate synthetase family: Unique interferon-inducible enzymes catalyzing 2'-5' instead of 3'-5' phosphodiester bond formation. *Biochimie*, **89**, 779-788.

11. Han, Y., Whitney, G., Donovan, J. and Korennykh, A. (2012) Innate immune messenger 2-5A tethers human RNase L into active high-order complexes. *Cell Rep*, **2**, 902-913.

12. Huang, H., Zeqiraj, E., Dong, B., Jha, B.K., Duffy, N.M., Orlicky, S., Thevakumaran, N., Talukdar, M., Pillon, M.C., Ceccarelli, D.F. *et al.* (2014) Dimeric structure of pseudokinase RNase L bound to 2-5A reveals a basis for interferon-induced antiviral activity. *Mol Cell*, **53**, 221-234.

13. Malathi, K., Dong, B., Gale, M., Jr. and Silverman, R.H. (2007) Small self-RNA generated by RNase L amplifies antiviral innate immunity. *Nature*, **448**, 816-819.

14. Banerjee, S., Li, G., Li, Y., Gaughan, C., Baskar, D., Parker, Y., Lindner, D.J., Weiss, S.R. and Silverman, R.H. (2015) RNase L is a negative regulator of cell migration. *Oncotarget*, **6**, 44360-44372.

15. Rath, S., Donovan, J., Whitney, G., Chitrakar, A., Wang, W. and Korennykh, A. (2015) Human RNase L tunes gene expression by selectively destabilizing the microRNA-regulated transcriptome. *Proc Natl Acad Sci U S A*, **112**, 15916-15921.

16. Siddiqui, M.A., Mukherjee, S., Manivannan, P. and Malathi, K. (2015) RNase L Cleavage Products Promote Switch from Autophagy to Apoptosis by Caspase-Mediated Cleavage of Beclin-1. *Int J Mol Sci*, **16**, 17611-17636.

17. Donovan, J., Rath, S., Kolet-Mandrikov, D. and Korennykh, A. (2017) Rapid RNase L-driven arrest of protein synthesis in the dsRNA response without degradation of translation machinery. *RNA*, **23**, 1660-1671.

18. Chitrakar, A., Rath, S., Donovan, J., Demarest, K., Li, Y., Sridhar, R.R., Weiss, S.R., Kotenko, S.V., Wingreen, N.S. and Korennykh, A. (2019) Real-time 2-5A kinetics suggest that interferons beta and lambda evade global arrest of translation by RNase L. *Proc Natl Acad Sci U S A*, **116**, 2103-2111.

19. Wreschner, D.H., McCauley, J.W., Skehel, J.J. and Kerr, I.M. (1981) Interferon action--sequence specificity of the ppp(A2'p)nA-dependent ribonuclease. *Nature*, **289**, 414-417.

20. Malathi, K., Saito, T., Crochet, N., Barton, D.J., Gale, M., Jr. and Silverman, R.H. (2010) RNase L releases a small RNA from HCV RNA that refolds into a potent PAMP. *RNA*, **16**, 2108-2119.

21. Cayley, P.J., Davies, J.A., McCullagh, K.G. and Kerr, I.M. (1984) Activation of the ppp(A2'p)nA system in interferon-treated, herpes simplex virus-infected cells and evidence for novel inhibitors of the ppp(A2'p)nA-dependent RNase. *Eur J Biochem*, **143**, 165-174.

22. Drappier, M., Jha, B.K., Stone, S., Elliott, R., Zhang, R., Vertommen, D., Weiss, S.R., Silverman, R.H. and Michiels, T. (2018) A novel mechanism of RNase L inhibition: Theiler's virus L* protein prevents 2-5A from binding to RNase L. *PLoS Path*, **14**, e1006989.

23. Han, J.Q. and Barton, D.J. (2002) Activation and evasion of the antiviral 2'-5' oligoadenylate synthetase/ribonuclease L pathway by hepatitis C virus mRNA. *RNA*, **8**, 512-525.

24. Keel, A.Y., Jha, B.K. and Kieft, J.S. (2012) Structural architecture of an RNA that competitively inhibits RNase L. *RNA*, **18**, 88-99.

25. Min, J.Y. and Krug, R.M. (2006) The primary function of RNA binding by the influenza A virus NS1 protein in infected cells: Inhibiting the 2'-5' oligo (A) synthetase/RNase L pathway. *Proc Natl Acad Sci U S A*, **103**, 7100-7105.

26. Silverman, R.H. (2007) Viral encounters with 2',5'-oligoadenylate synthetase and RNase L during the interferon antiviral response. *J Virol*, **81**, 12720-12729.

27. Silverman, R.H. and Weiss, S.R. (2014) Viral Phosphodiesterases That Antagonize Double-Stranded RNA Signaling to RNase L by Degrading 2-5A. *J Interferon Cytokine Res*, **34**, 455-463.

28. Taguchi, T., Nagano-Fujii, M., Akutsu, M., Kadoya, H., Ohgimoto, S., Ishido, S. and Hotta, H. (2004) Hepatitis C virus NS5A protein interacts with 2',5'-oligoadenylate synthetase and inhibits antiviral activity of IFN in an IFN sensitivity-determining region-independent manner. *J Gen Virol*, **85**, 959-969.

29. Thornbrough, J.M., Jha, B.K., Yount, B., Goldstein, S.A., Li, Y., Elliott, R., Sims, A.C., Baric, R.S., Silverman, R.H. and Weiss, S.R. (2016) Middle East Respiratory Syndrome Coronavirus NS4b Protein Inhibits Host RNase L Activation. *mBio*, **7**, e00258.

30. Townsend, H.L., Jha, B.K., Han, J.Q., Maluf, N.K., Silverman, R.H. and Barton, D.J. (2008) A viral RNA competitively inhibits the antiviral endoribonuclease domain of RNase L. *RNA*, **14**, 1026-1036.

31. Townsend, H.L., Jha, B.K., Silverman, R.H. and Barton, D.J. (2008) A putative loop E motif and an H-H kissing loop interaction are conserved and functional features in a group C enterovirus RNA that inhibits ribonuclease L. *RNA Biol*, **5**, 263-272.

32. Zhang, R., Jha, B.K., Ogden, K.M., Dong, B., Zhao, L., Elliott, R., Patton, J.T., Silverman, R.H. and Weiss, S.R. (2013) Homologous 2',5'-phosphodiesterases from disparate RNA viruses antagonize antiviral innate immunity. *Proc Natl Acad Sci U S A*, **110**, 13114-13119.

33. Zhao, L., Jha, B.K., Wu, A., Elliott, R., Ziebuhr, J., Gorbalenya, A.E., Silverman, R.H. and Weiss, S.R. (2012) Antagonism of the interferon-induced OAS-RNase L pathway by murine coronavirus ns2 protein is required for virus replication and liver pathology. *Cell Host Microbe*, **11**, 607-616.

34. Yakub, I., Lillibridge, K.M., Moran, A., Gonzalez, O.Y., Belmont, J., Gibbs, R.A. and Tweardy, D.J. (2005) Single nucleotide polymorphisms in genes for 2'-5'-oligoadenylate synthetase and RNase L inpatients hospitalized with West Nile virus infection. *J Infect Dis*, **192**, 1741-1748.

35. Lim, J.K., Lisco, A., McDermott, D.H., Huynh, L., Ward, J.M., Johnson, B., Johnson, H., Pape, J., Foster, G.A., Krysztof, D. *et al.* (2009) Genetic variation in OAS1 is a risk factor for initial infection with West Nile virus in man. *PLoS Path*, **5**, e1000321.

36. Bigham, A.W., Buckingham, K.J., Husain, S., Emond, M.J., Bofferding, K.M., Gildersleeve, H., Rutherford, A., Astakhova, N.M., Perelygin, A.A., Busch, M.P. *et al.* (2011) Host genetic risk factors for West Nile virus infection and disease progression. *PLoS One*, **6**, e24745.

37. Field, L.L., Bonnevie-Nielsen, V., Pociot, F., Lu, S., Nielsen, T.B. and Beck-Nielsen, H. (2005) OAS1 splice site polymorphism controlling antiviral enzyme activity influences susceptibility to type 1 diabetes. *Diabetes*, **54**, 1588-1591.

38. Fedetz, M., Matesanz, F., Caro-Maldonado, A., Fernandez, O., Tamayo, J.A., Guerrero, M., Delgado, C., Lopez-Guerrero, J.A. and Alcina, A. (2006) OAS1 gene haplotype confers susceptibility to multiple sclerosis. *Tissue Antigens*, **68**, 446-449.

39. O'Brien, M., Lonergan, R., Costelloe, L., O'Rourke, K., Fletcher, J.M., Kinsella, K., Sweeney, C., Antonelli, G., Mills, K.H., O'Farrelly, C. *et al.* (2010) OAS1: a multiple sclerosis susceptibility gene that influences disease severity. *Neurology*, **75**, 411-418.

40. Mandal, S., Abebe, F. and Chaudhary, J. (2011) 2'-5' oligoadenylate synthetase 1 polymorphism is associated with prostate cancer. *Cancer*, **117**, 5509-5518.

41. Li, H., Reksten, T.R., Ice, J.A., Kelly, J.A., Adrianto, I., Rasmussen, A., Wang, S., He, B., Grundahl, K.M., Glenn, S.B. *et al.* (2017) Identification of a Sjogren's syndrome susceptibility locus at OAS1 that influences isoform switching, protein expression, and responsiveness to type I interferons. *PLoS Genet*, **13**, e1006820.

42. Liu, X., Xing, H., Gao, W., Yu, D., Zhao, Y., Shi, X., Zhang, K., Li, P., Yu, J., Xu, W. *et al.* (2017) A functional variant in the OAS1 gene is associated with Sjogren's syndrome complicated with HBV infection. *Sci Rep*, **7**, 17571.

43. Wu, S., Wang, Y., Chen, G., Zhang, M., Wang, M. and He, J.Q. (2018) 2'-5'-Oligoadenylate synthetase 1 polymorphisms are associated with tuberculosis: a case-control study. *BMC Pulm Med*, **18**, 180.

44. Kondratova, A.A., Cheon, H., Dong, B., Holvey-Bates, E.G., Hasipek, M., Taran, I., Gaughan, C., Jha, B.K., Silverman, R.H. and Stark, G.R. (2020) Suppressing PARylation by 2',5'-oligoadenylate synthetase 1 inhibits DNA damage-induced cell death. *EMBO J*, **39**, e101573.

45. Banerjee, S., Gusho, E., Gaughan, C., Dong, B., Gu, X., Holvey-Bates, E., Talukdar, M., Li, Y., Weiss, S.R., Sicheri, F. *et al.* (2019) OAS-RNase L innate immune pathway mediates the cytotoxicity of a DNA-demethylating drug. *Proc Natl Acad Sci U S A*, **116**, 5071-5076.

46. Hartmann, R., Justesen, J., Sarkar, S.N., Sen, G.C. and Yee, V.C. (2003) Crystal structure of the 2'-specific and double-stranded RNA-activated interferon-induced antiviral protein 2'-5'-oligoadenylate synthetase. *Mol Cell*, **12**, 1173-1185.

47. Donovan, J., Dufner, M. and Korennykh, A. (2013) Structural basis for cytosolic double-stranded RNA surveillance by human oligoadenylate synthetase 1. *Proc Natl Acad Sci U S A*, **110**, 1652-1657.

48. Lohofener, J., Steinke, N., Kay-Fedorov, P., Baruch, P., Nikulin, A., Tishchenko, S., Manstein, D.J. and Fedorov, R. (2015) The Activation Mechanism of 2'-5'-Oligoadenylate Synthetase Gives New Insights Into OAS/cGAS Triggers of Innate Immunity. *Structure*, **23**, 851-862.

49. Hartmann, R., Norby, P.L., Martensen, P.M., Jorgensen, P., James, M.C., Jacobsen, C., Moestrup, S.K., Clemens, M.J. and Justesen, J. (1998) Activation of 2'-5' oligoadenylate synthetase by single-stranded and double-stranded RNA aptamers. *J Biol Chem*, **273**, 3236-3246.

50. Kodym, R., Kodym, E. and Story, M.D. (2009) 2'-5'-Oligoadenylate synthetase is activated by a specific RNA sequence motif. *Biochem Biophys Res Commun*, **388**, 317-322.

51. Vachon, V.K., Calderon, B.M. and Conn, G.L. (2015) A novel RNA molecular signature for activation of 2'-5' oligoadenylate synthetase-1. *Nucleic Acids Res*, **43**, 544-552.

52. Calderon, B.M. and Conn, G.L. (2018) A human cellular noncoding RNA activates the antiviral protein 2'-5'-oligoadenylate synthetase 1. *J Biol Chem*, **293**, 16115-16124.

53. Nielsen, S., Yuzenkova, Y. and Zenkin, N. (2013) Mechanism of eukaryotic RNA polymerase III transcription termination. *Science*, **340**, 1577-1580.

54. Koul, A., Deo, S., Booy, E.P., Orriss, G.L., Genung, M. and McKenna, S.A. (2020) Impact of double-stranded RNA characteristics on the activation of human 2'-5'-oligoadenylate synthetase 2 (OAS2). *Biochem Cell Biol*, **98**, 70-82.

55. Justesen, J. and Kjeldgaard, N.O. (1992) Spectrophotometric pyrophosphate assay of 2',5'-oligoadenylate synthetase. *Anal Biochem*, **207**, 90-93.

56. Donovan, J., Whitney, G., Rath, S. and Korennykh, A. (2015) Structural mechanism of sensing long dsRNA via a noncatalytic domain in human oligoadenylate synthetase 3. *Proc Natl Acad Sci U S A*, **112**, 3949-3954.

57. Wang, Y., Holleufer, A., Gad, H.H. and Hartmann, R. (2019) Length dependent activation of OAS proteins by dsRNA. *Cytokine*, **126**, 154867.

58. Marie, I., Blanco, J., Rebouillat, D. and Hovanessian, A.G. (1997) 69-kDa and 100-kDa isoforms of interferon-induced (2'-5')oligoadenylate synthetase exhibit differential catalytic parameters. *Eur J Biochem*, **248**, 558-566.

59. Charley, P.A. and Wilusz, J. (2014) Sponging of cellular proteins by viral RNAs. *Curr Opin Virol*, **9**, 14-18.

60. Li, S., Olson, W.K. and Lu, X.J. (2019) Web 3DNA 2.0 for the analysis, visualization, and modeling of 3D nucleic acid structures. *Nucleic Acids Res*, **47**, W26-W34.

TABLES

Table 1. Summary of OAS1 activation by short dsRNAs *in vitro* and A549 cells.

3'-ssPy location	Initial rate (nmol PP_i/ min)[a]	Kinetic analysis[b]		Relative 28S rRNA cleavage[c]
		K_{app} (μM)	V_{max} (nmol PP_i/ min)	
None	1.4 ± 0.1	10.3 ± 1.0	36.0 ± 2.5	1.0
Top	3.5 ± 0.3	4.0 ± 0.3	36.5 ± 1.4	1.7 ± 0.5
Bottom	1.6 ± 0.2	6.5 ± 0.6	22.8 ± 1.5	0.6 ± 0.2
Both ends	4.0 ± 0.2	ND	ND	2.7 ± 0.2

	Initial rate (nmol PP_i/ min)[a]		
	Base Pair Move	Scramble (Consensus)	Consensus Strand Swap
None	2.0 ± 0.1	0.74 ± 0.05	0.68 ± 0.06
Top	2.4 ± 0.2	1.3 ± 0.1	1.0 ± 0.1
Bottom	2.7 ± 0.3	0.80 ± 0.04	0.64 ± 0.04
Both ends	2.8 ± 0.3	1.2 ± 0.1	0.95 ± 0.04

[a]Initial rates determined by linear regression analysis on the 0-10 minute time points for replicate time course experiments performed at a single dsRNA concentration (300 nM dsRNA), as shown in **Figures 2**,**5,** and **6**.

[b]Kinetic parameters (K_{app} and V_{max}) were determined from fits to data shown in **Figure 4**. ND, Not determined.

[c]Values from quantification of three independent experiments in wild-type A549 cells, exemplified in **Figure 3**.

CHAPTER FOUR

Basis for sequence-dependent activation of the innate immune dsRNA sensor oligoadenylate synthetase 1

Samantha L. Schwartz, Debayan Dey, Julia Tanquary, Camden R. Bair,
Anice C. Lowen and Graeme L. Conn

A version of this manuscript is in preparation for submission for publication.

Author Contributions: S.L.S., D.D., A.C.L., and G.L.C. participated in research design. S.L.S.*, D.D., J.T., and C.R.B. performed experiments. S.L.S., D.D., A.C.L., and G.L.C. analyzed data. S.L.S. and G.L.C. wrote the manuscript.

[*S.L.S. performed the majority of experiments shown in Figures 1-5, 7, and S1-S3.]

ABSTRACT

The 2'-5'-oligoadenylate synthetases (OAS) are innate immune sensors of cytosolic double-stranded RNA (dsRNA) that play a critical role in limiting viral infection. How these proteins are able to discriminate between foreign and "self" RNAs is not fully understood, but *ADAR1* deficiency has been proposed to result in over-stimulation of the OAS/RNase L pathway via accumulation of activating endogenous RNAs in the absence of adenosine-to-inosine (A-to-I) editing. Here, we aim to uncover whether and how such sequence modifications can restrict the ability of short, defined dsRNAs to activate the single domain form of OAS, OAS1. Unexpectedly, we find that all inosine-containing dsRNAs generated increased the capacity of the short dsRNA to activate OAS1, whether in a destabilizing (I•U) or standard Watson-Crick-like base pairing (I-C) context. Additional variants with strongly destabilizing A•C mismatches or stabilizing G-C pairs also exhibited increased capacity to activate OAS1, eliminating helical stability as a factor in the relative ability of the dsRNAs to activate OAS1. Using thermal difference spectra (TDS) and molecular dynamics (MD) simulations, we identify both increased flexibility and specific local changes in helical structure as important factors in the capacity of short dsRNAs to activate OAS1. These dsRNA features may allow more ready adoption of the distorted dsRNA conformation when bound to dsRNA. These studies thus reveal the basis for previously unappreciated "sequence independent" contributions of dsRNA to OAS1 activation.

INTRODUCTION

The 2'-5'-oligoadenylate synthetase (OAS) family of nucleotidyl transferases are responsible for detecting double-stranded RNA (dsRNA), a potent pathogen-associated molecular pattern, typically absent in the uninfected cell but abundant during viral infection. OAS requires dsRNA binding to promote structural rearrangements necessary to form its active site for synthesis of 2'-5' phosphodiester-linked oligoadenylate (2-5A) signaling molecules (2,3). 2-5A binds the monomeric latent endoribonuclease (RNase L), promoting formation of the functionally active RNase L dimer (4-6). Activated RNase L is responsible for restricting viral infection by degrading viral and cellular RNA, including rRNA, tRNA, and specific mRNA transcripts required for cell growth, proliferation, and differentiation (7-11).

The human OAS family is comprised of three catalytically active members: OAS1, OAS2, and OAS3, which possess one, two, or three OAS domains, respectively. In each enzyme only one domain retains 2-5A synthesis activity (12-14) and the additional domains are speculated to be responsible for expanding the dsRNA binding surface to allow detection of a wider range of dsRNA lengths. As such, OAS1 is capable of detecting short dsRNAs (~18 base pairs or more) (2) while OAS3 requires >50 base pairs (14).

While the OAS/RNase L pathway is most notable for limiting viral replication and the spread of infection, there is growing appreciation for potential role(s) in the context of normal cell function in the absence of infection. For example, OAS has been implicated in diseases unrelated to viral infection that arise from defects in the OAS/RNase L pathway, including autoimmune disorders (15-18), cancer (19,20), tuberculosis (21,22), malaria (23), and linked to resistance for the only approved treatment for gastric cancer (24). These human diseases allude to additional roles for the pathway beyond innate immunity and highlight potential for OAS as a drug target for effective therapeutic strategies. Importantly, however, despite these new advances, we still do not fully understand how OAS1 avoids unwanted self-activation by

cellular RNAs containing double-stranded regions or how specific features within a dsRNA, of viral or cellular origin, contribute collectively to promote OAS1 activity.

Recent studies have suggested that a cellular A-to-I editing enzyme, adenosine deaminase acting on RNA (ADAR1), may play a protective role against self-activation of the OAS/RNase L pathway and other innate immune sensors of dsRNA (25,26). *ADAR1* mutations have been shown to cause Aicardi-Goutières syndrome (AGS), an autoimmune disorder associated with the upregulation of interferon-stimulated genes (27), identifying a novel function for ADAR1 as a suppressor of Type I Interferon signaling. Deletion of *ADAR1* results in a lethal phenotype that can be reversed by knocking out *RNASEL* (28). Together these observations indicate that the absence of ADAR1 in these cells leads to an accumulation of cellular RNAs with the capacity to activate the OAS/RNase L pathway. A-to-I editing is proposed to destabilize dsRNA regions within cellular RNAs thus providing an essential mechanism by which their propensity to inadvertently activate OAS proteins (and other dsRNA sensors) is reduced (25,26). However, to date, whether or not OAS1 (or other OAS family members) has the propensity to be activated by edited cellular dsRNAs (containing inosine) has yet to be directly tested.

Several studies have identified molecular signatures, including nucleotide sequences and structural motifs, responsible for potentiating OAS1 activation *in vitro* and in human cells (29-32), but their mechanism of action is not well understood. Previously, it was thought that OAS1 required only two key determinants for activation: (i) perfectly double-stranded RNA that also (ii) meets the length requirements needed to span the entire dsRNA binding surface (>18 bp). The crystal structure of dsRNA-bound human OAS1 contained an 18 bp dsRNA (**Figure 1A**) with two overlapping, antiparallel copies of a previously identified OAS1 activation consensus sequence WWN_9WG, where W is A or U and N is any nucleotide (2,30). The structure revealed the partially conserved (WW/WG) nucleotides of one of these WWN_9WG motifs to be positioned on the same face of the RNA helix, allowing their minor groove base pair

edges to mediate key contacts with OAS1 residues. The relative lack of contacts between OAS1 and the central region of the consensus (*i.e.* "N_9") suggested that, consistent with its variable sequence, this intervening region's main function was simply to serve as the necessary spacer to ensure the WW/WG dinucleotides were positioned appropriately (30). However, our recent work with variants of the 18 bp dsRNA revealed that changes in the N_9 sequence also have the propensity to strongly influence the extent of activation (1). The OAS1-bound dsRNA is distorted from a canonical A-form helix, adopting a bent conformation to make direct contacts with OAS1 at each end of the RNA helix (2). N_9 sequences with greater inherent flexibility or otherwise more predisposed to adopt the required bent conformation might offer a plausible explanation for increased activation without the need for direct interaction with OAS1. Indeed, during the course of the present work, a molecular dynamics (MD) study revealed the propensity for an AU-tract in dsRNAs to induce helical bending (33). Such an AU-tract, of the minimum 3-nt length to induce bending, is present in the 18 bp dsRNA immediately preceding the conserved G nucleotide of the consensus sequence engaged by OAS1 (**Figure 1A**).

We began the present work with the goal of addressing whether OAS1 activation is reduced by A-to-I "editing" in the context of a short dsRNA, and, if so, whether this correlates with decreased stability or some other alteration in helical structure due to the non-canonical I•U base pairs. More broadly we aimed to assess the role of helical structure and flexibility in OAS1 activation and whether such properties might underpin the observed influence of the consensus N_9 region on OAS1 activation. We find that A-to-I substitutions within the N_9 region reduce dsRNA stability as anticipated but, contrary to expectation, do not ablate OAS1 activation. Rather, I•U pairs and diverse other sequence changes in the consensus N_9 region enhance OAS1 activation by either increasing overall helical dynamics or inducing specific local changes in helical structure.

MATERIALS AND METHODS

OAS1 protein expression and purification

Human OAS1 was expressed in *Escherichia coli* BL21(DE3) as an N-terminal 6xHis-SUMO fusion of amino acids 1-346 (OAS^{1-346}; corresponding to the core residues shared by all OAS1 splicing isoforms) from vector pE-SUMO (LifeSensors). Cells were grown in lysogeny broth (LB) at 37°C to mid-log phase (OD_{600} ~0.5), and OAS1 expression was induced with 0.5 mM isopropyl β-D-1-thiogalactopyranoside (IPTG) and growth continued overnight at 20°C. Cells were lysed by sonication in 50 mM Tris-HCl buffer (pH 8.0) containing 300 mM NaCl, 20 mM imidazole, 10% (v/v) glycerol, and 10 mM β-mercaptoethanol. SUMO-OAS^{1-346} fusion protein was purified from cleared lysate by Ni^{2+}-affinity chromatography on an ÄKTApurifier 10 FPLC system (GE Healthcare), dialyzed overnight against SUMO cleavage buffer (50 mM Tris-HCl (pH 8.0), 150 mM NaCl, 10% (v/v) glycerol, and 2 mM DTT), and stored at -80°C. Prior to each experiment, the N-terminal 6xHis-SUMO tag was cleaved with SUMO protease (Ulp1) for 90 minutes at 30°C and an additional hour at 4°C, followed by dialysis against the appropriate assay buffer. This process produces OAS^{1-346} with a native N-terminus after SUMO tag removal.

Generating 18 bp dsRNA duplexes

Each RNA strand was chemically synthesized (Integrated DNA Technologies) and used without further purification. Each 18 bp dsRNA was generated by mixing individual strands at equimolar concentrations and annealing by heating to 65°C for 10 minutes followed by slow cooling to room temperature. Native PAGE (20% acrylamide in 0.5X Tris-borate-EDTA) was used to verify the homogeneity of both single-strand RNAs and dsRNA duplexes prior to use (**Figure S1**). Each lane contained RNA (100 ng total) resolved on gels run at 120 V for 3 hours at 4°C, visualized by staining with SYBR Gold (Invitrogen, 1:10,000), and imaged on a Typhoon Trio Imager (GE Healthcare).

Chromogenic assay of OAS1 activity

After removal of the 6xHis-SUMO tag, OAS^{1-346} was dialyzed overnight against OAS1 activity assay buffer: 50 mM Tris-HCl (pH 7.4) containing 100 mM NaCl, 1 mM EDTA, and 1 mM DTT. Production of pyrophosphate (PP_i), the reaction by-product of 2-5A synthesis by OAS1, was monitored using a chromogenic assay adapted from previously established methods for measurement of OAS1 activity (1,31,32,34). OAS^{1-346} (100 nM) was incubated with 300 nM dsRNA or 0.5 µg/ml high molecular weight homopolymer in reactions containing final solution conditions of 25 mM Tris-HCl (pH 7.4), 10 mM NaCl, 7 mM $MgCl_2$, 1 mM DTT, and 2 mM ATP at 37°C in a 150 µl total reaction volume. Aliquots (10 µl) were removed over a 0-120 minute time course and the reaction immediately quenched by adding directly to the wells of a 96-well plate pre-dispensed with 250 mM EDTA (pH 8.0, 2.5 µl). At completion of the time course, 2.5% (w/v) ammonium molybdate in 2.5 M H_2SO_4 (10 µl) and 0.5 M β-mercaptoethanol (10 µl) were added to each well and the final volume brought to 100 µl with water. Absorbance at 580 nm was measured using a Synergy Neo2 plate reader (BioTek), background subtracted using an ATP-only control reaction (lacking both OAS^{1-346} and dsRNA), and converted to pyrophosphate produced (nmols) using a pyrophosphate standard curve. Experiments were performed as four independent assays using two different preparations of OAS^{1-346}, each comprising three technical replicates (technical replicates were averaged prior to plotting and data analysis). Final values were plotted with their associated standard error of the mean (SEM), and linear regression analysis was used to obtain initial rates of reaction (nmol PP_i produced/minute) for each dsRNA in GraphPad Prism 9.

OAS1/RNase L activation in A549 cells

Human wild-type and RNase L knock-out A549 cells, constructed using CRISPR-Cas9 gene editing technology as reported previously (35), were cultured in RPMI1640 cell culture medium (Corning) supplemented with 10% fetal bovine serum (Bio-Techne) and 100 µg/ml Normocin™

(Invivogen). Both cell lines were monitored regularly and tested negative for mycoplasma. Cells were seeded into 12-well plates at $3x10^5$ cells/well and were treated overnight (16 hours) with 500 U/ml IFN-β1a (PBL Assay Science). Cells were then transfected with dsRNAs (50 nM) or poly(rI:rC) (0.1 µg/ml) using siLentFect Lipid Reagent (Bio-Rad) and incubated at 37°C for 6 hours. Cells were lysed and total RNA was isolated using a RNeasy Plus Mini Kit (Qiagen) following manufacturer instructions. Total RNA was resolved using an Agilent 2100 Bioanalyzer system. At least two independent sets of experiments were performed with essentially identical results for both the wild-type (n = 3) and RNase L knock-out (n = 2) cells, respectively. Bands resulting from 28S rRNA cleavage in wild-type A549 cells were quantified using ImageJ and relative cleavage was plotted with standard deviation (SD) for each set of averaged technical replicates by normalizing to activity induced by the 18 bp dsRNA (AU3). Statistical significance was determined by one-way ANOVA with Dunnett's post-hoc test in GraphPad Prism 9.

Immunoblotting

Human wild-type and RNase L knock-out A549 cells were either untreated or treated overnight (16 hours) with 500 U/ml IFN-β1a (PBL Assay Science). Cells were harvested by rinsing once with phosphate-buffered saline (Corning), lysed by sonication in RIPA lysis buffer (ThermoFisher Scientific), and clarified by centrifugation for 10 minutes (16,100 x *g* at 4°C). Protein concentrations were determined by Bradford Assay using known amounts of bovine serum albumin (Bio-Rad) as a standard. Total protein (20 µg/well) was resolved on a 4-12% Bis-Tris polyacrylamide gel (ThermoFisher Scientific) and transferred to a nitrocellulose membrane (Bio-Rad) at 50 V for 1 hour at room temperature. Membranes were rinsed in Tris-buffered saline containing 0.1% Tween-20 (TBST) and blocked in TBST containing 5% (w/v) nonfat dry milk (Bio-Rad) for 1 hour at room temperature. After washing three times in TBST (5 minutes each), membranes were incubated in primary antibody diluted in TBST containing 5% (w/v) bovine serum albumin (Sigma) overnight at 4°C. Membranes were then washed again three

times in TBST (5 minutes each) before incubating with HRP-conjugated anti-mouse (Promega #W4021, 1:2,500) or anti-rabbit (Promega #W4011, 1:2,500) secondary antibodies diluted in TBST containing 5% (w/v) nonfat dry milk for 1 hour at room temperature. Blots were washed three times in TBST (5 minutes each) then incubated in Clarity Western ECL (Bio-Rad) according to the manufacturer's recommendations and imaged using a Chemidoc MP system (Bio-Rad). The primary antibodies used in this study were: RNase L (E-9, Santa Cruz #sc-74405, mouse monoclonal, 1:1,000), OAS1 (F-3, Santa Cruz #sc-374656, mouse monoclonal, 1:1,000), β-Tubulin (Cell Signaling Technology #2146, rabbit polyclonal, 1:1,000), and Vinculin (Cell Signaling Technology #4650, rabbit polyclonal, 1:1,000).

RNA UV melting analysis

UV melting curves were collected at 260 nm with a heating rate of 1°C/ minute on a Cary 3500 UV-Vis spectrophotometer (Agilent) using quartz cuvettes with an optical pathlength of 10 mm, and with a temperature probe placed in a buffer-only sample. Samples contained 25 µg of RNA in a solution of 25 mM MOPS (pH 7.4) and 0.1 mM EDTA containing either 10 mM NaCl ("low salt"), 100 mM NaCl ("high salt"), or 100 mM NaCl and 7 mM $MgCl_2$ ("high salt with Mg^{2+}"). The first derivative was calculated for each UV absorbance curve in GraphPad Prism 9 to obtain the "melting profile," and melting temperatures (T_m) were determined using the mid-point of the peak. At least two independent experiments were performed with essentially identical results (**Table S1**).

Thermal difference spectra (TDS)

To assess dsRNA helical structure using TDS (36), we measured the absorbance spectra (225-340 nm) at two temperatures, one above (95°C) and one below (20°C) the T_m of all dsRNAs under study. Samples contained 25 µg of RNA in a solution of 25 mM MOPS (pH 7.4) containing 10 mM NaCl, 7 mM $MgCl_2$, and 0.1 mM EDTA. Data were collected on a Cary 3500 UV-Vis spectrophotometer (Agilent) using quartz cuvettes with an optical pathlength of 10 mm,

and with a scan speed of 3000 nm/ minute and a data interval of 1 nm. Individual spectra were normalized and difference spectra obtained by subtracting the low temperature spectrum from the high temperature spectrum (**Figure S2A**). Final plots were trimmed at 240 nm due to variability at shorter wavelengths (225-240 nm; **Figure S2B**) despite minimal variability between dsRNA preparations (**Figure S2C**). Three independent experiments were plotted with standard error of the mean (SEM) in GraphPad Prism 9.

dsRNA molecular dynamics (MD) simulations

Molecular dynamics (MD) simulations were performed on select dsRNA sequences after addition of short terminal sequences of four G-C base pairs (GGGG/CCCC; "G4") to give computational constructs in the form of G4-X-G4, where X = AU3, IU3, IC3, AC3, GC3, GC2, or GC1 dsRNAs. This design was used to prevent end fraying or other improper conformational changes during the MD production run at the helix ends from impacting our analysis of each 18 bp sequence. Three additional dsRNAs from our prior study (1) (X = "Scramble", "Scramble (Consensus)", and "Consensus Strand Swap") and three dsRNAs with highly biased sequences (X = $(AU)_{18}$, $(GC)_{18}$, $(IC)_{18}$) were also analyzed by MD in the same way. Finally, before analysis of the 18 bp dsRNAs, we analyzed one previously reported dsRNA sequence ("Seq3"; (33)) as a benchmark for our MD protocol.

dsRNA structures were built using the biopolymer building panel and MD simulation was performed in Desmond using the OPLS3e force field of the Schrödinger software (2020-4; Schrödinger, New York, NY, USA). Each system was first neutralized by adding Na^+ around the dsRNA using the System Builder module. The neutralized dsRNA was then placed in TIP3P water, and random water molecules substituted with Na^+ in order to obtain a total ionic strength of 10 mM NaCl. The solvated system was relaxed using a series of minimization stages, each of 1 ns duration, with all heavy atoms of the RNA restrained with force constant: 1) 100; 2) 25; 3) 5 kcal/mol$Å^2$; and finally, 4) with no constraints. Each dsRNA system was heated to 300 K and

equilibrated in the isobaric-isothermal (NPT) ensemble (P = 1 atm, T = 300 K) for 20 ns. Production simulations were then performed in the NVT ensemble using the last configuration of the NPT equilibration for a 200 ns production run. For unrestrained MD simulations, Langevin thermostat and barostat were used with relaxation times of 1 and 2 ps, respectively. The equations of motion were integrated using multiple time steps for short-range (2 fs) and long-range (6 fs) interactions with a 9 Å cutoff applied for non-bonded interactions. Coordinates were saved every 100 ps.

Representative structures in each 10 ns window (100 frames) over the 200 ns run were selected by using the Schrödinger software to determine the closest structure to the average of all structures within each window based on RMSD and low energy. The resulting 20 structures for each dsRNA were analyzed for helical bending, intra- and inter-base pair parameters, and groove dimensions using the Curves+ webserver (37,38) after removal of the G4 cap regions from each of the dsRNAs, where applicable. Plots of RMSD (Schrödinger software) and dsRNA helical parameters (Curves+) were generated in GraphPad Prism 9.

RESULTS

A-to-I "editing" does not prevent OAS1 activation

To test the effect of A-to-I "editing" on OAS1 activation in the context of a short defined dsRNA, we generated new variants of the RNA construct used in the human OAS1-dsRNA crystal structure (2) and our previous analyses of OAS1 activation (1,31). As both the crystal structure and our previous functional analyses revealed that OAS1 engages productively with only one of the two OAS1 activation consensus sequences in this dsRNA (highlighted green in **Figure 1A**), we focused on the intervening N_9 region within this "top" strand consensus. Three A-U base pairs were selected for A-to-I editing (**Figure 1A**) following the considerations that changes should not be immediately adjacent to the conserved WW/WG top strand consensus nucleotides nor directly alter the conserved nucleotides of the "bottom" strand consensus. Thus,

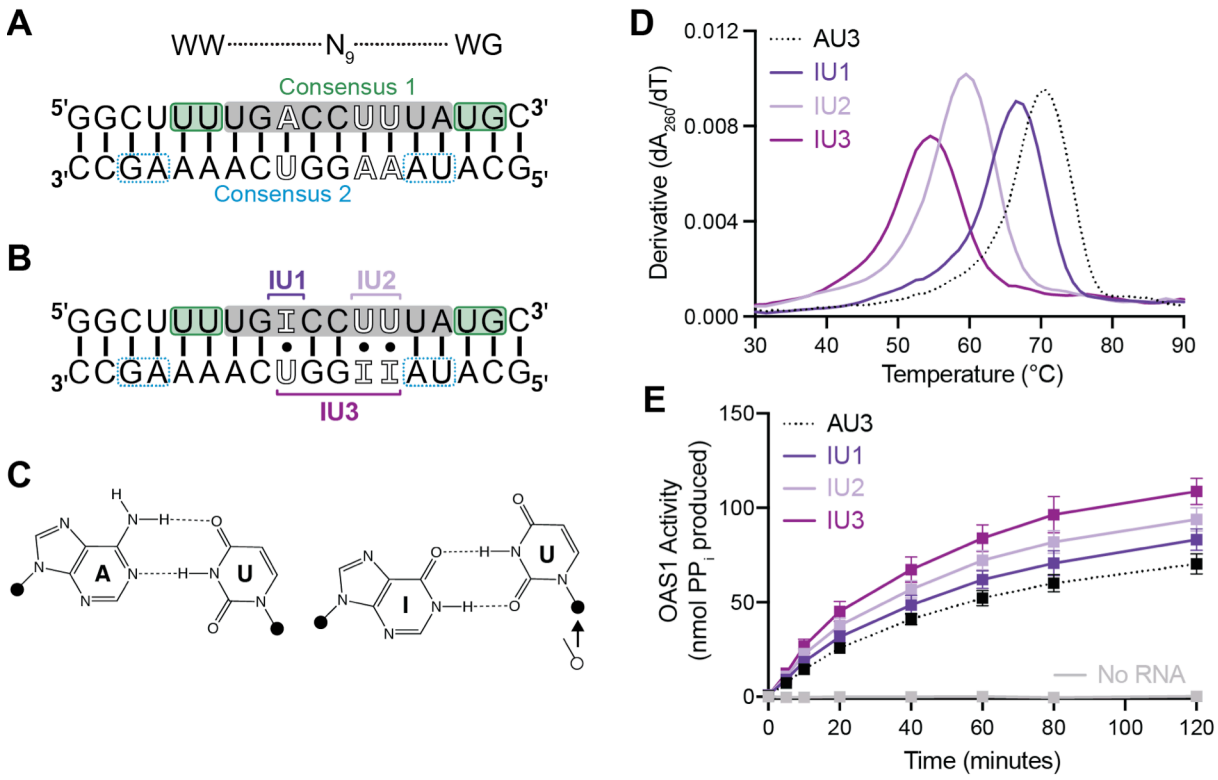

Figure 1. I•U base pairs do not diminish OAS1 activation by a short dsRNA. ***A,*** Schematic of the 18 bp dsRNA with two overlapping, antiparallel WWN_9WG OAS1 activation consensus sequences (conserved WW/WG nucleotides, *green and blue* respectively). Non-conserved (N_9, *grey*) nucleotides are only highlighted for the "top" strand which is engaged by OAS1 in the OAS1-dsRNA crystal structure (2). The A-U base pairs selected to generate dsRNA variants for these studies are indicated in outline font. ***B,*** Three inosine-containing dsRNAs were generated by introducing one (IU1), two (IU2), or three (IU3; combined IU1 and IU2) adenosine to inosine (A-to-I) substitutions. ***C,*** Comparison of canonical Watson-Crick A-U (*left*) and non-canonical I•U (*right*) base pairing, noting a shift in base and phosphodiester backbone positions necessary to maintain two hydrogen-bonding interactions (open and closed circles with arrow). ***D,*** UV thermal melting profiles (shown for the 100 mM NaCl condition) indicate that I•U containing dsRNAs (*purple shades*) are progressively destabilized (lower T_m) with increasing number of changes compared to the original dsRNA (AU3, *black dotted line*). ***E,*** Reaction progress curves from an *in vitro* chromogenic assay of OAS1 activity using a single dsRNA concentration (300 nM) with the same dsRNAs showing OAS1 activation is concomitantly enhanced as the number of I•U base pairs increases.

any changes in OAS1 activation should arise due to alterations in helical structure within the central region of the dsRNA, which is not directly contacted by OAS1, and not because of alterations to important interactions with the conserved consensus residues.

Following the above strategy, we generated three inosine-containing 18 bp dsRNAs by making one (IU1), two (IU2), or three (IU3; combined IU1 and IU2) I•U base pair substitutions in the center of the 18 bp dsRNA (**Figure 1B,C**). The parent 18 bp dsRNA which retains the original three A-U base pairs will be referred to as "AU3" for consistency in naming of these constructs. Each dsRNA was generated by annealing two complementary single-strand RNAs and stable duplex formation confirmed by native polyacrylamide gel electrophoresis (**Figure S1**). To maintain hydrogen bonding, I•U base pair have altered backbone geometry and base positioning compared to canonical Watson-Crick base pairing (**Figure 1C**), disrupting the dsRNA helical shape and stability. First, we measured melting temperature (T_m) values for each variant by UV thermal melting analyses under three conditions distinguished by low salt (10 mM NaCl), high salt (100 mM NaCl), and high salt with Mg^{2+} (100 mM NaCl, 7 mM $MgCl_2$). We selected these conditions as they reflect the components used in our OAS1 activation assay (*i.e.* 10 mM NaCl and 7 mM $MgCl_2$); however, Mg^{2+} was added only in the presence of high salt to reduce potential for RNA hydrolysis by the divalent ion at higher temperatures. Under all three solution conditions, dsRNA T_m decreases concomitantly as the number of inosine substitutions increases (**Figure 1D**), consistent with reduced dsRNA stability, as expected. Increasing solution ionic strength, *i.e.* low salt vs. high salt and high salt vs. high salt with Mg^{2+}, shifts the T_m of each I•U base pair-containing dsRNA higher by similar amounts (ΔT_m ~10-12°C) such that relative differences between the three dsRNAs remain the same regardless of the solution condition. The dsRNA T_m values in high salt (100 mM NaCl) therefore likely most closely reflect dsRNA stability under OAS1 *in vitro* assay conditions and these are reported as average values in **Table 1** for the IU variants and all other dsRNAs tested in subsequent experiments (individual measurements in all three conditions are also shown in **Table S1**).

As a consequence of the reduced stability with I•U base pairs, we also expected to observe a corresponding strongly decreasing trend in each dsRNA's ability to activate OAS1. However, when the I•U dsRNAs were tested in an established *in vitro* OAS1 activation assay,

the inosine-containing dsRNAs all unexpectedly enhanced OAS1 activation (**Figure 1E** and **Table 1**). Further, this modest increase in OAS1 activation directly correlated with the number of I•U base pairs incorporated (*i.e.* trend in OAS1 activation: AU3 < IU1 < IU2 < IU3). Thus, contrary to expectation, changes in the short dsRNA of the type arising from natural A-to-I editing do not decrease OAS1 activation, despite the anticipated reduction in dsRNA stability.

OAS1 activation is enhanced by inosine and mismatches in the center of short dsRNAs

The ability of I•U pair-containing dsRNAs to modestly enhance OAS1 activation by the short dsRNA could arise through generally increased helical flexibility, specific change in helical structure to accommodate the non-isosteric base pairs, or a property of the non-standard inosine base itself. To begin addressing these possibilities, we generated two further series of 18 bp dsRNAs containing either I-C or A•C pairings with one, two, or three sets of substitutions at the same sites and with the same naming convention as before (**Figure 2** and **S1**). These base pair substitutions were selected because I-C pairs place inosine in the same locations while maintaining Watson-Crick-like base pairing and geometry, whereas A•C pairings introduce a different strongly destabilizing mismatch that does not contain inosine.

I-C base pair-containing dsRNAs were prepared as before (**Figure S1**) and assessed for thermal stability by UV melting analysis (**Figure 2B**). As expected, T_m values for the three I-C dsRNAs were similar (within ~3°C) under each given solution condition and also similar to AU3 dsRNA (**Figure 2B**, **Tables 1** and **S1**). Again, no specific differences in stability were observed between the low and high salt, or with Mg^{2+} conditions (**Table S1**). Thus, unlike I•U pairs, I-C pairs do not destabilize the short dsRNA. Next, we assessed the three IC dsRNAs in the *in vitro* OAS1 activity assay and found that despite their identical stability to each other and AU3 dsRNA, OAS1 activation was again modestly enhanced (**Figure 2C** and **Table 1**). However, we note these base pair changes result in a different order of relative ability to activate OAS1 compared to the IU dsRNAs: both IC1 and IC2 cause the same intermediate level of activation

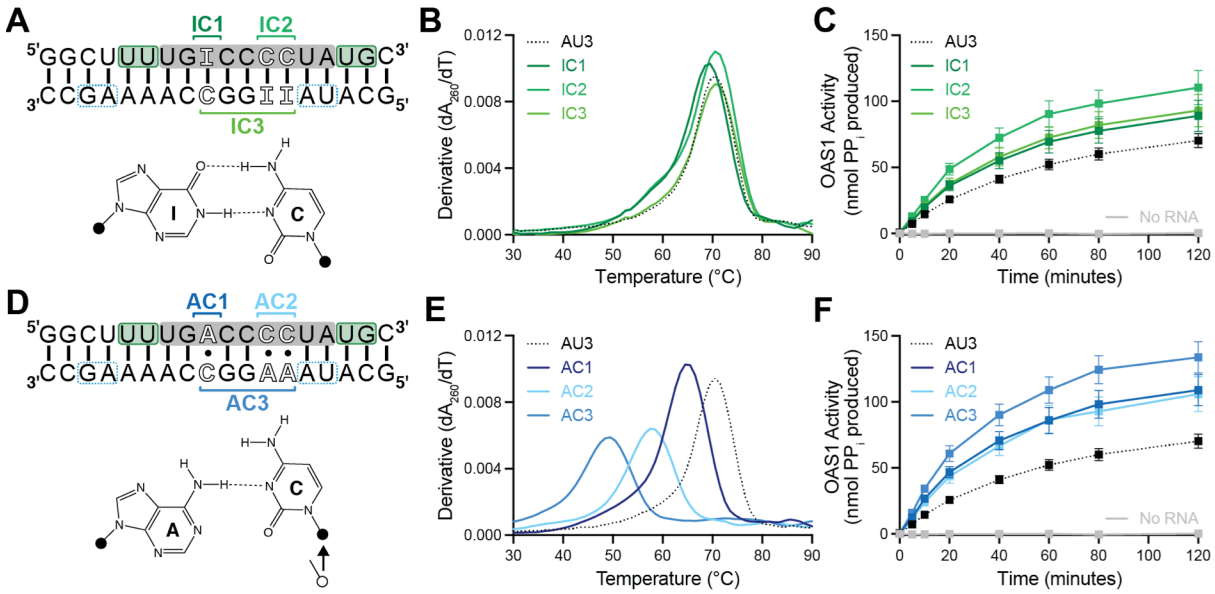

Figure 2. OAS1 activation is potentiated by inosine substitutions and mutations that introduce non-canonical Watson Crick base pairing. ***A,*** Schematic of the inosine-containing model 18 bp dsRNA with I-C base pairing (shown below), which adopts normal Watson-Crick base pair geometry. ***B,*** UV thermal melt analysis shows little to no change in melting temperature for the I-C substitutions (*green*) compared to AU3 (*black dotted line*). ***C,*** Reaction progress curves for *in vitro* OAS1 activation for all I-C variants (*green*) and AU3 (*black dotted line*). ***D,*** same as in *panel A*, but for A•C mismatches to test the correlation between OAS1 activation and dsRNA stability. For the A•C mismatch, the shift in base and phosphodiester backbone positions necessary to form a single hydrogen-bonding interaction is noted (open and closed circles with arrow). ***E,*** UV thermal melt analysis shows that destabilization of the dsRNA duplex by introducing A•C mismatches in this region shifts to lower melting temperatures compared to AU3 (*black dotted line*). ***F,*** same as in *panel C*, but for all A•C variants (*blue*) and AU3 (*black dotted line*).

between AU3 and IC3, while three I-C pairs in IC3 most significantly increase OAS1 activity (*i.e.* order AU3 < IC1 ~ IC2 < IC3).

Next, we tested the 18 bp dsRNA with one (AC1), two (AC2), or three (AC3) A•C mismatched base pairs (**Figure 2D** and **S1**) using the same two assays. As expected, there is a large shift to lower T_m under all conditions as the number of A•C mismatches increases (**Figure 2E**, **Tables 1** and **S1**). The same consistent shifts in T_m between the different conditions are observed again, albeit somewhat reduced for AC3 with a ΔT_m of only ~6°C on addition of Mg^{2+} (**Table S1**). Remarkably, addition of A•C mismatches robustly enhanced OAS1 activation

compared to AU3 dsRNA (**Figure 2F**). Further, as for the I-C dsRNAs, all three A•C substitutions are required to achieve the largest enhancement in OAS1 activation, whereas AC1 and AC2 produced a similar intermediate level of OAS1 activity (*i.e.* order AU3 < AC1 ~ AC2 < AC3).

The results thus far show that base pair changes in the middle of the OAS1 consensus sequence that reduce helical stability (I•U and A•C base pairs) unexpectedly enhance the capacity of the short dsRNA used here to activate OAS1. Further, inosine-containing dsRNAs are also modestly better activators regardless of whether the dsRNA is destabilized (I•U-containing dsRNAs) or not (I-C-containing dsRNAs) by incorporation of the modified base. As noted earlier, OAS1-bound dsRNA adopts a distorted structure to make contacts from both ends of the helix to the protein. Thus, destabilization of the dsRNA central region with I•U or A•C pairs could increase OAS1 activation by allowing this necessary helical structure to be more readily adopted. The potential for short dsRNA regions containing destabilizing pairings, such as mismatched base pairs, to retain an ability to activate OAS1 is particularly intriguing. This finding suggests that searches for perfectly paired regions of >18 base pairs in cellular RNAs likely significantly underestimate the number of potential endogenous OAS1-activators. We therefore decided to further test this idea by examining dsRNAs with additional G-C base pairs that would be expected to have the opposite effect on helical stability.

Stabilization with G-C substitutions can also enhance OAS1 activation by short dsRNAs

As a first test of the idea that dsRNAs enriched in G-C base pairs should result in lower OAS1 activity due to increased helical stability or rigidity, we used the *in vitro* OAS1 activation assay to test two high molecular weight homopolymers, poly(rA:rU) and poly(rG:rC), in comparison with the known potent OAS1 activator poly(rI:rC). Each homopolymer had widely different capacities to activate OAS1 with poly(rI:rC) dsRNA (**Figure 3**, green triangle) being the most potent and poly(rG:rC) dsRNA (**Figure 3**, red circle) promoting the least amount of OAS1 activation. The

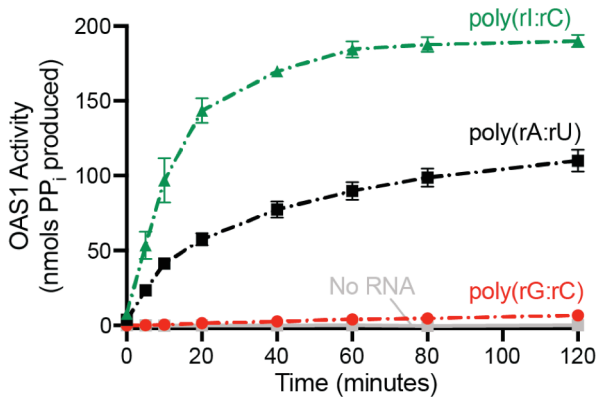

Figure 3. Homopolymer sequence strongly influences OAS1 activation. Reaction progress curves for *in vitro* OAS1 activation by three long synthetic dsRNAs: poly(rA:rU) (*black square*), poly(rI:rC) (*green triangle*), and poly(rG:rC) (*red circle*) at a single concentration (0.5 µg/ml).

poly(rG:rC) dsRNA was found to only be capable of weakly activating at 60-fold higher concentration (**Figure S3**). Thus, the results with dsRNAs containing highly biased sequences support the idea that more stable and, likely, more rigid dsRNA is a poor activator of OAS1. These results also underscore that poly(rI:rC) is an unusually potent activator relative to dsRNAs of similar length containing only the four standard bases.

Next, to test whether addition of G-C base pairs has the same effect in the context of the 18 bp dsRNA, we generated dsRNAs with one (GC1), two (GC2), or three (GC3) G-C substitutions as before (**Figure 4A** and **S1**). As expected, UV thermal melting analysis revealed overall higher melting temperatures for all three GC variants compared to AU3 with a clear positive correlation between the number of G-C base pairs and the increase in T_m under all solution conditions (**Figure 4B**, **Tables 1** and **S1**). Surprisingly, however, the addition of G-C base pairs in the 18 bp dsRNA, once again resulted in increased OAS1 activation (**Figure 4C** and **Table 1**). In this set of dsRNAs, a further distinct pattern of relative activation was observed with the tandem G-C substitutions of GC2 being sufficient to achieve the same highest level of activation as GC3 (*i.e.* order AU3 < GC1 < GC2 ~ GC3). These results suggest there must be some other features, in addition to the destabilizing effects of the I•U and A•C pairs, that can lead to increased activation capacity.

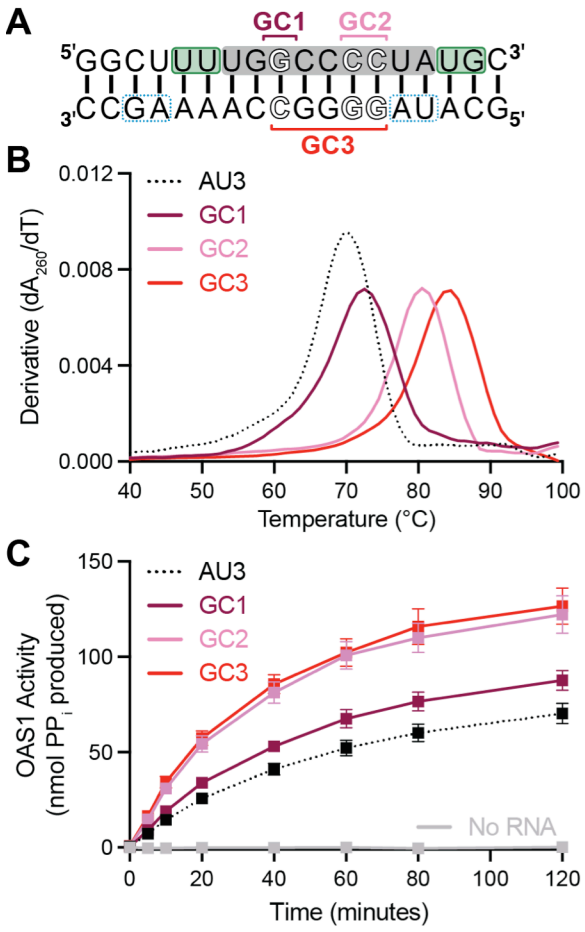

Figure 4. dsRNA helix stabilizing G-C base pairs enhance OAS1 activation. ***A,*** Schematic of model 18 bp dsRNA modified to include one (GC1), two (GC2), or three (GC3) G-C base pairs (*white*). ***B,*** UV thermal melt profiles indicate that increased G-C content (*red*) corresponds to an increase in respective melting temperatures compared to AU3 (*black dotted line*). ***C,*** Reaction progress curves for *in vitro* OAS1 activation of all G-C variants (*red*) and AU3 (*black dotted line*).

Differences in dsRNA structure correlate with their capacity to activate OAS1

Next, we used thermal difference spectra (TDS) to determine whether specific dsRNA helical structure differences in each dsRNA variant series could be identified that might underpin the observed increases in OAS1 activity. TDS for nucleic acids are obtained by measuring UV absorbance at a range of wavelengths at two temperatures, one above and one below the T_m corresponding to the unfolded and folded states of the molecule, respectively. The difference

between these two spectra (the TDS) arises through changes in base stacking interactions and thus contains valuable information characteristic of a given nucleic acid structure (36).

The TDS spectrum for AU3 dsRNA is characterized by three major features: a broad positive peak at ~270-280 nm flanked by two minima, a broad, likely double, minimum at ~285-295 and a weaker but sharper minimum at ~260 nm (**Figure 5A**). Features below ~250 nm were more variable between replicate experiments (**Figure S2**) and were not considered further. Clear differences in TDS spectra for each dsRNA variant series are observed compared to AU3 dsRNA, with common changes largely centered on an increase and/or rightward shift in the broad positive peak at ~270-280 nm and an increase (to less negative value) in one or both components of the double negative peak at ~285-295 nm. Importantly, excellent correlation between these spectral changes and order of ability to activate OAS1 within each series is also observed, as discussed further below, indicating that the TDS differences reflect dsRNA base stacking and helical features relevant for OAS1 activation.

I•U pair-containing dsRNAs alter each of the three major TDS spectral features in specific ways (**Figure 5B**). IU1 dramatically increases the broad ~270-280 nm peak and also slightly increases the negative peak at 260 nm while the other negative peak at ~285-295 nm is essentially unaffected. In contrast, IU2 significantly increases the negative ~285-295 nm peak, but only more modestly increases the ~270-280 nm peak and has no effect on the peak at 260 nm. In IU3, these distinct effects are almost perfectly combined with this dsRNA having the most pronounced increase in the ~270-280 nm peak, the strongest increase in the negative peak at ~285-295 nm (particularly in the shorter wavelength half, ~285-290 nm), and an identical increase as observed for IU1 at 260 nm. Thus, these base pair changes and the base stacking and helical alterations they induce, are consistent with *in vitro* OAS1 activation by these dsRNAs where IU1 and IU2 exhibit distinct intermediate levels of activation that are additive to make IU3 the most activating in this dsRNA series.

The I-C base pair changes also appear to impart unique differences in base stacking and helical structure as revealed by TDS. IC1 increases the positive ~270-280 nm peak but has essentially no effect on the other two regions. In contrast, IC2 sharply decreases (more negative) the 260 nm peak but also reduces the lower wavelength half of the positive ~270-280 nm peak (**Figure 5C**). Finally, IC3 contains spectra features of both variants, including increased 260 nm (IC2) and ~270-280 nm (IC1) peaks, but with pronounced rightward shift of the latter peak and loss of the shorter wavelength half of the negative ~285-290 nm peak. As for the IU dsRNAs, the changes in structure reflected in the TDS are consistent with the

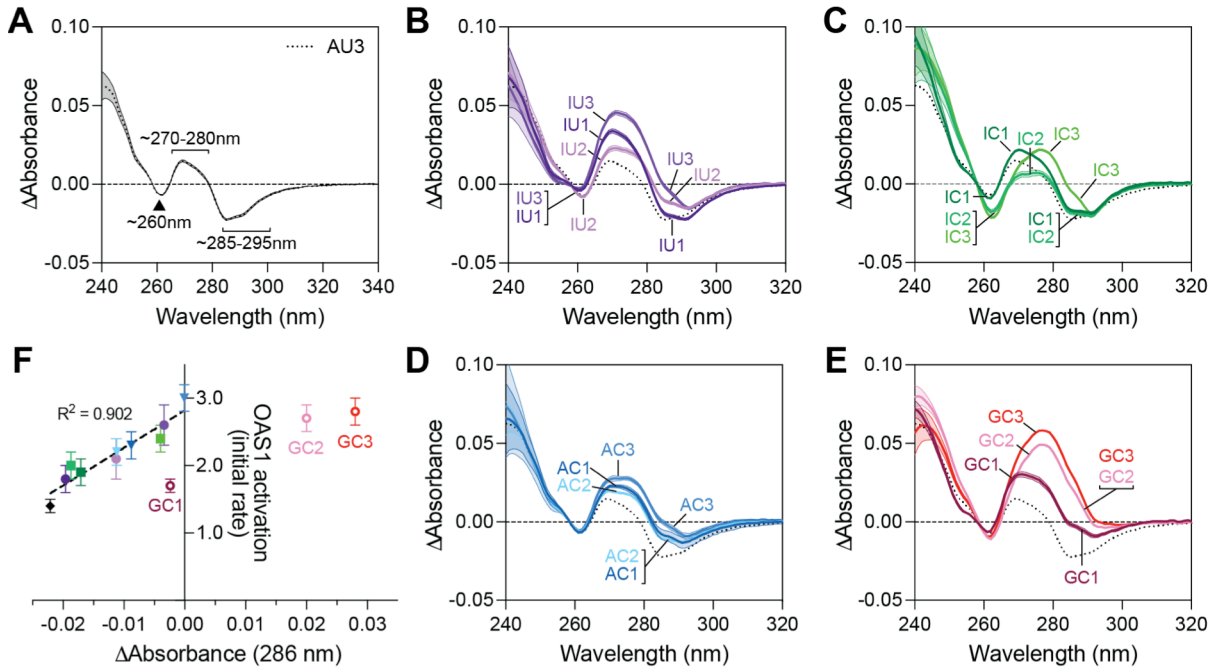

Figure 5. Thermal difference spectra (TDS) identify structural changes in dsRNA that correlate with increased OAS1 activation. ***A-E,*** UV absorbance was monitored for each indicated dsRNA over a range of wavelengths (240-320 nm) for the unfolded (95°C) and folded (20°C) states. TDS was obtained by normalizing individual data sets before subtracting absorbance values collected at 20°C from values collected at 95°C. All plots contain AU3 (*black dotted line*) for comparison and standard error of the mean (SEM) is shown for three independent experiments as transparent shading on each curve. Spectral features discussed in the main text are marked in *panel A* and labeled on each curve with specific dsRNAs in *panels B-E*. ***F,*** Plot of TDS at 286 nm against initial rate of OAS1 activation for each dsRNA shows a strong positive correlation for this spectral feature.

intermediate increase in OAS1 activation for IC1 and IC2 that combine in IC3 to make the strongest activator in this series of dsRNAs.

dsRNAs with A•C base pairs each result in similar changes in TDS (**Figure 5D**), with increases in both the positive ~270-280 nm and negative ~285-295 nm peaks (particularly in the shorter wavelength half, as for IU3). Here, AC1 and AC2 produce almost identical changes in the spectra, and these effects are additive in the spectrum for AC3. These results suggest that the A•C pairs induce similar, more global helical structure destabilization regardless of their location and, again, the changes in TDS accurately mirror the order of OAS1 activation: AC1 ~ AC2 < AC3.

Finally, the G-C base pairs result in the most pronounced changes in TDS of all the variant series, again centered on the peaks at ~270-280 nm and ~285-295 nm, with the negative 260 nm peak unaffected in all three dsRNAs (**Figure 5E**). While GC1 induces an increase in both peaks, the changes for GC2 and GC3 dsRNA are more pronounced and extremely similar in magnitude. In both latter dsRNAs, the negative ~285-295 nm is completely lost and appears in part as a shoulder on a broadened positive peak from ~270-290 nm. Thus, in contrast to the other dsRNA variants, for the G-C base pairs there appears to be relatively little additive effect in changes caused by GC1 and GC2. Instead, the effect of the tandem G-C pair of GC2 appears to dominate in both GC2 and GC3 dsRNAs, again mirroring the order of activation: GC1 < GC2 ~ GC3.

In summary, the TDS reveal that specific changes in base stacking and/ or helical structure arise from the distinct base pair changes in each dsRNA variant series and that the nature and extent of these changes faithfully reflect the extent of OAS1 activation by each RNA. Further, many of these changes appear to be shared among several of the dsRNA variants. For example, change in TDS at 286 nm is highly correlated within and between the I•U, I-C, and A•C base pair containing dsRNAs (**Figure 5F**). At this wavelength, G-C base pair containing dsRNAs also show an increase consistent with OAS1 activation (*i.e.* GC1 < GC2 ~ GC3), but

additional helical structure changes, that do not impact OAS1 activation, apparently result in significantly greater TDS. Together, these data clearly support the idea that dsRNA helical structure and dynamics, as dictated by specific sequence changes, play an important role in regulating the extent of OAS1 activation. While many changes in TDS observed are consistent between the most potent OAS1 activators in each dsRNAs variant series, the specific helical structures and/or dynamics underpinning these changes cannot be directly discerned. To gain such insights, we turned to molecular dynamics (MD) simulations of these dsRNAs.

MD simulation reveals a role for helical dynamics in OAS1 activation

We used MD simulations to gain deeper insight into the helical and local base pair/ base step properties within the N_9 region of select dsRNAs to define the basis for the structural differences identified by TDS and which confer their increased capacity to activate OAS1. As noted earlier, a recent MD study identified alternating AU sequences of three or more consecutive nt in length as a potential source of helical bending within dsRNA (33). We therefore first used one of the test sequences ("Seq3") from this study to benchmark our MD production protocol which used the Desmond module of the Schrödinger software (release 2020-4; see Methods for details).

Seq3 contains the sequence AUAU in the center of a 24-nucleotide dsRNA and was found to induce the most pronounced helical bending angle of 16.0 +/- 1.1° among three AU-tract-containing sequences tested, as well as a characteristic narrowing of the major groove at this sequence (33). As our analysis of other dsRNAs (see below) revealed relevant structural fluctuations on shorter timescales than used in this study, we chose to analyze 20 representative structures from consecutive 10 ns segments of a 200 ns production run using Curves+ (37,38). This analysis produces an average bending angle of 14.5°, close to the published value (33). However, we note that our comparatively fine-grained analysis (20 PDBs over 200 ns vs. 5 PDBs over 1000 ns) appears to distinguish a minor cluster with lower bending angles (~5-8°), a major cluster with higher bending angles (~11-21°), and single high outlier.

Excluding the outlier and minor cluster gives an average bending angle of 16.5° (**Figure S4A**), essentially identical to the published value (33). Additionally, the Curves+ analysis of major groove width reveals the previous reported 3-4 Å narrowing centered on the AUAU sequence (**Figure S4B**). Thus, our MD procedure faithfully replicates previously reported dsRNA helical features of the type that could potentially influence OAS1 activation.

MD analysis was first performed for 200 ns for the parent 18 bp dsRNA (AU3) and the variants with three base pair changes of each type (*i.e.* IU3, IC3, AC3, and GC3) as these dsRNAs showed the most pronounced changes in TDS correlated with enhanced OAS1 activation within each group of variants. Consistent with their decreased helical stability in the thermal melting studies, both IU3 and AC3 exhibited an overall higher root mean square deviation (RMSD) compared to both AU3 and the other variants, IC3 and GC3 (**Figure S4C**). Greater flexibility in the structures of these two dsRNAs was also reflected by their significantly higher mean bending angle compared to the AU3, IC3, and GC3 dsRNAs (**Figure 6A**). The IU3 and AC3 dsRNAs also showed an overall expanded range of bending angles and, for AC3, an overall upward shift of this expanded range to higher values. Consistent with higher overall RMSD and increase in helical bending, alignment of all 20 structures reveals larger variation in overall helical structure for both the IU3 and AC3 compared to AU3 dsRNA (**Figure 6B**). In contrast, IC3 and, to an even greater extent, GC3 exhibit lower variation among the 20 representative structures.

Examination of a wide range of helical, base step, and base pair parameters determined using Curves+ reveals more detail on the wide-ranging impacts of these destabilizing base pair changes on dsRNA helical structure (**Figure S5A-D**). Notably however, in all cases the first 7-8 base pairs or base pair steps which comprise one region directly contacted by OAS1, are essentially indistinguishable in structure from AU3 dsRNA. In IU3 and AC3 dsRNAs, large deviations in these structural parameters are centered on the regions following one or both of the sites with altered base pairs. As such, changes in helical and local base pair structure are

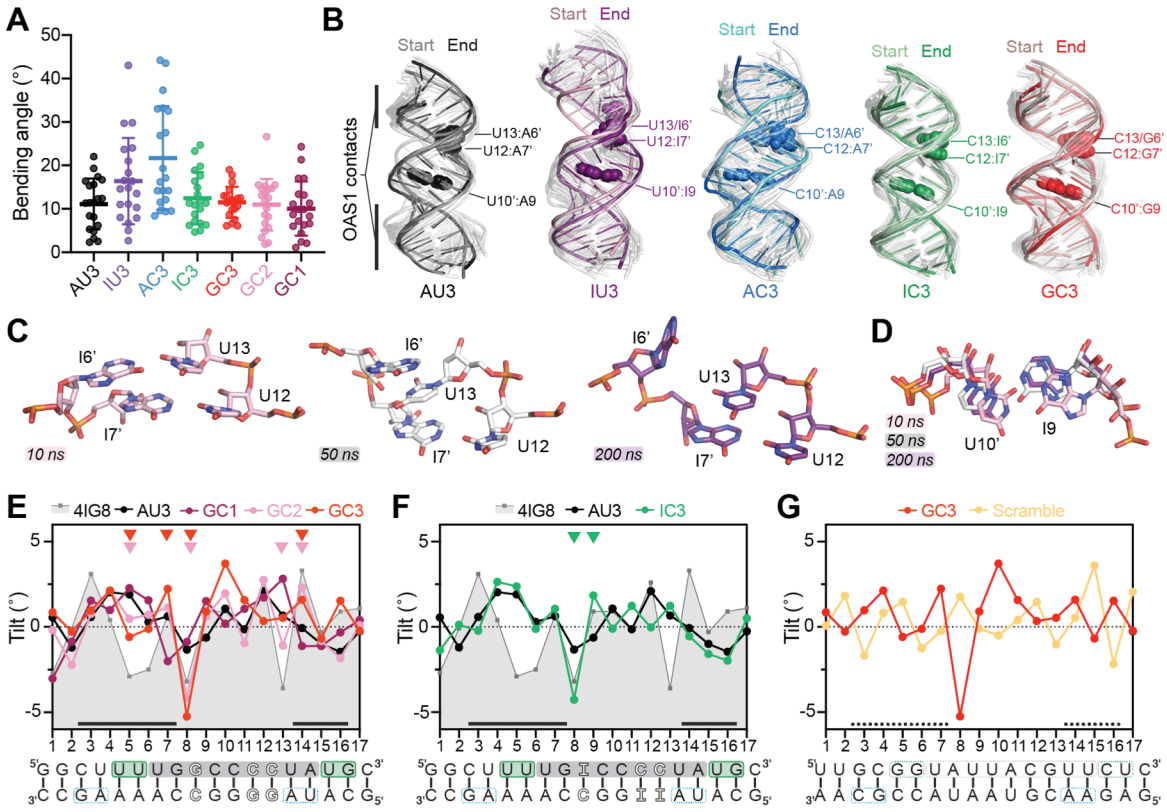

Figure 6. Increased dsRNA dynamics and specific helical features underpin enhanced OAS1 activation by short dsRNAs. ***A,*** Helical bending angle calculated for the 20 structures representative of each 10 ns of the 200 ns simulation of each dsRNA indicated. ***B,*** Alignment of all 20 representative structures for the indicated dsRNA simulation. The structure from the first (lighter color) and last (darker color) 10 ns segments of each simulation are highlighted, with the 18 intermediate structures shown as semi-transparent cartoons. The locations the base pairs changed in each dsRNA are indicated and the nucleobases highlighted (spheres). ***C,*** Interactions formed by the tandem I•U base pairs in representative structures at the indicated simulation time points, including the start and end, colored as in *panel B*. ***D,*** As for *panel C*, but for the single base pair change with the three structures overlaid. ***E,*** Comparison of base pair tilt for the 20 representative structures from MD simulation of AU3 and the GC series dsRNAs (GC1, GC2, and GC3) determined using Curves+. Values for the OAS1-bound RNA structure (PDB code 4IG8) are also indicated (gray shaded area). Steps with mean tilt values mirroring those in the bound dsRNA structure (4IG8) in the most activating GC2 and GC3 dsRNAs but not GC1 and AU3 are indicated above the plots with arrowheads. The black bar above the x-axis indicates the main regions (on either strand) of contact with OAS1 in the complex crystal structure. The sequence of GC3 dsRNA is shown underneath for reference. ***F,*** As in *panel E* but comparison of IC3 (sequence shown below for reference), AU3, and bound structure (4IG8). ***G,*** Comparison of mean tilt for strongly activating GC3 dsRNA and non-activating Scramble dsRNA. The Scramble sequence shown below for reference lacks consensus sequences but their positions in the other dsRNAs are indicated for comparison.

localized to the central region between the conserved OAS1 consensus dinucleotides (WW/WG). With only one exception (for axial bend; **Figure S5A**) structural parameters for IU3 and AC3 dsRNAs return to values similar to AU3 dsRNA by the final 2-3 base pairs or base steps (**Figure S5A-D**).

Examination of representative structures from the AC3 and IU3 simulations also reveals the potential for both tandem base pair substitutions (12:7' and 13:6', where ' denotes the bottom strand nucleotide) to induce large local changes in helical structure and base stacking (**Figure 6C,D** and **S5E**). Early in the IU3 simulation (within 30-50 ns) the U13:I6' pair becomes disrupted and U13 moves toward the helical axis forming a hydrogen bond via its base N3 to the 2'-OH of I6', creating a stack of three bases with the two inosines (I6':U13:I7'; **Figure 6C**). This structure subsequently persisted throughout the simulation, with only one minor variation near the end of the simulation in which I6' shifts up within the helical base stack nearer to A5' (exemplified by the 200 ns representative PDB in **Figure 6C**). In contrast, the single I•U base pair (base pair 9:10) maintained relatively consistent mismatched base pairing and base stacking interactions throughout the simulation (**Figure 6D**). In AC3 dsRNA, we observe formation of a similar structure in which a purine base (A7') rather than the pyrimidine shifts toward the central axis to form a similar single base stack (C13:A7':C12; **Figure S5E**). While this structure persists over several 10 ns segments of the simulation, these changes in AC3 appear more transient, returning to structures with distinct tandem mismatch A•C pairs and, finally, second distinct non-helical structure in which C13 is fully extruded from the helix, strongly kinking the RNA phosphodiester backbone (**Figure S5**).

In summary, the MD simulations reveal that inherent general deformability in the dsRNA region between the major contacts with OAS1, likely underpins the ability of the IU3 and AC3 dsRNA more strongly drive allosteric activation of the enzyme. The potential formation non-A-form helical structures, in particular by the tandem I•U pairs may also have implications for the

mechanism by which editing masks cellular dsRNAs from other innate immune sensors (see Discussion).

Specific base pair changes pre-dispose helical parameters to favor the short dsRNA adopting an OAS1-bound-like conformation

In contrast to AC3 and IU3 dsRNAs, the increased capacity of IC3 and GC3 dsRNAs to activate OAS1 cannot result from a general increase in helical flexibility or deformability. To provide additional comparisons which might aid in pinpointing any specific helical parameters that contribute to increased OAS1 activation in these dsRNAs, we ran additional simulations of GC1 (activation similar to AU3) and GC2 (activation similar to GC3). Both exhibited similar overall RMSD and overall bending angle to AU3 dsRNA (**Figures S4C** and **6A**, respectively). As before, helical and base pairing/ base step parameters were determined using Curves+ (37,38) for comparison with each other and to the structure of the 18 bp dsRNA corresponding to AU3 bound to human OAS1 (2) (**Figures 6E** and **S6**). Of these parameters, base pair tilt is particularly characteristic of local helical bending and three regions apparent in GC3 where the simulation suggests a propensity to adopt a more OAS1-bound-like structure (**Figure 6E**; regions marked with arrowheads). Importantly, most of these sites in GC3 dsRNA which more closely match the OAS1-bound dsRNA in their base pair tilt, are also present in GC2 dsRNA; in contrast, GC1 dsRNA appears consistently more similar to AU3, in both cases mirroring the respective differences between these pairs of dsRNAs in both their OAS1 activation capacity and TDS. While less pronounced in IC3, at least one region mirroring the bound structure is also apparent (**Figure 6F**). Further, a simulation of a randomized sequence (Scramble) previously shown to lack any capacity to activate OAS1 (1), appears close to anti-correlated in tilt values throughout (**Figure 6G**). Collectively, these insights reveal that local changes in base pair tilt likely have pronounced impact on OAS1 activation by short dsRNAs.

These dsRNAs also share an UAUG (underlined nts are the conserved WG of the OAS1 consensus sequence) immediately after the site where our tandem base pair changes are introduced. AU3 and both GC2 and GC3 all show modest narrowing of the major groove around this sequence (**Figure S6A**), consistent with the reported effect of AU-tract sequences on helical structure (33). It is possible that G-C base pairs preceding this sequence help stabilize a structure in this region that promotes OAS1 activation by this short dsRNA, in ways that are not fully apparent from simulations of the free dsRNAs. However, in further support of this idea, Scramble dsRNA which does not activate OAS1, lacks the UAUG sequence and has a markedly widened major groove in this region (**Figure S6E**). Finally, differences in other helical or base pair parameters between GC2/ GC3 and AU3 dsRNA (**Figure S6A-D**) could also contribute to greater activation in subtle ways that are apparent from simulation of the free dsRNAs or by comparison to the OAS1-bound structure.

Additive effects of distinct helical features on OAS1 activation

The MD simulations with short dsRNAs revealed two distinct mechanisms by which alterations in sequence can impact helical structure or dynamics to effect greater OAS1 activation: generally increased dynamics in the central region of the helix or specific local changes in helical structure, in particular, base pair tilt. An obvious next question is where these distinct effects can be combined in a single dsRNA to produce an even more potent OAS1 activator. To test this idea, we combined the AC1 and GC2 base pair changes (AC1-GC2 dsRNA) and did indeed find this dsRNA to be a significantly better activator than either individual variant (**Figure 7A,B**). Consistent with our interpretation of MD simulations thus far, analysis of AC1-GC2 dsRNA revealed, an increased overall RMSD compared to AU3 or any of the G-C pair-containing dsRNAs (**Figure S4C**) and an overall mean bending angle comparable to these other dsRNAs (**Figure 7C**). Additionally, AC1-GC2 exhibited the same local structural features reflected by base pair tilt as observed in GC2 and GC3 dsRNAs (**Figure 7D**, marked with

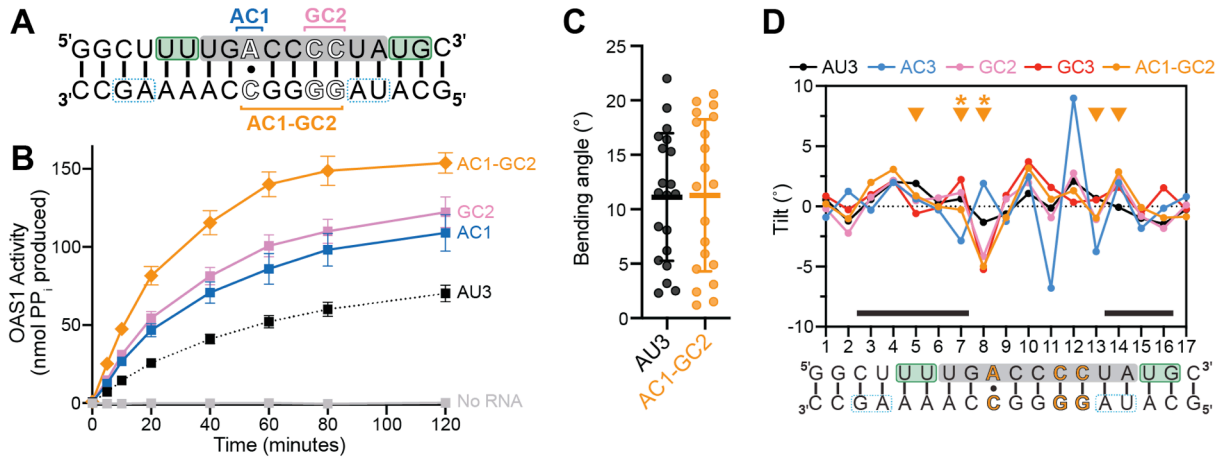

Figure 7. Sequence changes resulting of enhancement of OAS1 distinct via distinct molecular mechanisms have additive activity. *A*, Schematic of the 18 bp dsRNA AC1-GC2 combining the AC1 and GC2 bas pair changes. ***B***, Reaction progress curves from an *in vitro* chromogenic assay of OAS1 activity using a single dsRNA concentration (300 nM) showing OAS1 activation is enhanced by combination of the AC1 and GC2 base pair changes in AC1-GC2 dsRNA. Data for AU3, AC1 and GC2 dsRNAs shown for comparison are the same as in **Figures 2** and **4**). ***C***, Helical bending angle calculated for the 20 structures representative of each 10 ns segment of the 200 ns simulation of AC1-GC2 dsRNA. Data for AU3 shown for comparison are the same as in **Figure 6**. ***E***, Comparison of base pair tilt for the 20 representative structures from MD simulation of AC1-GC2 dsRNA and other indicated dsRNAs determined using Curves+. Arrowheads denote sites with mean tilt values mirroring those in the bound dsRNA structure (4IG8) as indicated for GC2 and GC3 dsRNAs in **Figure 6E**. Asterisks denote sites where tilt parameters in in AC1-GC2 match the two G-C base pair dsRNAs but differ from AC3 dsRNA. The black bar above the x-axis indicates the main regions (on either strand) of contact with OAS1 in the complex crystal structure (PDB 4IG8). The sequence of AC1-GC2 dsRNA is shown underneath for reference.

arrowheads), including two sites where opposite distortions in AC3 dsRNA are reversed to the more OAS1-bound-like conformation (marked * in **Figure 7D**). Similarly, combination of AC1 and GC2 base pair changes results in other helical and base pair parameters more like AU3 and GC dsRNAs (**Figure S7**).

Short dsRNA-mediated OAS1/RNase L activation in human cells mirrors their activity *in vitro*

We next assessed whether these dsRNAs with different base pair changes retain their ability to activate the OAS1/RNase L pathway in human lung carcinoma A549 cells. Wild-type and RNase L KO A549 cells were pre-treated with interferon to induce the expression of OAS1 (**Figure 8A,B**) and transfected with either AU3 or with three base pair changes from each dsRNA series, *i.e.* IU3, IC3, AC3, or GC3, alongside mock transfection and poly(rI:rC) dsRNAs as negative and positive controls, respectively. Transfection of A549 cells with each short dsRNA or poly(rI:rC) dsRNA results in the degradation of 28S and 18S rRNA (**Figure 8A**) consistent with OAS/RNase L pathway activation. In contrast, no rRNA cleavage was observed in the RNase L KO cells (**Figure 8A**) confirming that dsRNA-induced cleavage is a direct consequence of OAS/RNase L pathway activation. Additionally, our previous demonstration that Scramble dsRNA does not activate OAS1 *in vitro* or induce rRNA cleavage in A549 cells (1) further confirms the dependence of the observed pathway activation on the specific dsRNA sequence used. It is also important to note that the short dsRNAs are the minimal length (~18 bp) required to activate only OAS1; therefore, the greater observed rRNA cleavage for poly(rI:rC) dsRNA is likely due to both its potency as an activator of OAS1 and also its ability to activate additional OAS family members (*i.e.* OAS2 and OAS3).

To compare the degree of rRNA cleavage among the short dsRNAs, the major 28S cleavage product (**Figure 8A**, solid arrow) was quantified and normalized to AU3 dsRNA (**Figure 8C** and **Table 1**). Overall, the cell-based assays correlate well with the respective capacity of each dsRNA to activate OAS1 in the *in vitro* chromogenic assay: all dsRNA variants exhibit increased activity mirroring relative *in vitro* activation of OAS1 with one exception, AC3 dsRNA (**Figure 8C,D**). The variability observed for the AC3 dsRNA could be due to lower transfection efficiency (*e.g.* A•C pairs may be protonated to form two hydrogen bonds) and/or the multiple mismatched base pairs could render these short dsRNA more susceptible to strand dissociation and degradation by cellular RNases.

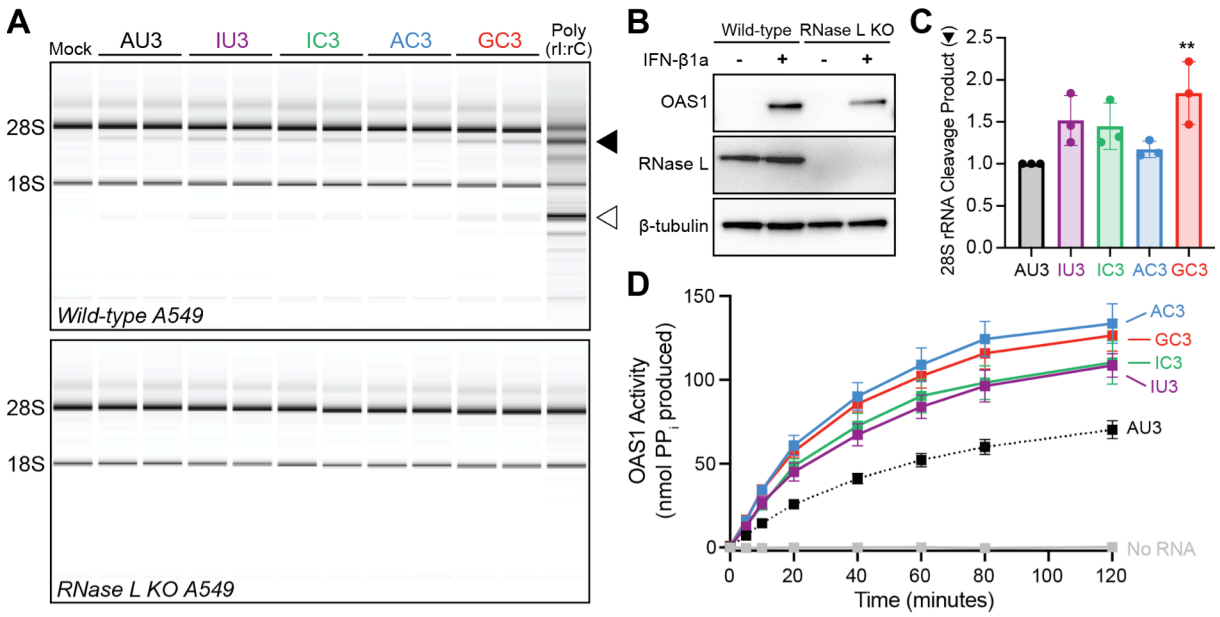

Figure 8. Activation of the OAS1/RNase L pathway by WWN$_9$WG dsRNA variants mirrors their capacity to activate OAS1 *in vitro*. *A,* Analysis of rRNA integrity in wild-type (*top*) or RNase L KO (*bottom*) A549 cells following transfection with dsRNAs: AU3 (*black*), IU3 (*purple*), IC3 (*green*), AC3 (*blue*), and GC3 (*pink*). Mock transfection and transfection with poly(rI:rC) dsRNA serve as negative and positive controls, respectively. 28S/18S rRNA degradation (*arrows*) is indicative of OAS1/RNase L pathway activation. A representative experiment with technical duplicates for each dsRNA is shown. ***B,*** Western blot analysis confirming both OAS1 expression following interferon (IFN-β1a) treatment and absence of RNase L in the RNase L KO cells. ***C,*** Quantification of the 28S rRNA cleavage product (panel A, *solid arrow*) for each dsRNA normalized to cleavage induced by AU3 (*black*). Data is shown as the mean with standard deviation (SD) for three independent experiments, and one-way ANOVA with Dunnett's post-hoc test was used to determine statistical significance, $p < 0.01$ (**). ***D,*** Reaction progress curves for *in vitro* OAS1 activation by AU3 (*black dotted line*) and the third variant in each mutation series: IU3 (*purple*), IC3 (*green*), AC3 (*blue*), and GC3 (*pink*) are shown for comparison (these data are the same as shown in **Figures 1, 2,** and **4** for each dsRNA).

DISCUSSION

A recent report indicated that A-to-I editing by ADAR1 is responsible for eliminating inadvertent activation of the OAS/RNase L pathway by endogenous dsRNAs in uninfected cells (28). Thus, we set out to determine OAS1 sensitivity to inosine modifications within a short 18 bp dsRNA. We also used these tools to extend our prior work showing that the N_9 sequence within the

OAS1 activation consensus sequence (WWN_9WG) plays an important, and to date, unappreciated role in OAS1 activation. As observed in the human OAS1-dsRNA crystal structure (2), dsRNAs adopt a bent, imperfect A-form helix when bound to OAS1 allowing interactions with the protein at two locations on its surface. Thus, sequence changes that alter dsRNA structure or dynamics, either making the helix too flexible or too rigid, would undoubtedly alter the dsRNA's ability to regulate OAS1 activation. Surprisingly, our studies revealed that, at least in the context of short dsRNAs, OAS1 is still able to sense inosine-containing dsRNAs. Not only was OAS1 activated by inosine-containing dsRNAs, but these modifications in fact generated dsRNAs that were even better OAS1 activators.

Both *in vitro* and cell-based assays of OAS1 activation showed that incorporating mismatched base pairs, such as those introduced by A-to-I editing, does not eliminate OAS1's ability to sense these short dsRNAs. Unexpectedly, all of the substitutions made to alter RNA shape, conformation, and/or flexibility resulted in markedly better activators of OAS1. TDS analysis showed that nucleotide substitutions can alter base stacking revealing unique structural fingerprints corresponding to differences in dsRNA helical structure which precisely mirrored the trends observed in OAS1 activation *in vitro*. MD simulations also identified both local and global changes in dsRNA shape and flexibility that correlate with their respective impacts on OAS1 activation. Taken together, we have identified that dsRNA structure and amenability to adopting the appropriate OAS1-bound-like conformation, are new criteria to consider when determining the capacity of OAS1 recognition of dsRNAs.

In the absence of infection, A-to-I editing of cellular RNAs by ADAR1 was proposed to be a protective measure to aid in differentiation between "self" and "non-self" dsRNAs preventing unnecessary activation of the OAS/RNase L pathway. This post-transcriptional modification alters base pair geometry, decreases RNA stability, and increases the susceptibility for degradation by cellular RNases. Additionally, A-to-I editing also removes double-stranded regions thought to be an absolutely indispensible characteristic required for OAS1 activation.

However, contrary to what has been proposed in the literature, inosine-containing pairs or mutations that otherwise disrupt the RNA helical structure were found to inversely correlate with OAS1 activation, *i.e.* IU and AC dsRNAs with the lowest melting temperatures were also observed to have the largest enhancements in OAS1 activation. MD simulations demonstrated that IU3 and AC3 dsRNAs are more prone to global changes in dsRNA structure and flexibility which contributes to their increased capacity to potently impact OAS1 activation. By increasing flexibility in the central region, the dsRNA may more readily adopt a bent conformation required for OAS1 recognition while not disrupting direct contacts made between OAS1 and the conserved consensus sequence dinucleotides (WW/WG) located on each end of the dsRNA helix.

The long poly(rG:rC) dsRNA was found to be an exceptionally poor activator consistent with the idea that forming a more rigid dsRNA should dampen OAS1's ability to sense these dsRNAs. However, in the context of the short dsRNA, additional G-C base pairs within the consensus N_9 region resulted in a substantial and unexpected increase in OAS1 activation. For these stabilized short dsRNAs, MD revealed specific changes in local helical parameters, in particular base pair tilt angle that appears to predispose the dsRNA to adopt a conformation more similar to the dsRNA-bound form. By reducing the need for OAS1 binding to induce required conformational changes in the dsRNA, these local helical structures thus lead to the increased OAS1 activation we observed both *in vitro* and in A549 cells. However, a general increase in helix rigidity, in the case of the long homopolymer poly(rG:rC) dsRNA, can almost completely abrogate any activating ability conferred by the dsRNA.

Our novel finding of OAS1 showing tolerance for inosine bases was also matched by revealing greater than appreciated complexity in the OAS1 activation consensus sequence suggesting that dsRNA helical dynamics (flexibility) and/or specific structural features such as helical bending may be dictated by the N_9 sequence and are necessary features required to promote optimal OAS1 activation. These insights also provide a basis for better understanding

of how more complex, structured RNAs may accomplish their strong OAS1 activation. More importantly, these data also greatly expand the potential sequences (of either viral or cellular origin) capable of OAS1 activation with the tolerance of, or even preference for, mismatched bases.

ACKNOWLEDGEMENTS

We thank Dr. Susan Weiss (University of Pennsylvania School of Medicine) for generously providing RNase L KO and associated parental A549 cells. We also thank Drs. Christine M. Dunham, Richard A. Kahn, and Daniel Reines for discussions and comments on the manuscript.

FUNDING INFORMATION

This work was supported by National Institutes of Health awards R01-AI144067 (to GLC), T32-GM008367 (to SLS), and F31-AI133950 (to SLS); the Emory University Research Council (to GLC); and the Emory University School of Medicine Bridge Funding Program (to GLC). SLS also gratefully acknowledges support from the Atlanta Chapter of The ARCS Foundation. This study was supported in part by the Emory Integrated Genomics Core (EIGC), which is subsidized by the Emory University School of Medicine and is one of the Emory Integrated Core Facilities.

REFERENCES

1. Schwartz, S.L., Park, E.N., Vachon, V.K., Danzy, S., Lowen, A.C. and Conn, G.L. (2020) Human OAS1 activation is highly dependent on both RNA sequence and context of activating RNA motifs. *Nucleic Acids Res*, **48**, 7520-7531.
2. Donovan, J., Dufner, M. and Korennykh, A. (2013) Structural basis for cytosolic double-stranded RNA surveillance by human oligoadenylate synthetase 1. *Proc Natl Acad Sci U S A*, **110**, 1652-1657.
3. Lohofener, J., Steinke, N., Kay-Fedorov, P., Baruch, P., Nikulin, A., Tishchenko, S., Manstein, D.J. and Fedorov, R. (2015) The Activation Mechanism of 2'-5'-Oligoadenylate Synthetase Gives New Insights Into OAS/cGAS Triggers of Innate Immunity. *Structure*, **23**, 851-862.

4. Dong, B., Xu, L., Zhou, A., Hassel, B.A., Lee, X., Torrence, P.F. and Silverman, R.H. (1994) Intrinsic molecular activities of the interferon-induced 2-5A-dependent RNase. *J Biol Chem*, **269**, 14153-14158.

5. Han, Y., Whitney, G., Donovan, J. and Korennykh, A. (2012) Innate immune messenger 2-5A tethers human RNase L into active high-order complexes. *Cell Rep*, **2**, 902-913.

6. Huang, H., Zeqiraj, E., Dong, B., Jha, B.K., Duffy, N.M., Orlicky, S., Thevakumaran, N., Talukdar, M., Pillon, M.C., Ceccarelli, D.F. *et al.* (2014) Dimeric structure of pseudokinase RNase L bound to 2-5A reveals a basis for interferon-induced antiviral activity. *Mol Cell*, **53**, 221-234.

7. Al-Ahmadi, W., Al-Haj, L., Al-Mohanna, F.A., Silverman, R.H. and Khabar, K.S. (2009) RNase L downmodulation of the RNA-binding protein, HuR, and cellular growth. *Oncogene*, **28**, 1782-1791.

8. Fabre, O., Salehzada, T., Lambert, K., Boo Seok, Y., Zhou, A., Mercier, J. and Bisbal, C. (2012) RNase L controls terminal adipocyte differentiation, lipids storage and insulin sensitivity via CHOP10 mRNA regulation. *Cell Death Differ*, **19**, 1470-1481.

9. Brennan-Laun, S.E., Li, X.L., Ezelle, H.J., Venkataraman, T., Blackshear, P.J., Wilson, G.M. and Hassel, B.A. (2014) RNase L attenuates mitogen-stimulated gene expression via transcriptional and post-transcriptional mechanisms to limit the proliferative response. *J Biol Chem*, **289**, 33629-33643.

10. Banerjee, S., Li, G., Li, Y., Gaughan, C., Baskar, D., Parker, Y., Lindner, D.J., Weiss, S.R. and Silverman, R.H. (2015) RNase L is a negative regulator of cell migration. *Oncotarget*, **6**, 44360-44372.

11. Rath, S., Donovan, J., Whitney, G., Chitrakar, A., Wang, W. and Korennykh, A. (2015) Human RNase L tunes gene expression by selectively destabilizing the microRNA-regulated transcriptome. *Proc Natl Acad Sci U S A*, **112**, 15916-15921.

12. Sarkar, S.N., Ghosh, A., Wang, H.W., Sung, S.S. and Sen, G.C. (1999) The nature of the catalytic domain of 2'-5'-oligoadenylate synthetases. *J Biol Chem*, **274**, 25535-25542.

13. Ibsen, M.S., Gad, H.H., Thavachelvam, K., Boesen, T., Despres, P. and Hartmann, R. (2014) The 2'-5'-oligoadenylate synthetase 3 enzyme potently synthesizes the 2'-5'-oligoadenylates required for RNase L activation. *J Virol*, **88**, 14222-14231.

14. Donovan, J., Whitney, G., Rath, S. and Korennykh, A. (2015) Structural mechanism of sensing long dsRNA via a noncatalytic domain in human oligoadenylate synthetase 3. *Proc Natl Acad Sci U S A*, **112**, 3949-3954.

15. Field, L.L., Bonnevie-Nielsen, V., Pociot, F., Lu, S., Nielsen, T.B. and Beck-Nielsen, H. (2005) OAS1 splice site polymorphism controlling antiviral enzyme activity influences susceptibility to type 1 diabetes. *Diabetes*, **54**, 1588-1591.

16. Fedetz, M., Matesanz, F., Caro-Maldonado, A., Fernandez, O., Tamayo, J.A., Guerrero, M., Delgado, C., Lopez-Guerrero, J.A. and Alcina, A. (2006) OAS1 gene haplotype confers susceptibility to multiple sclerosis. *Tissue Antigens*, **68**, 446-449.

17. Feng, X., Wu, H., Grossman, J.M., Hanvivadhanakul, P., FitzGerald, J.D., Park, G.S., Dong, X., Chen, W., Kim, M.H., Weng, H.H. *et al.* (2006) Association of increased interferon-inducible gene expression with disease activity and lupus nephritis in patients with systemic lupus erythematosus. *Arthritis Rheumatol*, **54**, 2951-2962.

18. Li, H., Reksten, T.R., Ice, J.A., Kelly, J.A., Adrianto, I., Rasmussen, A., Wang, S., He, B., Grundahl, K.M., Glenn, S.B. *et al.* (2017) Identification of a Sjogren's syndrome susceptibility locus at OAS1 that influences isoform switching, protein expression, and responsiveness to type I interferons. *PLoS Genet*, **13**, e1006820.

19. Mandal, S., Abebe, F. and Chaudhary, J. (2011) 2'-5' oligoadenylate synthetase 1 polymorphism is associated with prostate cancer. *Cancer*, **117**, 5509-5518.

20. Dar, A.A., Pradhan, T.N., Kulkarni, D.P., Shah, S.U., Rao, K.V., Chaukar, D.A., D'Cruz, A.K. and Chiplunkar, S.V. (2016) Extracellular 2'5'-oligoadenylate synthetase 2 mediates T-cell receptor CD3-zeta chain down-regulation via caspase-3 activation in oral cancer. *Immunology*, **147**, 251-264.

21. Wu, S., Wang, Y., Chen, G., Zhang, M., Wang, M. and He, J.Q. (2018) 2'-5'-Oligoadenylate synthetase 1 polymorphisms are associated with tuberculosis: a case-control study. *BMC Pulm Med*, **18**, 180.

22. Leisching, G., Cole, V., Ali, A.T. and Baker, B. (2019) OAS1, OAS2 and OAS3 restrict intracellular M. tb replication and enhance cytokine secretion. *Int J Infect Dis*, **80S**, S77-S84.

23. Lee, H.J., Georgiadou, A., Walther, M., Nwakanma, D., Stewart, L.B., Levin, M., Otto, T.D., Conway, D.J., Coin, L.J. and Cunnington, A.J. (2018) Integrated pathogen load and dual transcriptome analysis of systemic host-pathogen interactions in severe malaria. *Sci Transl Med*, **10**, eaar3619.

24. Yu, C., Xue, P., Zhang, L., Pan, R., Cai, Z., He, Z., Sun, J. and Zheng, M. (2018) Prediction of key genes and pathways involved in trastuzumab-resistant gastric cancer. *World J Surg Oncol*, **16**, 174.

25. Lamers, M.M., van den Hoogen, B.G. and Haagmans, B.L. (2019) ADAR1: "Editor-in-Chief" of Cytoplasmic Innate Immunity. *Front Immunol*, **10**, 1763.

26. Samuel, C.E. (2019) Adenosine deaminase acting on RNA (ADAR1), a suppressor of double-stranded RNA-triggered innate immune responses. *J Biol Chem*, **294**, 1710-1720.

27. Rice, G.I., Kasher, P.R., Forte, G.M., Mannion, N.M., Greenwood, S.M., Szynkiewicz, M., Dickerson, J.E., Bhaskar, S.S., Zampini, M., Briggs, T.A. *et al.* (2012) Mutations in ADAR1 cause Aicardi-Goutieres syndrome associated with a type I interferon signature. *Nat Genet*, **44**, 1243-1248.

28. Li, Y., Banerjee, S., Goldstein, S.A., Dong, B., Gaughan, C., Rath, S., Donovan, J., Korennykh, A., Silverman, R.H. and Weiss, S.R. (2017) Ribonuclease L mediates the cell-lethal phenotype of double-stranded RNA editing enzyme ADAR1 deficiency in a human cell line. *Elife*, **6**, e25687.

29. Hartmann, R., Norby, P.L., Martensen, P.M., Jorgensen, P., James, M.C., Jacobsen, C., Moestrup, S.K., Clemens, M.J. and Justesen, J. (1998) Activation of 2'-5' oligoadenylate synthetase by single-stranded and double-stranded RNA aptamers. *J Biol Chem*, **273**, 3236-3246.

30. Kodym, R., Kodym, E. and Story, M.D. (2009) 2'-5'-Oligoadenylate synthetase is activated by a specific RNA sequence motif. *Biochem Biophys Res Commun*, **388**, 317-322.

31. Vachon, V.K., Calderon, B.M. and Conn, G.L. (2015) A novel RNA molecular signature for activation of 2'-5' oligoadenylate synthetase-1. *Nucleic Acids Res*, **43**, 544-552.

32. Calderon, B.M. and Conn, G.L. (2018) A human cellular noncoding RNA activates the antiviral protein 2'-5'-oligoadenylate synthetase 1. *J Biol Chem*, **293**, 16115-16124.

33. Marin-Gonzalez, A., Aicart-Ramos, C., Marin-Baquero, M., Martin-Gonzalez, A., Suomalainen, M., Kannan, A., Vilhena, J.G., Greber, U.F., Moreno-Herrero, F. and Perez, R. (2020) Double-stranded RNA bending by AU-tract sequences. *Nucleic Acids Res*, **48**, 12917-12928.

34. Justesen, J. and Kjeldgaard, N.O. (1992) Spectrophotometric pyrophosphate assay of 2',5'-oligoadenylate synthetase. *Anal Biochem*, **207**, 90-93.

35. Li, Y., Banerjee, S., Wang, Y., Goldstein, S.A., Dong, B., Gaughan, C., Silverman, R.H. and Weiss, S.R. (2016) Activation of RNase L is dependent on OAS3 expression during infection with diverse human viruses. *Proc Natl Acad Sci U S A*, **113**, 2241-2246.

36. Mergny, J.L., Li, J., Lacroix, L., Amrane, S. and Chaires, J.B. (2005) Thermal difference spectra: a specific signature for nucleic acid structures. *Nucleic Acids Res*, **33**, e138.

37. Lavery, R., Moakher, M., Maddocks, J.H., Petkeviciute, D. and Zakrzewska, K. (2009) Conformational analysis of nucleic acids revisited: Curves+. *Nucleic Acids Res*, **37**, 5917-5929.

38. Blanchet, C., Pasi, M., Zakrzewska, K. and Lavery, R. (2011) CURVES+ web server for analyzing and visualizing the helical, backbone and groove parameters of nucleic acid structures. *Nucleic Acids Res*, **39**, W68-73.

TABLES

Table 1. Summary of short dsRNA stability and OAS1 activation

dsRNA	T_m (°C)[a]	Initial Rate (nmol PP_i/ min)[b]	Relative 28S rRNA Cleavage[c]
AU3	70.5	1.4 ± 0.1	1.0
IU1	66.8	1.8 ± 0.2	-
IU2	59.5	2.1 ± 0.3	-
IU3	54.5	2.6 ± 0.3	1.5 ± 0.3
IC1	69.3	1.9 ± 0.2	-
IC2	70.8	2.0 ± 0.2	-
IC3	71.0	2.4 ± 0.2	1.4 ± 0.3
AC1	64.8	2.3 ± 0.2	-
AC2	57.5	2.2 ± 0.2	-
AC3	49.3	3.0 ± 0.2	1.2 ± 0.1
GC1	72.3	1.7 ± 0.1	-
GC2	80.5	2.7 ± 0.2	-
GC3	84.0	2.8 ± 0.2	1.8 ± 0.4

[a]Melting temperature (T_m) in the high salt (100 mM NaCl) condition; values are the average of at least two independent experiments. Individual values are shown in **Table S1**.

[b]Initial rates of the reaction were determined for OAS1 activation assays by linear regression analysis on the first three or four time points of the reaction progress curve.

[c]Quantification of the major 28S cleavage product (**Figure 5A**, *solid arrow*) from three independent experiments in wild-type A549 cells. Values are normalized to AU3 dsRNA; -, not determined.

SUPPLEMENTAL FIGURES

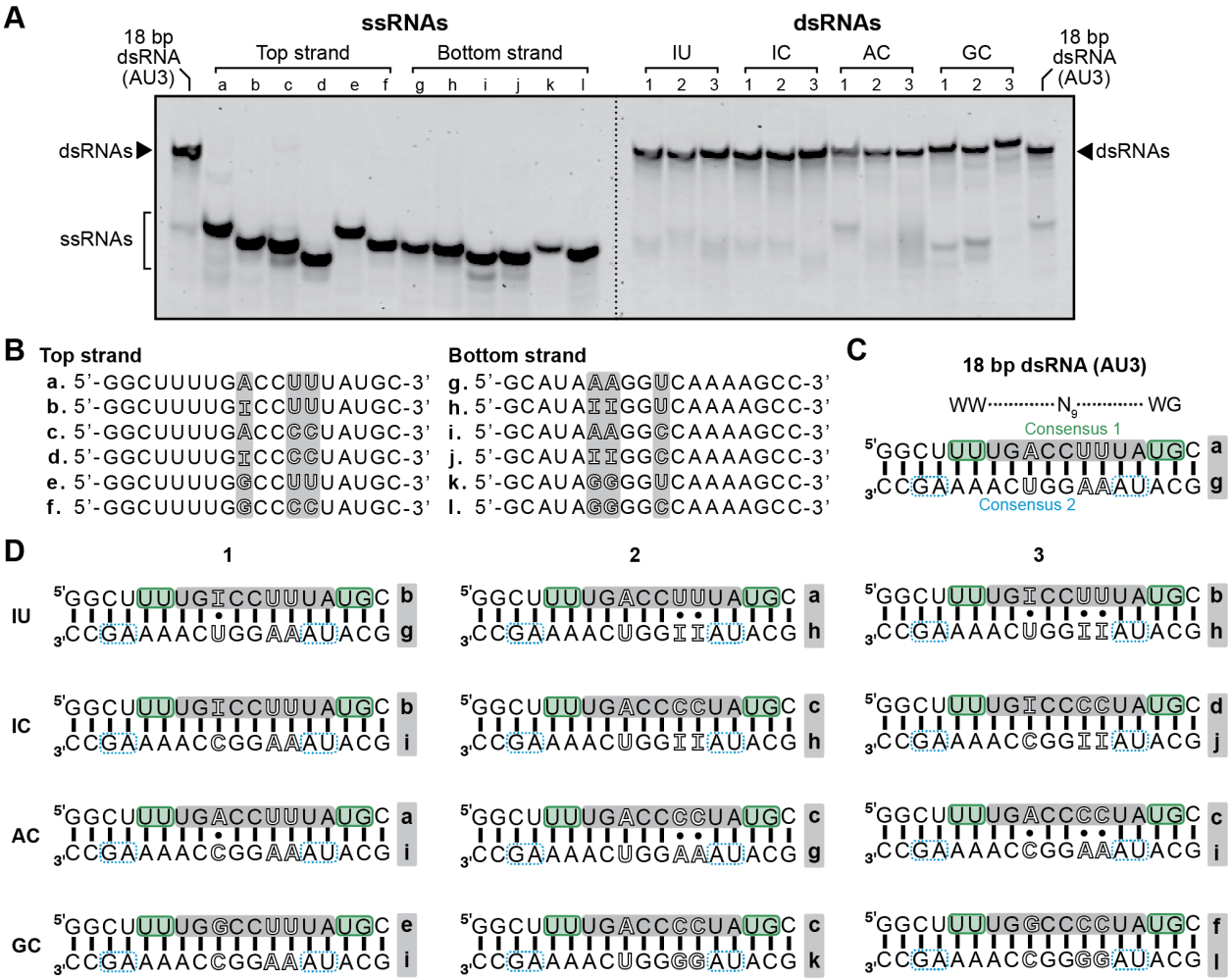

Figure S1. Native gel analysis showing purity of ssRNAs and stable formation of each dsRNA. ***A,*** Assessed the quality and homogeneity of chemically synthesized single-stranded RNAs (ssRNAs, *left)* and their respective 18 bp double-stranded RNA duplexes (dsRNAs, *right)*. ***B,*** Sequences for each ssRNA are shown with mutations highlighted in grey and correspond to the lanes as indicated in *panel A* (*left*). ***C,*** Schematic for the 18 bp dsRNA (AU3) which serves as the "background" in which all mutations were made. ***D,*** Specific combinations of ssRNAs (*grey* and as labeled in *panel B*) were annealed to form each dsRNA variant. dsRNA schematics show complete sequence composition and correspond to the lanes as indicated in *panel A* (*right*).

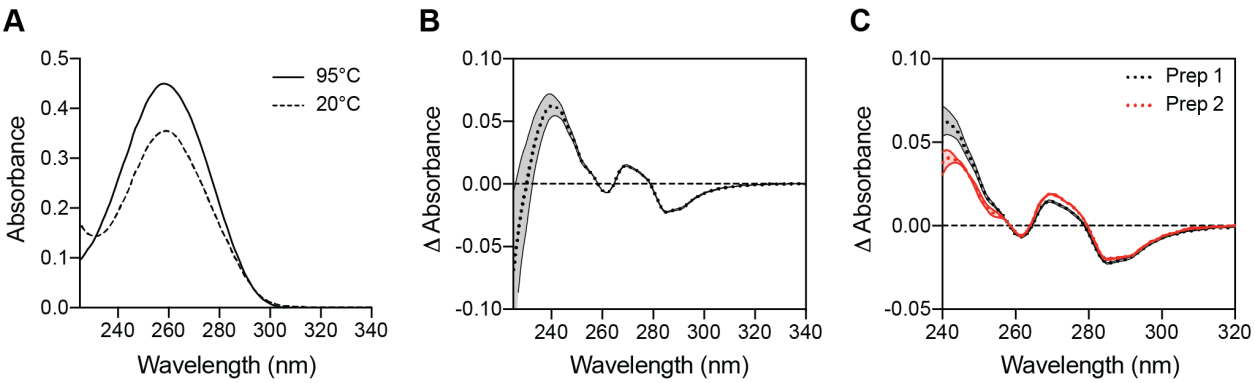

Figure S2. Workflow for determining thermal difference spectra (TDS). ***A,*** Two UV absorbance spectra were measured over a range of wavelengths from 225 to 340 nm at a temperature above (95°C, *solid black line*) and below (20°C, *dashed black line*) the melting temperature for AU3 dsRNA. ***B,*** Individual data sets for AU3 dsRNA were normalized and the thermal difference spectra (TDS) was obtained by subtracting the data collected at 20°C from the data collected at 95°C (as shown in *panel A*). Due to consistent variability observed at shorter wavelengths (<240 nm), all final graphs were trimmed to highlight structural changes occurring between 240-320 nm. ***C,*** TDS showing minimal variability between two AU3 dsRNA preparations. Error for *panels B and C* are reported as standard error of the mean (SEM) and are shown as transparent shading for each curve.

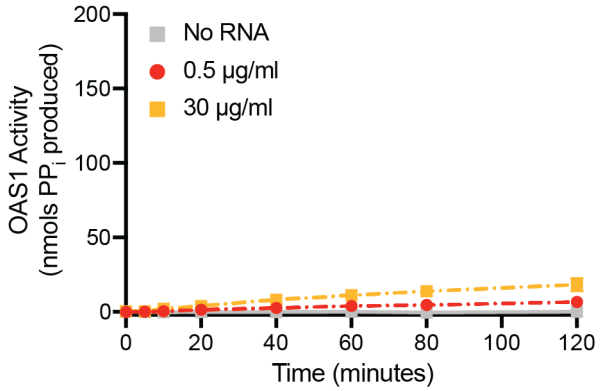

Figure S3. The poly(rG:rC) homopolymer is a poor activator even at high concentrations. Reaction progress curves for *in vitro* OAS1 activation by the poly(rG:rC) homopolymer at two concentrations: 0.5 µg/ml (*red circle*, as shown in the main text) and 30 µg/ml (*orange square*). OAS1 activity is observed above background levels (No RNA, *grey square*) at a concentration 60-fold higher (30 µg/ml) than the assay conditions used for poly(rA:rU) and poly(rI:rC) (**Figure 3**).

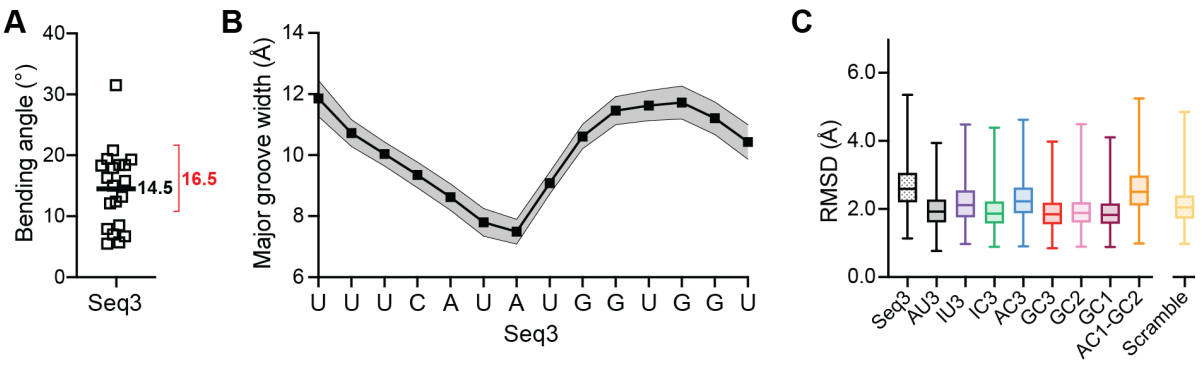

Figure S4. MD analysis of benchmark sequence and dsRNA RMSD. ***A,*** Helical bending angle calculated in Curves+ for the 20 representative structures from the Seq3 simulation (overall average 14.5°). As noted in the main text, greater sampling in our analysis (20 vs. 5 representative structures), reveals two clusters of structures with low (5 structures) and high (14 structures) bending angles; the average for the high bending angle cluster only (denoted with the red bracket) is 16.5°, matching the reported value within error. ***B,*** Major groove width narrows at the AUAU sequence at the center of Seq3, as previously reported (33). ***C,*** RMSD for Seq3 and all 18 bp dsRNAs analyzed in MD simulations. RMSD values were calculated by comparison of each representative structure with all other structures within each 10 ns segment (yielding 20 RMSD values for each dsRNA).

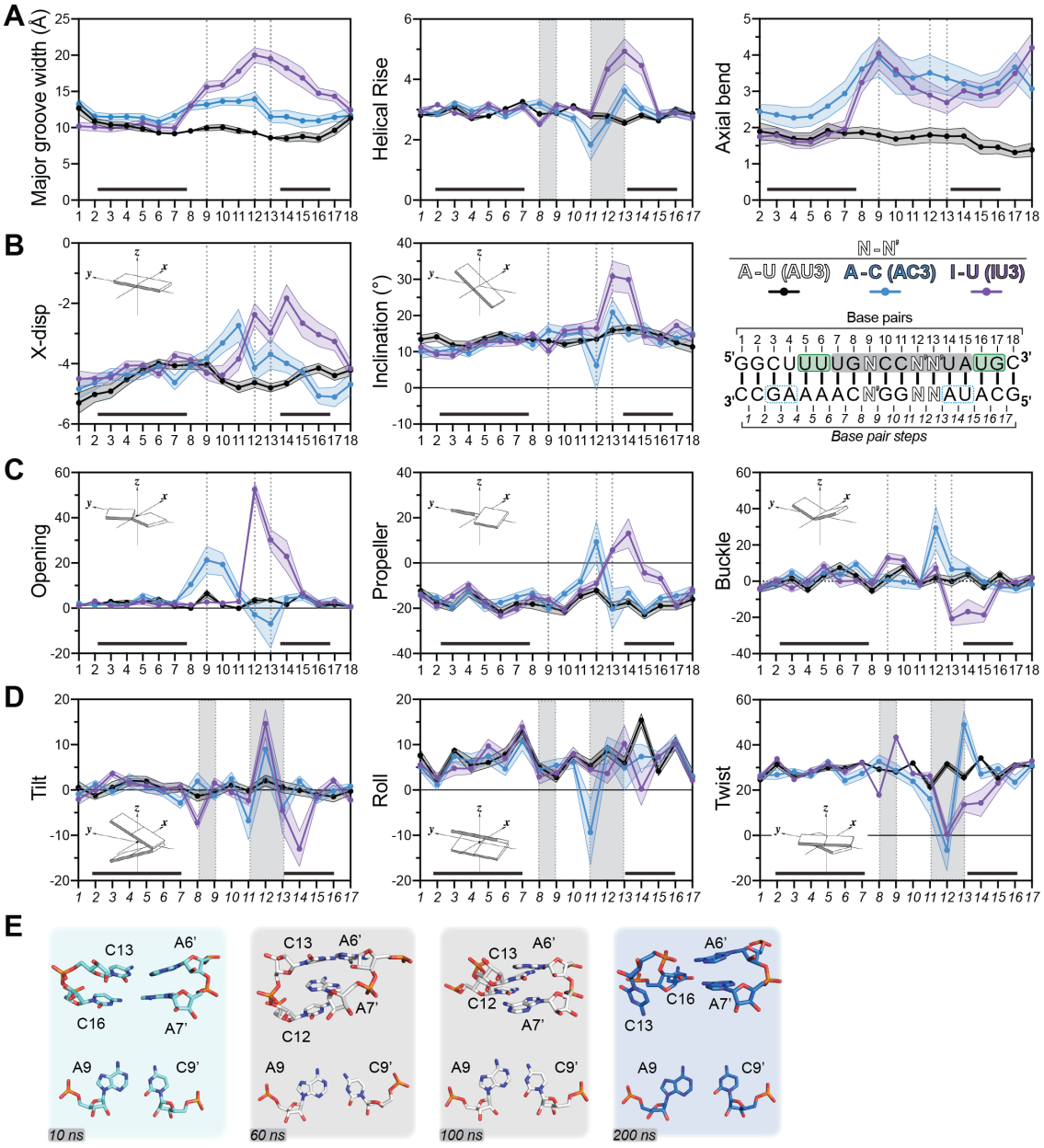

Figure S5. Mismatch base pairings (I•U *and* A•C) cause major alterations helical structure. Output from Curves+ analysis of 20 representative structures from simulations of AU3, IU3 and AC3 dsRNAs shown as mean values at each base pair or base pair step for ***A***, helical, ***B,C*** base pair and ***D***, base step parameters (as shown on the y axis). Shaded areas are standard error of the mean. Vertical dotted lines and shaded regions mark the sites of base pair changes in the dsRNAs compared for AU3, for each base pair or base pair step, respectively. The black bars above the x-axis indicate the main regions (on either strand) of contact with OAS1 in the complex crystal structure (PDB 4IG8). ***E*****,** The tandem A•C mismatches adopt multiple distinct structures in the MD simulation of AC3 dsRNA. Structures formed by the tandem A•C base pairs (*top*) and single A•C base pair (*bottom*) in representative structures at the indicated simulation time points, including the start (10 ns) and end (200 ns). The tandem pairs, but not the single base pair, are capable of adopting multiple different structures that likely increase helical flexibility and decrease dsRNA stability.

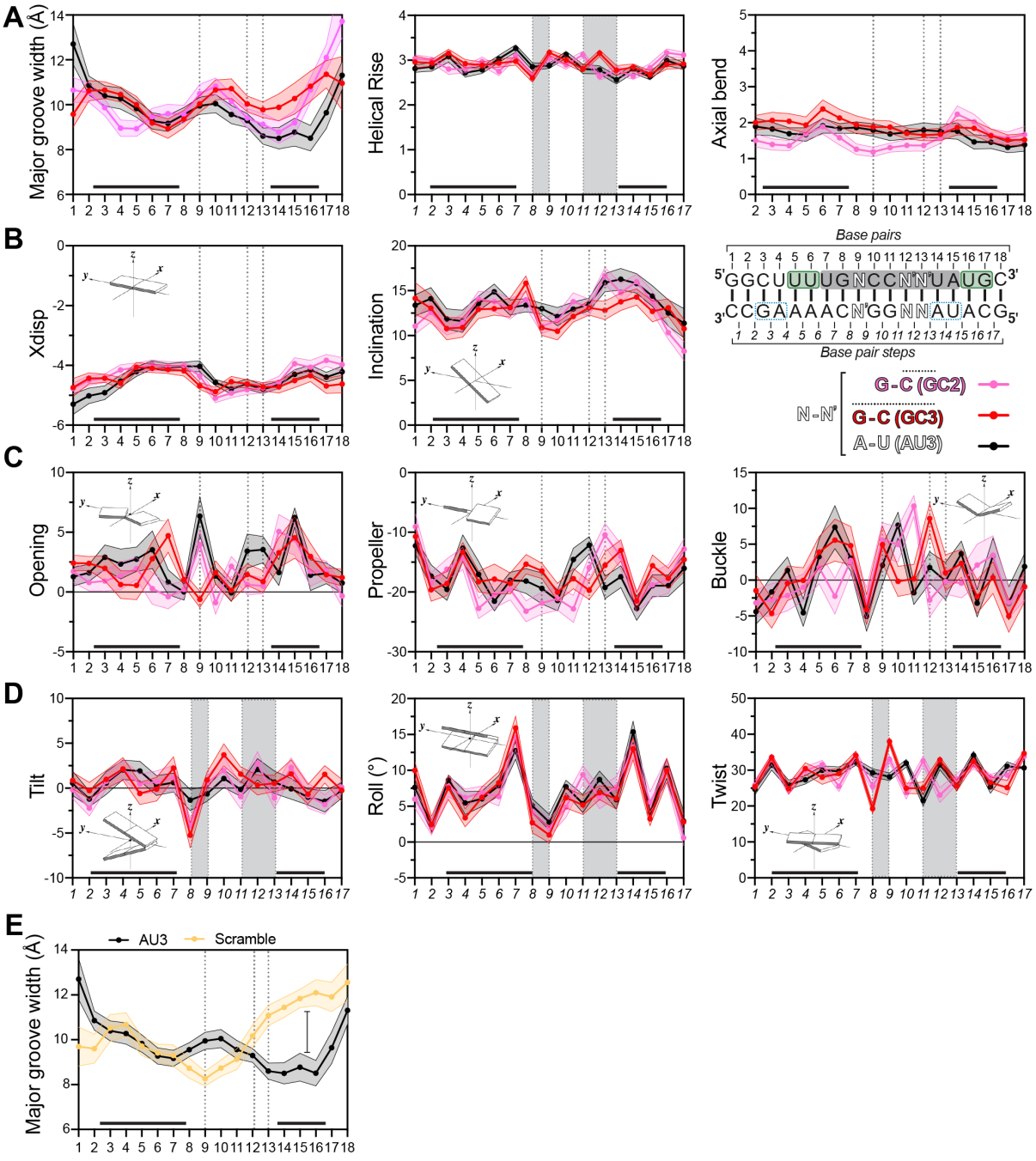

Figure S6. Analysis of helical and base pair/ base step parameters for GC2 and GC3 dsRNAs. Output from Curves+ analysis of 20 representative structures from simulations of AU3, GC2 and GC3 dsRNAs shown as mean values at each base pair or base pair step for ***A***, helical, ***B,C*** base pair and ***D***, base step parameters (as shown on the y axis). Shaded areas are standard error of the mean. Vertical dotted lines and shaded regions mark the sites of base pair changes in the dsRNAs compared for AU3, for each base pair or base pair step, respectively. The black bars above the x-axis indicate the main regions (on either strand) of contact with OAS1 in the complex crystal structure (PDB 4IG8). ***E***, Comparison of major groove width for AU3 dsRNA and the non-OAS1 activator Scramble dsRNA.

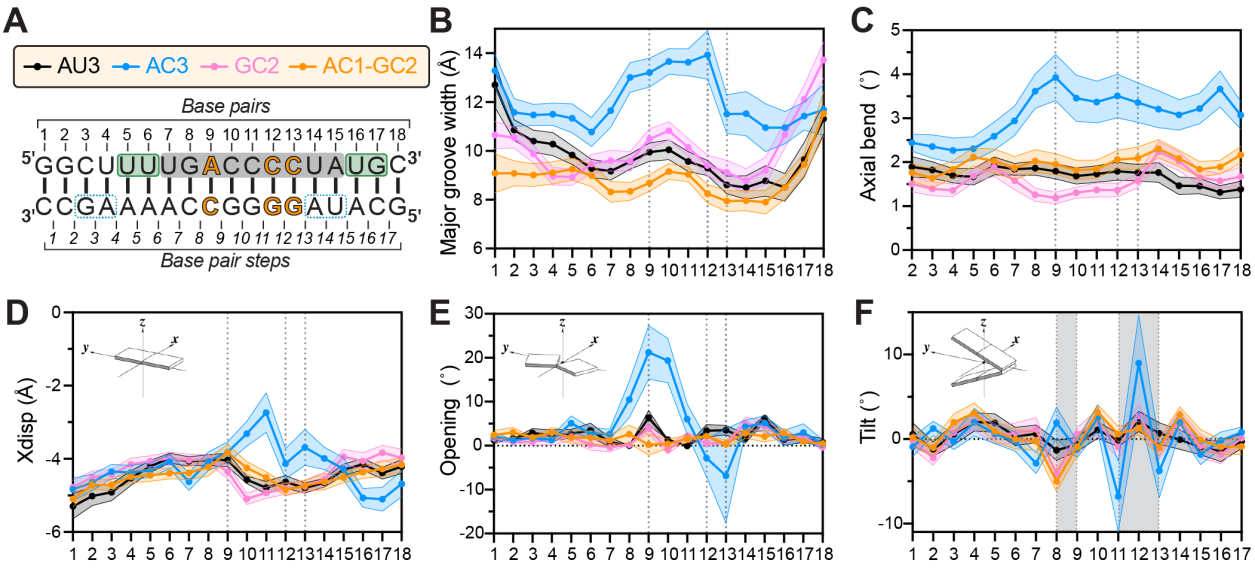

Figure S7. Analysis of helical and base pair/ base step parameters for AC1-GC2 dsRNA. ***A*****,** Sequence of the dsRNA with combined AC1 and GC2 base pair changes. ***B-F*****,** Output from Curves+ analysis of 20 representative structures from simulation of AC1-GC2 dsRNA as mean values at each base pair or base pair step for select helical and base pair parameters (as shown on the y axis). AU3, AC3 and GC2 dsRNA values are shown for comparison and are the same as in **Figures S5** and **S6**. Shaded areas are standard error of the mean. Vertical dotted lines and shaded regions mark the sites of base pair changes in the dsRNAs compared for AU3, for each base pair or base pair step, respectively. The black bars above the x-axis indicate the main regions (on either strand) of contact with OAS1 in the complex crystal structure (PDB 4IG8).

Table S1. Summary of dsRNA UV melting analysis

dsRNA	dsRNA Melting Temperature (Tm), ºC[a]								
	10 mM NaCl			**100 mM NaCl**			**100 mM NaCl + 7 mM $MgCl_2$**		
	Expt. 1	Expt. 2	**Average**	Expt. 1	Expt. 2	**Average**	Expt. 1	Expt. 2	**Average**
AU3	59.0 59.5	59.5 59.0	**59.3**	70.5 70.5	70.5 70.5	**70.5**	80.5 79.5	79.5 79.5	**79.8**
IU1	54.5	55.0	**54.8**	67.0	66.5	**66.8**	76.5	76.0	**76.3**
IU2	47.5	48.0	**47.8**	59.5	59.5	**59.5**	69.0	70.0	**69.5**
IU3	42.5	42.0	**42.3**	54.5	54.5	**54.5**	65.0	65.0	**65.0**
IC1	57.0	57.5	**57.3**	69.5	69.0	**69.3**	78.5	78.5	**78.5**
IC2	59.5	60.0	**59.8**	71.0	70.5	**70.8**	80.5	80.5	**80.5**
IC3	58.5	58.0	**58.3**	71.5	70.5	**71.0**	81.5	80.5	**81.0**
AC1	54.5	54.5	**54.5**	65.0	64.5	**64.8**	73.0	72.5	**72.8**
AC2	47.0	46.5	**46.8**	57.5	57.5	**57.5**	68.0	68.0	**68.0**
AC3	40.0	40.0	**40.0**	49.0	49.5	**49.3**	55.0	55.5	**55.3**
GC1	60.0	60.5	**60.3**	72.0	72.5	**72.3**	82.5	83.5	**83.0**
GC2	69.0	69.5	**69.3**	80.5	80.5	**80.5**	89.5	89.5	**89.5**
GC3	72.0	72.0	**72.0**	84.0	84.0	**84.0**	94.0	93.5	**93.8**

[a]For each dsRNA, absorbance was measured at 260 nm in buffer containing 10 mM NaCl, 100 mM NaCl, or 100 mM NaCl + 7 mM $MgCl_2$. Melting temperatures (Tm) were determined by calculating the first derivative for each UV absorbance curve to identify the inflection point. Average Tm is reported for two independent experiments (n = 2) except AU3 (n = 4), which was used as a control for all assays.

CHAPTER FIVE

OAS1 activation is determined by competing activating and non-activating binding sites in double-stranded RNA

Samantha L. Schwartz, Camden R. Bair, Anice C. Lowen and Graeme L. Conn

This work is unpublished.

Author Contributions: S.L.S., A.C.L., and G.L.C. participated in research design. S.L.S.* and C.R.B. performed experiments. S.L.S., A.C.L., and G.L.C. analyzed data.

[*S.L.S. performed the experiments shown in Figures 1, 2, and 4-6.]

INTRODUCTION

OAS1 lacks a canonical RNA-binding motif and instead interacts with dsRNA through a relatively flat protein surface enriched with positive residues. This surface is located on the opposite side of OAS1 from its ATP binding sites and 2-5A synthesis catalytic center, such that dsRNA binding is necessary to induce activation by an allosteric mechanism (1-3). Despite appearing suited to binding dsRNA in a sequence-independent manner, there have been several reports indicating that OAS1 activation can be enhanced by specific RNA sequences or structural motifs (4-7).

One such RNA sequence is the OAS1 activation consensus sequence WWN_9WG, where W is A or U, and N is any nucleotide (5). This consensus sequence was identified using 109 random dsRNAs of which ~88% of those able to induce robust OAS1 activation were found to contain the sequence WWN_9WG. These findings were further rationalized by the observation that the partially conserved dinucleotide sequences (WW and WG) would be perfectly spaced by nine non-conserved base-paired nucleotides (N_9), thus presenting these nucleotides in two adjacent minor grooves on the same face of the RNA helix for OAS1 recognition. About four years later, the co-crystal structure of human OAS1 bound to dsRNA was solved using an 18 bp dsRNA containing, what we later noted to be, two overlapping, antiparallel OAS1 activation consensus sequences (2,5). Despite containing two potential OAS1 binding sites (Consensus 1 and Consensus 2; **Figure 1A**, *top*), the human OAS1-dsRNA crystal structure contained the dsRNA bound in a single orientation. We therefore asked whether this could be a crystallographic artifact or might OAS1 also show such binding preference in solution?

To begin answering this open question, we used a second OAS1 activation motif, the 3'-end single-stranded pyrimidine (3'-ssPy) motif (6), as a molecular tool to introduce directionality in the model 18 bp dsRNA to identify whether both dsRNA orientations could bind and activate OAS1 equivalently (8). The 3'-ssPy motif was appended to each end of the 18 bp dsRNA in each combination (*i.e.* to "top" strand only, "bottom" strand only, or both ends), and analysis of

OAS1 activation showed that the 3'-ssPy motif could not be sensed equally, with strong preference for addition to the top strand adjacent to Consensus 1 (**Figure 1A**, *top*). These studies suggested that the consensus sequence dictates binding position and orientation on the dsRNA and, only when correctly positioned in this way, can the 3'-ssPy exert its effect on OAS1 activation. In a subsequent study, we also revealed the basis for previously unappreciated complexity in the non-conserved (N_9) nucleotides. The N_9 region is not recognized in a sequence-specific manner, but its nucleotide identity strongly influences the dsRNA shape and flexibility (Schwartz, *et al.*, *submitted*). These dsRNA features are important to consider when seeking to identify new dsRNA activators of OAS1.

Having discovered important roles for the consensus sequence in positioning dsRNA on OAS1 and for the nine intervening non-conserved nucleotides, a final critical piece of the puzzle is to define the role of the partially conserved nucleotides (WW/WG) in dictating the extent of OAS1 activation. As revealed by our work and in the original identification of the WW/WG motif, not all consensus sequences are equal in their ability to activate OAS1 (5,8). For the present studies, we used the same 18 bp dsRNA as in the human OAS1-dsRNA crystal structure and our previous work, with two overlapping, antiparallel copies of the WWN_9WG consensus sequence and thus two potential OAS1 binding sites (**Figure 1A**, *green and blue*). Here, this system is used to identify the respective capacity for each OAS1 activation consensus sequence to activate OAS1, and to determine whether there is competition between two OAS1 binding sites within the same dsRNA molecule. These studies reveal that two OAS1 binding sites that fit the "rules" of the OAS1 activation consensus sequence unexpectedly displayed vastly different capacities to activate OAS1 *in vitro* and in human cells. Additionally, we observe competition between these two non-equivalent OAS1 binding sites which can be eliminated or enhanced by introducing specific sequence substitutions.

MATERIALS AND METHODS

OAS1 protein expression and purification

Human OAS1 was expressed in *Escherichia coli* BL21(DE3) as an N-terminal 6xHis-SUMO fusion of amino acids 1-346 (corresponding to the common, core residues of all OAS1 splicing isoforms) from vector pE-SUMO (LifeSensors). Cells were grown in lysogeny broth (LB) at 37°C to mid-log phase (optical density at 600 nm of ~0.5), and protein expression was induced with 0.5 mM isopropyl β-D-1-thiogalactopyranoside (IPTG) with continued growth overnight at 20°C. Cells were lysed by sonication in 50 mM Tris-HCl buffer (pH 8.0) containing 300 mM NaCl, 20 mM imidazole, 10% (v/v) glycerol, and 10 mM β-mercaptoethanol. SUMO-OAS^{1-346} fusion protein was purified from cleared lysate by Ni^{2+}-affinity chromatography on an ÄKTApurifier 10 FPLC system (GE Healthcare) and dialyzed overnight against SUMO cleavage buffer, containing 50 mM Tris-HCl (pH 8.0), 150 mM NaCl, 10% (v/v) glycerol, and 2 mM DTT. The partially purified fusion protein was then stored at -80°C. Prior to each experiment, the N-terminal 6xHis-SUMO tag was cleaved by incubating SUMO-OAS^{1-346} fusion protein with SUMO protease (Ulp1) for 90 minutes at 30°C and an additional hour at 4°C, followed by dialysis against the appropriate assay buffer. This process produces OAS^{1-346} with a native N-terminus after SUMO tag removal.

Generating 18 bp dsRNA duplexes

Each RNA strand was chemically synthesized (Integrated DNA Technologies) and used without further purification. Each 18 bp dsRNA duplex was generated by mixing individual strands at equimolar concentrations and annealing by heating to 65°C for 10 minutes followed by slow cooling to room temperature. Native PAGE (20% acrylamide in 0.5x Tris-Borate-EDTA) was used to verify the homogeneity of both single-strand RNAs and dsRNA duplexes prior to use. Each lane contained RNA (100 ng total) resolved on gels run at 120V for 3 hours at 4°C,

visualized by staining with SYBR Gold (1:10,000, Invitrogen), and imaged on a Typhoon Trio Imager (GE Healthcare).

Chromogenic assay of OAS1 activity

OAS^{1-346} was dialyzed overnight against OAS1 activity assay buffer: 50 mM Tris-HCl (pH 7.4) containing 100 mM NaCl, 1 mM EDTA, and 1 mM DTT. Pyrophosphate (PP_i), the reaction by-product of 2-5A synthesis by OAS1, was monitored using a chromogenic assay adapted from previously established methods for measurement of OAS1 activity (6,7,9). OAS^{1-346} (100 nM) was incubated with 300 nM dsRNA in reactions containing final solution conditions of 25 mM Tris-HCl (pH 7.4), 10 mM NaCl, 7 mM $MgCl_2$, 1 mM DTT, and 2 mM ATP at 37°C in a 150 µl total reaction volume. Aliquots (10 µl) were removed over a 0-120 minute time course and the reaction immediately quenched by adding directly to the wells of a 96-well plate pre-dispensed with 250 mM EDTA (pH 8.0, 2.5 µl). At completion of the time course, 2.5% (w/v) ammonium molybdate in 2.5 M H_2SO_4 (10 µl) and 0.5 M β-mercaptoethanol (10 µl) were added to each well and the final volume brought to 100 µl with water. Absorbance at 580 nm was measured using a Synergy Neo2 plate reader (BioTek). Readings were subtracted from background using an ATP-only control reaction (lacking both OAS^{1-346} and dsRNA) and then converted to pyrophosphate produced (nmols) using a pyrophosphate standard curve. Experiments were performed as four independent assays using two different preparations of OAS^{1-346}, each comprising three technical replicates which were averaged prior to data analysis. Final values were plotted with their associated standard error of the mean (SEM) in GraphPad Prism 9.

Kinetic analyses were performed similarly but using a range of dsRNA concentrations (0.1-5 µM) and measuring PP_i production only for the initial 12 minutes of the reaction with two technical replicates for each experiment. Linear regression analysis was used to obtain initial rates of reaction (nmol PP_i produced/minute) for each dsRNA concentration. These values were

plotted and a non-linear regression analysis performed to obtain V_{max} and K_{app} values using the Michaelis-Menten model equation: $Y=(V_{max}X)/(K_{app}+X)$ in GraphPad Prism 9.

OAS1/RNase L activation in A549 cells

Human wild-type and RNase L knock-out A549 cells, constructed using CRISPR-Cas9 gene editing technology as reported previously (10), were cultured in RPMI1640 cell culture medium (Corning) supplemented with 10% fetal bovine serum (Bio-Techne) and 100 µg/ml Normocin™ (Invivogen). Both cell lines were monitored regularly and tested negative for mycoplasma. Cells were seeded into 12-well plates at $3x10^5$ cells/well and were treated with 500 U/ml IFN-β1a (PBL Assay Science) prior to dsRNA transfection. Following overnight interferon treatment (16 hours), cells were transfected with dsRNAs (50 nM) or poly(rI:rC) (0.1 µg/ml) using siLentFect Lipid Reagent (Bio-Rad) and incubated at 37°C for 6 hours. Cells were lysed and total RNA was isolated using a RNeasy Plus Mini Kit (Qiagen) following manufacturer instructions. Total RNA was resolved using an Agilent 2100 Bioanalyzer system. Two independent sets of experiments were performed with essentially identical results for both the wild-type (n = 2) and RNase L knock-out (n = 2) cells, respectively.

OAS1-dsRNA 4-thiouridine (4-thioU) crosslinking

RNA strands containing a 3'-ssPy motif modified with a 4-thiouridine were chemically synthesized and purified by high performance liquid chromatography (Dharmacon). RNAs were supplied in protected form and were 2'-deprotected before use according to manufacturer instructions. RNA strands containing the 4-thiouridine modification (3'-end) were 5'-end labeled using [γ-^{32}P]-ATP and T4 polynucleotide kinase (PNK). Excess [γ-^{32}P]-ATP was removed using an Illustra MicroSpin G-25 column (GE Healthcare), and radiolabel incorporation was quantified by scintillation counting. The radiolabeled 18 bp dsRNA duplexes were generated by mixing the radiolabeled strand (containing 4-thiouridine) with the same unlabeled strand and a slight total excess of unlabeled complement. The mixed strands were annealed by heating to 65°C for 10

minutes followed by slow cooling to room temperature. OAS^{1-346} was dialyzed overnight against OAS1 activity assay buffer but lacking DTT, *i.e.* 50 mM Tris-HCl (pH 7.4) containing 100 mM NaCl and 1 mM EDTA.

OAS^{1-346} (5 μM) was incubated with radiolabeled, 4-thiouridine containing 18 bp dsRNA duplex (500 nM) for 30 minutes on ice with UV exposure at 365 nm and using a 96-well plate format at a distance of 3 cm. Reactions were stopped by addition of SDS loading buffer and heating to 95°C for 5 minutes. Reaction products were resolved on a 10% SDS-PAGE run at 200V for 45 minutes to allow for sufficient separation of OAS1-dsRNA complex and free RNA. Gels were soaked in destain solution (50:40:10% ethanol:water:acetic acid; 15 minutes), fixed (20% ethanol, 2% glycerol; 15 minutes), dried, and imaged using a Typhoon FLA 7000 PhosphorImager and ImageQuant software (GE Healthcare).

RESULTS

Mutation of the conserved guanine nucleotide (WWN_9WG) reveals that two activating consensus sequences within the same dsRNA are not equivalent

We started our mutagenesis analysis beginning with the conserved guanine (WWN_9WG) within the previously identified OAS1 activation consensus sequence (5). The human OAS1-dsRNA co-crystal structure showed that the guanine located in Consensus 1 on the top strand (**Figure 1A**, *top*) made one of few base-specific interactions with OAS1. Specifically, a hydrogen bond between the backbone of OAS1 residue Ser56 and the guanine base amino group, revealed at least part of the basis for the specificity of this consensus sequence (2).

First, we mutated the conserved G to an A to identify how critical this guanine base-specific interaction is in driving potent OAS1 activation. For these analyses, we made three separate constructs incorporating G-to-A mutation(s) in Consensus 1 (CS1-AC), Consensus 2 (CS2-AC), and a Consensus 1/2 double mutant (CS1/CS2-AC) (**Figure 1A**). All dsRNAs were generated by annealing the corresponding single-strand RNAs to form stable duplexes, as

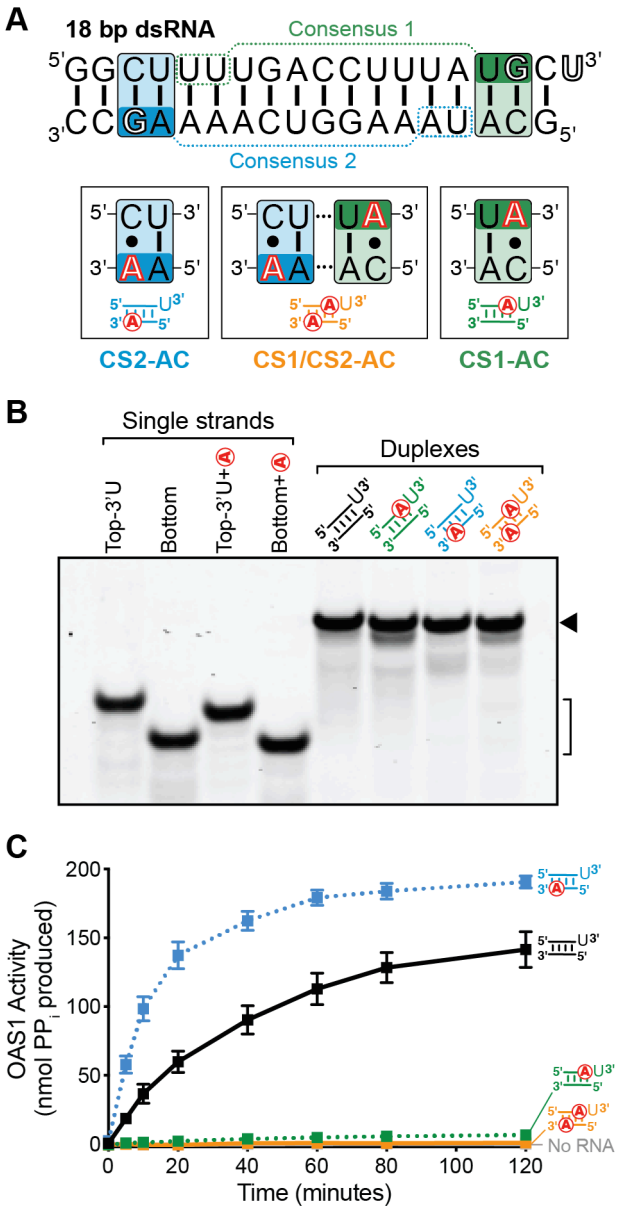

Figure 1. A short 18 bp dsRNA can contain two OAS1 activation consensus sequences (WWN$_9$WG) with vastly different capacities to activate OAS1. ***A, Top*** Sequence of the model 18 bp dsRNA containing two overlapping, antiparallel copies of the OAS1 activation consensus sequence WWN$_9$WG (where W is A or U, and N is any nucleotide), highlighted for top strand Consensus 1 (*green*) and bottom strand Consensus 2 (*blue*). The 3'-ssPy motif and conserved guanine are also indicated (outline font). ***Bottom*** Schematics showing the site of each conserved guanine (G) to adenine (A) substitution (*red outline font*) for Consensus 1 (CS1-AC; *green*), Consensus 2 (CS2-AC; *blue*), or both (CS1/CS2-AC; *orange*). ***B,*** Native gel analysis showing purity of chemically synthesized ssRNAs (*bracket*) and stable formation of each dsRNA (*solid arrow*). ***C,*** Reaction progress curves from an *in vitro* chromogenic assay of OAS1 activity performed under previously established conditions using a single dsRNA concentration (300 nM) for the 18 bp dsRNA (*solid black line*), CS1-AC (*dotted green line*), CS2-AC (*dotted blue line*), and CS1/CS2-AC (*solid orange line*). A control reaction (No RNA, *grey*) confirms there is no OAS1 activation in the absence of dsRNA.

confirmed by native polyacrylamide gel electrophoresis (**Figure 1B**). The dsRNAs were then tested in an established *in vitro* OAS1 activation assay, which measures the inorganic pyrophosphate (PP_i) produced as a consequence of 2-5A synthesis. The dsRNA with G-to-A mutation in Consensus 1 (CS1-AC) was barely able to activate beyond levels seen for the control reaction without dsRNA (**Figure 1C**; compare green and grey curves, respectively). This result confirms the critical role of the conserved G within the top strand consensus sequence that is specifically recognized by OAS1 in the crystal structure. Remarkably, however, when the corresponding G-to-A mutation was made in the bottom strand Consensus 2 (CS2-AC) we observed a dramatic increase in OAS1 activation, significantly surpassing that of the original 18 bp dsRNA (**Figure 1C**; compare blue and black curves, respectively). Thus, in the context of the bottom strand consensus, the same base identity change generating a non-consensus sequence has a strongly positive effect on the dsRNA's capacity to activate OAS1. Consistent with a dominant effect of changes in the top strand consensus, the double mutant (CS1/CS2-AC) was unable to activate OAS1 (**Figure 1C**; orange) mirroring the activity of CS1-AC.

Together, these results indicate that in the context of this dsRNA, only an intact Consensus 1 with conserved guanosine on the top strand is necessary for OAS1 activation. Additionally, the finding that elimination of Consensus 2 on the bottom enhances activation, suggests that the two consensus sequences effectively create two alternate competing binding sites in opposite orientations in the dsRNA. One of these sites (with OAS1 engaging Consensus 1) activates OAS1 and is ablated by the G-to-A mutation. In contrast, the second binds but does not activate (with OAS1 engaging Consensus 2) and its elimination "frees" OAS1 for more time in productive interaction with the top strand consensus. With their divergent effects on OAS1 activation compared to the 18 bp dsRNA, we refer to these two dsRNAs as "non-activator" (CS1-AC) and "hyper-activator" (CS2-AC) dsRNA.

To begin testing the model for competing binding sites, we first wanted to confirm that the non-activator (CS1-AC) and hyper-activator (CS2-AC) dsRNAs were indeed able to

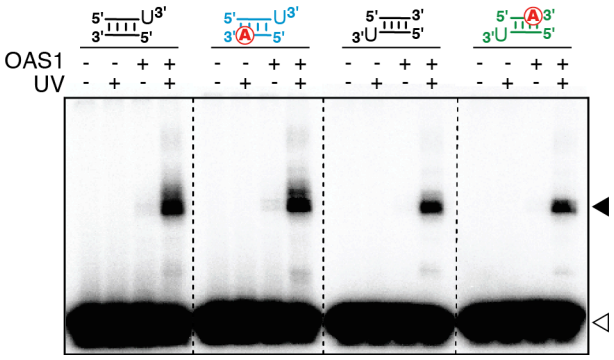

Figure 2. CS1-AC (non-activator) and CS2-AC (hyper-activator) form stable OAS1-dsRNA complexes. OAS1-dsRNA crosslinking induced by irradiation with UV light (365 nm) resolved by SDS-PAGE to separate crosslinked complex (solid arrow) from free RNA (open arrow). The ssRNA with 4-thioU modifications was 5'-end labeled with ^{32}P for visualization prior to annealing. *Left to right*, 18 bp dsRNA with 4-thioU on the "top" strand, CS2-AC (*blue*), 18 bp dsRNA with 4-thioU placed on the "bottom" strand, and CS1-AC (*green*). Data for the two 18 bp dsRNAs were previously published (8) but are shown here for comparison with their corresponding G-to-A variant dsRNAs.

equivalently bind and form stable complexes with OAS1. Specifically, we wanted to rule out the possibility that CS1-AC is no longer able to activate OAS1 simply because it does not bind the protein. To assess whether or not CS1-AC can still form a stable OAS1-dsRNA complex, we used OAS1-dsRNA crosslinking by exploiting the presence of the 3'-ssPy motif to site-specifically incorporate the photoreactive crosslinker 4-thiouridine (4-thioU). The modified single uridine (3'-ssPy motif) was added individually to each end of the dsRNA to generate CS2-AC (top 3'-ssPy) or CS1-AC (bottom 3'-ssPy) dsRNAs, which were crosslinked to OAS1 by exposure to 365 nm ultraviolet (UV) light. The RNA strand containing the 4-thioU modification was also 5'-end ^{32}P-labeled for visualization by autoradiography. Crosslinking and control reactions were resolved by SDS-PAGE to separate crosslinked OAS1-dsRNA complexes from free dsRNA (**Figure 2**). These experiments revealed that both CS1-AC and CS2-AC were able to similarly form stable complexes with OAS1 compared to each other as well as matched dsRNAs containing the 4-thioU modification but lacking the G-to-A substitution. Thus, the

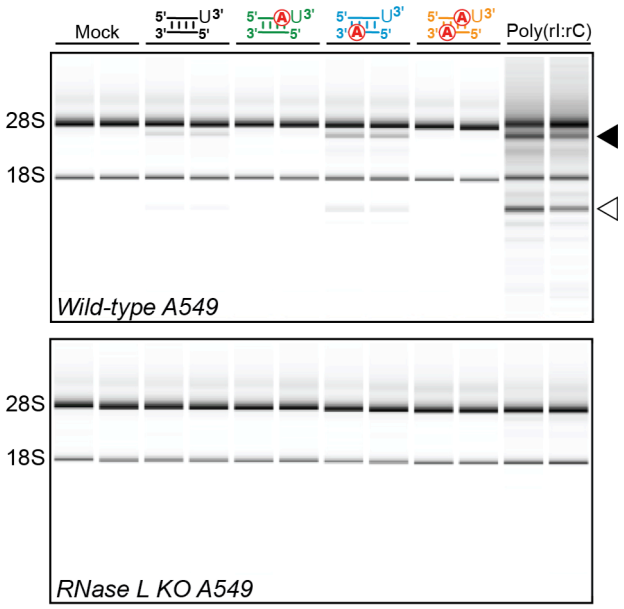

Figure 3. OAS/RNase L pathway activation in A549 cells mirrors OAS1 activity by the short dsRNAs *in vitro*. Bioanalyzer analysis of rRNA integrity in A549 cells following transfection with the indicated dsRNAs: 18 bp dsRNA (*black*), CS1-AC (*green*), CS2-AC (*blue*), and CS1/CS2-AC (*orange*). Mock transfection and transfection with poly(rI:rC) dsRNA serve as negative and positive controls, respectively. OAS1/RNase L pathway activation is indicated by 28S and 18S rRNA degradation (top, *arrows*). The same experiment was also performed using RNase L KO A549 cells (bottom) to ensure degradation observed is exclusively due to activation of the OAS1/RNase L pathway. A representative analysis with technical duplicates for each dsRNA is shown for one of two independent experiments.

observed differences in *in vitro* OAS1 activity for these two dsRNAs (**Figure 1C**; green and blue) are not likely due to significant differences in OAS1-dsRNA interaction (**Figure 2**).

OAS/RNase L pathway activation in human A549 cells mirrors OAS1 activity *in vitro*

We next tested the ability of the same four 18 bp dsRNAs to activate the OAS1/RNase L pathway in human lung carcinoma A549 cells as assessed by rRNA cleavage triggered by RNase L activation. Importantly, our dsRNAs were designed to be the approximate minimum length needed to activate OAS1 only and should therefore be too short to activate other OAS family members (OAS2 or OAS3). For these experiments, A549 cells were transfected with one of the four dsRNAs: 18 bp dsRNA, non-activator (CS1-AC), hyper-activator (CS2-AC), or double

mutant (CS1/CS2-AC). Poly(rI:rC) dsRNA and mock transfected cells served as positive and negative controls, respectively. Transfections with the 18 bp dsRNA and hyper-activator (CS2-AC) revealed these to be the only dsRNAs capable of inducing rRNA cleavage in addition to the poly(rI:rC) dsRNA positive control (**Figure 3**; compare black and blue to green and orange). These cell-based assays were also sufficiently sensitive to detect differences in the relative amount of rRNA cleavage between the 18 bp dsRNA and the hyper-activator, with the latter inducing more pronounced cleavage (**Figure 3**; compare black and blue). Activation of the OAS1/RNase L pathway in human A549 cells thus precisely mirrors the respective capacity of each dsRNA to activate OAS1 as observed in the *in vitro* activity assay (**Figure 1C** and **Figure 3**). While activation by even the most potent 18 bp dsRNA was lower than for poly(rI:rC) dsRNA, this difference is likely due to the synthetic dsRNA's greater length and additional capacity to activate OAS2 and OAS3 (11). Finally, we also observed no rRNA cleavage in A549 cells lacking RNase L (RNase L KO A549) confirming that the rRNA cleavage induced by these dsRNAs results from exclusively activating the OAS1/RNase L pathway (**Figure 3**).

Consensus 1, but not Consensus 2, requires both the guanine and Watson-Crick base pairing for potent OAS1 activation

To better define the basis for the differing capacity of the 18 bp dsRNA to activate OAS1, we made additional substitutions at the same conserved guanine position in both Consensus 1 and Consensus 2. These new dsRNAs were designed to test other nucleotides (C) as well as base pairing preferences (A-U, C-G) and tolerance for mismatches (G:U, C:C) (**Figure 4A** and **Figure 5A**). All base or base pair changes made to Consensus 1 resulted in dsRNAs with severely reduced capacity to activate OAS1 compared to the original 18 bp dsRNA (**Figure 4B**). However, of this series of dsRNA variants, one possessing a C-G base pair produces the greatest OAS1 activation, alternate Watson-Crick (A-U) or wobble (G:U) pairings produce intermediate OAS1 activation, while mismatches (C:C and the original A:C of non-activator CS1-

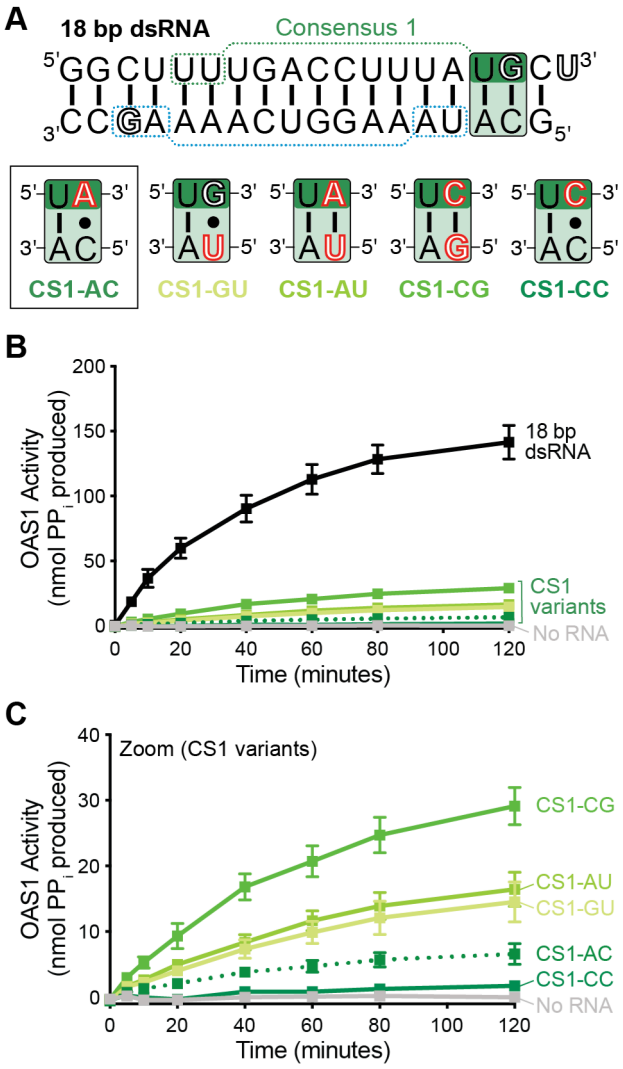

Figure 4. Consensus 1 requires both the conserved guanine and Watson-Crick base pairing for potent OAS1 activation. ***A,*** Schematic of individual Consensus 1 (CS1) substitutions (*red outline font*) generated to probe base identity requirement at the conserved guanine position. The original 18 bp dsRNA is shown for comparison. ***B,*** Reaction progress curves from the OAS1 *in vitro* activity assay comparing all CS1 variants (*solid green lines*, as labeled on the plot) to the 18 bp dsRNA (*black*) and non-activator CS1-AC (*dotted green line*). ***C,*** as in *panel B*, but showing a zoomed in view of Consensus 1 variants only. The No RNA (*grey*) control is also shown for each panel.

AC) are the most attenuated (**Figure 4C**). These data suggest that the nucleotide identity (*i.e.* guanine), orientation, and requirement for Watson-Crick base pairing are all essential for Consensus 1 to effectively drive OAS1 activation.

We next tested the equivalent substitutions in Consensus 2, revealing a more complex dependence on the base pair identity for OAS1 activation. The A:C mismatch in hyper-activator CS2-AC was the only mutation to significantly enhance OAS1 activation. Re-establishing Watson-Crick base pairing with the alternative A-U pair (CS2-AU) or replacement of the G as a G:U wobble pair (CS2-GU) resulted in activation capacity similar to the 18 bp dsRNA (**Figure 5B**). Finally, the two other dsRNA mutations which place a cytosine at the conserved position, either in the form of a C:C mismatch (CS2-CC) or Watson-Crick C-G base pair (CS2-CG) showed only weak OAS1 activation, at levels similar to that of the Consensus 1 variants (**Figure**

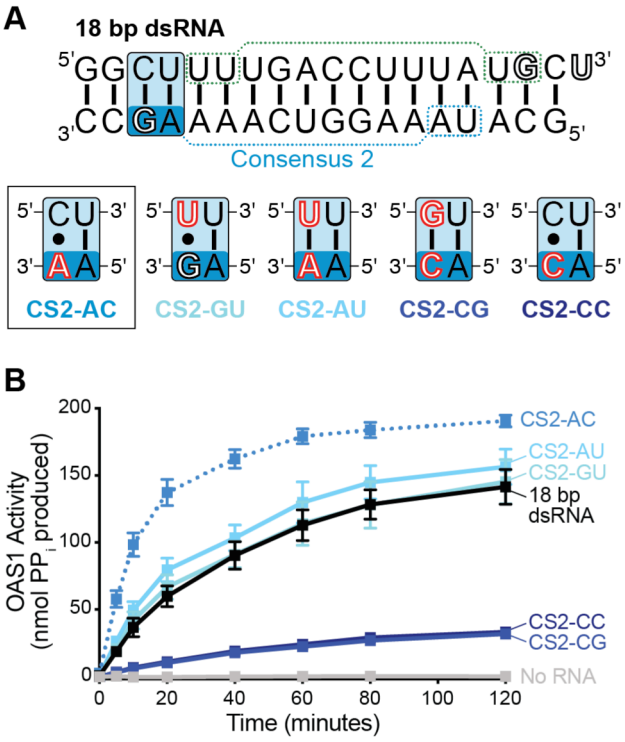

Figure 5. OAS1 activation does not require the conserved guanine in Consensus 2, and in specific contexts, altering the base content in this location significantly improves OAS1 activity. ***A,*** Schematic of individual Consensus 2 (CS2) substitutions (*red outline font*) generated to probe base identity requirement at the conserved guanine position. The original 18 bp dsRNA is shown for comparison. ***B,*** Reaction progress curves from the OAS1 *in vitro* activity assay comparing all CS2 variants (*solid blue lines*, as labeled on the plot) to the 18 bp dsRNA (*black*) and the hyper-activator CS2-AC (*dotted blue line*). The No RNA (*grey*) control is also shown.

4B and **Figure 5B**). These data suggest that the OAS1 binding site containing Consensus 2 is not the preferred OAS1 binding site in terms of productive OAS1 activation as substitutions at this position are more broadly accommodated with only a few exceptions.

Consensus sequence changes impact both dsRNA affinity (K_{app}) and maximal OAS1 activation (V_{max})

To define the basis for these observed differences in consensus sequence contribution, we used the *in vitro* OAS1 activation assay to assess enzyme activation over a wide range of dsRNA concentrations. Initial rates of reaction at each dsRNA concentration were determined and used to derive the maximum reaction velocity (V_{max}) and apparent RNA dissociation constant (K_{app}) (**Figure 6A-C** and **Table 1**). Both the non-activator (CS1-AC) and hyper-activator (CS2-AC) exhibited significant differences in K_{app} compared to the 18 bp dsRNA, corresponding to lower (~10.5-fold for CS1-AC) and higher (~6-fold for CS2-AC) apparent dsRNA affinity, respectively (**Figure 6D**). In contrast, there was no measurable difference in V_{max} for the hyper-activator (CS2-AC) compared to the 18 bp dsRNA, while we observed a ~2.5-fold decrease in V_{max} for the non-activator (CS1-AC) (**Figure 6D** and **Table 1**). Select consensus substitutions were also tested, and in general, we observed that Consensus 1 variants have a weaker apparent dsRNA affinity with similar maximal OAS1 activation, while Consensus 2 variants affect both parameters (**Table 1**). Therefore, the differences observed in OAS1 activity for these dsRNAs appear to be due in large part to changes in both apparent RNA affinity and maximum rate of 2-5A produced by OAS1.

DISCUSSION

Here, we used a model 18 bp dsRNA to define how the partially conserved (WW/WG) nucleotides within the OAS1 activation consensus sequence (WWN_9WG) contribute to enhanced OAS1 activity, and how the level of activation is affected when a dsRNA molecule contains more than one potential OAS1 binding site. Our studies revealed that (i) the two OAS1

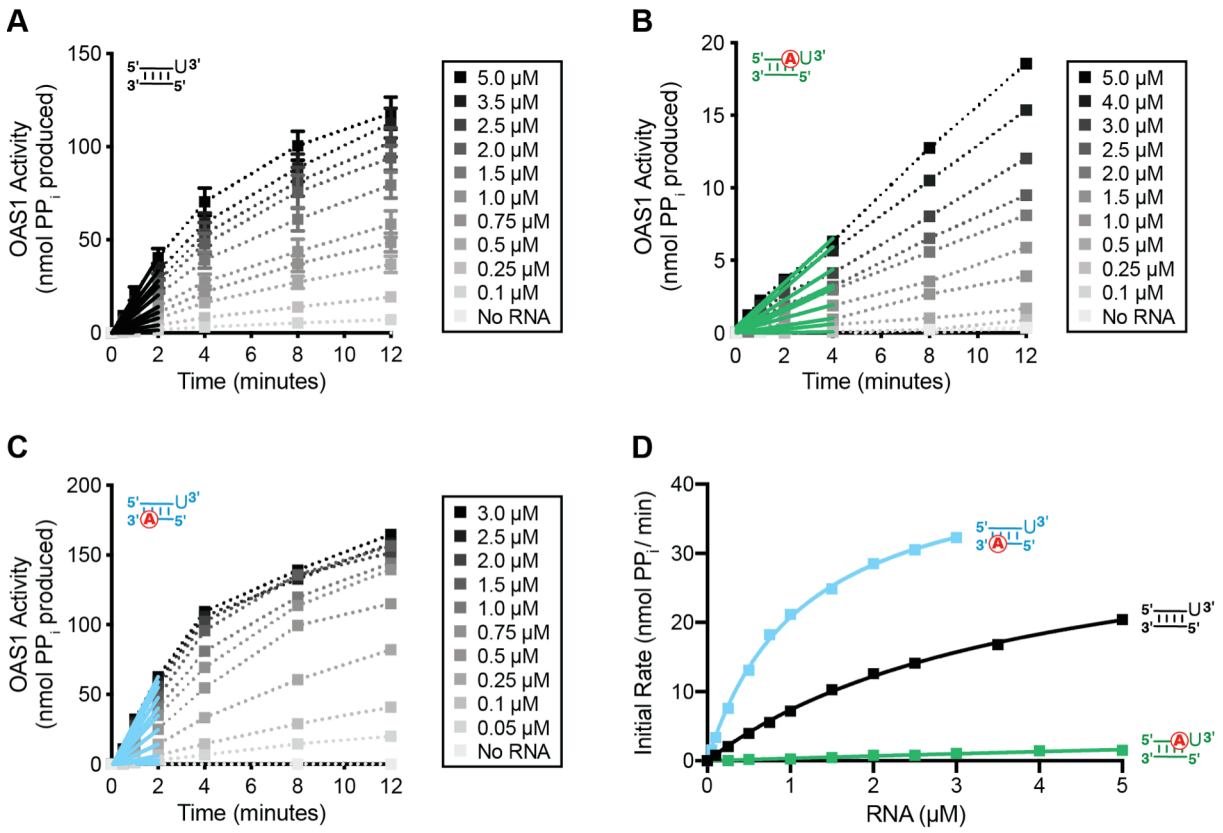

Figure 6. Changes in the two OAS1 activation consensus sequences dramatically alter apparent dsRNA affinity and maximal OAS1 activation. ***A-C,*** Progress curves for 18 bp dsRNA (*black*), CS1-AC (*green*), and CS2-AC (*blue*) over a range of dsRNA concentrations (0-5 μM) to determine initial rates of pyrophosphate (PP_i) production. Data were fit using linear regression analysis for the first 2-4 minutes of the reaction (*color-coded solid lines*) in order to obtain the initial rate. ***D,*** Kinetic analyses using calculated initial rates from *panels A-C* for OAS1 activation by each dsRNA. Data were fit using non-linear regression analysis to obtain kinetic parameters: apparent dsRNA affinity (K_{app}) and maximal OAS1 activation (V_{max}).

activation consensus sequences are not equivalent even though both meet the previously determined requirements for the consensus, (ii) these two OAS1 activation consensus sequences are in competition for OAS1 binding which is eliminated when the conserved guanine ($WWN_9W\underline{G}$) is mutated, and (iii) mutagenesis of the conserved guanine demonstrated that the OAS1 binding site containing “Consensus 1” is preferred and requires both the critical guanine and Watson-Crick base pairing to induce OAS1 activation.

These mutagenesis studies of the conserved guanine nucleotide within each consensus sequence ($WWN_9W\underline{\mathbf{G}}$) suggest that two "equivalent" binding sites within the same dsRNA molecule have disparate abilities to direct binding and activate OAS1. Additionally, Consensus 1 appears to be the preferred, "productive" OAS1 binding site because all mutations made at this position result in a dramatic loss in OAS1 activation. Thus, a guanine with canonical Watson-Crick base pairing is not only preferred, but is required. On the other hand, Consensus 2 mutations demonstrated that more variation is possible in which nucleotides or base pair geometry can be accommodated in this position giving us an indication that this is likely not the preferred OAS1 binding site. Based on these results, we speculate that an A:C mismatch in Consensus 2 reduces residence time on the non-activating binding site (*i.e.* drives binding to Consensus 1), while C-G and C:C mutations increase residence time at this (non-activating) site blocking efficient OAS1 activation. A-U and G:U mutations in Consensus 2 have a neutral effect which does not alter the bias in OAS1 binding in one or the other orientation allowing OAS1 to equally sample both binding sites similar to the 18 bp dsRNA. Thus, we predict that OAS1 is able to sense both binding sites because they each contain a consensus sequence recognized by OAS1, but introducing specific substitutions in Consensus 2, can disrupt the competition between the two OAS1 binding sites and drive binding to the preferred binding site on the top strand containing Consensus 1.

The 18 bp dsRNA contains two overlapping and competing OAS1 binding sites, each containing a copy of an OAS1 activation consensus sequence, with vastly different capacities to activate OAS1. Mutation of the critical guanine on the top strand (Consensus 1) to generate non-activator (CS1-AC) prevented the dsRNA from being able to activate OAS1 *in vitro* and in human cells despite retaining ability to bind OAS1. Mutation of the equivalent guanine on the bottom strand (Consensus 2) dramatically enhanced OAS1 activation in the context of an A:C mismatch compared to the 18 bp dsRNA. We propose the following model to summarize our findings: the extent of OAS1 activation is dictated by dsRNA sequence and context of activating

motifs, including the contributions of competing activating and non-activating binding sites. Consensus sequence mutations, particularly at the conserved guanine position, eliminated competition between these two dsRNA orientations driving binding to the productive (Consensus 1) or non-productive (Consensus 2) binding sites. These findings underscore the complex interplay two OAS1 binding sites can have within a short 18 bp dsRNA, which would be further complicated in long, more structured dsRNAs. Viruses could also use this mechanism as a potent viral evasion strategy generating decoy RNAs able to bind, but not activate, would sequester the nucleic acid sensor and allow the virus to go undetected by the innate immune system.

Further work is needed to test our two OAS1 binding site model, including competition assays that are important to test the dsRNA's ability to displace one another and compete for binding. In this experiment, we would incubate OAS1 with "hyper-activator" dsRNA and measure if increasing amounts of "non-activator" can compete for binding allowing us to extract a half maximal inhibitory concentration (IC_{50}) and would help further support our hypothesis of a two OAS1 binding site competition model. Additionally, we should test the other partially conserved (WW/WG) nucleotides to monitor the impact they have on OAS1 activation. It would also be important to gain mechanistic insight to define the molecular basis for how dsRNAs with small sequence changes have dramatically differing capacities for OAS1 activation. Several avenues are possible to address this point, including the use of hydrogen-deuterium exchange coupled with mass spectrometry (HDX-MS) or molecular dynamics simulations to assess protein conformational changes driven by the hyper-activator (CS2-AC) and non-activator (CS1-AC), or x-ray crystallography to reveal potential structural differences when OAS1 is bound to these dsRNAs. One possibility is that the non-activator is able to bind but not induce the correct structural rearrangements necessary for OAS1 allosteric regulation, and conversely, the hyper-activator could be driving additional allosteric changes or known necessary structural changes with greater efficiency. Identifying the precise molecular mechanism exploited by these dsRNAs

is important for our general understanding of OAS biology and regulation by dsRNA, and will undoubtedly form the basis needed to begin developing novel therapeutic strategies required to combat both viral infection and OAS1 dysregulation in the uninfected cell.

REFERENCES

1. Hartmann, R., Justesen, J., Sarkar, S.N., Sen, G.C. and Yee, V.C. (2003) Crystal structure of the 2'-specific and double-stranded RNA-activated interferon-induced antiviral protein 2'-5'-oligoadenylate synthetase. *Mol Cell*, **12**, 1173-1185.
2. Donovan, J., Dufner, M. and Korennykh, A. (2013) Structural basis for cytosolic double-stranded RNA surveillance by human oligoadenylate synthetase 1. *Proc Natl Acad Sci U S A*, **110**, 1652-1657.
3. Lohofener, J., Steinke, N., Kay-Fedorov, P., Baruch, P., Nikulin, A., Tishchenko, S., Manstein, D.J. and Fedorov, R. (2015) The Activation Mechanism of 2'-5'-Oligoadenylate Synthetase Gives New Insights Into OAS/cGAS Triggers of Innate Immunity. *Structure*, **23**, 851-862.
4. Hartmann, R., Norby, P.L., Martensen, P.M., Jorgensen, P., James, M.C., Jacobsen, C., Moestrup, S.K., Clemens, M.J. and Justesen, J. (1998) Activation of 2'-5' oligoadenylate synthetase by single-stranded and double-stranded RNA aptamers. *J Biol Chem*, **273**, 3236-3246.
5. Kodym, R., Kodym, E. and Story, M.D. (2009) 2'-5'-Oligoadenylate synthetase is activated by a specific RNA sequence motif. *Biochem Biophys Res Commun*, **388**, 317-322.
6. Vachon, V.K., Calderon, B.M. and Conn, G.L. (2015) A novel RNA molecular signature for activation of 2'-5' oligoadenylate synthetase-1. *Nucleic Acids Res*, **43**, 544-552.
7. Calderon, B.M. and Conn, G.L. (2018) A human cellular noncoding RNA activates the antiviral protein 2'-5'-oligoadenylate synthetase 1. *J Biol Chem*, **293**, 16115-16124.
8. Schwartz, S.L., Park, E.N., Vachon, V.K., Danzy, S., Lowen, A.C. and Conn, G.L. (2020) Human OAS1 activation is highly dependent on both RNA sequence and context of activating RNA motifs. *Nucleic Acids Res*, **48**, 7520-7531.
9. Justesen, J. and Kjeldgaard, N.O. (1992) Spectrophotometric pyrophosphate assay of 2',5'-oligoadenylate synthetase. *Anal Biochem*, **207**, 90-93.
10. Li, Y., Banerjee, S., Wang, Y., Goldstein, S.A., Dong, B., Gaughan, C., Silverman, R.H. and Weiss, S.R. (2016) Activation of RNase L is dependent on OAS3 expression during infection with diverse human viruses. *Proc Natl Acad Sci U S A*, **113**, 2241-2246.
11. Marie, I., Blanco, J., Rebouillat, D. and Hovanessian, A.G. (1997) 69-kDa and 100-kDa isoforms of interferon-induced (2'-5')oligoadenylate synthetase exhibit differential catalytic parameters. *Eur J Biochem*, **248**, 558-566.

TABLES

Table 1. Summary of OAS1-dsRNA kinetic parameters.

dsRNA	**K_{app}** (μM)	**V_{max}** (nmol PP_i/min)	**n**
18 bp dsRNA	4.0 ± 0.3	36.5 ± 1.4	4
CS1-AC	42.6	15.4	1
CS1-AU	15.4	9.2	1
CS2-AC	0.7	35.4	1
CS2-AU	2.2	9.9	1
CS2-CC	15.6	18.5	1

CHAPTER SIX

Discussion

Nucleic acid sensing is one essential strategy used by the innate immune system to detect, respond to, and clear infection. The OAS enzymes are allosterically regulated by dsRNA, driving the necessary conformational changes to form the catalytic site and produce the second messenger 2-5A required to activate RNase L in the OAS/RNase L pathway (1,2). Previously, it was determined that the minimum requirement for OAS activation is a perfectly base-paired dsRNA of an optimal length that spans the RNA binding surface. As such, OAS1 with a single OAS domain is activated by the shortest dsRNAs (>18 bp) while OAS3 requires dsRNA of at least 50 bp in length (1,3). However, recent work has identified consensus sequences and other activating motifs that aid in potentiating OAS1 activity (4-7). Since OAS relies on dsRNA for activation, it is important to understand how OAS is regulated by dsRNA, specifically the dsRNA features and their context that are necessary or dispensable for OAS enzyme activity. Tight regulation of OAS1 activity is required for proper cell function and misregulation of this essential cellular pathway can leave the cell susceptible to viral infection and disease.

The work described in this thesis focused on elucidating the molecular features within dsRNA that impact activation of OAS1 by utilizing a short 18 bp dsRNA containing two OAS1 activation sequences, WWN_9WG consensus (5) and 3'-ssPy motif (6), as a model. These studies were essential to begin understanding the molecular basis of how OAS1 activation is affected by dsRNA sequence, structure, and context of these activating motifs.

In **Chapter 3**, we showed that the 3'-ssPy motif is a biologically important RNA signature capable of enhancing OAS1 activation *in vitro* and in human cells. Our data demonstrated that adding the 3'-ssPy motif to the top strand of the model 18 bp dsRNA enhances OAS1 activation while adding the same modification to the bottom strand had no effect. These data suggest that OAS1 binds preferentially to one of the two supposedly "equivalent" WWN_9WG consensus sequence binding sites. Additional permutations altering the context of the OAS1 activation consensus sequence, 3'-ssPy motif, or both, showed that the potency of the 3'-ssPy motif was determined by optimal dsRNA positioning via the OAS1 activation consensus sequence. We

also determined, utilizing a series of scrambled sequences, that OAS1 is unexpectedly sensitive to sequence and that not any perfectly double-stranded RNA of appropriate length is able to induce activation. Our work with a partially scrambled sequence indicated that the identity of the nine intervening nucleotides within the OAS1 activation consensus sequence (WW$\underline{N_9}$WG) were also important contributors to the enhancement of OAS1 activation. We were able to use the 3'-ssPy motif as a molecular tool to measure dsRNA-binding directionality in solution as well as demonstrate that OAS1 activity can be driven by sequence preferences and the context of activating motifs.

In **Chapter 4**, we initially set out to investigate the propensity of inosine-containing dsRNAs to evade detection by OAS1. A recent report had indicated that accumulation of endogenous dsRNAs lacking A-to-I editing resulting from ADAR1 deficiency could activate the OAS/RNase L pathway (8). Further, rescue of this phenotype by subsequent deletion of RNase L implied that such editing is a mechanism by which the cell avoids aberrant OAS/RNase L pathway activation. In contrast to our initial expectation, we found that OAS1 could be activated by dsRNA with inosine modifications in both mismatched (I•U) and Watson-Crick-like base paired (I-C) contexts. Changing A to I did not eliminate the ability of OAS1 to sense these particular short dsRNAs. Unexpectedly, all of the inosine substitutions also had an enhancing effect on OAS1 activity. As a consequence of the location and relative position of these nucleotide changes, we also determined that the extent of OAS1 activation was partially determined by dsRNA shape and flexibility. We speculate that the nine non-conserved nucleotides (N_9) forming the intervening region within the OAS1 activation consensus sequence (WWN_9WG) may not be sensed in a sequence-specific manner, but nonetheless have at least two critical functions: (i) achieve the adequate spacing to position conserved nucleotides (WW/WG) within the dsRNA minor grooves on the same surface of the helix for interactions with OAS1 (5), and (ii) dictate the shape and flexibility of the dsRNA for OAS1 recognition. When bound to OAS, dsRNA adopts a slightly bent conformation, as observed in the human OAS1-

dsRNA crystal structure (1), so changes in nucleotide content or base pair composition could strongly influence dsRNA bending and activity. Our finding that OAS1 exhibits tolerance for dsRNAs that contain non-standard nucleotides and/or include regions with mismatches or imperfect base pairing also greatly expands the number of potential RNA activators in the cell. What then prevents short cellular dsRNA segments from activating OAS1 if A-to-I editing alone is insufficient? One possible explanation could be that most cellular RNAs are coated in RNA-binding proteins, which offer protection from degradation or inducing a cellular response at the wrong place at the wrong time. We also cannot eliminate the possibility that there could simply be other cellular pathways at work that help prevent inadvertent activation of OAS1.

In **Chapter 5**, we wanted to identify the role of the conserved nucleotides (WW/WG) within the OAS1 activation consensus sequence (WWN_9WG) and determine the molecular mechanism employed by this consensus to potentiate OAS1 activation. We introduced guanine (G) to adenine (A) mutations, generating two separate A:C mismatches, one in each copy of the OAS1 activation consensus sequence. Surprisingly, despite occupying the same location in their respective consensus sequence, the two G to A mutations were non-equivalent: one greatly reduced the level of OAS1 activity, while the other dramatically enhanced OAS1 activation. Thus, we demonstrated that our 18 bp dsRNA contains two, non-equivalent OAS1 binding sites with vastly different capacities to activate OAS1. Our current model suggests that mutation of the conserved guanine removes the competition driving dsRNA binding to either the "preferred" or "non-preferred" consensus sequence in the opposite orientation. These data support our findings in **Chapter 3** that showed that the 3'-ssPy motif, although appended to both ends of the dsRNA, were not equally sensed by OAS1. Taken together, we have demonstrated that the two consensus strands in the model 18 bp dsRNA are not equal.

These advances in the field of OAS biology and innate immune system regulation by dsRNA have helped us begin filling in the gaps, as we better understand what features within a dsRNA molecule contribute to the extent of OAS1 activation (**Figure 1**). However, despite

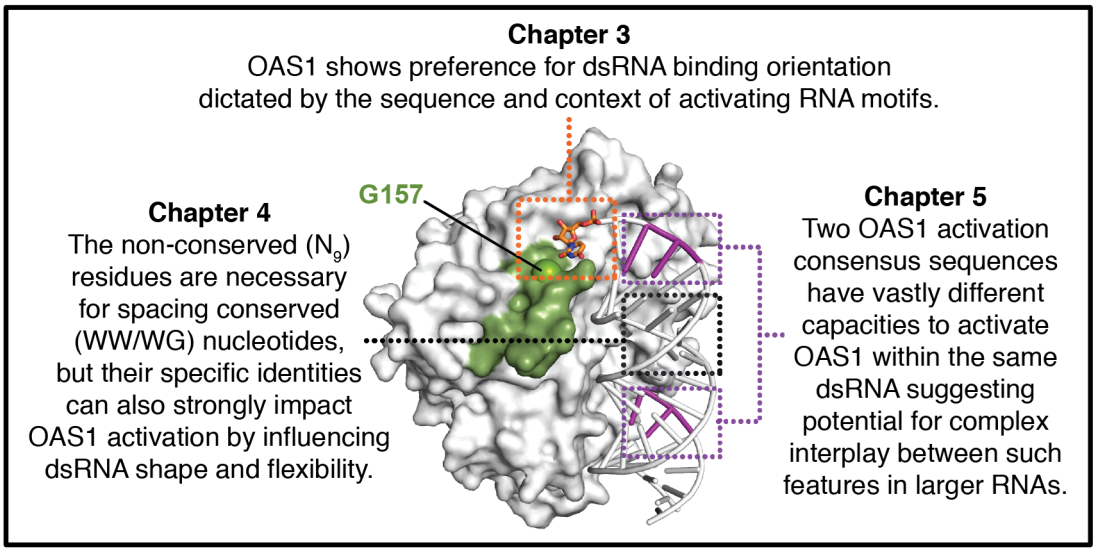

Figure 1. Overview of main research findings. As discussed in extensive detail in the preceding chapters, OAS1 (*grey*) activation is regulated by dsRNA (*white*) and can be enhanced by the presence of unique molecular signatures, such as the 3'-ssPy motif (*orange box*) or WWN_9WG activation consensus sequence (*purple and black boxes*). These statements summarize the main takeaways for each of the three results chapters of this work (**Chapters 3-5**).

garnering all of this new information, a number of questions remain unaddressed. For example, identifying the 3'-ssPy motif as a molecular signature with the propensity to (if positioned optimally) enhance OAS1 activation, still begs the question: what is the mechanism by which the 3'-ssPy motif exerts its effect? Determining the molecular mechanisms utilized by these OAS1 activating sequences (or structures) would give us another layer of detail into how dsRNA is able to precisely tune the level of OAS1 activity. The sections below detail general gaps in our knowledge as well as logical future directions for this work.

Define the molecular mechanism(s) of action for enhancement of OAS1 activation by RNA sequence and structural motifs.

Our lab has identified two novel molecular signatures with the capacity to potentiate OAS1 activation: the 3'-ssPy motif produced as a result of RNA polymerase III transcription termination (6,9) and the unique tertiary structure formed by the apical stem loop of the human non-coding

RNA 886 (nc886) (7). We have determined that OAS1 binding to either the model 18 bp dsRNA or nc886 is dictated primarily by the OAS1 activation consensus sequence (10) or the ~18 bp region of the non-coding RNA's central stem (7), respectively. Once positioned optimally by the OAS1 binding site, these RNA signatures dramatically increase OAS1 activation. However, the precise mechanism of activation by these two RNA features has remained elusive. Bioinformatics approaches could be used to identify the frequency of these motifs in viral genomes, but would not necessarily provide mechanistic insights employed by these sequences. However, based on my work, this method could be adapted to identify or predict sequences that potently activate or inhibit OAS1, as a useful new tool for studying viral evasion strategies and for the development of therapies required to combat these infections.

Based on modeling and mutagenesis analyses, it seems likely that the 3'-ssPy motif acts as an allosteric enhancer of activation. Our lab previously demonstrated that substitution of OAS1 residue Gly157 with the bulkier Gln eliminated the enhancing effect of the 3'-ssPy motif, but did not otherwise reduce OAS1 activity significantly (6). This finding provided convincing evidence that the 3'-ssPy motif may interact with a loop containing Gly157 to promote enhanced OAS1 activation. However, given the location of this OAS1 loop adjacent to the dsRNA binding surface and distant from its catalytic center, the molecular basis for 3'-ssPy action was unclear. More recent studies in our lab using molecular dynamics (MD) simulations have revealed a potential additional allosteric mechanism in OAS1. These MD studies were performed to understand the impacts of four distinct OAS1 amino acid substitutions identified in patients with immunodeficiencies that give rise to low-level constitutive "gain-of-function" activity (see details below; Magg *et al.*, *submitted*). However, despite the distant location of all four sites of substitution, each resulted in an overlapping set of changes in protein dynamics, surrounding the catalytic center on one side of the protein and within the Gly157 loop on the other. These initial insights into the possible molecular mechanism are valuable, but moving forward it will be important to utilize more high-resolution experimental techniques, such as x-ray crystallography,

in addition to further MD simulations (*e.g.* of Gly157 loop substitutions in the free and dsRNA-bound form of OAS1) to determine the structure and step-by-step mechanistic details of these allosteric interactions.

Expand the model dsRNA to test the action of the OAS1 activation consensus sequence and other activating motifs in the context of longer or more structured RNA.

All of these studies have been done in the context of a "simple" model 18 bp dsRNA that can be easily manipulated and dissected. The interplay between OAS1-activating molecular signatures in RNA are likely to become exponentially more complicated in larger dsRNA molecules with many potential overlapping binding sites. Based on our work to date, it seems that it is not simply the presence or absence of an RNA feature, but also their placement within the dsRNA that determines how much each motif contributes to OAS activation.

These RNA molecular signatures could also act in concert or competition to affect the level of OAS activity. It will therefore be important to fully address open questions pertaining to how the context of OAS1 activation sequences affects the extent of OAS1 activation within a longer and/or more structured RNA. For example, a viral dsRNA containing a preferred OAS binding site with a weaker ability to activate OAS1 could potentially diminish activation by other sites within the same dsRNA. These important new insights would give us valuable information on how viruses could potentially mask an otherwise activating motif to evade detection by the host innate immune system. As a precedence for such a viral strategy, a previous study showed that a non-coding RNA from Dengue virus could act as a molecular "sponge" dampening the activity of three cellular RNA-binding proteins (G3BP1, G3BP2, and CAPRIN1) restricting the translation of interferon-stimulated mRNA transcripts (11).

Identify the impact (if any) these OAS1 activation sequences have on other OAS family members, OAS2 and OAS3.

A recent study of OAS2 tested dsRNAs ranging from 19-123 bp in length and each construct was subjected to RNase treatment to generate a minimal 3'-ssPy motif (12). However, the 3'-ssPy motif had no effect on OAS2 activation. The dsRNA constructs used in this study contained multiple WWN_9WG consensus sequences, but these were not located in the same position as the model 18 bp dsRNA (6,10). These findings suggest that RNA signatures, like the 3'-ssPy motif, may not directly influence OAS1 (or OAS2) binding to dsRNAs but when positioned optimally by other features of the adjacent dsRNA binding site can serve to strongly enhance 2-5A synthesis. Another possible explanation could be that OAS2 activity is simply not enhanced by the 3'-ssPy and this OAS protein may not rely on RNA sequence at all; activation may just require binding a dsRNA long enough to span both OAS domains (and/or dimer interface) in order to activate the catalytic subunit(s). This phenomenon has only begun to be teased apart for OAS1, so whether or not specific sequences can similarly enhance OAS2 or OAS3 activity remains to be elucidated. This work further emphasizes a longstanding gap in the field and that by defining the dsRNA sequences and the mechanisms that lead to potent OAS1 activation is critical to our understanding of OAS protein function and regulation.

Pathway crosstalk and the additional role RNAs could play in regulating multiple arms of the innate immune system.

Another important consideration is the role RNA may play in potentially regulating multiple cellular pathways. Our lab showed that human nc886 is a regulator of two distinct innate immune system pathways required for translational control (7,13). Specifically, we showed that nc886 adopts two structural conformations with opposing functions: Conformer 1 is a potent *inhibitor* of PKR but activator of OAS1, while Conformer 2 is a weak activator of both proteins (7,13). The two conformations share largely the same structure, specifically in the central and terminal stem, but they differ in the apical stem region. The apical region of nc886 was found to be essential for both PKR inhibition and OAS1 activation, through its presumed formation of a

complex tertiary structure (7). This finding led to speculation that nc886 may serve as a potential mediator of communication between these two pathways. The overlapping yet distinct mechanisms (*e.g.* inhibition of PKR versus activation of OAS1) suggest that these two dsRNA sensors may compete for nc886 binding depending on the "current" cellular requirements. In the absence of a viral infection, nc886 is bound to PKR to prevent PKR activation while also preventing inadvertent activation of OAS1. However, during a viral invasion, nc886 can be displaced from PKR by viral dsRNA allowing nc886 to bind and activate OAS1 limiting the spread of infection two-fold. Future experiments could include using PKR/OAS1-nc886 competition assays to directly assess this proposed model for direct competitive binding between these two dsRNA sensors. However, several open questions still remain to be answered: How does the cell prevent nc886 from activating the OAS/RNase L pathway unnecessarily? Does the cell precisely tune the level of each nc886 conformer to impact OAS1 activity? Does nc886 fall under the short list of potential RNase L targets? What role(s) does nc886 play (as a cellular non-coding RNA) in the uninfected cell compared to during a viral infection? Future studies should focus on answering these pertinent questions while also potentially identifying other RNAs with the ability to selectively inhibit or activate different arms of the innate immune system.

Determine the molecular basis of dsRNA-independent OAS1 activation conferred by clinical mutations with gain-of-function phenotypes.

Pursuing studies to fully define how OAS1 is regulated in the uninfected cell will also be critical. In collaboration with research groups from around the world, we helped identify the possible molecular mechanism responsible for immune system dysregulation caused by four human heterozygous missense *OAS1* mutations that result in four different amino acid substitutions (A76V, C109Y, V121G, and L198V; Magg *et al.*, *submitted*). These mutations cause lethal early-onset symptoms linked to a previously uncharacterized autoinflammatory immunodeficiency

syndrome: OAS1-associated polymorphic autoinflammatory immunodeficiency disorder (OPAID). We speculate that such OAS1 mutations in genomic databases are underrepresented due to the lethal nature of the phenotype. Our mechanistic insights based on *in vitro* OAS1 activation assays coupled with *in silico* modeling and MD simulations suggest that these patient mutations conferred a dsRNA-independent mechanism of activation via common allosterically induced changes in OAS1 protein dynamics (**Figure 2**). Therefore, these symptoms likely arise from unconstrained regulation of OAS1 in the uninfected cell, where OAS1 exhibits a low level of basal activation without the need of a dsRNA allosteric activator.

As discussed previously, dsRNA is required to drive conformational changes necessary to form the OAS1 catalytic triad for ATP binding and 2-5A synthesis (1,2); however, the patient mutations identified in this particular study resulted in proteins able to partly undergo these structural rearrangements in the absence of dsRNA (**Figure 2**). These patient variants are yet another example underscoring the importance of the need for OAS1 activity to be tightly regulated. These studies should be followed up with additional biochemical, biophysical, and structural approaches to define the molecular mechanism(s) by which these OAS1 clinical variants act independently of dsRNA allosteric regulation. Defining the molecular details that dictate unconstrained OAS1 regulation will also help us understand more about general OAS function and could serve as an excellent candidate for the development of novel therapeutics against OAS1 gain-of-function phenotypes.

Develop novel OAS1 inhibitors (and activators) for therapeutic implementation.

As discussed in the previous section, OAS1 patient mutations were recently identified and shown to cause immune system dysregulation via OAS1 activation independent of dsRNA or viral infection (Magg *et al.*, *submitted*). OAS proteins are essential effectors of the cellular response to viral infections. However, OAS has also been implicated in other human diseases, including autoimmune disorders (14-17), cancer (18,19), tuberculosis (20,21), malaria (22), and

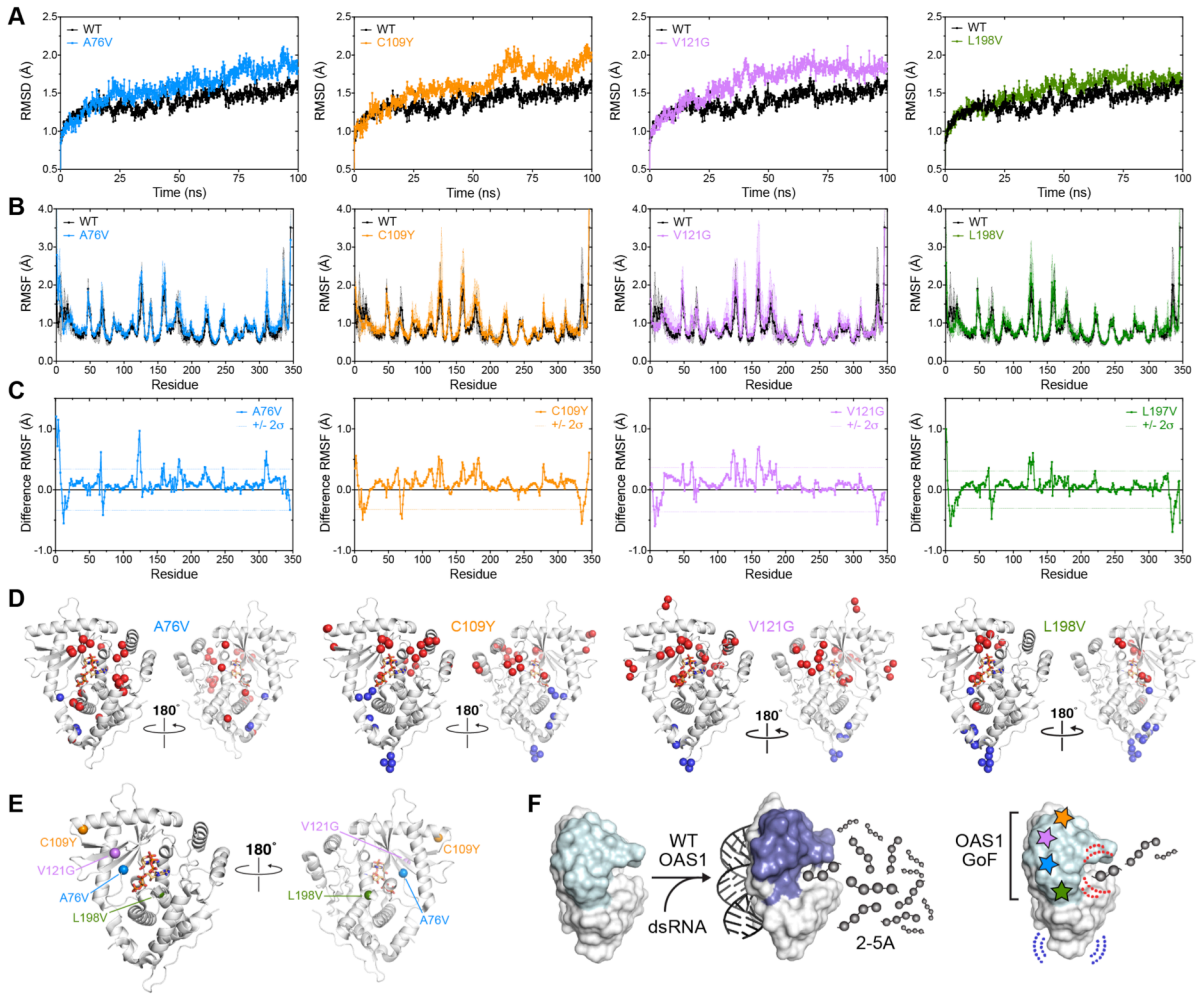

Figure 2. dsRNA-independent OAS1 gain-of-function activity is favored by allosteric loss of structural constraints.

MD simulation analysis of wild-type OAS1 (WT) and OAS1 clinical variants (A76V, C109Y, V121G, and L198V): ***A,*** overall protein root-mean-square deviation (RMSD) over the 100 ns MD production run, ***B,*** residue backbone atom root-mean-square fluctuation (RMSF), and ***C,*** difference RMSF (wild-type OAS1 subtracted from each clinical variant). Individual proteins are as noted in the plot legends (*left* to *right*): A76V (blue), C109Y (orange), V121G (purple) and L198V (green); wild-type OAS1 (black) is shown in *panels A* and *B* for comparison. Shaded regions on plots in *panel B* represent the error in each value (SD). In *panel C*, dotted lines denote two standard deviations (+/- 2σ) from the average difference RMSF for each protein (*i.e.* the most significant changes in residue dynamics). ***D,*** Residues with most significant changes in dynamics mapped onto OAS1 structure (shown in the dsRNA-bound conformation; PDB code 4RWN) as Cα spheres; color coding denotes increased dynamics (> 2σ; red) and decreased dynamics (< -2σ; blue) compared to wild-type OAS1. ***E,*** Locations of substituted residues are shown in the same views as *panel D*. ***F,*** Model for common action of OAS1 gain-of-function (GoF) variants. Wild-type OAS1 (*left*) strictly regulated by dsRNA binding-induced conformational changes, whereas amino acid substitutions (*right*) relieve this strict control by allosteric induction of changes around the enzyme catalytic center (red dotted lines) and mirroring changes that occur upon dsRNA binding (blue dotted lines). These changes promote low-level gain-of-function activity in the absence of dsRNA. MD simulations were run and analyzed, and figures prepared by Drs. Debayan Dey and Graeme L. Conn (Magg *et al.* submitted).

linked to resistance for the only approved treatment for gastric cancer (23). The importance of OAS in these human diseases and resistance to treatments cannot be overlooked, and the OAS proteins should be considered viable drug targets to improve immune modulation and existing treatments.

A recent report used homology modeling and high-throughput virtual screening to identify potential OAS1, OAS2, and OAS3 inhibitors (24). The thirty-seven small molecule drug targets identified in this study were proposed to act as competitive inhibitors of ATP, blocking substrate binding, and thus limiting 2-5A synthesis. The molecules were computationally predicted to bind to one of the two ATP binding sites (donor or acceptor) interacting with the same residues independent of the OAS activation state: Asp75, Asp77, Gln194, Gln229, and Tyr230 in OAS1 and analogous amino acids in OAS2 and OAS3. However, there was little correlation between specific chemical fragments and their intermolecular interactions with the OAS catalytic triad. This study provides candidates of possible OAS inhibitors that could be used as a jumping off point for future rational design and optimization. These OAS inhibitors would be essential for the treatment of patients with OAS1 gain-of-function mutations prior to stem cell transplant; however, one caveat to developing therapies that inhibit OAS activation would be the potential adverse effect of increasing patient susceptibility to viral infection.

Viruses have developed unique ways of evading the OAS/RNase L pathway, yet developing compounds to specifically target OAS regulation to treat patients has been severely under researched. Thus, I envisage another growing area of study would be to use OAS1 as a target for identifying novel small molecule inhibitors, or even activators, depending on therapeutic need. OAS1 inhibitors would be required for patients that have mutations in OAS1 that result in hyperactivity and/or lead to immune dysregulation. OAS1 activators may serve as broad-spectrum antivirals required to supplement the immune system of immunocompromised individuals at increased risk or susceptibility to viral infections. These drugs would serve as important modulators of OAS1 activity protecting the cell from spurious activation or aiding the

cell in viral takeover, respectively. Based on current knowledge of OAS1 structure and function, we can begin using computational approaches to design small molecule leads that target different parts of the enzyme, including the catalytic site, dsRNA binding surface, or other regions responsible for allosteric regulation. A useful tool to implement testing of OAS1 inhibitors is a high-throughput system that can effectively screen small molecule libraries using mammalian cells expressing OAS1 variants that are constitutively active in the absence of dsRNA. The OAS1 clinical mutations outlined in the previous section would be perfect candidates for such studies.

Final remarks

Prior to starting this work, there was little known about what features within a dsRNA constitute an activating or non-activating OAS1 binding site. My work has thus contributed to our essential understanding of how specific RNA sequence(s) and their context tune the level of OAS1 activation. I also identified the importance of dsRNA shape and flexibility (as dictated by nucleotide content) as an additional set of criteria that should be taken into consideration when probing for potent dsRNA activators. My thesis work began to fill in outstanding gaps, but moving forward, a complete understanding of the dsRNA features and their molecular mechanism(s) controlling OAS1 regulation will be critical for the development of essential therapeutic strategies.

References

1. Donovan, J., Dufner, M. and Korennykh, A. (2013) Structural basis for cytosolic double-stranded RNA surveillance by human oligoadenylate synthetase 1. *Proc Natl Acad Sci U S A*, **110**, 1652-1657.
2. Lohofener, J., Steinke, N., Kay-Fedorov, P., Baruch, P., Nikulin, A., Tishchenko, S., Manstein, D.J. and Fedorov, R. (2015) The Activation Mechanism of 2'-5'-Oligoadenylate Synthetase Gives New Insights Into OAS/cGAS Triggers of Innate Immunity. *Structure*, **23**, 851-862.
3. Donovan, J., Whitney, G., Rath, S. and Korennykh, A. (2015) Structural mechanism of sensing long dsRNA via a noncatalytic domain in human oligoadenylate synthetase 3. *Proc Natl Acad Sci U S A*, **112**, 3949-3954.

4. Hartmann, R., Norby, P.L., Martensen, P.M., Jorgensen, P., James, M.C., Jacobsen, C., Moestrup, S.K., Clemens, M.J. and Justesen, J. (1998) Activation of 2'-5' oligoadenylate synthetase by single-stranded and double-stranded RNA aptamers. *J Biol Chem*, **273**, 3236-3246.

5. Kodym, R., Kodym, E. and Story, M.D. (2009) 2'-5'-Oligoadenylate synthetase is activated by a specific RNA sequence motif. *Biochem Biophys Res Commun*, **388**, 317-322.

6. Vachon, V.K., Calderon, B.M. and Conn, G.L. (2015) A novel RNA molecular signature for activation of 2'-5' oligoadenylate synthetase-1. *Nucleic Acids Res*, **43**, 544-552.

7. Calderon, B.M. and Conn, G.L. (2018) A human cellular noncoding RNA activates the antiviral protein 2'-5'-oligoadenylate synthetase 1. *J Biol Chem*, **293**, 16115-16124.

8. Li, Y., Banerjee, S., Goldstein, S.A., Dong, B., Gaughan, C., Rath, S., Donovan, J., Korennykh, A., Silverman, R.H. and Weiss, S.R. (2017) Ribonuclease L mediates the cell-lethal phenotype of double-stranded RNA editing enzyme ADAR1 deficiency in a human cell line. *Elife*, **6**, e25687.

9. Nielsen, S., Yuzenkova, Y. and Zenkin, N. (2013) Mechanism of eukaryotic RNA polymerase III transcription termination. *Science*, **340**, 1577-1580.

10. Schwartz, S.L., Park, E.N., Vachon, V.K., Danzy, S., Lowen, A.C. and Conn, G.L. (2020) Human OAS1 activation is highly dependent on both RNA sequence and context of activating RNA motifs. *Nucleic Acids Res*, **48**, 7520-7531.

11. Bidet, K., Dadlani, D. and Garcia-Blanco, M.A. (2014) G3BP1, G3BP2 and CAPRIN1 are required for translation of interferon stimulated mRNAs and are targeted by a dengue virus non-coding RNA. *PLoS Pathog*, **10**, e1004242.

12. Koul, A., Deo, S., Booy, E.P., Orriss, G.L., Genung, M. and McKenna, S.A. (2020) Impact of double-stranded RNA characteristics on the activation of human 2'-5'-oligoadenylate synthetase 2 (OAS2). *Biochem Cell Biol*, **98**, 70-82.

13. Calderon, B.M. and Conn, G.L. (2017) Human noncoding RNA 886 (nc886) adopts two structurally distinct conformers that are functionally opposing regulators of PKR. *RNA*, **23**, 557-566.

14. Field, L.L., Bonnevie-Nielsen, V., Pociot, F., Lu, S., Nielsen, T.B. and Beck-Nielsen, H. (2005) OAS1 splice site polymorphism controlling antiviral enzyme activity influences susceptibility to type 1 diabetes. *Diabetes*, **54**, 1588-1591.

15. Fedetz, M., Matesanz, F., Caro-Maldonado, A., Fernandez, O., Tamayo, J.A., Guerrero, M., Delgado, C., Lopez-Guerrero, J.A. and Alcina, A. (2006) OAS1 gene haplotype confers susceptibility to multiple sclerosis. *Tissue Antigens*, **68**, 446-449.

16. Feng, X., Wu, H., Grossman, J.M., Hanvivadhanakul, P., FitzGerald, J.D., Park, G.S., Dong, X., Chen, W., Kim, M.H., Weng, H.H. *et al.* (2006) Association of increased interferon-inducible gene expression with disease activity and lupus nephritis in patients with systemic lupus erythematosus. *Arthritis Rheumatol*, **54**, 2951-2962.

17. Li, H., Reksten, T.R., Ice, J.A., Kelly, J.A., Adrianto, I., Rasmussen, A., Wang, S., He, B., Grundahl, K.M., Glenn, S.B. *et al.* (2017) Identification of a Sjogren's syndrome susceptibility locus at OAS1 that influences isoform switching, protein expression, and responsiveness to type I interferons. *PLoS Genet*, **13**, e1006820.

18. Mandal, S., Abebe, F. and Chaudhary, J. (2011) 2'-5' oligoadenylate synthetase 1 polymorphism is associated with prostate cancer. *Cancer*, **117**, 5509-5518.

19. Dar, A.A., Pradhan, T.N., Kulkarni, D.P., Shah, S.U., Rao, K.V., Chaukar, D.A., D'Cruz, A.K. and Chiplunkar, S.V. (2016) Extracellular 2'5'-oligoadenylate synthetase 2 mediates T-cell receptor CD3-zeta chain down-regulation via caspase-3 activation in oral cancer. *Immunology*, **147**, 251-264.

20. Wu, S., Wang, Y., Chen, G., Zhang, M., Wang, M. and He, J.Q. (2018) 2'-5'-Oligoadenylate synthetase 1 polymorphisms are associated with tuberculosis: a case-control study. *BMC Pulm Med*, **18**, 180.

21. Leisching, G., Cole, V., Ali, A.T. and Baker, B. (2019) OAS1, OAS2 and OAS3 restrict intracellular M. tb replication and enhance cytokine secretion. *Int J Infect Dis*, **80S**, S77-S84.

22. Lee, H.J., Georgiadou, A., Walther, M., Nwakanma, D., Stewart, L.B., Levin, M., Otto, T.D., Conway, D.J., Coin, L.J. and Cunnington, A.J. (2018) Integrated pathogen load and dual transcriptome analysis of systemic host-pathogen interactions in severe malaria. *Sci Transl Med*, **10**, eaar3619.

23. Yu, C., Xue, P., Zhang, L., Pan, R., Cai, Z., He, Z., Sun, J. and Zheng, M. (2018) Prediction of key genes and pathways involved in trastuzumab-resistant gastric cancer. *World J Surg Oncol*, **16**, 174.

24. Gonzalez, K.J., Moncada-Giraldo, D.M. and Gutierrez, J.B. (2020) In silico identification of potential inhibitors against human 2'-5'- oligoadenylate synthetase (OAS) proteins. *Comput Biol Chem*, **85**, 107211.